JOURNAL OF FLUID MECHANICS

VOLUME 10 PART 1

FEBRUARY 1961

PUBLISHED BY

CAMBRIDGE UNIVERSITY PRESS

BENTLEY HOUSE, 200 EUSTON ROAD, LONDON, N.W.1

AMERICAN BRANCH: 32 EAST 57TH STREET, NEW YORK 22, N.Y.

Price 30*s*. (*U.S.A.* $5.00)

The JOURNAL OF FLUID MECHANICS exists for the publication of theoretical and experimental investigations of all aspects of the mechanics of fluids, and is issued in four parts per volume.

EDITORS

DR G. K. BATCHELOR, DR T. BROOKE BENJAMIN

Department of Applied Mathematics and Theoretical Physics, University of Cambridge, Free School Lane, Cambridge, England

ASSISTANT EDITORS

DR J. R. A. PEARSON, DR O. M. PHILLIPS

ASSOCIATE EDITORS

PROF. G. F. CARRIER

Pierce Hall, Harvard University, Cambridge 38, *Massachusetts, U.S.A.*

DR W. C. GRIFFITH

Lockheed Missiles and Space Division, Palo Alto, California, U.S.A.

M. J. LIGHTHILL

Royal Aircraft Establishment, Farnborough, Hampshire, England

PROF. R. R. LONG

School of Engineering, The Johns Hopkins University, Baltimore 18, *Maryland, U.S.A.*

DR P. G. SAFFMAN

Department of Mathematics, King's College, London, W.C. 2, *England*

Authors wishing to have papers published in the JOURNAL should communicate them to any one of the persons named above, choosing one in their own country where possible.

Authors are urged to ensure that their papers are written clearly and attractively, in order that their work will be readily accessible to readers.

Manuscripts should be typed in double spacing on one side of the paper only, with references listed at the end in alphabetical order of authors. Drawings should be done on a large scale in Indian ink on tracing cloth or drawing paper, the lettering being shown clearly in pencil for reproduction by the printer; the list of captions should be typed at the end of the manuscript. Proofs of papers from overseas will usually be despatched to authors by airmail. There is no charge for publication. Authors are entitled to receive 50 offprints of a paper in the JOURNAL free of charge, and additional offprints can be purchased if ordered in advance.

SUBSCRIPTIONS

The subscription price for a volume of four parts is £5. 10*s*. net, post free, payable in advance; separate parts 30*s*. net, plus postage. Subscriptions may be sent to any bookseller, or to the Cambridge University Press, Bentley House, 200 Euston Road, London, N.W.1.

Subscribers in the United States should send their orders to the Cambridge University Press, American Branch, 32 East 57th Street, New York 22, N.Y. The subscription price per volume is $18.50, post free, payable in advance; separate parts $5.00, plus postage.

Quotations for available back volumes and parts may be obtained on application to the Cambridge University Press.

Diffraction of strong shocks by cones, cylinders, and spheres

By A. E. BRYSON
Harvard University

AND R. W. F. GROSS*
Douglas Aircraft Company, Inc.

(Received 24 July 1960)

This paper presents experimental investigations of the diffraction of plane strong shocks by several cones, a cylinder, and a sphere. The diffraction pattern, in particular the loci of Mach triple points and the shape of the diffracted shocks are compared with theoretical results obtained from a diffraction theory proposed by Whitham (1957, 1958, 1959). The agreement between theory and experiment is shown to be good. Also given are extensive numerical results supplementing Whitham's papers, and theoretical considerations applying Whitham's theory to very blunt bodies.

1. Introduction

Whitham (1957, 1958, 1959) has presented an approximate theory for the dynamics of two- and three-dimensional shock waves. He applied this theory to the description of shock diffractions on wedges and a cone of 28·8° semi-angle. The present paper presents experimental results of shock diffractions by several cones with different apex angles at shock Mach numbers between 3·5 and 4·0 and compares them with numerical solutions obtained using Whitham's theory. In addition, Whitham's theory is extended to blunt two- and three-dimensional bodies, in particular a cylinder and a sphere. A theory based on Whitham's ideas is presented to describe the diffraction pattern near the nose of very blunt bodies. This theory was used to find initial values, at a distance sufficiently far from the nose to start a characteristics solution of Whitham's equations for the sphere and the cylinder. The agreement between theory and experiment at shock Mach numbers near 3·00 for certain features of the diffraction pattern was found to be good.

2. Experimental investigations and their results

The experimental investigations were performed in the Harvard University 4 in. × 12 in. × 40 ft. shock tube in air. A Schlieren optical system using a spark light source of approximately 0·2 μsec duration was used to photograph the

* Formerly Harvard University.

diffraction patterns. The shock speed was measured between two Schlieren light screens by means of an electronic counter. The second light screen also triggered a variable time delay which in turn triggered the spark light source.

Diffraction on cones

A series of Schlieren pictures of diffractions on cones with semi-apex angles θ_w varying between 9·7° and 44·7° was taken at a mean shock Mach number of $3{\cdot}68 \pm 0{\cdot}16$. Figure 1 (plate 1) gives a typical photograph from this series.

The feature of the diffraction pattern predicted by Whitham's theory is the shape and location of the diffracted shock (Mach shock) at any time. The theory

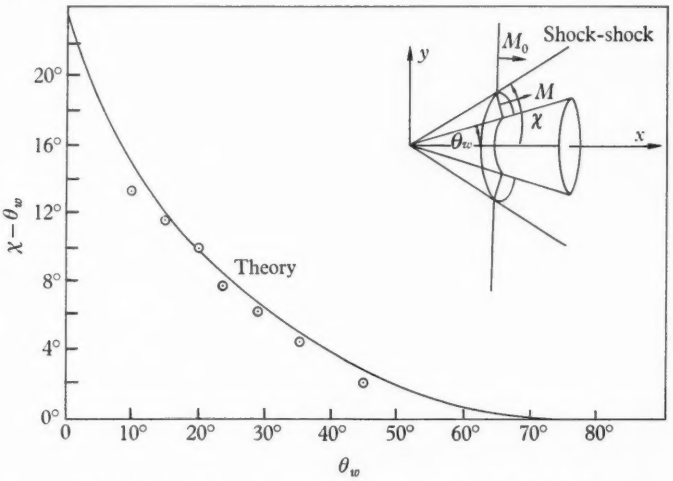

FIGURE 2. Shock-shock angle χ *vs* cone semi-apex angle θ_w for shock Mach number $M_0 = 3{\cdot}68$. ⊙ Exp. points.

does not predict the shape or location of reflected shocks. As part of the description of the Mach shock, the locus of successive positions of the Mach triple point can be found. Whitham calls this locus a 'shock-shock', since it represents a (Mach) shock moving along the incident shock.

Shock-shocks of any conical diffraction are straight lines inclined by an angle χ (shock-shock angle) with respect to the axis of symmetry. This angle was determined from the photographs. Figure 2 shows $\chi-\theta_w$ *vs* θ_w compared with the curve predicted by Whitham's theory for incident Mach number $M_0 = 3{\cdot}68$. As is seen the experimental points lie below the theoretical curve. This is the same discrepancy as that reported by Whitham (1957) on wedges. It appears to be connected with the fact that this theory does not allow for the possibility of a regular reflexion. Instead, this theory predicts Mach reflexion for all angles θ_w up to 90°, although $\chi-\theta_w$ becomes so small for $\theta_w > 70°$ that one could consider it a regular reflexion for all practical purposes.

Except for very small semi-apex angles θ_w the Mach shock is predicted to

be almost a straight line. This is shown to be true (figure 1, plate 1) although at very small θ_w the shock is so weak that an accurate determination from the Schlieren pictures was not possible.

Diffraction on a cylinder

The most extensive results were obtained for a cylinder of diameter $D = \frac{1}{2}$ in. Each shock-tube run produced one picture of the diffraction in a certain stage of development. Figures 3–5 (plates 2–4) show typical examples.

Two series of experiments were performed at the same mean shock Mach number of 2·82 but at two different pressures P_2 behind the undisturbed shock

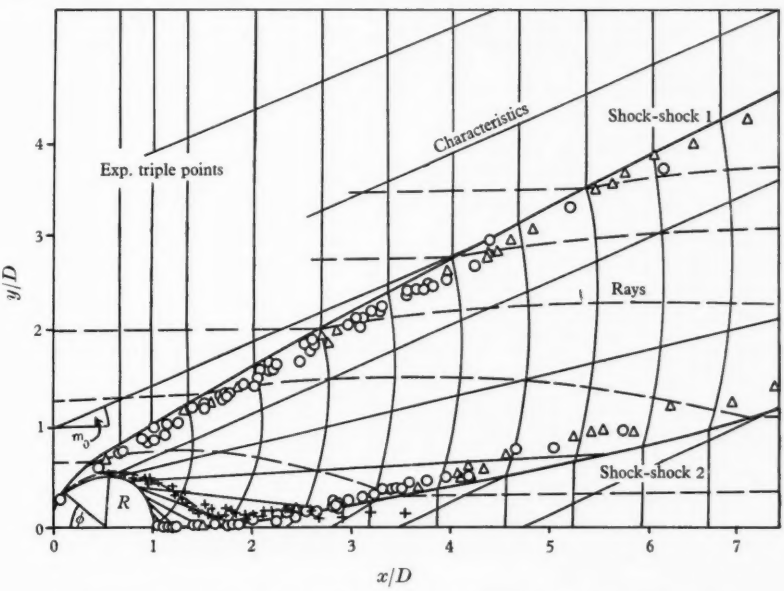

FIGURE 6. Diffraction on a cylinder. $M_0 = 2{\cdot}81$. ○ $Re = 7{\cdot}79 \times 104$, △ $Re = 0{\cdot}87 \times 10^4$, +vortex locus.

and, therefore, at two different Reynolds numbers, $Re = uD/\nu$ (u being the velocity of the undisturbed shock afterflow, D the diameter of the cylinder and ν the kinematic viscosity behind the undisturbed shock):

Series 1, $P_2 = 9{\cdot}94$ p.s.i., $Re = 7{\cdot}79 + 10^4$;

Series 2, $P_2 = 1{\cdot}08$ p.s.i., $Re = 0{\cdot}78 + 10^4$.

The diffraction was followed through about 7 diameters of travel of the incident shock past the cylinder.

On a cylinder two loci of triple points appear on either side of the plane of symmetry of the flow, one starting at the front of the cylinder, and the other at the plane of symmetry behind the cylinder (figures 4 and 5, plates 3 and 4). One half of the symmetrical diffraction pattern is shown in figure 6, which summarizes the data of the two series of experiments on the cylinder, together with the predicted shock-shocks using Whitham's theory.

When the incident shock first impinges on the cylinder a regular reflexion is formed since $\theta_w > \theta_{w\max}$, the cut-off angle. Between 40° and 50° from the forward stagnation point Mach reflexion begins. Figure 3 (plate 2), therefore, shows two curved Mach shocks and the corresponding slip surfaces just before the Mach shocks meet at the rear end of the cylinder. Note that the slip surface has 'rolled up' into a vortex (not to be mistaken for the vortices formed in viscous flow *behind* a cylinder). This vortex is formed in a boundary-layer shock-wave interaction at the time when the Mach shock is first created. The vortex was not observed in series 2 experiments; the low density and resulting decreased Schlieren sensitivity probably rendered it invisible. If the assumption is made that the circulation of the vortex does not change very much with time, it should follow a particle path. The locus of vortex positions is also shown in figure 6. Whitham, calling the orthog[illegible]al trajectories of the shock positions rays, assumes that they are identical [illegible] particle paths; note that the vortex follows a ray closely except as it near [illegible] plane of symmetry of the flow behind the cylinder.

The interaction of the two Mach shocks as they collide behind the cylinder may be considered as a reflexion off a solid wall in place of the plane of symmetry. Here again the reflexion is at first regular, Mach reflexion beginning between 0·5 and 1·0 diameters behind the cylinder. This second Mach reflexion is evident in figures 4 and 5 (plates 3 and 4).

In figure 3 (plate 2) boundary-layer separation is seen to take place on the aft sides of the cylinder. Figures 4 and 5 (plates 3 and 4) show the flow field resulting from the interaction between reflected shocks and the separated boundary-layer material behind the cylinder during the process of wake formation. In spite of this complicated flow behind the diffracted shocks, agreement between the predicted diffraction pattern and experiments appears to be good. Note in particular that a change of Reynolds number by a factor of 10 did not result in any change of the loci of the triple points in the diffraction pattern.

Diffraction on a sphere

Two series of Schlieren photographs of the diffraction on a sphere were taken in the same manner as for the cylinder. An English table-tennis ball of 1 in. diameter filled with Wood's metal and suspended in the test section from 8 nylon strings was used for a sphere. Having found the Reynolds number of no influence on the diffraction pattern, it was kept (approximately) constant and the diffraction investigated at two incident shock Mach numbers $M_0 = 2{\cdot}85$ and $M_0 = 4{\cdot}41$. Due to the larger size of the sphere the experiments cover the diffraction over a range of only 3·5 sphere-diameters of travel of the incident shock. The diffraction pattern for a sphere is qualitatively the same as for the cylinder: two pairs of triple-point loci appear on either side of the axis of symmetry. Figures 7 and 8 (plates 5 and 6) show instances in the development of the diffraction (the radial lines are the nylon strings). The diffraction pattern behind the sphere shows a spherical shock penetrating the straight Mach shock (figure 8, plate 6). This spherical shock is the reflected shock resulting from the point collision of the converging cylindrical Mach shock at the rear stagnation point of the sphere.

Due to the small extension of the disturbed flow field normal to the direction of propagation, the viscous wake development as well as the slip surfaces are almost invisible to the Schlieren system.

Figure 9 shows the experimentally found loci of the triple points plotted together with the shock-shock obtained from the theory by the method of characteristics for incident Mach numbers $M_0 \gg 1$. Due to difficulties in extending the

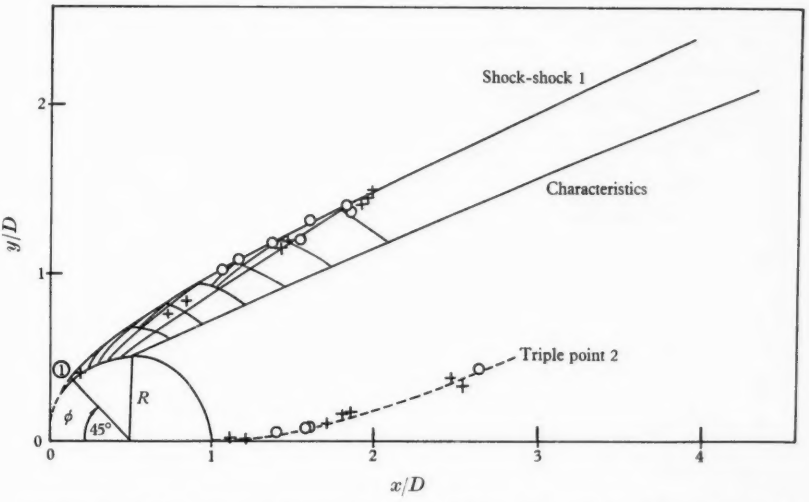

FIGURE 9. Diffraction on a sphere; characteristics solution for $M_0 \gg 1$. Exp. triple points: ○ $M_0 = 2{\cdot}85$, + $M_0 = 4{\cdot}41$, ① starting of characteristic solution.

characteristics net around the sphere to its back side, no theoretical prediction for the second shock-shock could be obtained. The agreement between theory and experiment along the first shock-shock is good. Whitham's theory predicts that the diffraction pattern should be the same for incident Mach numbers $M_0 \geqslant 3$. This is substantiated by the coincidence of the loci of the triple points found experimentally for the two incident shock Mach numbers ($M_0 = 2{\cdot}85$ and $M_0 = 4{\cdot}41$) and the shock-shock predicted for $M_0 \gg 1$.

3. Theoretical calculations

Theoretical calculations cover (1) the numerical solutions of the equations governing conical flows (with a number of by-products, which have been tabulated for future reference); (2) a semi-graphical solution by the method of characteristics for the cylinder; and (3) a purely graphical solution by characteristics for the sphere. An attempt was made in the latter two cases to simplify the calculations as much as possible by exploiting the peculiarities of the diffraction equations. In order to find an initial value curve from which to start the characteristics solution, an approximate solution for the nose region of the cylinder and the sphere was developed, based on the fundamental ideas of

Whitham's theory. The approximation was also extended to cones of large semi-apex angles.

Solution of the conical equations

The equations governing conical diffractions given by Whitham (1959, equations 52, 53, 54) for finite incident Mach number M_0 were solved on a high-speed digital computer by simultaneous integrations, starting from the shock-shock and calculating backwards to the cone surface. The method has been described by Whitham (1959). Figure 10 shows the hodograph shock-shock

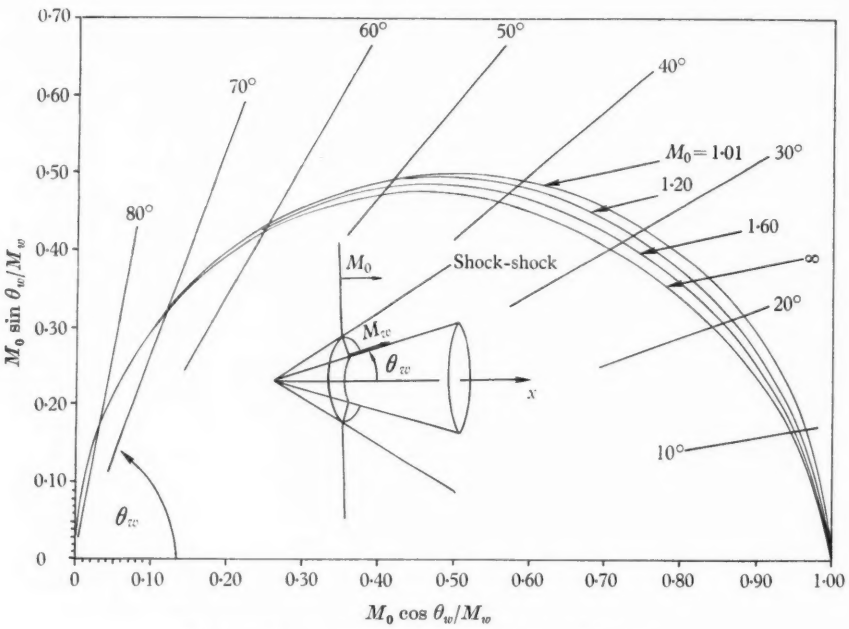

FIGURE 10. Crescent curves for conical diffractions.

polars which we will call 'crescent curves': M_0/M_w *vs* θ_w corresponding to one branch of Busemann's 'apple curves' in supersonic flow (M_0/M_w = relative Mach number on wall, θ_w = semi-apex angle) with M_0 as a parameter. Figure 11 gives $(\chi - \theta_w)$ *vs* θ_w with M_0 as a parameter. Also shown is the curve obtained from the approximate theory for cones of large semi-apex angles. Finally, figure 12 shows the full 'crescent curve' for $M_0 \gg 1$, including the curves representing the solutions of the conical diffraction in the hodograph plane. In order to make these calculations, it was necessary to determine, as functions of Mach number, the ray area A, the characteristic angle m, the integral function analogous to the Prandtl–Meyer function, ω, and the shock-shock jump conditions. Since these functions are not tabulated elsewhere, and appear to be of general interest for any further application of this theory, they are reproduced in table 1.

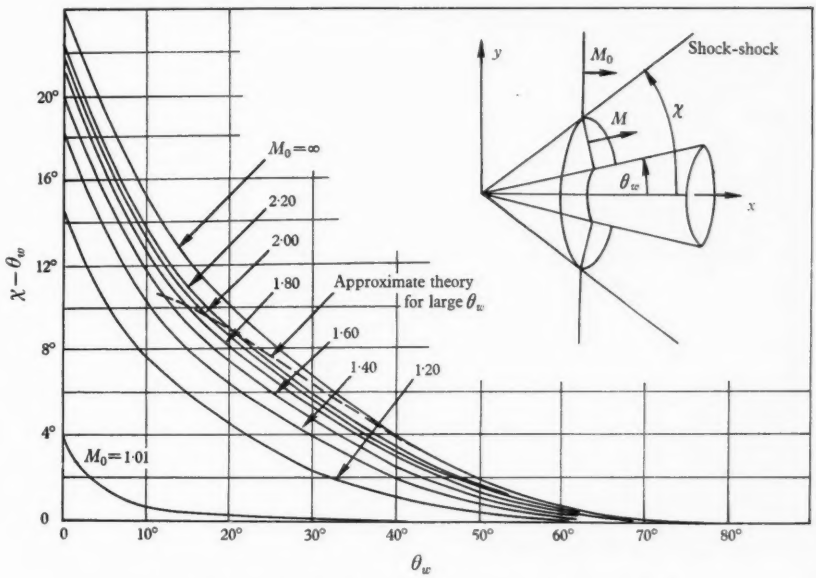

FIGURE 11. Shock-shock angle χ *vs* cone semi-apex angle θ_w.

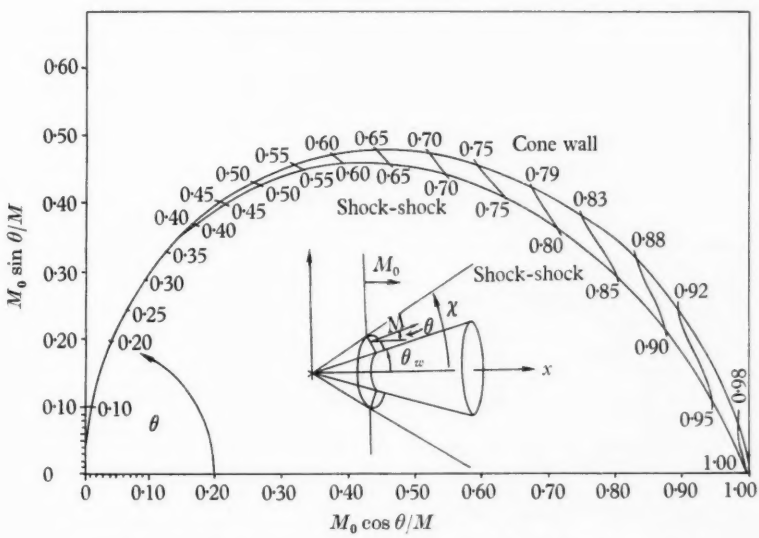

FIGURE 12. Complete crescent curves for conical diffractions. $M_0 \gg 1$.

The respective equations are given by Whitham (1957).

(1) Ray area, $A = A(M)$:

$$A = k \exp\left\{-\int \frac{2M\,dM}{(M^2-1)\,K(M)}\right\} = kf(M),$$

where

$$K(M) = 2\left[\left(1+\frac{2}{\gamma+1}\frac{1-\mu^2}{\mu}\right)\left(2\mu+1+\frac{1}{M^2}\right)\right]^{-1},$$

$$\mu^2 = \frac{(\gamma-1)\,M^2+2}{2\gamma M^2-(\gamma-1)},$$

and k is an arbitrary constant. As noted by Whitham this integral has an analytical solution which was found to be

$$\begin{aligned} f(M) = \exp\Bigg[\Bigg[&-\Bigg\{\log\frac{M^2-1}{M}+\frac{1}{\gamma}\log\left(M^2-\frac{\gamma-1}{2\gamma}\right)+\log\frac{1-\mu}{1+\mu} \\ &+\left(\frac{\gamma-1}{2\gamma}\right)^{\frac{1}{2}}\log\left[\mu+\left(\frac{2\gamma}{\gamma-1}\right)^{\frac{1}{2}}\right]-\left(\frac{\gamma-1}{2\gamma}\right)^{\frac{1}{2}}\log\left[\mu-\left(\frac{2\gamma}{\gamma-1}\right)^{\frac{1}{2}}\right] \\ &+\left(\frac{2}{\gamma(\gamma-1)}\right)^{\frac{1}{2}}\log\left[\left(M^2-\frac{2}{\gamma-1}\right)^{\frac{1}{2}}+\left(M^2-\frac{\gamma-1}{2\gamma}\right)^{\frac{1}{2}}\right] \\ &+\left[\frac{1}{2(\gamma-1)}\right]^{\frac{1}{2}}\tan^{-1}\left\{\frac{[4\gamma-(\gamma-1)^2]\,M^2-4(\gamma-1)}{4\gamma^{\frac{1}{2}}(\gamma-1)\,(M^2+2/\gamma-1)^{\frac{1}{2}}\,(M^2-(\gamma-1)/2\gamma)^{\frac{1}{2}}}\right\}\Bigg\}\Bigg] \end{aligned}$$

choosing $k = 1$. $A = f(M)$ is tabulated in table 1.

(2) The characteristic angle $m = m(M)$ is given by

$$m = \tan^{-1}\left[\frac{(M^2-1)\,K(M)}{2M^2}\right]^{\frac{1}{2}}.$$

Values for $m = m(M)$ are also tabulated in table 1.

(3) The integral ω corresponding to the Prandtl–Meyer function in supersonic flow is given by

$$\omega = \int_1^M \left[\frac{2}{(M^2-1)\,K(M)}\right]^{\frac{1}{2}} dM.$$

Therefore for two-dimensional diffractions the characteristics of Whitham's diffraction equations are given by

$$\theta \pm \omega = \text{const.}$$

along curves of slope

$$\frac{dy}{dx} = \tan(\theta \pm m).$$

Values for $\omega = \omega(M)$ are given in column 3 of table 1.

(4) The shock-shock jump conditions for oblique shock-shocks are

$$\tan(\theta_1-\theta_0) = \frac{(M_1^2-M_0^2)^{\frac{1}{2}}\,(A_0^2-A_1^2)^{\frac{1}{2}}}{A_1M_1+A_0M_0}$$

and

$$\tan(\chi-\theta_0) = \frac{A_0}{M_0}\left(\frac{M_1^2-M_0^2}{A_0^2-A_1^2}\right)^{\frac{1}{2}},$$

Mach no. M	Ray area A $A \times 10^{-n}$	n	Characteristic angle m (degrees)	Prandtl–Meyer integral ω
1	∞		0	0
1·000001	3·668749	+10	—	0·003
1·00001	3·668672	+ 8	—	0·009
1·0001	3·667902	+ 6	0·403	0·028
1·001	3·660213	+ 4	1·280	0·089
1·01	3·584696	+ 2	4·002	0·283
1·05	1·310728	+ 1	8·544	0·633
1·10	2·946288	+ 0	11·474	0·896
1·15	1·184152	+ 0	13·142	1·097
1·20	6·053638	− 1	14·843	1·266
1·25	3·536658	− 1	15·958	1·414
1·30	2·250720	− 1	16·859	1·547
1·35	1·520662	− 1	17·604	1·669
1·40	1·074028	− 1	18·231	1·728
1·45	7·850741	− 2	18·766	1·887
1·50	5·898186	− 2	19·228	1·984
1·55	4·531934	− 2	19·630	2·077
1·60	3·548150	− 2	19·983	2·165
1·65	2·822580	− 2	20·295	2·249
1·70	2·276434	− 2	20·572	2·330
1·75	1·858064	− 2	20·820	2·406
1·80	1·532637	− 2	21·042	2·480
1·85	1·276079	− 2	21·242	2·551
1·90	1·071389	− 2	21·423	2·619
1·95	9·063299	− 3	21·587	2·685
2·00	7·719471	− 3	21·736	2·749
2·05	6·615861	− 3	21·872	2·811
2·10	5·702352	− 3	21·997	2·871
2·15	4·940726	− 3	22·111	2·929
2·20	4·301517	− 3	22·216	2·985
2·25	3·761766	− 3	22·312	3·040
2·30	3·303423	− 3	22·401	3·094
2·40	2·576553	− 3	22·560	3·203
2·50	2·037086	− 3	22·696	3·302
2·60	1·630023	− 3	22·814	3·388
2·70	1·318343	− 3	22·916	3·477
2·80	1·076566	− 3	23·006	3·563
2·90	8·868121	− 4	23·085	3·645
3·00	7·363072	− 4	23·154	3·724
3·20	5·184216	− 4	23·271	3·875
3·40	3·740925	− 4	23·364	4·015
3·60	2·757067	− 4	23·439	4·148
3·80	2·069662	− 4	23·501	4·272
4·00	1·578970	− 4	23·552	4·398
4·50	8·519558	− 5	23·647	4·660
5·00	4·926060	− 5	23·710	4·900
6·00	1·921342	− 5	23·788	5·314
7·00	8·705958	− 6	23·832	5·672
8·00	4·395269	− 6	23·859	5·966
9·00	2·408270	− 6	23·876	6·232
10·00	1·407051	− 6	23·889	6·470
15·00	1·786391	− 7	23·917	7·385
20·00	4·141420	− 8	23·926	8·033
100·00	1·172427	−11	23·937	11·67
∞	0		23·938	∞

TABLE 1

where index 0 refers to the flow before, index 1 to the flow behind, the shock-shock, θ_1 is the angle between the ray direction and the fixed co-ordinate system, and χ is the shock-shock angle between the shock-shock and the fixed co-ordinate system. The relationship between θ_1 and M_1 with M_0 as parameter ($\theta_0 = 0$) is shown in the form of hodograph shock-polars in figure 16; $(\chi - \theta_1)$ as a function of θ_1 with M_0 as parameter ($\theta_0 = 0$) is shown in figure 17.

Approximate analysis of shock-shock locus on cones of large semi-apex angle, $M_0 \gg 1$

For large semi-apex angles it can be assumed that the Mach shock is approximately straight (see figure 13). The velocity of point P is the same for both shocks, therefore

$$M_0 \sec \chi = M \sec (\chi - \theta). \tag{1}$$

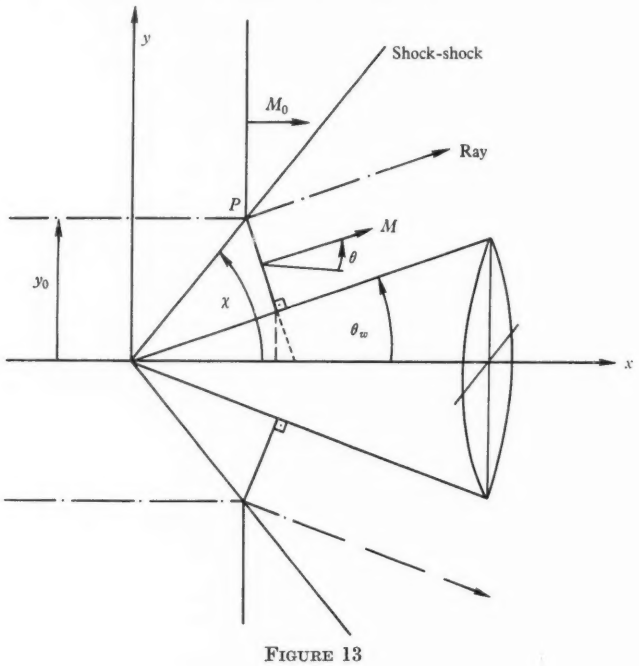

FIGURE 13

All the rays contained in the undisturbed ray tube of area $A_0 = \pi y_0^2$ must pass through a ray tube of area A behind the shock-shock, where

$$A = \pi y_0^2 \sec \theta \{1 - [1 - \cos\theta \csc \chi \sin (\chi - \theta)]^2\},$$

so that

$$\frac{A}{A_0} = \sec \theta \{1 - [1 - \cos\theta \csc \chi \sin(\chi - \theta)]^2\}. \tag{2}$$

But, for $M \gg 1$,

$$\frac{A}{A_0} = \left(\frac{M_0}{M}\right)^n \quad (n = 5{\cdot}0743), \tag{3}$$

assuming that this also holds across the shock-shock.

From (1), (2) and (3) we obtain a relationship between θ and χ, for $\theta \to \frac{1}{2}\pi$

$$\frac{\cos^n \chi}{\cos^n (\chi-\theta)} = 2\frac{\sin(\chi-\theta)}{\sin\chi} - \cos\theta \frac{\sin^2(\chi-\theta)}{\sin^2\chi}. \tag{4}$$

In the limit χ, $(\frac{1}{2}\pi-\theta) \ll 1$, (4) reduces to

$$\chi-\theta \simeq \tfrac{1}{2}(\tfrac{1}{2}\pi-\theta). \tag{5}$$

Equation (4) has been plotted in figure 12.

Approximate analysis of shock-shock locus on front of cylinders, $M_0 \gg 1$

It is again assumed that the Mach shock is almost straight and radial (see figure 14). Here the undisturbed rays contained in a stream tube of area $A_0 = (1+\lambda)\sin\phi$ pass through the area $A = \lambda$ per unit length of the cylinder.

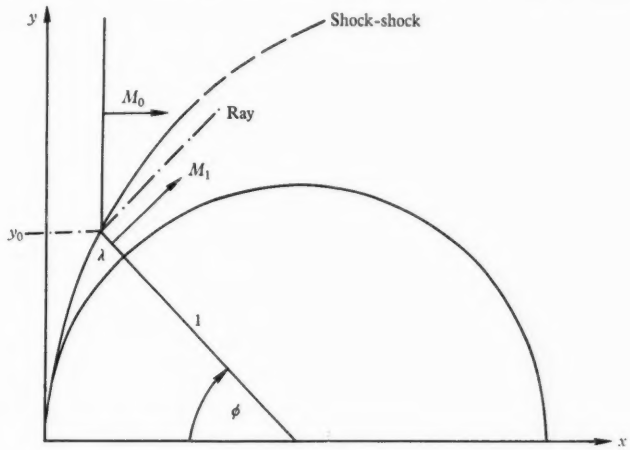

FIGURE 14

Mach shock and incident shock are parts of the same surface $\alpha(x, y, t)$ at any instant, where (Whitham 1959) in our case

$$\alpha = \alpha_0 t = \frac{x}{M_0} = \frac{1-(1+\lambda)\cos\phi}{M_0}. \tag{6}$$

By definition (Whitham 1959),

$$M|\nabla\alpha| = 1. \tag{7}$$

Since the Mach shock is normal to the wall, for the cylinder,

$$|\nabla\alpha| \simeq \frac{\partial\alpha}{R\partial\phi}. \tag{8}$$

Remembering that

$$\frac{A}{A_0} = \left(\frac{M_0}{M}\right)^n \quad (M_0 \gg 1),$$

we find a differential equation connecting λ and ϕ for $\phi \to 0$

$$\frac{d\lambda}{d\phi} = (1+\lambda)\tan\phi - \frac{1+\frac{1}{2}\lambda}{\cos\phi}\left[\frac{\lambda}{(1+\lambda)\sin\phi}\right]^{1/n}, \tag{9}$$

with the initial condition $\lambda = 0$ at $\phi = 0$ since at the nose the reflexion must be regular. In the limit $\lambda, \phi, (d\lambda/d\phi) \ll 1$ we find

$$\lambda = \sin^{n+1}\phi. \tag{10}$$

The solution of equation (9) is plotted in figure 15.

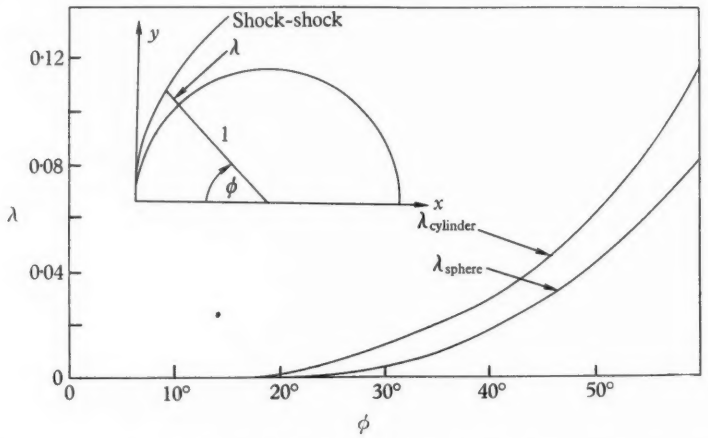

FIGURE 15. Position of shock-shock as given by approximate theory for blunt bodies, $M_0 \gg 1$.

Approximate analysis of shock-shock locus on front of sphere, $M_0 \gg 1$

The assumptions and notations are the same and equations (6), (7) and (8) hold also in this case, except that now

$$\left.\begin{aligned} A_0 &= \pi y_0^2 = \pi(1+\lambda)^2\sin^2\phi, \\ A &= 2\pi\lambda(1+\tfrac{1}{2}\lambda)\sin\phi. \end{aligned}\right\} \tag{11}$$

We obtain a differential equation analogous to (9), for $\phi \to 0$

$$\frac{d\lambda}{d\phi} = (1+\lambda)\tan\phi - \frac{1+\frac{1}{2}\lambda}{\cos\phi}\left[\frac{2(1+\frac{1}{2}\lambda)\,\lambda}{(1+\lambda)^2\sin\phi}\right]^{1/n}, \tag{12}$$

with $$\lambda = 0 \quad \text{at} \quad \phi = 0.$$

In the limit $\lambda, \phi, (d\lambda/d\phi)$ all $\ll 1$ the solution can be obtained explicitly

$$\lambda = \tfrac{1}{2}\sin^{n+1}\phi. \tag{13}$$

Very close to the nose the shock-shock 'stand off' distance on a sphere is half as large as on the cylinder for the same ϕ. The numerical solution obtained for (12) is also given in figure 15.

Assuming that the approximations for the positions of the shock-shock for cylinder and sphere are good up to $\phi = 50°$, we may chose a value of $\phi = 45°$, say, to find the shock-shock angle χ, shock-shock strength $(M_0/M_1)_s$, and ray angle θ_1

behind the shock-shock, which then can serve as a starting point for a characteristics solution (λ is so small near 45°, the shock-shock so close to the wall, that one point on the shock-shock appears sufficient).

The angle χ between the shock-shock and the x-axis is found, for the cylinder and the sphere, from

$$\tan\chi = \left(\frac{dy}{dx}\right)_{ss} = \frac{(1+\lambda)\tan\phi + d\lambda/d\phi}{(1+\lambda) - d\lambda/d\phi \,.\, \tan\phi}, \tag{14}$$

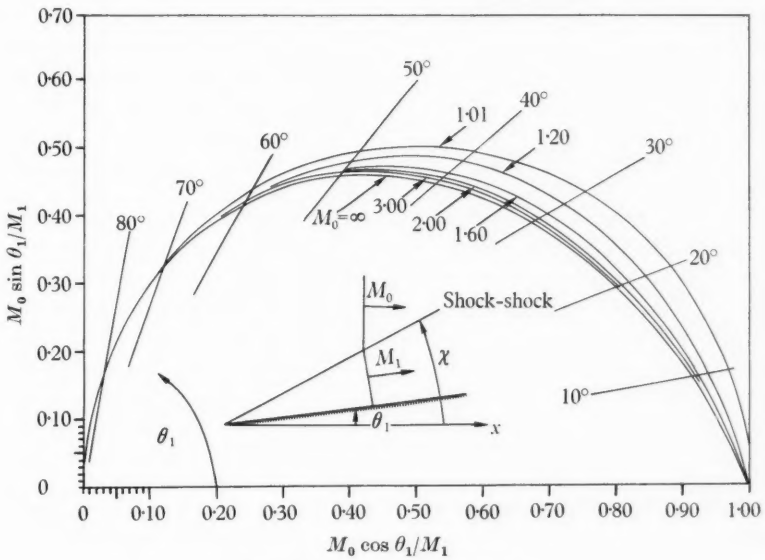

FIGURE 16. Shock-shock polars.

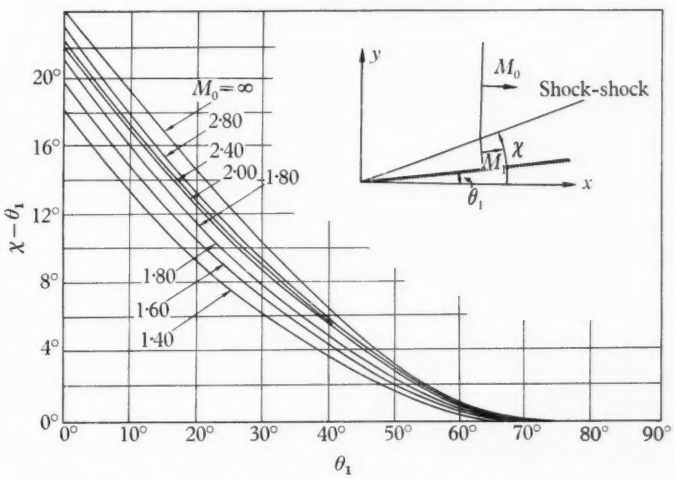

FIGURE 17. Shock-shock angle χ *vs* deflexion angle θ_1; shock-shock jump conditions; M_0 = incident Mach number.

where the origin of the x-y system is now located at the front stagnation point. Knowing χ, (M_0/M_1) and θ_1 are found from figures 16 and 17, and m from table 1. These values define the starting point for a characteristics solution in the physical and hodograph planes.

Characteristics solution for cylinder

If we neglect reflexions of the characteristics from the shock-shocks in this case, then the left-running characteristics are straight lines along which all flow properties are constant. In particular, the ray angle θ is constant between wall and shock-shock and equal to $\theta_{\text{wall}} = \frac{1}{2}\pi - \phi$. Knowing $\theta = \theta_w$, we may find (M_0/M_1) on the appropriate shock-shock-polar of figure 16, and the corresponding values for χ and m are given by figure 17 and table 1, respectively. This allows us to draw the left-running characteristic from any point on the wall. At the initial point 1 which lies on the shock-shock with χ, θ, M_0/M_1, and m given this scheme is inverted. The point 0 on the wall from which the left-running characteristic through the initial point issues is obviously defined by $\phi = \frac{1}{2}\pi - \theta$. From point 1 the shock-shock is continued with a slope $\tan\chi_3$, $\chi_3 = \chi(M_3)$, up to a point 3 where it intersects the characteristic from the next wall point 2. This semi-graphical method of constructing the shock-shock is illustrated by figure 18.

This procedure is continued up to $\phi = \frac{1}{2}\pi$; the characteristic from this point on the wall meets the shock-shock at infinity, $(M_0/M_1) = 1$ and $m = m_0$ along this characteristic.

The back side of the cylinder is obtained by a simple wave expansion along its wall. Again $\theta = \theta_{\text{wall}} = \frac{1}{2}\pi - \phi$ is known and assumed to be constant along a straight left-running characteristic. Then by means of the characteristic equation

$$\omega = -\theta,$$

where

$$\omega = \int_1^M \left[\frac{2}{(M^2-1)K(M)}\right]^{\frac{1}{2}} dM,$$

M and m are found from Table 1, $\omega = 0$ at $M = 1$ (which is in error in Whitham's paper of 1957).

When the diffraction reaches the plane of symmetry a second shock-shock is formed since the diffraction is again turned through a 'compressive' angle of $0 \leqslant \Delta\theta \leqslant \frac{1}{2}\pi$; the rays must be parallel to the plane of symmetry. All characteristics on the back side, therefore, intersect a second shock-shock. Observing that θ_1 (before the second shock-shock) is given and θ_2 (behind the second shock-shock) is equal to zero, χ can be found again from the shock-shock polar diagram, if we use the polar on which $M_0 = M_{\text{wall}}$. The second shock-shock starts at the rear stagnation point with $\chi = 0$, and is constructed piece-wise in the same manner as the first shock-shock.

Figure 6 shows the full characteristic field, the constructed shock-shapes and rays, and the experimental data. Also shown is the locus of the vortex in the slip surface, which should trace a particle path. The correspondence between theory and experiment appears to be good.

Characteristic solution for sphere

For axisymmetric shock diffraction problems, viz. a sphere, the characteristic equations in the hodograph plane have a term containing the radius r, which implies that the left-running characteristics are not straight lines. Also the diffraction around the back side is no longer a simple wave.

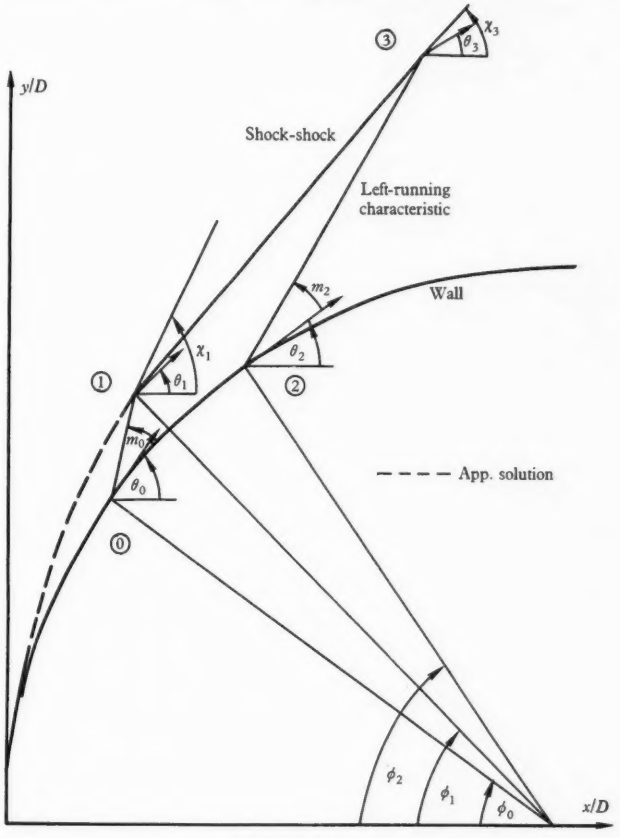

FIGURE 18

A purely graphical method proposed by de Haller (1945) and modified to apply to shock diffraction problems was used. Since the experimental incident Mach numbers were quite high, it was assumed that $M_0 \gg 1$. In this case the characteristic angle $m = 23{\cdot}9°$ becomes constant and independent of Mach number.

De Haller's method, also described in Shapiro (1954), solves the axisymmetrical characteristic equations in the physical and hodograph planes simultaneously making use of the two-dimensional hodograph characteristics, which are logarithmic spirals in our case. The term in the axisymmetrical characteristics equations containing the radius vector is found graphically in the physical plane and introduced as a correction term into the hodograph plane. A simple template

drawing device was made to mechanize the calculation. It was found, however, that the left-running characteristics in the hodograph plane became highly divergent on the aft portion of the sphere. A reliable solution for this part and the second shock-shock could, therefore, not be obtained.

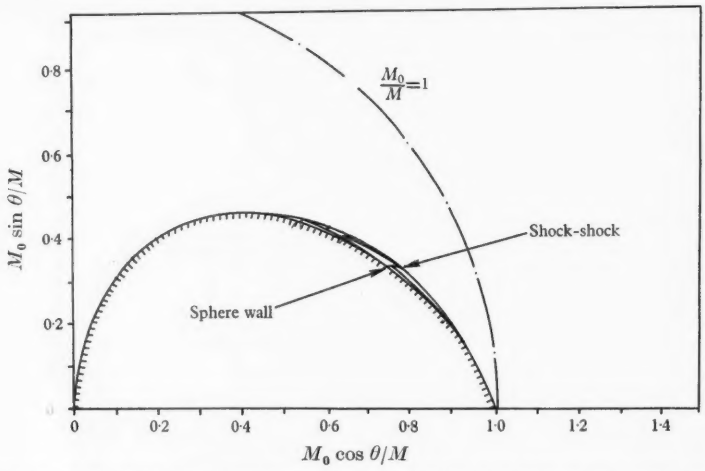

FIGURE 19. Hodograph plane for characteristics solution on a sphere fore-body, $M_0 \gg 1$. Numbers refer to successive points of the characteristic net in physical plane.

Figure 9 shows the result of the solution for the front of the sphere starting from an input point on the shock-shock as described previously. The experimental points for two different Mach numbers are also plotted. The correspondence appears to be very good. Figure 19 is a reproduction of the hodograph plane corresponding to this part of the diffraction field. It is seen that at an azimuth angle $\phi = 90°$, $\theta_{\text{wall}} = 0$ and the Mach number $(M_0/M_1) = 1$, as was found for the cylinder.

The experimental investigation was sponsored by the National Science Foundation under Grant 7008 to Harvard University, Cambridge, Mass. The theoretical calculations were sponsored by Douglas Aircraft Co. Inc., and performed on the Bendix G-15 computer at Douglas Aircraft Co. Inc., Missiles and Space Systems Engineering Department. We are particularly indebted to Mr W. A. Anderson, Douglas Aircraft Co. Inc., Santa Monica, for programming and performing the numerical calculations, and to Mr G. Brownell of Harvard University, Gordon McKay Laboratory machine shop for his unfailing assistance in the experiments.

REFERENCES

HALLER, P. DE 1945 *Revue tech. Sulzer*, no. 1.

SHAPIRO, A. 1954 *Dynamics and Thermodynamics of Compressible Fluid Flow*, vol. 2. New York: The Ronald Press.

WHITHAM, G. B. 1957 *J. Fluid Mech.* **2**, 145.

WHITHAM, G. B. 1958 *J. Fluid Mech.* **4**, 337.

WHITHAM, G. B. 1959 *J. Fluid Mech.* **5**, 369.

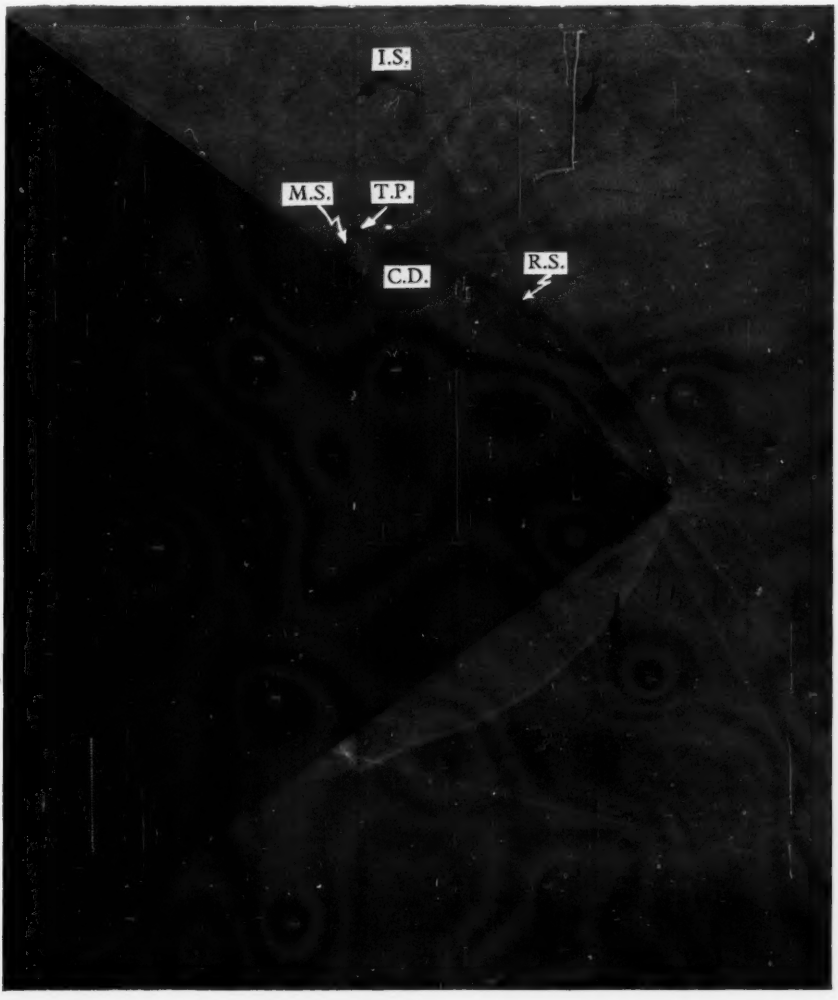

FIGURE 1 (plate 1). Schlieren photograph of shock diffraction on a cone of semi-apex angle $\theta_w = 35{\cdot}1°$. $M_0 = 3{\cdot}55$. Notation: I.S., incident shock; M.S., mach shock; R.S., reflected shock; C.D., contact discontinuity; T.P., triple point.

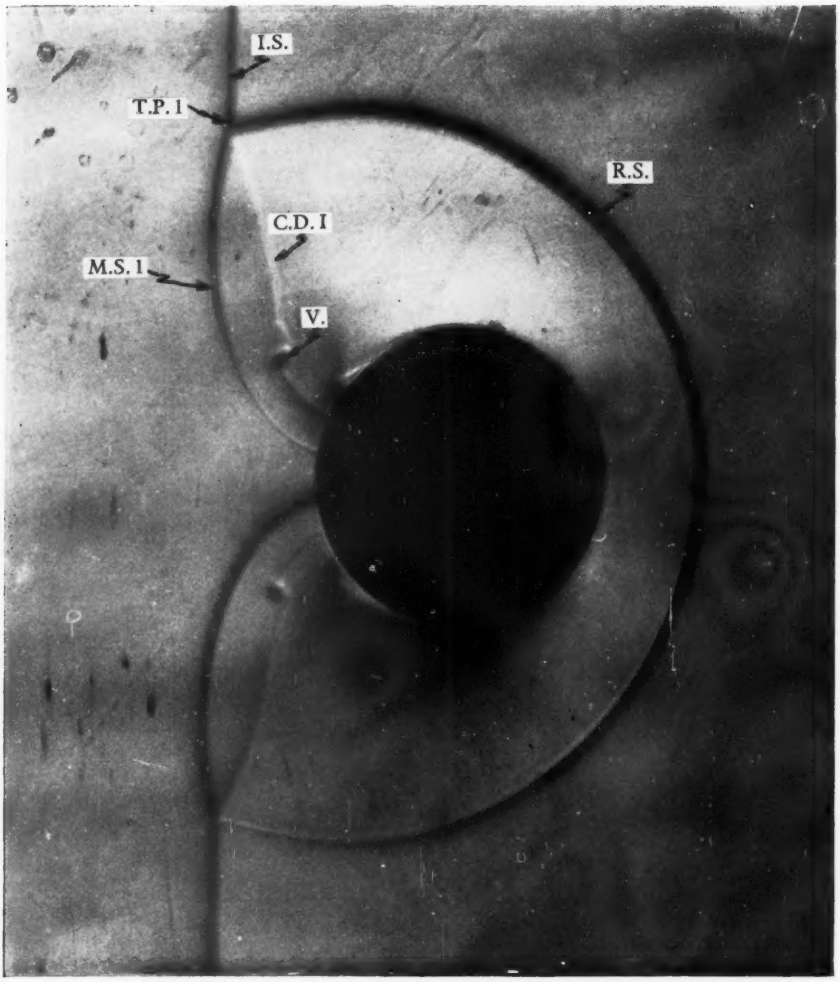

FIGURE 3 (plate 2). Schlieren photograph of shock diffraction on a cylinder of $\frac{1}{2}$ in. diameter. $M_0 = 2{\cdot}82$. Note the boundary-layer separation starting. Notation: I.S., incident shock; M.S., mach shock; R.S., reflected shock; C.D., contact discontinuity; T.P., triple point; V., vortex.

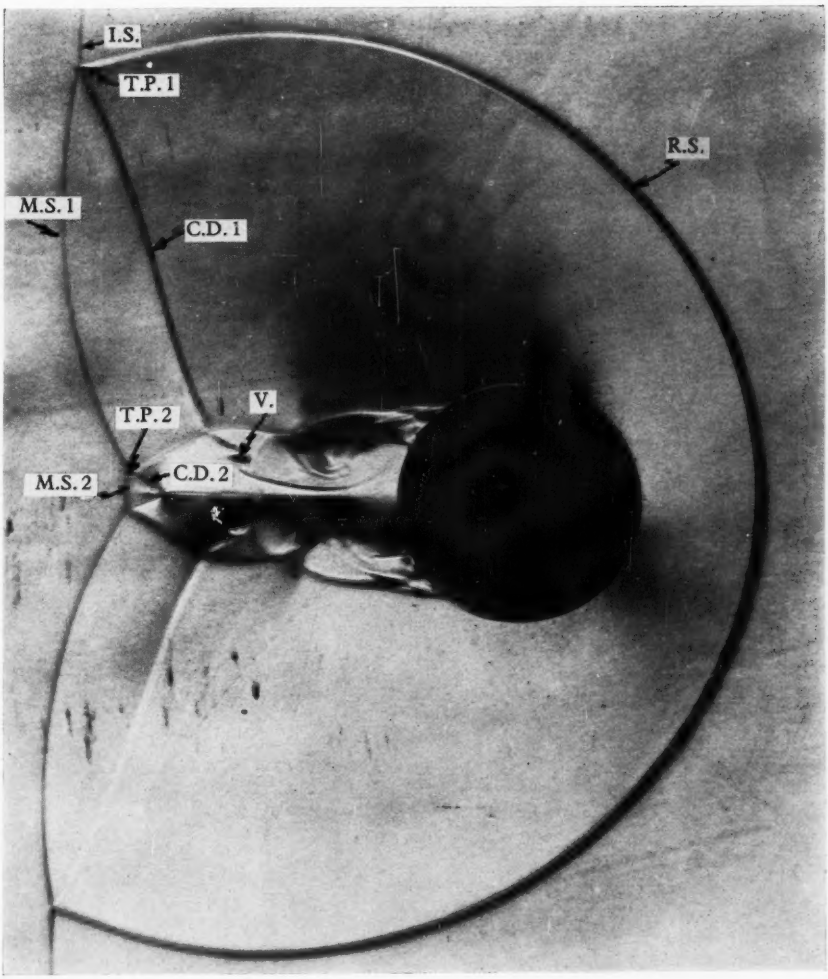

FIGURE 4 (plate 3). Schlieren photograph of shock diffraction on a cylinder of $\frac{1}{2}$ in. diameter. $M_0 = 2{\cdot}81$. Notation: I.S., incident shock; M.S., mach shock; R.S., reflected shock; C.D., contact discontinuity; T.P., triple point; V., vortex.

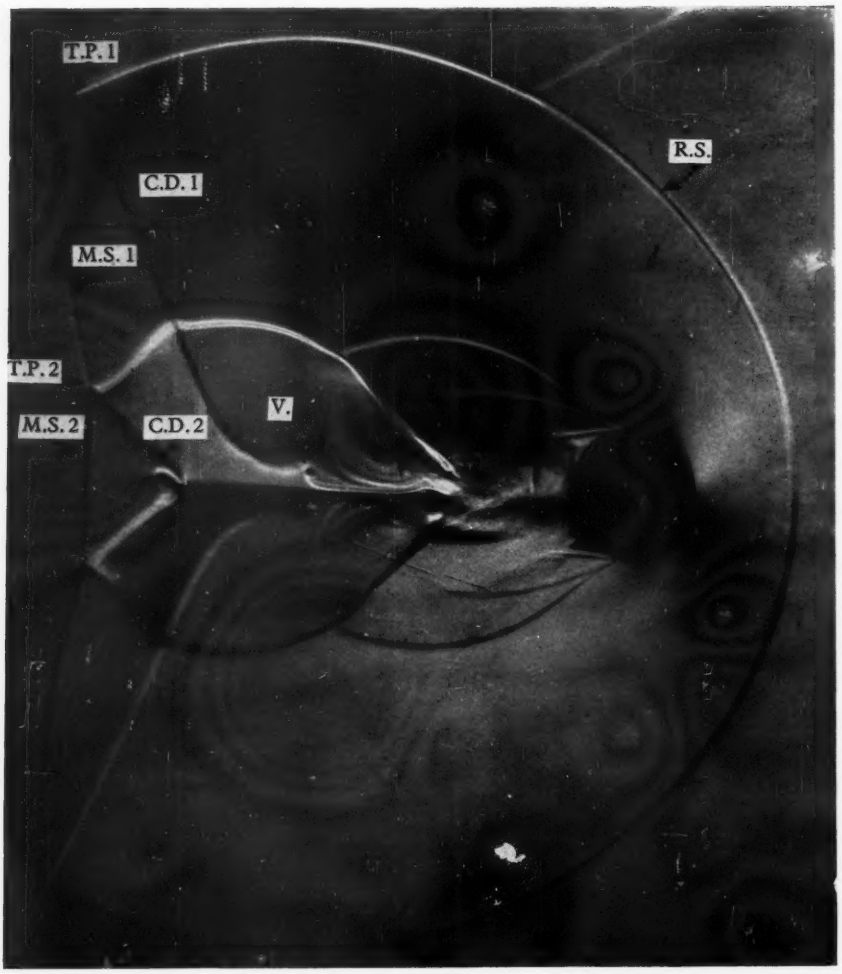

FIGURE 5 (plate 4). Schlieren photograph of shock diffraction on a cylinder of $\frac{1}{2}$ in. diameter. $M_0 = 2{\cdot}84$. Notation: M.S., mach shock; R.S., reflected shock; C.D., contact discontinuity; T.P., triple point; V., vortex.

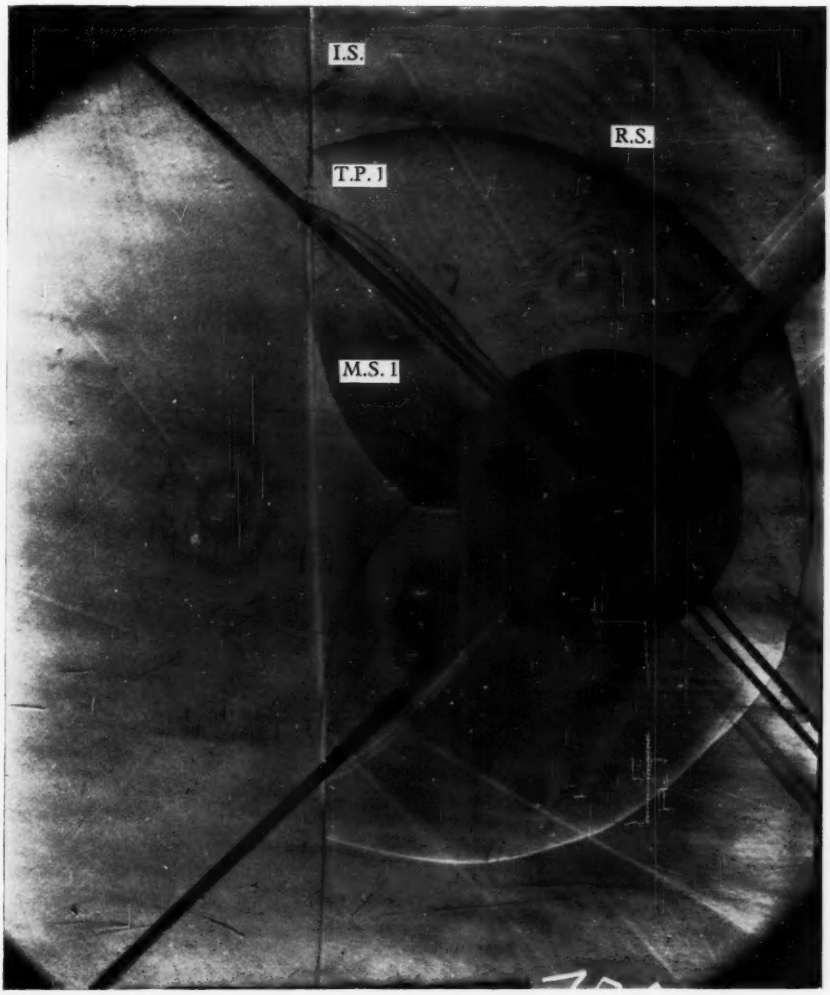

FIGURE 7 (plate 5). Schlieren photograph of shock diffraction on a sphere of 1 in. diameter. $M_0 = 2{\cdot}89$. Note the second Mach shock just forming. The eight radial lines are strings by which the sphere was suspended in the test section. Notation: I.S., incident shock; M.S., mach shock; R.S., reflected shock; T.P., triple point.

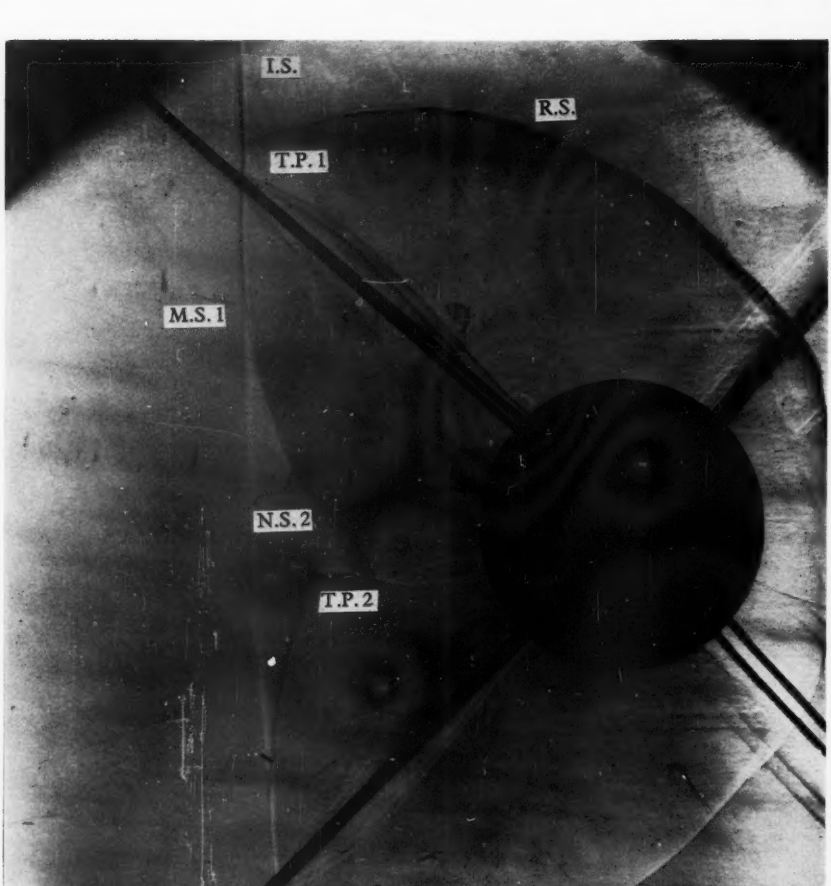

FIGURE 8 (plate 6). Schlieren photograph of shock diffraction on a sphere of 1 in. diameter. $M_0 = 2{\cdot}89$. Note the second Mach shock pierced by the spherical shock wave. Notation: I.S., incident shock; M.S., mach shock; R.S., reflected shock; T.P., triple point.

Slow steady rotation of axially symmetric bodies in a viscous fluid

By R. P. KANWAL

Department of Mathematics, The Pennsylvania State University, University Park, Pennsylvania

(Received 22 July 1960)

The Stokes flow problem is considered here for the case in which an axially symmetric body is uniformly rotating about its axis of symmetry. Analytic solutions are presented for the heretofore unsolved cases of a spindle, a torus, a lens, and various special configurations of a lens. Formulas are derived for the angular velocity of the flow field and for the couple experienced by the body in each case.

1. Introduction

The value of the couple experienced by axially symmetric bodies, rotating steadily in a viscous and incompressible fluid, is needed in designing and calibrating viscometers. Therefore, many attempts have been made to evaluate such a couple for various bodies of revolution. When inertial effects can be validly ignored, so that Stokes's linearized theory applies, the solutions have been found for some configurations. These configurations are a sphere (Lamb 1945), spheroids and a pair of spheres (Jeffery 1915). Jeffery has also given the solution for a circular disk as a limiting case of the solution for an oblate spheroid. The value of the angular velocity of the flow has also been calculated for each of the above-mentioned cases by the same authors.

The purpose of this paper is to discuss the flow when a spindle, a torus and a lens are rotating steadily in an incompressible viscous fluid. Various special configurations of a lens, e.g. a hemisphere and a spherical cap, are also considered and explicit calculation of the couple has been made in each of these cases. Following other workers in the field, we assume the motion to be slow enough to justify the neglect of the inertial terms in the Navier–Stokes equations.

The procedure for solving the present problem is similar to the one given by Payne & Pell (1960). They have discussed the Stokes flow problem of axially symmetric bodies when the flow at points distant from the body is uniform and parallel to the axis of symmetry. They solve their problem with the help of the generalized axially symmetric potential theory. Furthermore, they derive a relation between the drag on a body and the stream function of the flow. In the present analysis we find a corresponding relation between the couple experienced by a body and the angular velocity of the flow. Furthermore, it is found in the following analysis that there is a relation between such a couple on a body and the polarization potential of that body.

The known cases of spheroids and a pair of spheres can be solved in a relatively simple way by this method. Since the simplicity of this method in solving these cases has been demonstrated by Payne & Pell, we omit the solutions for these configurations in the present work. The other two known cases, namely, a sphere and a circular disk, are briefly mentioned in the following work since they form special cases of a lens and thus provide a check on our analysis.

2. Equations of motion

Let the z-axis be the axis of symmetry and the x- and y-axes be mutually orthogonal axes in a plane perpendicular to the z-axis. Let u_i $(i = 1, 2, 3)$ denote the components of the velocity vector, p the pressure, and μ the coefficient of viscosity. Then for rotation about the z-axis, the Stokes-flow equations in a region $\mathscr{D}$ exterior to a closed boundary B may be expressed as

$$\mu \Delta u_i = p_{,i} \quad (u_{i,i} = 0), \tag{1}$$

where we have used the summation convention. On B

$$u_1 = -\omega_0 y, \quad u_2 = \omega_0 x, \quad u_3 = 0, \tag{2}$$

where ω_0 is the uniform angular velocity of the body of revolution.

These equations can be satisfied if we choose

$$u_1 \equiv -\omega_0 \phi_2, \quad u_2 \equiv \omega_0 \phi_1, \quad u_3 \equiv 0, \quad p = \text{constant}, \tag{3}$$

where

$$\left.\begin{aligned} \Delta\phi_1 = 0, \quad \Delta\phi_2 = 0, \quad &\text{in} \quad \mathscr{D}, \\ \phi_1 = x, \quad \phi_2 = y, \quad &\text{on} \quad B. \end{aligned}\right\} \tag{4}$$

By this choice of u_i, the equation of continuity may be automatically satisfied.

Clearly ϕ_1 and ϕ_2 are polarization potentials (Schiffer & Szegö 1949) and are of the form

$$\phi_1 = \frac{x}{r^2}\,\Omega(r, z), \quad \phi_2 = \frac{y}{r^2}\,\Omega(r, z), \tag{5}$$

where $r^2 = x^2 + y^2$ and Ω satisfies the equation

$$L_{-1}\,\Omega \equiv \left(\frac{\partial^2}{\partial z^2} + \frac{\partial^2}{\partial r^2} - \frac{1}{r}\frac{\partial}{\partial r}\right)\Omega = 0. \tag{6}$$

This equation could also have been derived in a different way (Kanwal 1955). If ω denotes the angular velocity of the flow, then we observe that $\omega/\omega_0 = \Omega/r^2$. Moreover, from (4) we find that

$$\Omega = r^2 \text{ on } B. \tag{7}$$

3. Couple on an axially symmetric body

Payne & Pell have given an elegant formula for the drag experienced by an axially symmetric body in terms of the stream function. We now derive a similar formula for the couple in terms of the angular velocity of the flow. The value of the couple can, however, be found in another way also. It turns out that the couple on a body in the present problem can be related to the polarization of that body. Furthermore, since there is a tie between the polarization and the

virtual mass of a body (Payne 1956), we can get a relation between the couple on a body and the virtual mass of that body. We first set out to investigate these relations.

Now the couple N is given by the expression

$$N = \frac{\mu}{2\omega_0}\iiint_{\mathscr{D}} (u_{i,j}+u_{j,i})(u_{i,j}+u_{j,i})\,dV, \tag{8}$$

where we have adopted the summation convention. If we put

$$D(u_i) = \iiint_{\mathscr{D}} |\mathrm{grad}\, u_i|^2\,dV, \tag{9}$$

we get

$$N = \frac{\mu}{\omega_0}\left[D(u_1)+D(u_2)+\iiint_{\mathscr{D}} (u_{i,j}u_{j,i})\,dV\right],$$

$$= \mu\omega_0[D(\phi_1)+D(\phi_2)]+\frac{\mu}{\omega_0}\iint_B u_i[u_{j,i}n_j-u_{j,j}n_i]\,dS, \tag{10}$$

where n_i are the components of the unit normal to B. The integral over B involves only u_i and its tangential derivatives so that we may replace u_i throughout by its boundary values. Thus

$$N = \mu\omega_0\left[D(\phi_1)+D(\phi_2)-\iint_B (xn_x+yn_y)\,dS\right],$$

$$= 2\mu\omega_0[P+V], \tag{11}$$

where V is the volume of the body B and $P = D(\phi_1) = D(\phi_2)$ is the suitably normalized polarization. Now Schiffer & Szegö (1949) have shown that

$$P+V = 4\pi e_x = 4\pi e_y, \tag{12}$$

where e_x and e_y are the dipole coefficients. Thus

$$N = 8\pi\mu\omega_0 e_x. \tag{13}$$

In their paper, Schiffer & Szegö have tabulated e_x for spheroids, spindle, torus, two spheres, and lenses, giving several particular examples for the lens.

If the meridian section ($r > 0$) of $\mathscr{D}$ is simply connected, then it has been shown by Payne (1956) that the virtual mass M, due to a potential flow along the z-axis, is given by the relation

$$P+V = 2(M+V). \tag{14}$$

Thus from (11) and (14) we get the relation between the couple and the virtual mass as

$$N = 4\mu\omega_0(M+V). \tag{15}$$

In a previous paper (1952) Payne has calculated the value of the virtual mass for the cases of a spindle and a lens.

We finally derive the value of the couple in terms of the angular velocity ω of the flow. The relation (8) can be written as

$$N = C+4\mu\omega_0 V, \tag{16}$$

where

$$C = \frac{\mu}{2\omega_0}\iiint_{\mathscr{D}} (u_{i,j}-u_{j,i})(u_{i,j}-u_{j,i})\,dV. \tag{17}$$

In view of the axial symmetry we may restrict attention to any single meridian half plane ($r > 0$). Now let B^* denote the curve of intersection of the boundary B of the body with this half plane and let R be the region in ($r > 0$) bounded by B^* and a large semicircle Γ whose radius we shall ultimately let tend to infinity.

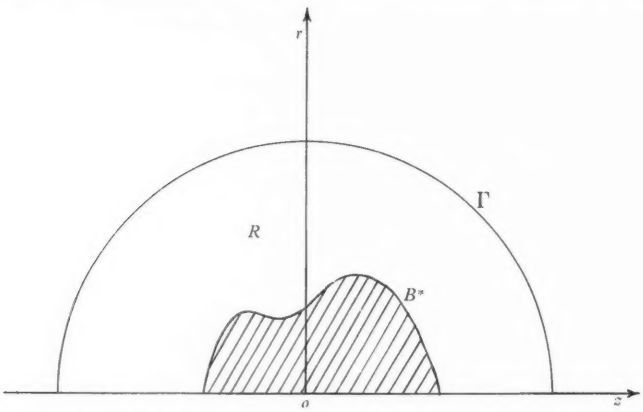

FIGURE 1. Configuration of flow field in meridian half plane.

The relation (17) then becomes

$$\frac{C}{2\pi\mu\omega_0} = \iint_R \frac{1}{r} |\text{grad}\,\Omega|^2 \, dr\,dz,$$

$$= \iint_R \frac{1}{r} \Omega L_{-1}\Omega \, dr\,dz + \oint_{B^*+\Gamma} \frac{1}{r} \Omega \frac{\partial \Omega}{\partial n} ds, \tag{18}$$

where the normal is directed outward from R. The integral along $r = 0$, between B^* and Γ vanishes since Ω is $O(r^2)$ as $r \to 0$ (Hyman 1954). Since $L_{-1}\Omega = 0$, the relation (18) gives

$$\frac{C}{2\pi\mu\omega_0} = \oint_{B^*+\Gamma} \frac{1}{r} r^2 \frac{\partial \Omega}{\partial n} ds + \oint_{\Gamma} \frac{1}{r} (\Omega - r^2) \frac{\partial \Omega}{\partial n} ds. \tag{19}$$

But since both r^2 and Ω satisfy the equation (6), we have from Green's second identity

$$\oint_{B^*+\Gamma} \frac{1}{r} r^2 \frac{\partial \Omega}{\partial n} ds = \oint_{B^*+\Gamma} \frac{1}{r} \Omega \frac{\partial r^2}{\partial n} ds. \tag{20}$$

From (19) and (20) we get

$$\frac{C}{2\pi\mu\omega_0} = 2\oint_{B^*} r^2 \frac{\partial r}{\partial n} ds + \oint_{\Gamma} \frac{1}{r} (\Omega - r^2) \frac{\partial \Omega}{\partial n} ds + \oint_{\Gamma} \frac{1}{r} \Omega \frac{\partial r^2}{\partial n} ds. \tag{21}$$

Letting the radius of Γ tend to infinity and noting that as $\rho^2 = r^2 + z^2 \to \infty$

$$\Omega = \frac{br^2}{\rho^3} + O\left(\frac{1}{\rho^2}\right), \tag{22}$$

we have

$$\frac{C}{2\pi\mu\omega_0} = 2\oint_{B^*} r^2 \frac{\partial r}{\partial n}\, ds + 3b\int_0^\pi \sin^3\theta\, d\theta,$$

$$= -4\iint_{\text{interior of } B^*} r\, dz\, dr + 4b,$$

$$= -\frac{2V}{\pi} + 4b. \tag{23}$$

Finally from (16), (22) and (23) we have our result:

$$N = 8\pi\mu\omega_0 \lim_{\rho\to\infty}\left[\rho^3\frac{\Omega}{r^2}\right], = 8\pi\mu \lim_{\rho\to\infty}[\rho^3\omega]. \tag{24}$$

It is of interest to compare it with the formula for the drag given by Payne & Pell (1960):

$$D = 8\pi\mu \lim_{\rho\to\infty}\left[\rho\frac{\psi^1}{r^2}\right].$$

We now turn to the consideration of a specific flow configuration.

4. The flow about a rotating spindle

A curve $\xi = \xi_0$ in dipolar co-ordinates defines the profile of a spindle. The dipolar transformation is given by

$$z + ir = ic\cot\tfrac{1}{2}(\xi + i\eta), \tag{25}$$

where c is a positive constant. The range of co-ordinates is chosen as $-\infty < \eta < \infty$, $0 < \xi \leqslant \pi$. The boundary of the spindle is given by $\xi = \xi_0 < \pi$, and the exterior region is defined by $0 < \xi < \xi_0$. Let us put

$$s = \cosh\eta, \quad t = \cos\xi.$$

We assume the solution of the equation (6) in the form

$$\Omega = r^2(s-t)^{-\frac{3}{2}}\int_0^\infty A(\alpha)\, K_\alpha^{(1)}(t)\cos\alpha\eta\, d\alpha, \tag{26}$$

where $^{(q)}$ denotes the qth partial derivative with respect to the argument and $K_\alpha(t)$ is a Legendre function of a complex degree commonly called a conal function (Hobson 1931, p. 445). It is defined as

$$K_\alpha(t) = \frac{2}{\pi}\cosh\alpha\pi\int_0^\infty (2\cosh u + 2\cos\xi)^{-\frac{1}{2}}\cos\alpha u\, du. \tag{27}$$

If we replace ξ by $(\pi - \xi)$ in (27), we obtain

$$K_\alpha(-t) = \frac{2}{\pi}\cosh\alpha\pi\int_0^\infty [2\cosh u - 2\cos\xi]^{-\frac{1}{2}}\cos\alpha u\, du. \tag{28}$$

The boundary condition gives the value of $A(\alpha)$ occurring in the equation (26), and the complete solution to our problem is

$$\Omega = 2^{\frac{3}{2}}(s-t)^{\frac{3}{2}} r^2\int_0^\infty \frac{K_\alpha^{(1)}(-t_0)\, K_\alpha^{(1)}(t)\cos\alpha\eta}{K_\alpha^{(1)}(t_0)\cosh\alpha\pi} d\alpha. \tag{29}$$

The couple experienced by the spindle is given by the formula

$$N = 8\pi\mu\omega_0 c^3\int_0^\infty \frac{(4\alpha^2+1)\, K_\alpha^{(1)}(-t_0)}{K_\alpha^{(1)}(t_0)\cosh\alpha\pi} d\alpha. \tag{30}$$

5. The flow about a rotating lens-shaped body

Let us introduce the peripolar transformation

$$z+ir = -c\cot\tfrac{1}{2}(\xi+i\eta), \tag{31}$$

where c is a positive constant. The profile of a lens is defined by two curves $\xi = \xi_1$, and $\xi = \xi_2$. We shall assume that $0 < \xi_1 < \xi_2 < 2\pi$. The external region is chosen as $\eta > 0$.

Let us assume the solution of the equation (6) in the form

$$\Omega = 2^{\frac{3}{2}}(s-t)^{\frac{3}{2}} r^2 \int_0^\infty F(\alpha,\xi)\,\mathrm{sech}\,\alpha\pi K_\alpha^{(1)}(s)\,d\alpha, \tag{32}$$

where the quantities s, t and $^{(q)}$ are the same as defined in the previous section. The function $K_\alpha(s)$ is

$$K_\alpha(s) = \frac{2}{\pi}\cosh\alpha\pi \int_0^\infty [2\cosh u + 2\cosh\eta]^{-\frac{1}{2}}\cos\alpha u\,du. \tag{33}$$

Furthermore, the quantity $F(\alpha,\xi)$ is assumed to be of the form

$$F(\alpha,\xi) = \{A(\alpha)\cosh\alpha\xi + B(\alpha)\sinh\alpha\xi\}. \tag{34}$$

It can be shown that (Hobson 1931, p. 451)

$$(s-t)^{-\frac{1}{2}} = \sqrt{2}\int_0^\infty \frac{\cosh\alpha(\xi-\pi)}{\cosh\alpha\pi} K_\alpha(s)\,d\alpha. \tag{35}$$

If we differentiate this relation with respect to s, we obtain

$$[2(s-t)]^{-\frac{3}{2}} = -\int_0^\infty \frac{\cosh\alpha(\xi-\pi)}{\cosh\alpha\pi} K_\alpha^{(1)}(s)\,d\alpha. \tag{36}$$

With the help of the above relation, the boundary condition provides the expression for $F(\alpha,\xi)$, as

$$\begin{aligned}&\sinh\alpha(2\pi-\xi_2+\xi_1)\,F(\alpha,\xi)\\ &\quad = \sinh\alpha(\xi_1-\xi)\cosh\alpha(\pi-\xi_2) + \cosh\alpha(\pi-\xi_1)\sinh\alpha(2\pi-\xi_2+\xi).\end{aligned} \tag{37}$$

The corresponding couple is

$$N = 8\pi\mu\omega_0 c^3 \int_0^\infty \frac{\{\sinh\alpha\xi_1\cosh\alpha(\pi-\xi_2)+\cosh\alpha(\pi-\xi_1)\sinh\alpha(2\pi-\xi_2)\}(4\alpha^2+1)}{\sinh\alpha(2\pi+\xi_1-\xi_2)\cosh\alpha\pi}\,d\alpha. \tag{38}$$

6. Special cases of the lens

(*a*) *Hemisphere.* In this case $\xi_1 = \frac{1}{2}\pi$, $\xi_2 = \pi$. The expression (37) becomes

$$\sinh\left(\frac{3\alpha\pi}{2}\right)F(\alpha,\xi) = \sinh\alpha\left(\frac{\pi}{2}-\xi\right) + \cosh\frac{\alpha\pi}{2}\sinh\alpha(\pi+\xi). \tag{39}$$

Similarly, the expression for the couple is obtained as

$$\begin{aligned}N &= \frac{8(135-59\sqrt{3})}{81}\pi\mu\omega_0 c^3,\\ &= 10{\cdot}18\mu\omega_0 c^3.\end{aligned} \tag{40}$$

(*b*) *The symmetrical (biconvex) lens.* In this instance, if $\xi = \xi_1$ is one face of the lens, then the other is $\xi = \xi_2 = 2\pi - \xi_1$. Thus, from the expressions (37) and (38) we have the corresponding values of the quantity $F(\alpha, \xi)$, and the couple N, as

$$\cosh\alpha\xi_1 F(\alpha,\xi) = \cosh\alpha(\pi-\xi_1)\cosh\alpha\xi, \tag{41}$$

and

$$N = 8\pi\mu\omega_0 c^3 \int_0^\infty (4\alpha^2+1)(1-\tanh\alpha\pi\tanh\alpha\xi_1)\,d\alpha. \tag{42}$$

In the case of a sphere $\xi_1 = 2\pi$, so the expression (41) gives

$$F(\alpha,\xi) = \cosh\alpha\xi.$$

Thus from the equation (32), we obtain

$$\Omega = 2^{\frac{3}{2}}(s-t)^{\frac{3}{2}} r^2 \int_0^\infty \cosh\alpha\xi\,\operatorname{sech}\alpha\pi K_\alpha^{(1)}(s)\,d\alpha. \tag{43}$$

If we put ξ for $(\xi-\pi)$ in the relation (36), we readily derive the result

$$[2(s+t)]^{-\frac{3}{2}} = -\int_0^\infty \cosh\alpha\xi\,\operatorname{sech}\alpha\pi K_\alpha^{(1)}(s)\,d\alpha. \tag{44}$$

From (43) and (44), we finally have

$$\Omega = -r^2\frac{(s-t)^{\frac{3}{2}}}{(s+t)^{\frac{3}{2}}}. \tag{45}$$

If a is the radius of the sphere, then $(\rho/a)^2 = (s+t)/(s-t)$. Therefore, we get the well-known results

$$\Omega = r^2\frac{a^3}{\rho^3}, \tag{46}$$

and

$$N = 8\pi\mu\omega_0 a^3. \tag{47}$$

(*c*) *Spherical cap.* If $\xi_2 = \xi_1$, the two bounding surfaces of the lens coincide, the body becomes a portion of a spherical surface bounded by a circle of latitude and we have a spherical cap. The expression for $F(\alpha, \xi)$ is given by the equation (37) with $\xi_2 = \xi_1$. The value of the couple is

$$N = 4\pi\mu\omega_0 c^3\left\{f''(\xi_1)+f(\xi_1)+\frac{1}{3\pi}\right\}, \tag{48}$$

where

$$f(\xi_1) = \frac{1}{\pi}+\left(1-\frac{\xi_1}{\pi}\right)\frac{1}{\sin\xi_1}. \tag{49}$$

When $\xi_1 \to \pi$, we get the case of the circular disk and N becomes

$$N = \tfrac{32}{3}\pi\mu\omega_0 c^3, \tag{50}$$

which is well known. Finally, when $\xi_1 \to \frac{1}{2}\pi$, the cap becomes hemispherical and the couple in this case is given as

$$N = 8\pi\mu\omega_0 c^3\left(\frac{1}{2}+\frac{2}{3\pi}\right). \tag{51}$$

7. The flow about a rotating torus

In order to calculate the flow about a torus, we introduce toroidal co-ordinates ξ, η in a meridian plane by the transformation

$$\left.\begin{aligned} x &= \frac{c\sin\xi}{s-t}, \quad r = \frac{c\sinh\eta}{s-t}, \\ s &= \cosh\eta, \quad t = \cos\xi. \end{aligned}\right\} \tag{52}$$

The curves η = constant in $r \geqslant 0$ are circles which nest about $(0, c)$. Hence, any curve $\eta = \eta_0$ = constant, defines the boundary of a torus whose exterior is given by

$$\eta_0 \geqslant \eta \geqslant 0, \quad 0 \leqslant \xi < 2\pi.$$

We assume the solution to be given as

$$\Omega = r^2(s-t)^{\frac{3}{2}} \sum_{n=0}^{\infty}{}' A_n P^{(1)}_{n-\frac{1}{2}}(s) \cos n\xi, \tag{53}$$

where Σ' indicates that the term for $n = 0$ is to be multiplied by the factor $\frac{1}{2}$. The boundary condition gives

$$(s_0-t)^{-\frac{3}{2}} = \sum_{n=0}^{\infty}{}' A_n P^{(1)}_{n-\frac{1}{2}}(s_0) \cos n\xi. \tag{54}$$

If we differentiate the relation (Hobson 1931, p. 443)

$$(s-t)^{-\frac{1}{2}} = \frac{2\sqrt{2}}{\pi} \sum_{n=0}^{\infty}{}' Q_{n-\frac{1}{2}}(s) \cos n\xi, \tag{55}$$

with respect to s, we have

$$(s-t)^{-\frac{3}{2}} = -\frac{4\sqrt{2}}{\pi} \sum_{n=0}^{\infty}{}' Q^{(1)}_{n-\frac{1}{2}}(s) \cos n\xi. \tag{56}$$

From (54) and (56) we obtain the value of A_n as

$$A_n = -\frac{4\sqrt{2}}{\pi} \frac{Q^{(1)}_{n-\frac{1}{2}}(s_0)}{P^{(1)}_{n-\frac{1}{2}}(s_0)}. \tag{57}$$

The couple experienced by the torus is

$$N = -16\mu\omega_0 c^3 \sum_{n=0}^{\infty}{}' (4n^2-1) \frac{Q^{(1)}_{n-\frac{1}{2}}(s_0)}{P^{(1)}_{n-\frac{1}{2}}(s_0)}. \tag{58}$$

Finally, I wish to thank Prof. L. E. Payne for his very generous help in the preparation of this article.

REFERENCES

HYMAN, M. A. 1954 Concerning analytic solutions of the generalized potential equation. *Proc. K. Akad. Wet.*, Amst. A, **57**, 408–13.

HOBSON, E. W. 1931 *The Theory of Spherical and Ellipsoidal Harmonics.* Cambridge University Press.

JEFFERY, G. B. 1915 Steady rotation of a solid of revolution in a viscous fluid. *Proc. Lond. Math. Soc.* **14**, 327–38.

KANWAL, R. P. 1955 Rotary and longitudinal oscillations of axisymmetric bodies in a viscous fluid. *Quart. J. Mech. Appl. Math.* **8**, 146–63.

LAMB, H. 1954 *Hydrodynamics.* Dover Publications.

PAYNE, L. E. 1952 On axially symmetric flow and the method of generalized electrostatics. *Quart. Appl. Math.* **10**, 197–204.

PAYNE, L. E. 1956 New Isoperimetric inequalities for eigenvalues and other physical quantities. *Comm. Pure Appl. Math.* **9**, 531–42.

PAYNE, L. E. & PELL, W. H. 1960 The Stokes flow problem for a class of axially symmetric bodies. *J. Fluid Mech.* **7**, 529–49.

SCHIFFER, M. & SZEGÖ, G. 1949 Virtual mass and polarization. *Trans. Amer. Math. Soc.* (1), **67**, 130–205.

Analysis of vibrational relaxation regions by means of the Rayleigh-line method

By N. H. JOHANNESEN

Department of the Mechanics of Fluids, The University of Manchester

(Received 4 September 1960)

The physics of shock-waves with vibrational relaxation regions is recapitulated, and it is shown that exact methods of analysis can be developed from the classical Rayleigh-line equations by treating the real gas as an ideal gas with heat transfer. By using these methods to analyse experimental records of density distributions in relaxation regions, a large number of local values of the relaxation frequency, rather than a single over-all value, may be obtained from each shock-wave record.

1. Introduction

When a one-dimensional compression wave of finite amplitude travels into a gas at rest, the ultimate stable waveform, which propagates with constant velocity, is the result of a balance between two sets of influences. These are, as discussed in detail by Lighthill (1956), the convection which tends to steepen the waveform, and the various types of lag which resist this steepening.

We shall in this paper refer to the particular case of gases in which the lags in the various degrees of freedom of the molecule have markedly different effects. The translational and rotational degrees of freedom reach equilibrium in a very short time (after a few collisions) and the effects of their lag are confined to a narrow region at the front of the wave, the diffusion-resisted part of the wave. This is followed by a generally much wider region in which the vibrational degrees of freedom reach equilibrium. This region is called the relaxation region.

Waves in which both types of lag have an effect are called partly dispersed shock-waves. In some cases of very weak waves the relaxation alone gives sufficient resistance to the convective effects and the diffusion-resisted part of the wave is absent. Such waves are called fully dispersed.

In the present discussion we shall, in the case of partly dispersed waves, assume that the relaxation region is long compared with the diffusion-resisted region, in fact so much so that the thickness of the latter can be put equal to zero in the calculations. It is assumed throughout that the temperature is low enough and the pressure high enough for dissociation effects to be negligible.

Although the development of the stable waveform is most conveniently discussed in terms of a wave travelling into a stationary gas (this is also the case met with in the shock tube), for calculation purposes it is more convenient to consider the flow in a co-ordinate system fixed in the wave. This corresponds to the case

of a gas passing through a stationary wave. Both distances and times will be measured from the downstream end of the diffusion-resisted part of the wave. Because of the assumption about the relative thicknesses of the two regions of the shock-wave, this definition is sufficiently accurate in most cases. It does, however, need modification in the case of a fully dispersed shock-wave.

It will be noted that in the definition adopted here the shock-wave is the whole of the wave. In the literature the wave is often described as a shock-wave followed by a relaxation region, and the term shock-wave therefore used for that part of the wave which in this paper, following Lighthill, is called the diffusion-resisted part of the wave.

Looking now at the passage of a diatomic gas through a stationary partly dispersed shock-wave, the processes may be described physically as follows. The gas approaches the shock-wave with conditions (1) and is compressed very rapidly in the diffusion-resisted part of the wave, so rapidly that the vibrational degrees of freedom are inactive. This means that the conditions at (a), just behind this part of the wave, can be calculated from the shock-wave equations ignoring the vibrational degrees of freedom. After (a) energy is fed into the vibrational degrees of freedom at a rate which depends on the pressure and temperature and on the difference between the local value of the vibrational energy and its equilibrium value at the local temperature. Temperature in this context means translational temperature, and it is assumed that the approach to vibrational equilibrium is so slow that the translational and rotational energies are in local equilibrium throughout the relaxation region. The final state with all the degrees of freedom in energy equilibrium is reached at (2), which is theoretically at infinity downstream.

The main theme of this paper is a discussion of the structure of the relaxation region, a problem which has received considerable treatment in the literature, but nevertheless remains far from clarified.

The ultimate goal from a practical point of view is to be able to predict the structure of the relaxation region for any shock-wave with given initial conditions. It will be shown that it is possible to do this very rapidly provided the rate of approach to equilibrium is known throughout the relaxation region.

We shall, for the time being, assume that the rate of change of vibrational energy at any point in the relaxation region is proportional to the difference between its local equilibrium value, $\overline{\sigma}$ (which is a function of the local temperature T), and its actual value, σ, so that a relaxation equation may be written

$$\frac{d\sigma}{dt} = \omega[\overline{\sigma}(T) - \sigma(t)]. \tag{1}$$

Here t is the time and ω is assumed to be a function of pressure and temperature only. Although (1) is strictly speaking only valid for a system of harmonic oscillators with small deviations from equilibrium (Landau & Teller, 1936; Herzfeld, 1955), nearly all work on the structure of relaxation regions has been done using this equation. It certainly forms a reasonable basis for the discussion of diatomic

gases in which there is only one mode of vibration, in particular as neither theoretical nor experimental evidence is yet available which can suggest the form of a more complicated equation including the effects of anharmonicity and large departures from equilibrium.

For polyatomic molecules the situation is more complicated. In the case of several completely independent modes of vibration excited in parallel, it would be reasonable to write an equation of the form (1) for each mode. In actual molecules the energy transfer is probably a combination of simple transfer in parallel and various types of transfer in series, and the form of the appropriate relaxation equation is not known. Some slight progress has been made theoretically, but it seems likely that further progress must depend, at least in part, on more detailed experimental results than those already available.

All theoretical predictions of ω show that for an ideal gas, in which the specific heats depend on temperature only, ω is directly proportional to the pressure and may be written

$$\omega = p\Omega(T). \tag{2}$$

The temperature dependence of Ω is far more complicated. Relations similar to the one given by Gunn (1946),

$$\Omega = AT^{-1}\exp(-BT^{-\frac{1}{3}})\{1-\exp(-\theta/T)\}, \tag{3}$$

have been used in the plotting of most experimental results. A and B are constants depending on the gas only and θ is the characteristic temperature of vibration. The important term in this expression is $\exp(-BT^{-\frac{1}{3}})$ which follows from the Landau & Teller (1936) theory for the excitation probability. The power of T in the factor preceding the exponential depends, among other things, on the assumptions made in integrating this probability over the velocity distribution of the molecules. The bracket is often replaced by unity.

Experimental results confirm the general dependence of Ω on T but are not yet sufficiently accurate for judging the merits of the various forms of the less important terms in the expression. Ω must therefore be determined experimentally, and the present investigation was in fact started because of the apparent confusion in the literature as to the correct way of determining Ω from experimental observations of relaxation regions. As ω depends on both pressure and temperature and these both vary through the relaxation region (the temperature in strong shock-waves varying by a very large amount) it was felt that the common practice of ascribing to any particular relaxation region *one* value of ω and taking this as the value corresponding to certain 'mean' values of p and T was likely to lead to errors (or uncertainties) in Ω larger than those inherent in the experimental techniques used.

In § 2 it is shown that the variables in the relaxation region can be simply related by means of universal functions using the Rayleigh-line approach, and this approach is shown to lead to a simple method of determining local values of Ω throughout the relaxation region.

Most writers have used $\tau = 1/\omega$ to characterize the rate of approach to equilibrium and called it a relaxation time. This notation derived from the fact that if

in (1) both ω and $\overline{\sigma}$ are taken to have constant values the equation integrates to give $\sigma-\overline{\sigma}_1=(\overline{\sigma}_2-\overline{\sigma}_1)[1-\exp(-\omega t)]$ and $1/\omega$ is a conventional relaxation time. However, for the general case, in which we are interested in local rates of approach rather than over-all times, we prefer to use ω and call it a relaxation frequency.

2. Exact solutions using the Rayleigh-line method

The equations governing the transition through the shock-wave are:

$$\text{Continuity:} \quad \rho v=\rho_1 v_1. \tag{4}$$

$$\text{Momentum:} \quad p+\rho v^2=p_1+\rho_1 v_1^2. \tag{5}$$

$$\text{Energy:} \quad h+\tfrac{1}{2}v^2=h_1+\tfrac{1}{2}v_1^2. \tag{6}$$

$$\text{State:} \quad p=\rho RT. \tag{7}$$

Here h is the enthalpy and R is the gas constant. These equations relate variables at any point in the shock-wave, except in the diffusion-resisted part. They do not, however, relate the conditions at a point to the position of the point. Hence to introduce the x-co-ordinate we must use the relaxation equation (1) which can with $dx/dt=v$, $T=T(x)$, and $t=t(x)$, be written

$$v\frac{d\sigma}{dx}=p\Omega(T)[\overline{\sigma}(x)-\sigma(x)]. \tag{8}$$

If we know all the variables at a series of points $x_1, \ldots, x_p$ in the relaxation region we can at once find the local value of Ω in, say, the region x_n to x_{n+1}:

$$\Omega\left(\frac{T_n+T_{n+1}}{2}\right)=2\frac{(v_n+v_{n+1})(\sigma_{n+1}-\sigma_n)}{(p_n+p_{n+1})(x_{n+1}-x_n)}[\overline{\sigma}_n+\overline{\sigma}_{n+1}-(\sigma_n+\sigma_{n+1})]^{-1}, \tag{9}$$

and each relaxation region will give values of Ω over the whole temperature range from T_a to T_2.

Experimental results are usually obtained as interferometer photographs and only one variable, the density ρ, is initially known as a function of x. In principle, all other variables can, using equations (4) to (7), be expressed as functions of ρ and the conditions at (a), but the expressions are very lengthy and numerical calculations of Ω using (9) would be very tedious. This is probably the reason why previous writers have not used (9) to find the local values of Ω, but instead introduced certain approximations and found a single value of Ω for each relaxation region.

We shall now show that it is possible to rearrange the exact equations so that the relations between the variables can be expressed as universal functions which have already been tabulated. This reduces very considerably the time involved in finding values of Ω from a known density distribution and makes calculations practicable.

The energy equation may be written

$$c_{pa}T+\tfrac{1}{2}v^2+\sigma=c_{pa}T_1+\tfrac{1}{2}v_1^2+\overline{\sigma}_1, \tag{10}$$

where $c_{p\alpha}$ is the specific heat at constant pressure ignoring vibration. If we put

$$\sigma - \overline{\sigma}_1 = q, \tag{11}$$

this becomes

$$c_{p\alpha} T + \tfrac{1}{2} v^2 = c_{p\alpha} T_1 + \tfrac{1}{2} v_1^2 - q. \tag{12}$$

We note that the equations (4), (5), (6), (7) and (12) are the equations governing the steady constant-area flow of an ideal gas with constant specific heats with heating or (as in the present case) cooling. We may therefore treat the non-equilibrium flow of the real gas through the shock-wave as that of an ideal gas (which we shall call the α-gas) from which heat is being extracted at a rate equal to that at which the energy increases in the vibrational modes of the real gas.

The real gas and the α-gas have at each point the same values of p, ρ, T and v, as these depend only on the translational energy which is in equilibrium. Other variables, such as stagnation temperature and Mach number, are useful parameters in the calculations when referred to the α-gas, but have no obvious meaning in the real gas except at stations (1) and (2).

To find all the required relations for the variables in the relaxation region we need only consider the α-gas and note that the quantity q increases monotonically from zero at station (a) to $\overline{\sigma}_2 - \overline{\sigma}_1$ at station (2). For the α-gas we know all quantities at station (1), namely m_1, T_1, T_{01}, p_1, v_1 and ρ_1. These are the same as for the real gas except the Mach number m_1, which is related to the Mach number M_1 of the real gas by

$$m_1 = M_1 (\gamma_1/\gamma_\alpha)^{\frac{1}{2}}, \tag{13}$$

and the stagnation temperature, T_{01}, which is only of interest for the α-gas and is

$$T_{01} = T_1 (1 + \tfrac{1}{2}(\gamma_\alpha - 1) m_1^2). \tag{14}$$

Conditions (a) immediately behind the diffusion-resisted part of the shock-wave are found as those behind a normal shock-wave in the α-gas (the α-shock) with initial conditions (1). T_0 does not change through the diffusion-resisted part of the wave.

In the region (a) to (2) the ratio of the values of a certain quantity at two points can be expressed as a function of the Mach numbers of the α-gas at the two stations. Choosing as a reference station that at which $m = 1$, and using suffix b to indicate values at the reference station, we have the well-known Rayleigh-line relations (e.g. see Shapiro 1953):

$$\frac{T}{T_b} = \frac{(\gamma_\alpha + 1)^2 m^2}{(1 + \gamma_\alpha m^2)^2}, \tag{15}$$

$$\frac{T_0}{T_{0b}} = \frac{2(\gamma_\alpha + 1) m^2 (1 + \frac{1}{2}[\gamma_\alpha - 1] m^2)}{(1 + \gamma_\alpha m^2)^2}, \tag{16}$$

$$\frac{v}{v_b} = \frac{\rho_b}{\rho} = \frac{(\gamma_\alpha + 1) m^2}{1 + \gamma_\alpha m^2}, \tag{17}$$

and

$$\frac{p}{p_b} = \frac{\gamma_\alpha + 1}{1 + \gamma_\alpha m^2}. \tag{18}$$

These relations have been tabulated for $\gamma_\alpha = 7/5$, the value for diatomic and linear molecules (Shapiro 1953; Zucrow 1958). Available tabulations may not

be detailed enough, but the range of m required for practical calculations is quite small and if necessary more detailed tables can be prepared very quickly.

So far we have described how to find the conditions at (a) and how to relate the variables within the relaxation region. Before describing the actual calculations in the relaxation region we must discuss the general behaviour of the variables in this region.

First let us look at the possible values of m_a. The minimum possible value of M_1 is unity which gives $m_1 = (\gamma_1/\gamma_\alpha)^{\frac{1}{2}}$. As M_1 increases, m_1 reaches a maximum value of unity for $M_1 = (\gamma_\alpha/\gamma_1)^{\frac{1}{2}}$. In the range $1 \leqslant M_1 \leqslant (\gamma_\alpha/\gamma_1)^{\frac{1}{2}}$, the shock-wave is fully dispersed and $m_1 = m_a \leqslant 1$. When $M_1 > (\gamma_\alpha/\gamma_1)^{\frac{1}{2}}$, $m_1 > 1$ and a diffusion-resisted part (α-shock) is present, corresponding to a normal shock-wave in the α-gas changing m from a value $m_1 > 1$ to a value $m_a < 1$. We therefore conclude that for all waves $m_a \leqslant 1$.

Equation (10) may be written

$$q/c_{p\alpha} = T_{01} - T_0 = T_{0a} - T_0. \tag{19}$$

As q increases when x increases through the relaxation region, T_0 must decrease. Differentiating (16) we find that $dT_0/dm > 0$ for $m < 1$, so that m decreases through the relaxation region. Similarly we find, by differentiating (17) and (18), that p and ρ increase while v decreases.

The behaviour of T is more complicated. Here we find that for decreasing m, T increases in the interval $1 > m > 1/(\gamma_\alpha)^{\frac{1}{2}}$ and decreases for $m < 1/(\gamma_\alpha)^{\frac{1}{2}}$. If, therefore, $1 > m_a > 1/(\gamma_\alpha)^{\frac{1}{2}}$ the temperature increases at the beginning of the relaxation region. Whether T increases throughout the relaxation region or reaches a local maximum depends on the range of m covered in the relaxation region. This again depends on the function $\overline{\sigma} = \overline{\sigma}(T)$ for the particular gas and cannot be discussed simply in terms of the initial conditions.

The calculation of the relaxation region can now be carried out as follows.

(1) From Equations (15) to (18), or using tables, find the reference values (suffix b) using the known conditions at either station (1) or station (a).

(2) Choose a succession of decreasing values of m, starting with m_a. For each value of m read from the tables of the values of T, T_0, v, ρ and p. (By taking as values of m those appearing as arguments in the table, interpolation is avoided.)

(3) From T and tabulated values of $\overline{\sigma}(T)$ find $\overline{\sigma}$.

(4) From T_0 find q from (19) and hence σ from (11).

(5) Continue this process until at station (2) $\sigma_2 = \overline{\sigma}_2$. The exact conditions at (2) are found very easily by 'overshooting' slightly and interpolating once.

It is interesting to compare this method of finding the equilibrium conditions at (2) with the usual method due to Bethe & Teller (1941). In their method the temperature at (2) is chosen and conditions at (1) calculated. If the equilibrium conditions behind a shock-wave with known initial conditions are required it is therefore necessary to carry out the calculations for at least two values of T_2 before interpolating, whereas in the method suggested above, the final values follow from a single calculation starting with the known initial conditions.

Having determined the variables through the relaxation region it is now straightforward to apply the results to the two cases of interest.

If ρ is known as an experimentally determined function of x, we can find the values of x at the points used in the tabulation of the variables in the relaxation region, in other words find $x = x(m)$, and (9) at once gives the local values of Ω.

If Ω is known as a function of T we know all quantities in the relaxation region except x, and (8) can be rewritten as

$$dx = \frac{v\,d\sigma}{p\Omega(\bar{\sigma} - \sigma)}, \tag{20}$$

and integrated numerically to give the values of x.

A good deal of thought was given to the choice of the most convenient parameter to be used in the calculations, and it was found that using the Mach number, m, of the α-gas gave by far the quickest calculation procedure. With the variables tabulated as functions of m with sufficiently small steps in m, interpolation in the tables is only necessary at stations (a) and (2). If, for example, a series of values of ρ, or equidistant values of x, were chosen, interpolation would be necessary at all points in the relaxation region.

3. Discussion and conclusions

It has been shown that the use of the Rayleigh-line equations reduces the numerical work involved in the calculation of the structure of relaxation regions or the derivation of relaxation frequencies from experimentally determined density distributions to such an extent that exact calculations become just as easy as approximate ones.

The use of the Rayleigh-line equations has the major advantage that a whole series of values of the relaxation frequency, each corresponding to a definite pressure and temperature, can be determined from each relaxation region density distribution. This reduces the experimental work very considerably, and, what is perhaps more important, it offers a method for detailed study of the relaxation equation. If the simple equation (1) is valid it will be found that values of Ω (i.e. ω reduced to a pressure of one atmosphere) depend on T only and not on where in the relaxation region they have been found. If, however, Ω depends also on the departure from equilibrium, this should be easily detectable, and it might be possible to find the form of the dependence.

Similarly, in the case of gases for which the simple relaxation equation would not be expected to hold, detailed analysis of the relaxation region may help to determine the more complicated relaxation equation.

The method is at present being used in this department to evaluate experimental results on strong (large departures from equilibrium) shock-waves in nitrogen and on weaker waves in carbon dioxide which has several modes of vibration with different relaxation frequencies.

In the following paper Blythe (1961) uses the exact calculation method outlined in the present paper to assess the various approximate methods which have been proposed in the literature, and he also includes illustrative numerical examples.

The author is indebted to Mr H. K. Zienkiewicz and Mr P. A. Blythe for many helpful discussions.

REFERENCES

BETHE, H. & TELLER, E. 1941 *Deviations from Thermal Equilibrium in Shock-Waves.* Cornell University.

BLYTHE, P. A. 1961 Comparison of exact and approximate methods for analysing vibrational relaxation regions. *J. Fluid Mech.* **10**, 33.

GUNN, J. C. 1946 Relaxation time effects in gas dynamics. *Aero. Res. Counc., Rep. & Mem.* no. 2338.

HERZFELD, K. F. 1955 Relaxation phenomena in gases. Section H of *Thermodynamics and Physics of Matter* (Vol. 1 of *High Speed Aerodynamics and Jet Propulsion*). Princeton University Press.

LANDAU, L. & TELLER, E. 1936 Zur Theorie der Schalldispersion. *Phys. Z. Sowjet.* **10**, 34.

LIGHTHILL, M. J. 1956 Viscosity in waves of finite amplitude. Article in *Surveys in Mechanics.* Cambridge University Press.

SHAPIRO, A. H. 1953 *The Dynamics and Thermodynamics of Compressible Fluid Flow.* Ronald Press.

ZUCROW, M. J. 1958 *Aircraft and Missile Propulsion*, Vol. 1. John Wiley and Sons.

Comparison of exact and approximate methods for analysing vibrational relaxation regions

By P. A. BLYTHE

Department of the Mechanics of Fluids, The University of Manchester

(Received 4 September 1960)

The validity of various solutions for the vibrational relaxation region in shock-waves, and of the assumptions on which they are based, has been assessed by comparison with an exact solution obtained by numerical integration of the relaxation equation, and also by use of the Rayleigh-line equations. Estimates of errors in the values of the relaxation frequency, determined by means of these solutions, are given.

1. Introduction

In the preceding paper (Johannesen 1961) a discussion of the basic physics of vibrational relaxation regions in shock-waves was given. The paper presented a method whereby the exact shock-wave equations (equations (4), (5) and (6) of Johannesen) could be solved for any given temperature dependence of the relaxation frequency ω, assuming the simple relaxation equation

$$\frac{d\sigma}{dt} = \omega(\overline{\sigma} - \sigma) \tag{1}$$

to hold. (The notation used in this paper is the same as that used by Johannesen, unless otherwise stated.)

Alternatively the method could be used to obtain, from experimental records, local values of ω, rather than over-all ones.

In this paper an exact numerical integration has been carried out for a strong shock-wave in nitrogen using Gunn's expression for ω,

$$\omega = ApT^{-1}\exp(-BT^{-\frac{1}{3}})[1-\exp(-\theta/T)], \tag{2}$$

where A and B are constants.

This numerical solution is referred to as the exact solution and previously published solutions are compared with it. These previous solutions are all approximate in the sense that they either use simplified forms of the shock-wave equations or make certain other simplifying assumptions (e.g. ω constant).

For weak waves the previous solutions are compared with an analytical solution which is based on ω and c_{vib} constant. These are valid assumptions for such waves.

By regarding the exact numerical solution as a representation of an experimental record it is possible to assess the accuracy with which ω would be deter-

mined from such a record by means of the previous approximate solutions. (Note that these previous solutions obtain over-all values of ω, and not local values.)

The numerical integration was done for a shock-wave in nitrogen of Mach number $M_1 = 8{\cdot}0$, and with T_1, the temperature ahead of the shock-wave, equal to 300 °K. Values of $\overline{\sigma}$ were taken from N.B.S. Circular no. 564. The results were obtained in the form of the density ratio, etc., as functions of $\omega_m x/v_m$, where the suffix m denotes the value of the quantity at the point in the relaxation region corresponding to $T = \frac{1}{2}(T_a + T_2)$, so that only the value of the constant B, occurring in equation (2), was required. By fitting (2) to Blackman's experimental results it was found that $B = 223$ (°K)$^{\frac{1}{2}}$.

It is unlikely that the use of a slightly different relationship between ω and T would alter the main conclusions reached in this paper.

Because of the labour involved, prior to Johannesen's paper, in obtaining solutions to the exact shock-wave equations for varying ω, previous workers made various assumptions in an attempt to simplify matters.

Many of these assumptions concerned the energy equation, and this fact affords a convenient means of classifying the solutions. Energy equations that have been used are: (*a*) exact, (*b*) constant-enthalpy, (*c*) Bethe–Teller ($d\overline{\sigma}/d\sigma$ = constant), and (*d*) constant-internal-energy. All these assumptions have the advantage that they eliminate the velocity from the energy equation. The validity of these assumptions is assessed by means of the Rayleigh-line equations and numerical checks.

The other main type of assumption is to consider ω and c_{vib} constant in the relaxation region. When the assumption of constant ω is made it is, of course, only possible to obtain an over-all value of ω from such a solution.

A full list of solutions discussed in this paper, together with the assumptions made in obtaining any particular one of them, is given in table 1. When a solution is mentioned in the text it will be followed by a Roman numeral corresponding to its position in this list.

Sections 2 to 6 deal with these solutions and assumptions. The conclusions reached in these sections are summarized in section 7. In section 8 previous methods of determining ω are discussed.

2. Exact-energy-equation solutions

The numerical solution already mentioned belongs to this class and, as stated, is called the exact solution.

If ω and c_{vib} are assumed constant in the relaxation region, then it is possible to integrate the relaxation equation analytically using the correct shock-wave equations. This can be done for both fully and partly dispersed shock-waves (ii and vi).

The assumption of constant ω is by no means valid for strong shock-waves in which departures from a mean value can be as high as 20 or 30 %. Even for fairly weak waves, if the temperature ahead of the shock is high, some account may have to be taken of the variation in ω.

The latter of the two assumptions, constant c_{vib}, predicts that the equilibrium vibrational energy will be a linear function of the temperature in the relaxation region, and for most shock-waves this is a reasonable assumption.

No.	Solution	Form of energy equation used	Assumptions concerning ω	Assumptions concerning c_{vib}	Further assumptions
(i)	Exact	Exact	—	—	—
(ii)	Analytical solution for partly dispersed shock-waves (Blythe)	Exact	Constant	Constant	—
(iii)	Broer's analytical solution	Exact	Constant	Constant $= (c_{vib})_1$	—
(iv)	Approximate form of analytical solution (ii)	Exact	Constant	Constant	Assume that the term $\log\{(v-v_2)/v_1\}$ dominates the relaxation
(v)	Lighthill solution for partly dispersed shock-waves	Exact	Constant $= \omega_2$	~ 0	Assume that the term $\log\{(v-v_2)/v_1\}$ dominates the relaxation
(vi)	Analytical solution for fully dispersed shock-waves (Blythe)	Exact	Constant	Constant	—
(vii)	Griffith–Kenney solution for fully dispersed shock-waves	Exact	Constant	Constant	Neglect variation of the v/v_1 term
(viii)	Lighthill solution for fully dispersed shock-waves	Exact	Constant	Constant	See Lighthill (1956); assumptions valid only for very weak waves
(ix)	Bethe–Teller and Gunn solutions for fully dispersed shock-waves	Exact	Constant	Constant	See Gunn (1946)
(x)	Constant enthalpy numerical solution	Constant-enthalpy	—	—	—
(xi)	Gunn	Constant-enthalpy	Constant	Constant	—
(xii)	Blackman	Constant-enthalpy	Constant	Constant	Constant pressure
(xiii)	Approximate form of Blackman's solution	Constant-enthalpy	Constant	Constant	Constant pressure, $x = \bar{v}t$, and $\rho_2/\{\rho_a + (\rho_2 - \rho_a) \times \exp(-c_{pm}\omega_m x/c_{p_a}\bar{v})\} \doteqdot 1$
(xiv)	Bethe–Teller numerical solution	Bethe–Teller	—	—	—
(xv)	Smiley–Winkler	Bethe–Teller	Exponential variation in v/ω; see equation (24)	—	—
(xvi)	Constant internal energy numerical solution (Herman & Rubin)	Constant-internal-energy	—	—	—
(xvii)	Constant $\bar{\sigma}$	—	—	—	Assume that $\bar{\sigma} = \bar{\sigma}_2$ in the relaxation region

TABLE 1

In order to integrate (1) analytically it is convenient to express the variables as functions of the velocity v. Equation (1) becomes

$$\frac{r\omega_m}{v_1}\frac{dx}{du} = \frac{u[b_1-(\gamma_\alpha+1)u]}{u^2-d_1u+d_2}, \tag{3}$$

where
$$\left.\begin{aligned} &u = v/v_1, \\ &b_1 = \gamma_\alpha + 1/m_1^2, \quad b_2 = \tfrac{1}{2}(\gamma_\alpha-1)+1/m_1^2, \\ &d_1 = \frac{2\gamma_m b_1}{\gamma_\alpha(\gamma_m+1)}, \quad d_2 = \frac{v_1^2 b_2+(\gamma_\alpha-1)(\overline{\sigma}_1+K)}{rv_1^2}, \\ \text{and} \quad &r = \frac{(\gamma_\alpha-1)(\gamma_m+1)}{2(\gamma_m-1)}. \end{aligned}\right\} \tag{4}$$

K is defined by $\overline{\sigma} = (c_{\text{vib}})_m T - K$. The constant value of ω was assumed to be ω_m.

Consider first of all partly dispersed shock-waves. The denominator on the right-hand side of equation (3) is proportional to $\overline{\sigma}-\sigma$. This is zero at the final equilibrium position and thus $v = v_2$ must be a root of the denominator. If the other root is λ then (3) is easily integrated to give

$$\frac{1}{\lambda-v_2/v_1}\left\{\left(\frac{v_2}{v_1}\right)^2\left(\frac{1}{m_2^2}-1\right)\log\left(\frac{v}{v_1}-\frac{v_2}{v_1}\right)-\lambda[b_1-(\gamma_\alpha+1)\lambda]\log\left(\lambda-\frac{v}{v_1}\right)\right\}+(\gamma_\alpha+1)\,v/v_1$$
$$= -\frac{r\omega_m x}{v_1}+\text{constant}. \tag{5}$$

A similar type of solution was obtained by Broer (1951), (iii), who assumed that $(c_{\text{vib}})_m = (c_{\text{vib}})_1$, an assumption that is valid only for weak waves.

A comparison between the above solution, (ii), (equation 5) and the exact solution (i) is shown in figure 1. As can be seen the solution appears to give a satisfactory mean prediction of the density as a function of x over the region in which the major portion of the density change occurs.

For strong shock-waves, the variations in the terms $\log(\lambda-v/v_1)$ and v/v_1 are small compared with the variation in $\log(v/v_1-v_2/v_1)$. Thus one can approximate equation (5) to

$$\frac{v-v_2}{v_a-v_2} = \exp\left\{-\frac{r(\lambda-v_2/v_1)}{(v_2/v_1)(1/m_2^2-1)}\frac{\omega_m x}{v_2}\right\}. \tag{6}$$

This solution, (iv), is also plotted in figure 1. For weak waves the agreement between (6) and (5) becomes worse, as the term $\log(\lambda-v/v_1)$ becomes important.

Lighthill (1956) obtained a solution, (v), of the form

$$\frac{v-v_2}{v_a-v_2} = \exp\left(-\frac{\omega_2 x}{v_2}\right) \tag{7}$$

by assuming that on the right-hand side of equation (3) v could be replaced by v_2 except in the term $v-v_2$ in the denominator. Furthermore he assumed that the constant value of ω was ω_2, and that $\gamma_m \doteqdot \gamma_\alpha$.

This solution, (v), is thus valid only for waves in which $\gamma_m \doteqdot \gamma_\alpha$, and it is not valid for weak waves. Obviously it has only a limited range of application. Figure 1 shows this solution for a strong shock-wave in which γ_m is noticeably

less than γ_α, and also ω_2 is considerably less than ω_m. It is immediately apparent that the errors which are introduced into the density curve by incorrect application of equation (7) are large.

In order to obtain the solution (vi) for fully dispersed shock-waves reconsider equation (3). The denominator on the right-hand side of this equation will now have roots $v = v_1$, and $v = v_2$, as there is now no diffusion-resisted part of the wave and (3) will be valid throughout the wave. Equation (3) can be integrated as before, and the result can be obtained from (5) by simply putting $\lambda = 1$. (In fact it can easily be shown that $\lambda = 1$ when $\gamma_m = \gamma_1$. Previously one distinguished between γ_m and γ_1 because of the presence of the diffusion-resisted part of the wave.)

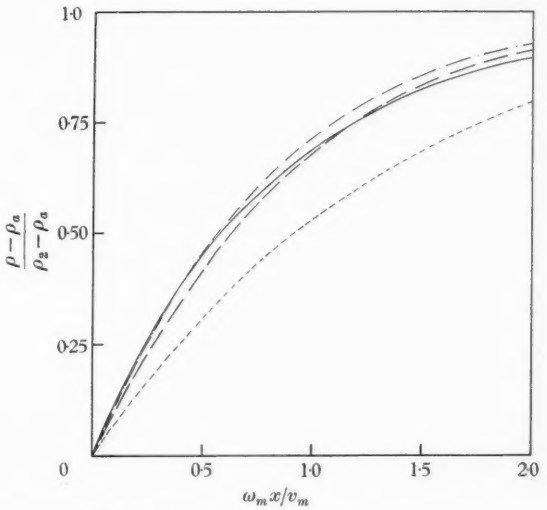

FIGURE 1. Comparison of solutions based on the exact energy equation. $M_1 = 8{\cdot}0$, $T = 300\,°\mathrm{K}$, in nitrogen. ———, Exact solution, (i); — —, analytical solution, (ii), (Blythe); — · —, approximate form of solution (ii); – – – –, Lighthill solution, (v).

Both the log terms are now equally important, though the term v/v_1 can be omitted without serious error (cf. Griffith & Kenny (1957), (vii)). Lighthill (1956), (viii), gives a full discussion of fully dispersed waves, but his analysis is only applicable to very weak weaves. Bethe & Teller (1941) and Gunn (1946), (ix), have also analysed fully dispersed waves but in terms of the temperature rather than the velocity. This solution, (ix), would be invalid if it were possible for the temperature to have a maximum in a fully dispersed shock-wave. This, however, is impossible for an ideal diatomic gas (neglecting anharmonicity) as the required condition is that $\gamma_1 < (13/11)$.

The preceding solution (ii) can be expressed in terms of the time t rather than the distance x. The expression corresponding to (5) is

$$\frac{1}{\lambda - v_2/v_1}\left\{\frac{v_2}{v_1}\left(\frac{1}{m_2^2}-1\right)\log\left(\frac{v}{v_1}-\frac{v_2}{v_1}\right)-[b_1-(\gamma_\alpha+1)\lambda]\log\left(\lambda-\frac{v}{v_1}\right)\right\} = -r\omega_m t + \text{constant}. \qquad (8)$$

One can obtain a result similar to (6) from which a relaxation time τ_m for the velocity can be obtained. In fact

$$\tau_m = \frac{v_2/v_1\,(m_2^{-2}-1)}{r(\lambda - v_2/v_1)}\,\frac{1}{\omega_m}, \tag{9}$$

which has the limiting value

$$\tau_m \to 11/(14\omega_m) \tag{10}$$

as $m_1 \to \infty$, for a system of fully excited harmonic oscillators.

3. Constant-enthalpy solutions

The assumption of constant enthalpy in the relaxation region is one of the more common approximations made in the literature on this subject.

The energy equation (equation (6) of Johannesen's paper) is now replaced by

$$h = \text{constant},$$

or

$$c_{p\alpha}T + \sigma = \text{constant}. \tag{11}$$

As σ is calculated from this assumption, the condition that constant enthalpy be a good approximation is that

$$\left|\frac{\Delta h}{\Delta \sigma}\right| \ll 1. \tag{12}$$

From the Rayleigh-line equations it can be shown that

$$\frac{dh}{d\sigma} = \frac{(\gamma_\alpha - 1)\,m^2}{1-m^2}. \tag{13}$$

Obviously (12) is not satisfied for weak waves where m and m_1 are of order unity. However, as $m_1 \to \infty$, for a system of fully excited harmonic oscillators, equation (13) gives

$$\left(\frac{dh}{d\sigma}\right)_a \to \frac{1}{15}; \quad \left(\frac{dh}{d\sigma}\right)_2 \to \frac{1}{22}.$$

(The effect of anharmonicity makes the second of these two limits smaller.)

This result, that the constant-enthalpy assumption is valid only for strong shock-waves, could have been anticipated from a knowledge of the temperature profile in weak shock-waves. For such shock-waves it is possible for the temperature to increase in the relaxation region, whereas the constant-enthalpy assumption predicts that the temperature must always decrease and hence leads to a totally incorrect qualitative picture. Further elaboration on this point is given later.

In order to check the conclusion concerning strong shock-waves numerical integration, (x), using the constant-enthalpy assumption, was performed for the case $M_1 = 8{\cdot}0$, $T_1 = 300\,^\circ\text{K}$, in nitrogen. Before this can be done one has to decide what value the enthalpy should take. It was found that the '2' position value gave a better result than did the 'a' position value. The comparison with the exact solution, (i), is shown in figure 2, and, as can be seen, the assumption introduced little error in the density as a function of distance.

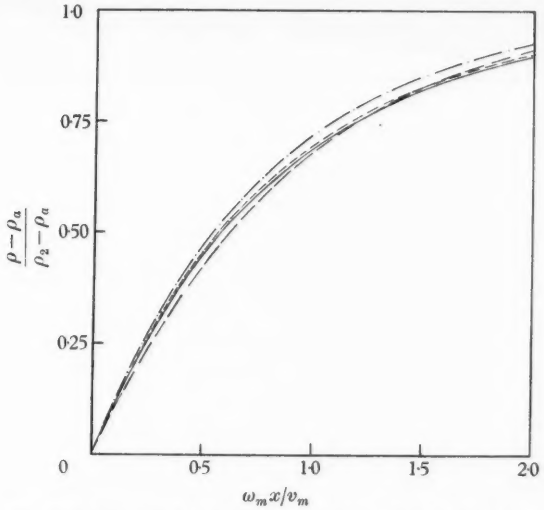

FIGURE 2. Comparison between the exact solution, (i), and the solutions based on the constant-enthalpy assumption. $M_1 = 8{\cdot}0$, $T_1 = 300$ °K, in nitrogen. ———, Exact solution, (i); – – –, constant enthalpy numerical solution, (x); — —, Blackman's solution, (xii); — · —, Blackman's approximate solution, (xiii).

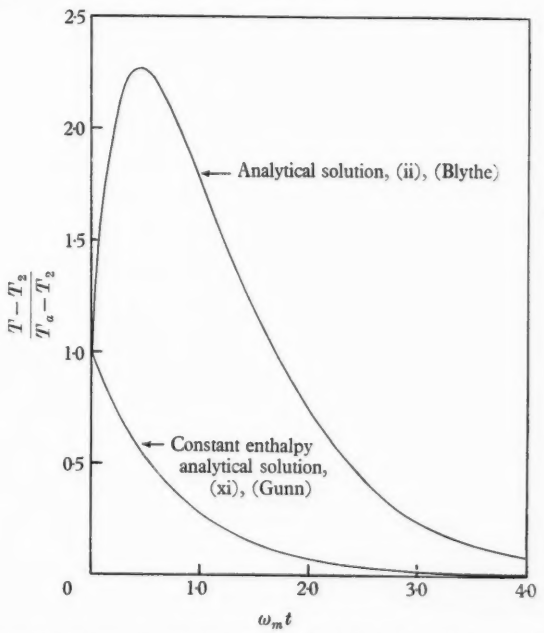

FIGURE 3. Comparison between solution (ii) which is based on the exact energy equation, and solution (xi), which is based on the constant-enthalpy assumption, for the temperature profile in the relaxation region in a weak shock-wave. $m_1 = 1{\cdot}15$, $T_1 = 3000$ °K, in nitrogen.

By the further assumption that ω and c_{vib} be constant an analytical solution for the temperature can be obtained using only the constant-enthalpy assumption and the relaxation equation. It is for this reason that the constant-enthalpy assumption has proved so useful in practice. (A similar remark could be made about the other energy equation assumptions.) This solution, (xi), was first obtained by Gunn (1946) and it can be written

$$\frac{T-T_2}{T_a-T_2} = \exp\left(-\omega_m t\, c_{pm}/c_{px}\right). \tag{14}$$

Equation (14) is, of course, invalid for weak waves. This is demonstrated quite strikingly in figure 3 where (14) is compared with the analytical solution (ii), which is based on the exact energy equation, for $m_1 = 1{\cdot}15$, $T_1 = 3000\,^{\circ}\text{K}$, in nitrogen. The temperature variation in this shock-wave is very small, even though $T_1 = 3000\,^{\circ}\text{K}$, and the assumptions of constant ω and constant c_{vib} are still valid. The discrepancy is thus due solely to the constant-enthalpy assumption.

(Note that ω_m as previously defined would not, in general, be a sound estimate of the constant value of ω for shock-waves which have a maximum in the temperature profile in the vibrational relaxation region. For such shock-waves ω_m should be taken to mean the constant value, whatever that constant value is.)

Blackman (1956), (xii), further assumed constant pressure in the relaxation region from which

$$\frac{v-v_2}{v_a-v_2} = \exp\left(-\omega_m t\, c_{pm}/c_{px}\right),$$

or

$$\frac{\rho_2-\rho}{\rho_2-\rho_a} = \frac{(\rho_2/\rho_a)\exp\left(-\omega_m t\, c_{pm}/c_{px}\right)}{1+(\rho_2/\rho_a-1)\exp\left(-\omega_m t\, c_{pm}/c_{px}\right)}. \tag{15}$$

The constant-pressure assumption is reasonable except for weak waves. (The density always increases in the relaxation region, hence the constant-pressure assumption implies that the temperature must fall, a condition not valid in weak waves.)

Note that in this case the relaxation time for the velocity is given by

$$\tau_m = c_{px}/(c_{pm}\omega_m), \tag{16}$$

which has the limiting value of $7/(9\omega_m)$ for a system of fully excited harmonic oscillators. Comparison with the previously derived result (10) reveals that the limiting values are different by less than $(100\,\omega_m)^{-1}$.

In order to analyse his experimental results Blackman made the further assumption that the term $\rho_2/\rho_a - 1$ was small and hence that

$$(\rho_2/\rho_a)/\{1+(\rho_2/\rho_a-1)\exp\left(-\omega_m t c_{pm}/c_{px}\right)\}$$

could be replaced by unity. Further he wrote $x = t/\bar{v}$ where $\bar{v} = \frac{1}{2}(v_a+v_2)$. Equation (15) then becomes

$$\frac{\rho_2-\rho}{\rho_2-\rho_a} = \exp\left(-\frac{c_{pm}}{c_{px}}\frac{\omega_m x}{\bar{v}}\right). \tag{17}$$

This exponential law (17), (xiii), has been deduced by means of a large number of assumptions and whether or not it is valid is very much open to question. It is

certainly true that Blackman found experimentally that the density varied exponentially with distance in the relaxation region. However this simply requires that

$$\frac{\rho_2-\rho}{\rho_2-\rho_a} = \exp(-Cx)$$

where C is some constant, not necessarily equal to $\frac{c_{pm}}{c_{px}}\frac{\omega_m}{\bar{v}}$.

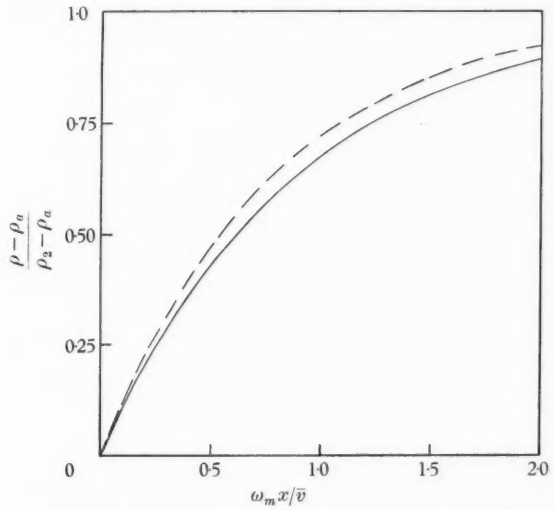

FIGURE 4. Comparison between the Blackman solution, (xiii), and solution (ii) for a weak wave. $m_1 = 1{\cdot}15$, $T_1 = 3000\,°\text{K}$, in nitrogen. ———, Analytical solution, (ii), (Blythe); — —, Blackman's approximate analytical solution (xiii).

Figure 2 compares equation (17) with the exact solution (i) for a strong wave. As can be seen there is a marked discrepancy between the two solutions. Inclusion of the term neglected by Blackman (i.e. solution (xii), equation (15)) lessens this discrepancy (see figure 2).

For weak waves it is expected that equation (17) will be invalid because of the assumption of constant enthalpy. This prediction is confirmed in figure 4 where a comparison between equation (17) and solution (ii), which is based on the exact energy equation, for $m_1 = 1{\cdot}15$, $T_1 = 3000\,°\text{K}$, is shown. (As previously pointed out the assumptions of constant ω and constant c_{vib} are perfectly valid in this wave.)

4. Solutions based on the Bethe–Teller assumption

Consider

$$\frac{d\bar{\sigma}}{d\sigma} = -\mu. \tag{18}$$

For $\mu = c_{\text{vib}}/c_{px}$ (18) is equivalent to the constant-enthalpy assumption. From the Rayleigh-line equations it can be shown that μ is strictly given by

$$\mu = \frac{c_{\text{vib}}}{c_{px}}\left[1-(\gamma_x-1)\frac{m^2}{1-m^2}\right]. \tag{19}$$

Bethe & Teller (1941) assumed that μ was constant and calculated μ by matching the integrated form of (18) for constant μ, namely

$$\overline{\sigma}+\mu\sigma = \phi, \text{ a constant}, \tag{20}$$

to the boundary conditions at 'a' and '2'. Thus

$$\mu = \frac{\overline{\sigma}_a-\overline{\sigma}_2}{\overline{\sigma}_2-\overline{\sigma}_1}, \quad \phi = \overline{\sigma}_2\frac{(\overline{\sigma}_a-\overline{\sigma}_1)}{\overline{\sigma}_2-\overline{\sigma}_1}. \tag{21}$$

The condition that (20) be a valid method of calculating σ is that

$$\left|\frac{\Delta(\overline{\sigma}+\mu\sigma)}{\Delta\sigma}\right| \ll 1, \tag{22}$$

where μ is given by (21).

It can be shown that as $m_1 \to \infty$, for a system of fully excited harmonic oscillators,

$$\left(\left|\frac{d(\overline{\sigma}+\mu\sigma)}{d\sigma}\right|\right)_a \to \frac{1}{315}, \quad \left(\left|\frac{d(\overline{\sigma}+\mu\sigma)}{d\sigma}\right|\right)_2 \to \frac{2}{693},$$

so that the assumption is valid for strong shock-waves.

The analysis for weak waves is a little more difficult. For m^2 of order $1/\gamma_\alpha$ it can be shown from (19) that it is possible for μ to change sign in the relaxation region, although the form used, (21), predicts that μ will be positive or negative according as T_a is greater or less than T_2. Hence, for weak waves, an incorrect qualitative picture would arise, even though the criterion (22) might predict a good quantitative agreement. For even weaker waves, m of order unity, it is easily shown that (22) is not satisfied.

Hence as in the case of constant enthalpy, it would appear that this assumption is valid only for strong shock-waves.

A numerical integration, (xiv), was carried out using the Bethe–Teller assumption for a shock-wave of Mach number $M_1 = 8{\cdot}0$ in nitrogen at $T_1 = 300\,°\text{K}$. Excellent agreement was obtained with the exact solution (i) (see figure 5), thus verifying the above conclusion.

By assuming ω constant, one can easily derive similar results to those obtained by Gunn, (xi), and by Blackman, (xii, xiii), for the constant-enthalpy case. In fact all one has to do is to replace $c_{pm}/c_{p\alpha}$ by $1+\mu$ in the previous expressions. The conclusions concerning such solutions would be similar to those obtained before.

Smiley & Winkler (1954), (xv), attempted to improve this type of analytical solution by allowing for the variation in ω. From the relaxation equation (1) and equation (18) it can be shown that

$$\frac{\overline{\sigma}_2-\sigma}{\overline{\sigma}_2-\overline{\sigma}_1} = \exp\left[-\int_0^x (1+\mu)\frac{\omega}{v}dx\right]. \tag{23}$$

Smiley & Winkler then assumed that the variation of ω/v could be represented by

$$\frac{v}{\omega} = \left(\frac{v}{\omega}\right)_a + \left[\left(\frac{v}{\omega}\right)_2 - \left(\frac{v}{\omega}\right)_a\right]\left[1-\exp\left\{-\left(\frac{\omega}{v}\right)_a x\right\}\right]. \tag{24}$$

This assumption has no physical foundation and is purely a curve-fitting approximation. Nevertheless, as will be seen later, it turns out that this assumption leads to very satisfactory results.

Equations (23) and (24) are easily combined to give

$$\frac{\overline{\sigma}_2-\sigma}{\overline{\sigma}_2-\overline{\sigma}_1}=\left[\left(\frac{v}{\omega}\right)_2\left(\frac{\omega}{v}\right)_a\exp\left\{\left(\frac{\omega}{v}\right)_a x\right\}-\left\{\left(\frac{v}{\omega}\right)_2\left(\frac{\omega}{v}\right)_a-1\right\}\right]^{-s}, \tag{25}$$

where $s=(1+\mu)\,(v/\omega)_a\,(\omega/v)_2$.

The comparison between this solution, (xv), and the exact solution (i) for $M_1=8{\cdot}0$, $T_1=300\,^\circ\mathrm{K}$, in nitrogen is shown in figure 5. The agreement is very good, confirming that (24) is a valid approximation. (It has already been established that the Bethe–Teller assumption is valid for strong shock-waves.)

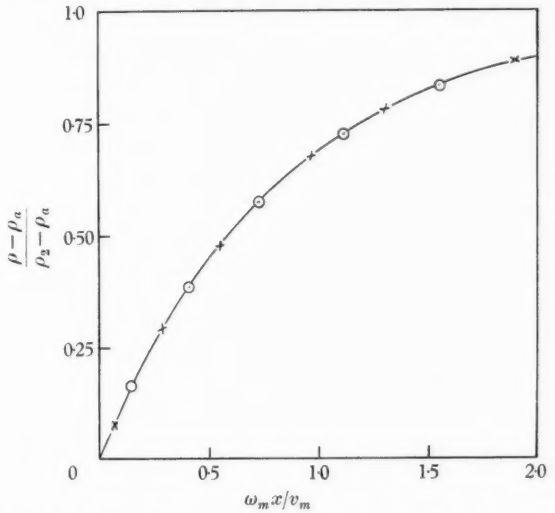

FIGURE 5. Comparison between the exact solution (i) and solutions based on Bethe–Teller assumption. $M_1=8{\cdot}0$, $T_1=300\,^\circ\mathrm{K}$, in nitrogen. ———, Exact solution, (i); ⊙, Bethe–Teller numerical solution, (xiv); ×, Smiley–Winkler analytical solution, (xv).

5. Constant-internal-energy solution

Herman & Rubin (1959) made the assumption of constant internal energy in the relaxation region. It is very difficult to justify this assumption. Certainly the values of the internal energy at the two 'end' points differ far more than the values, for example, of the enthalpy.

The condition for this assumption to be valid is that

$$\left|\frac{\Delta e}{\Delta\sigma}\right|\ll 1, \tag{26}$$

where e is the internal energy.

It can be shown from the Rayleigh-line equations that

$$\frac{de}{d\sigma}=\frac{\gamma_a-1}{\gamma_a(1-m^2)}. \tag{27}$$

For weak waves, $m\doteq 1$ and the assumption is obviously erroneous. As $m_1\to\infty$ it is found that for a system of fully excited harmonic oscillators

$$\left(\frac{de}{d\sigma}\right)_a\to\frac{1}{3},\quad\left(\frac{de}{d\sigma}\right)_2\to\frac{7}{22}.$$

Thus it can hardly be said, for *any* Mach number, that the assumption is valid.

A numerical integration, (xvi), confirmed this prediction for a strong shock-wave (figure 6). (e_2 was used as the constant value; if e_a were used the disagreement would be slightly more marked.)

No analytical solutions using this assumption have been given, although one could easily be obtained in a way similar to that used to derive the constant-enthalpy solution (xi). It would, admittedly, be of little use.

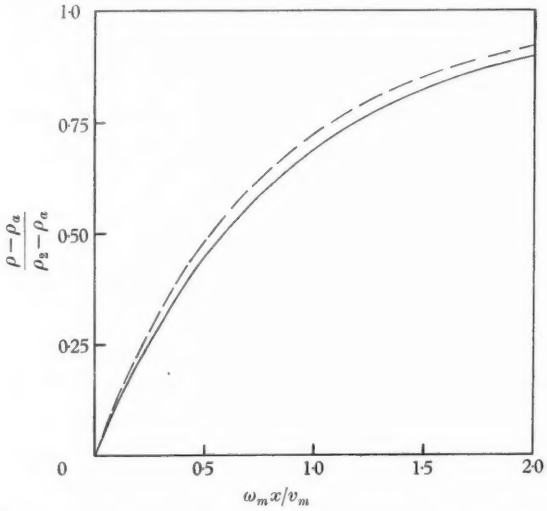

FIGURE 6. Comparison between the constant-internal-energy solution (xvi) and the exact solution (i). $M_1 = 8{\cdot}0$, $T_1 = 300$ °K, in nitrogen. ——— exact solution (i); — — constant-internal-energy numerical solution (xvi) (Herman & Rubin).

6. Constant-$\bar{\sigma}$ solution

If $\bar{\sigma}$ is assumed constant the relaxation equation can be integrated immediately for constant ω, (xvii). The constant value of $\bar{\sigma}$ must, of course, be $\bar{\sigma}_2$, and then

$$\frac{\bar{\sigma}_2-\sigma}{\bar{\sigma}_2-\bar{\sigma}_1} = \exp(-\omega_m t). \tag{28}$$

This was one of the earliest solutions obtained for vibrational relaxation regions.

It is expected that for strong shock-waves, in which both ω and $\bar{\sigma}$ vary by large amounts, this solution will give poor agreement with the exact solution (i). In fact from the Bethe–Teller assumption, which is valid for strong shock-waves, it can be shown that the relaxation equation will be of the form

$$\left.\begin{aligned} \frac{d\sigma}{dt} &= \omega'(\bar{\sigma}_2-\sigma), \\ \text{only if} \quad \omega' &= (1+\mu)\,\omega. \end{aligned}\right\} \tag{29}$$

For strong shock-waves in a diatomic gas μ is roughly $\frac{2}{7}$.

For weak shock-waves in which the variation of temperature, and hence of ω and $\overline{\sigma}$, is small, agreement will be much better,

In order to obtain the density, temperature, etc., from such a solution one can either use the correct shock-wave equations or any of the previously discussed assumptions.

7. Conclusions from the preceding sections

Before proceeding to discuss the inverse problem, namely, for a given density distribution, what errors are introduced in ω, measured from such a distribution, by using the various solutions so far considered, the results obtained in the previous sections are summarized.

These conclusions are:

(1) The assumptions of constant ω and c_{vib} alone do not lead to any serious error in the density distribution.

(2) The constant-enthalpy assumption is valid for strong shock-waves only.

(3) The Blackman approximate solution, (xiii), for ρ, which is partly based on the constant-enthalpy assumption, gives only fair agreement even for strong shock-waves. However, inclusion of the term neglected by Blackman lessens this discrepancy for strong waves (solution (xii)).

(4) The Bethe–Teller assumption is valid for strong shock-waves and is superior to the constant-enthalpy assumption.

(5) The Smiley–Winkler solution, (xv), is excellent for strong shock-waves.

(6) The constant-internal-energy assumption is invalid for all shock-waves.

(7) The relaxation equation can be written in the form

$$\frac{d\sigma}{dt} = \omega(\overline{\sigma}_2 - \sigma)$$

for weak waves only. For strong shock-waves ω should be replaced by $(1+\mu)\omega$.

8. The determination of ω from experimental records

In sections 2 to 6 the merits of the various solutions for predicting the structure of the relaxation region for a given $\omega(p, T)$ have been discussed. The results obtained there can also be used to indicate probable errors in the value of ω which would be obtained if any of these solutions were used for the reverse process of determining ω from experimental results.

For this purpose regard the exact solution (i) (which gives, say, ρ as a function of $\omega_m x/v_m$) as representing the experimental data. Any other solution, say A, can be written in the form

$$f_A(\rho) = \omega_m x/v_m.$$

Obviously ω_m would be determined from such a solution by plotting $f_A(\rho)$ against x and fitting the best straight line. Thus by plotting f_A against f_{expt} an immediate check on the value of ω_m determined from A as compared with the true value is obtained.

Of the analytical solutions discussed only two have actually been used to determine ω from experimental results. These are the Blackman, (xiii), and Smiley–Winkler, (xv), solutions.

For the Blackman approximate solution, (xiii), $f_A \leqslant f_{\text{expt}}$ throughout the relaxation region for all shock-waves. Hence the Blackman value of ω_m will be an underestimate of the true value. In particular for $M_1 = 8{\cdot}0$, $T_1 = 300\,^\circ\text{K}$, in nitrogen it was found that the Blackman value would be roughly 10 % too low. (This is provided that the variation in ω/ω_m is correctly predicted by the expression (2), which appears to be a reasonable assumption from the available experimental data.)

For the weak wave $m_1 = 1{\cdot}15$, $T_1 = 3000\,^\circ\text{K}$, in nitrogen, the Blackman value would be approximately 12 % too low.

These estimates were obtained by plotting f_{Blackman} against f_{expt}. An attempt to draw the best straight line through these points creates the difficulty of how far into the relaxation region one should plot the points. Theoretically the relaxation region stretches from $x = 0$ to ∞ (for a partly dispersed shock-wave). In practice, however, measurements will probably be confined to a distance of, say, $2\omega_m/v_m$, and it was for this region that the best straight line was obtained.

If Blackman had not replaced the term

$$\frac{\rho_2/\rho_a}{1+(\rho_2/\rho_a-1)\exp\left(-\omega_m t c_{pm}/c_{pa}\right)}$$

by unity, i.e. if he had used his original solution, (xii), then the value of ω_m obtained would have been much improved for strong waves. In fact for $M_1 = 8{\cdot}0$, $T_1 = 300^\circ\,\text{K}$, in nitrogen, the value would be only 1 % less than the true value.

It is perhaps worth mentioning that if one applies the same analysis to the analytical solution (ii), which is based on the exact energy equation, then it is found that the value of ω_m which would be obtained from this solution would differ by less than $\frac{1}{2}$ % from the true value for the strong shock-wave.

The second of the two solutions that have been used for evaluating ω is the one due to Smiley & Winkler, (xv). The agreement between this solution and the exact solution (i) was excellent for strong shock-waves. However, as (25) depends on both ω_a and ω_2 it is not possible to use this solution directly to obtain a value of ω from experimental records. To overcome this difficulty Smiley & Winkler assumed that

$$\left|\left(\frac{v}{\omega}\right)_2\left(\frac{\omega}{v}\right)_a - 1\right| \ll 1. \tag{30}$$

According to their results this assumption is permissible for carbon dioxide, the gas investigated by them, over the Mach-number range covered by them, $M_1 = 1{\cdot}5$ to 4. Equation (30) becomes invalid for stronger shock-waves in carbon dioxide. In general this will be true for most gases.

Also, it is doubtful whether it is permissible to use a relaxation equation of the form (1) for carbon dixoide, as presumably more than one relaxation frequency will exist (Greenspan & Blackman 1957). In the following discussion this last point will be ignored.

Smiley & Winkler measured the position at which

$$\frac{\rho_2-\rho}{\rho_2-\rho_a} = \frac{1}{e}.$$

Suppose this position was $x = S_l$, and that

$$\frac{\overline{\sigma}_2 - \sigma}{\overline{\sigma}_2 - \overline{\sigma}_1} = \exp(-l) \quad \text{at} \quad x = S_l. \tag{31}$$

Then from (25) and (31), using the approximation (30), it is found that

$$\left.\begin{aligned} \omega_a &\doteq \frac{v_a}{S_l}\left[\frac{l}{1+\mu} + k\left\{\left(\frac{v}{\omega}\right)_2 \left(\frac{\omega}{v}\right)_a - 1\right\}\right], \\ \text{where} \qquad k &= \frac{l}{1+\mu} - 1 + \exp\left(-\frac{l}{1+\mu}\right). \end{aligned}\right\} \tag{32}$$

From this equation, by first of all ignoring the small term $k\{(v/\omega)_2 (\omega/v)_a - 1\}$, a set of values of ω_a corresponding to p_a and T_a can be found. An empirical curve for ω as a function of T can then be established (assuming that ω is proportional to p). Secondly, by including the small term, obtained by means of the empirical curve, the final corrected value of ω can be found.

Smiley & Winkler assumed that $k = 1/e$, i.e. $l \sim 1 + \mu$. Unfortunately over the range covered by them k varied from 0·28 to 0·18, while $1/e \doteq 0{\cdot}37$. This discrepancy leads to errors in ω of the order of 15 to 20 % for the stronger shock-waves (M_1 of order 4).

The main drawback of the methods of evaluating ω discussed in this section is that they determine only one over-all value of ω per relaxation region. The Blackman method in particular also leads to errors of the order of 10 % in this value. It is obvious that a method whereby local values can be accurately determined is needed.

Such a method was developed by Johannesen in the preceding paper. The amount of numerical work necessary was reduced to a minimum by the use of the Rayleigh-line equations.

The author would like to thank Dr N. H. Johannesen for his advice and criticism during the preparation of this paper, and also Mr H. K. Zienkiewicz for many helpful discussions. The author was in receipt of a grant from the Department of Scientific and Industrial Research during the course of this work.

REFERENCES

Bethe, H. A. & Teller, E. 1941 *Deviations from Thermal Equilibrium in Shock-Waves.* Cornell University.

Blackman, V. H. 1956 *J. Fluid Mech.* **1**, 61.

Broer, L. J. F. 1951 *Appl. Sci. Res.* A, **2**, 447.

Greenspan, W. D. & Blackman, V. H. 1957 *Bull. Amer. Phys. Soc.* **2**, 217.

Griffith, W. C. & Kenney, A. 1957 *J. Fluid Mech.* **3**, 286.

Gunn, J. C. 1946 *Aero Res. Coun., Rep. & Mem.* no. 2338.

Herman, R. & Rubin, R. J. 1959 *Phys. Fluids*, **2**, 547.

Herzfeld, K. F. 1955 Section H of *Thermodynamics and Physics of Matter* (Vol. 1 of *High Speed Aerodynamics and Jet Propulsion*). Princeton University Press.

Johannesen, N. H. 1961 *J. Fluid. Mech.* **10**, 25.

Lighthill, M. J. 1956 Article in *Surveys in Mechanics*, p. 250. Cambridge University Press.

Smiley, E. F. & Winkler, E. H. 1954 *J. Chem. Phys.* **22**, 1018.

A further note on the speed of floating bodies in a stream

By J. R. D. FRANCIS
Imperial College, London

(Received 1 September 1960)

In an earlier contribution (Francis 1956), a report was made of the speed of small solid bodies floating in the upper layers of a free surface stream. The bodies were cylinders of several diameters floating with their axes vertical and ballasted to the same draft. All the floats travelled at the same speed in the long, wide stream which was of constant depth and was strongly sheared, and this speed was the mean speed of the upper layers of the stream. It was pointed out that this result is unexpected, since the solid boundaries of the floats prevent turbulent interchange there, so that the floats are not locked to the stream in the same way as the corresponding volume of turbulent water would be locked. Thus the floats would be expected to travel a little faster than the stream, large diameter floats travelling faster than small floats.

This contradiction led Prof. Hellström to send a photograph of a log of wood floating down a steeply sloping channel. There seems to be a clearly defined bow-wave as the log moves downward relative to the water. The question therefore arises as to the difference between the log and the floats used in the laboratory experiment.

A possible reason for the difference may be that the laboratory floats were never more than 6·3 cm diameter, and were floating in a stream of depth 7·5 cm, and so were still not very large in horizontal extent compared to the depth. The shear in the laboratory channel was developed largely by secondary current systems from regular roughness elements, so that the effective size of the momentum transporting systems was of the order of the depth and was large compared to the floats. Thus these small floats did not materially affect the turbulence in the stream, and so were restrained in the same way as the corresponding mass of water would be restrained.

On the above hypothesis, it seems necessary to have a float which is large in horizontal extent compared to the depth of water under it if the turbulence is to be modified and the float allowed to travel faster than the water. The float should still be appreciably smaller than the width of the channel to avoid side effects, and the channel must have efficient roughness on the bottom in order to give a large shear and so a large surface gradient.

An experiment has been conducted in order to see if very large floats travel faster than smaller ones of the same draft. A steel channel, 76 cm wide and 6·7 m long, had wooden battens 2·5 cm wide by 4 cm high, placed across the bottom, with clear spaces 5·4 cm between them. The channel could be tilted until the bed was parallel to the surface of the water. A discharge of 0·0101 $m^3 sec^{-1}$ was made

to flow down it, and it was found that a slope of 1/161 gave a uniform depth of 3·8 cm above the tops of the wooden battens all along the channel. Three wooden floats were used, the 6·3 and 1·9 cm diameter ones from the 1956 experiments and a new one 30·4 cm diameter. All three were ballasted to float to a 2·5 cm draft, but only an insignificant part projected into the air. Thus the new one was a cylinder of a length/diameter ratio of only 1/12.

The floats were timed over a 3·86 m test length of channel starting 1·9 m from the inlet and ending 1·0 m upstream of the outlet. Any drift in which the float came within 7 cm of the walls of the channel was neglected. The timing was by stopwatch calibrated to 1/100 sec, and the times are shown in table 1.

It will be seen that the largest float travelled faster and more consistently than the smaller floats. The slowest timing of the largest float was faster than the fastest timing of either of the others.

Float diam. (cm.)	30·4	6·3	1·9
Number of successful drifts	20	20	20
Mean time to traverse 3·86 m (sec)	8·01	8·82	8·89
Mean deviation (sec)	± 0·07	± 0·16	± 0·23
Mean speed (m/sec)	0·482	0·438	0·435

TABLE 1. Measured velocities of cylinders 2·5 cm long drifting in a stream 3·8 cm deep.

The largest float was also tested to find at what speed it would travel in still water if towed with a pull of 1/161 of its weight: this proved to be 20·5 cm/sec. Perhaps if this float had modified the turbulence in the water under it so completely that the stress there was zero, then it would travel 20·5 cm/sec faster than small floats. A float to do this would, of course, be nearly infinite in extent; the 30·4 cm diameter float was not large enough to modify all turbulence completely as it passed over so it only travelled some 4 cm/sec faster than the mean speed of the layer of water in which it floated. In fact, it travelled at approximately 1 cm/sec faster than the surface speed of the water, as shown by the relative motion of aluminium dust sprinkled on the water.

Another experiment carried out in the same channel confirms this observation. Cylindrical cup-like floats were made from 1 mm thick Perspex (methyl methycrylate) sheet, having only one end of the cylinder closed by a circular disk. One float was 30·4 cm diameter and 2·5 cm long, and two others were 2·5 cm diameter and 2·5 cm long. The large float was arranged to float full of water with its solid Perspex diaphragm uppermost and level with the water surface, buoyancy being provided by small pieces of a foam plastic fixed to the rim; the water within the float was therefore free to interchange with the rest of the water in the channel. The speed of this float was compared with that of the previous 30·4 cm float, made of wood and ballasted to the same depth. The two smaller Perspex floats were ballasted to float to the same 2·5 cm draft but one was arranged to float with the diaphragm uppermost, and the other with its diaphragm below. The former allowed interchange of fluid within it, and the latter did not allow interchange.

The flow in the 76 cm wide channel was now 0·0171 $m^3 sec^{-1}$ and a slope of 1:182 was found to give a uniform depth of 5·2 cm above the wooden battens. The floats were timed over a 2·40 m test length, and the times of ten successful drifts were taken of each float. These results are shown in table 2.

It is clear that although the solid wooden float *A* travels faster than the large open bottomed Perspex float *B*, both the two small floats travel at the same speed. Thus it appears that the solid lower end of the small float *C* is not sufficiently large to affect the turbulent fluctuations responsible for the interchange of momentum

	A	*B*	*C*	*D*
Float diam. (cm)	30·4	30·4	2·5	2·5
Type of float	Wood	Perspex diaph. uppermost	Perspex diaph. downward	Perspex diaph. uppermost
No. of successful drifts	10	10	10	10
Mean time to traverse 2·40 m (sec)	3·84	4·51	4·47	4·46
Mean speed m/sec	0·625	0·532	0·538	0·537

TABLE 2. Measured velocities of cylinders drifting in a 5·2 cm depth stream.

at these levels in the stream. So floats *C* and *D*, one allowing interchange by small-scale fluctuations only and the other allowing no interchange at all, both travel at the same speed with neither float modifying the large-scale fluctuations. Floats *A* and *B* travel at different speeds because *B* can accept large-scale fluctuations and *A* cannot. So *A* modifies the large fluctuations, while *B* does not and so moves at the same speed as *C* and *D*.

Thus it appears that floats can only travel faster than the water they sample if they are large compared to the scale of the turbulent fluctuations transporting momentum downwards in the stream. The log of Prof. Hellström's photograph is large compared to the depth of water and so can travel relative to the stream. Prandtl's (1952, p. 179) statement that ships drifting in rivers 'hurry ahead of the water' may therefore be true only if an important qualification is made: that the ship is of large horizontal extent compared to the depth of water under it, so that it greatly modifies the flow in its neighbourhood.

The experiments described above were carried out in the Civil Engineering Laboratories of Imperial College.

REFERENCES

FRANICS, J. R. D. 1956 *J. Fluid Mech.* **1**, 517.

PRANDTL, L. 1952 *Essentials of Fluid Dynamics.* London: Blackie.

Experiments on power generation from a moving plasma

By H. J. PAIN AND P. R. SMY*

Physics Department, Imperial College of Science and Technology, London, S.W.7

(Received 19 July 1960)

Electrical power of 0·32 MW has been extracted for a period of 100 μsec from a plasma of shock-ionized argon travelling at 4×10^5 cm per sec through a magnetic field of 10,000 G. Currents of more than 10,000 amp are drawn and the resulting modification of the applied field is considered.

Maximum power is obtained when the external load is matched to the plasma generator which has an internal impedance equivalent to its own electrical resistance in series with a resistance arising from its behaviour as a compressible fluid.

Values of the electrical conductivity of the plasma obtained in these experiments (about 3×10^3 mho per metre) show that the plasma resistance is controlled by electron motion and these values are in good agreement with those found by other methods.

Introduction

Experiments on the generation of electrical power by converting the energy of a fast-moving electrically conducting fluid are now being carried out in several laboratories. Pilot plants now operating employ the continuous flow system where the gas has a temperature in the region of 2000 °K and its conducting properties are enhanced by the introduction of easily ionized substances such as potassium. A report on some of the experiments at Avco, U.S.A., has been made by Rosa (1960). A theoretical analysis of the problem has recently appeared in this journal (Neuringer 1960).

The principle of all of these experiments is the same. A fast-moving plasma crosses a region of magnetic field the lines of which are transverse to its flow direction. If the flow velocity is u cm per sec and the field strength is B G an electric field $10^{-8}(\mathbf{u} \times \mathbf{B})$ V per cm is developed in the plasma. Currents of density $j = \sigma uB$, where σ is the electrical conductivity of the plasma, will flow when a short-circuit path is available. Such a path is provided by completing an external circuit via a pair of electrodes whose faces are parallel to the flow direction and to the lines of the magnetic field (figure 1).

In the experiments reported here the process is essentially a pulsed system and not a continuous flow method. Power is extracted from the plasma for periods of about 100 μsec which is the duration of plasma flow through the electrode and the magnetic field system. The flow velocity is about 4×10^5 cm

* Now at the Physics Department, University of British Columbia, Vancouver.

per sec and the field strength is 10,000 G so that the electric field across the plasma is about 40 V per cm.

Earlier experiments of a similar type were presented in a thesis by Brogan (1956) who considered in some detail the resistive effect of the cold boundary layer between the hot plasma and the cold electrodes. In the present experiments, boundary-layer effects appear to intrude only when the currents drawn

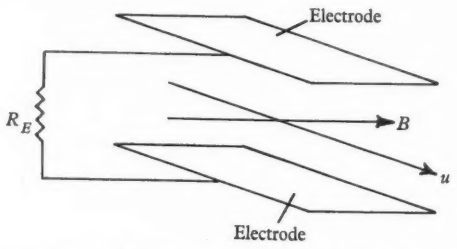

FIGURE 1. Disposition of the electrodes with respect to the plasma flow (velocity u) and the magnetic field (B). An electric field $\mathbf{u} \times \mathbf{B}$ generates a current which flows through the circuit closed by the external load R_E.

fall below 100 amp per cm^2 of electrode surface. At larger currents the resistance presented by the plasma between the electrodes leads to a value of the electrical conductivity which is in good agreement with results obtained by other methods.

This electrical conductivity is controlled by the motion of the electrons. In a recently published paper by Sakuntala, von Engel & Fowler (1960) a similar experimental arrangement is described; this yields values of the electrical conductivity which are governed by ionic mobility. The discussion at the end of this paper suggests that there is no discrepancy between these results, but that the significant conductivity depends upon the magnitude of the current flowing through the plasma.

Experimental conditions

The plasma is generated as a column of shock-ionized argon in a combustion-driven shock-tube, details of which are given in Pain & Smy (1960*a*). The length of the plasma column varies between 5 and 50 cm depending upon the initial conditions in the shock tube. The plasma has a velocity of 4×10^5 cm per sec, a temperature near 12,000 °K and a degree of ionization, α, of about 20 %.

It passes through a Pyrex glass tube 30 cm long, of 5 cm internal diameter and at the mid-point of which are located the magnetic field and the electrode system. The magnetic field is transverse to the plasma flow and is formed by two spirally wound coils arranged as a Helmholtz pair, one on each side of the shock tube.

Pulsed magnetic fields of more than 10,000 G, uniform across the shock tube, are developed when a condenser bank of 900 μF, rated at 5 kV, is discharged through the coils. The period of discharge is approximately 1 msec and the plasma is timed to pass through the region when the field is at its maximum. The flow duration is much less than 1 msec so that a constant field is seen by the plasma.

The electrode system is formed by a pair of conductors set in the walls of the Pyrex tube and machined flush with the inner surface.

The directions of plasma flow, of magnetic field and of the normal to the two electrode faces form a set of three mutually perpendicular axes as shown in figure 1.

Small electrode system

The first pair of electrodes was designed to carry out a preliminary investigation on the response of such systems. Each electrode was a 2 cm length of copper rod of circular cross-section 1 cm in diameter.

External resistances varying from 100 KΩ to 0·01 Ω were wired in symmetric array close to the glass walls of the tube to keep the external inductance to a

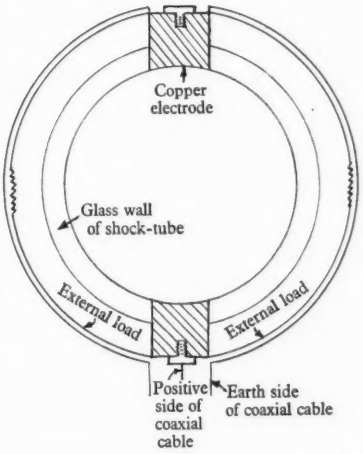

FIGURE 2. The small copper electrodes are inserted as studs in the glass walls of the shock-tube. The external load resistance is arranged symmetrically around the tube, very close to the tube wall and to the lead which connects one electrode to the earth side of a coaxial cable. The positive side of the cable feeds the signal from the other electrode to the C.R.O.

minimum. Electrical pick-up was also minimized by the voltage-measuring device shown in figure 2. The voltage developed across the external resistance R_E was recorded on a cathode-ray oscilloscope and typical traces obtained with initial shock-tube argon pressures of 10, 1 and 0·1 mm of mercury are shown in figure 3.

The recorded voltage allows the induced current and the power dissipated in the external load R_E to be calculated and the electrical conductivity of the plasma to be found. The small external resistances used in this experiment were made from resistance wire. The electrical energy dissipated in these resistances caused a negligible change in their value and their dimensions were such that the ohmic resistance was independent of frequency over the range of frequencies involved in the induced current pulse.

If R_p is the resistance of the plasma between the electrodes, R_E the external resistance, V_E the measured voltage across R_E, d the electrode separation and B the magnetic field strength, then the equivalent circuit yields the relation

$$V_E = uBdR_E/(R_E+R_p),$$

that is

$$\frac{1}{V_E} = \frac{1}{uBd} + \frac{1}{uBd}\frac{R_p}{R_E}. \tag{1}$$

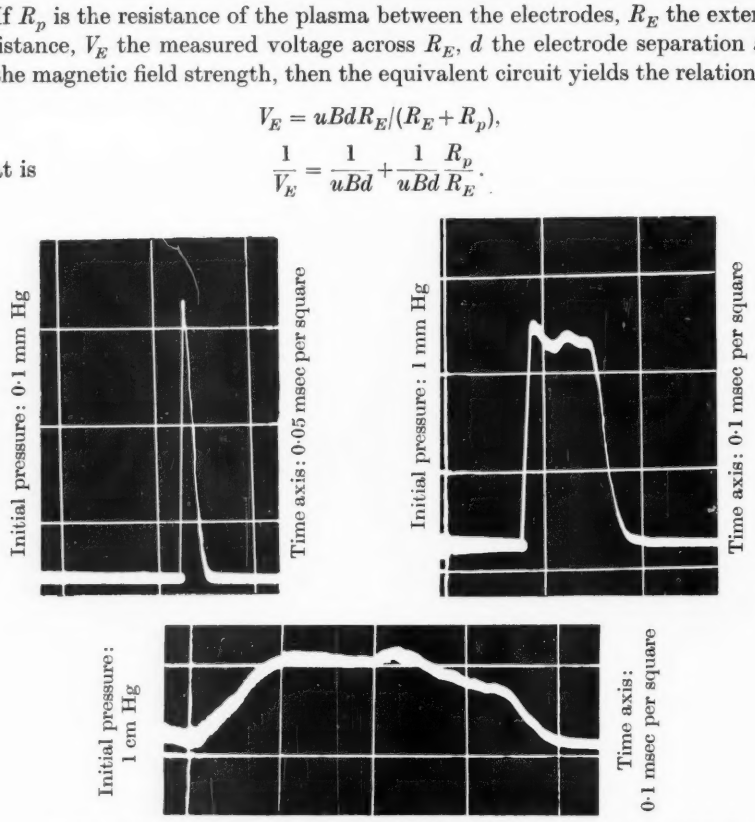
Initial pressure: 0·1 mm Hg
Time axis: 0·05 msec per square
Initial pressure: 1 mm Hg
Time axis: 0·1 msec per square
Initial pressure: 1 cm Hg
Time axis: 0·1 msec per square

FIGURE 3. Typical voltage traces obtained with the small electrodes for initial channel pressures of 1 cm, 1 mm, and 0·1 mm of mercury. The rise and decay of the 1 cm trace is attributed to the variation of the applied field of half-period equal to the flow duration.

Except where stated all experiments were carried out with an initial argon pressure of 1 mm of mercury in the shock-tube.

The plasma resistance R_p is not simply $d/(A\sigma)$, where A is the electrode area and σ is the electrical conductivity of the plasma. This formula is valid only when $A \gg d^2$. In the present case $A \ll d^2$, so that electrode end-effects must be considered.

The effective resistance presented by the plasma between the electrodes was found by filling the space between the electrodes with a salt solution of known concentration and electrical conductivity σ'. The resistance R' of this solution between the electrodes was then found using an alternating current source and the relation $R_p = R'\sigma'/\sigma$ effectively determines R_p. Keeping the plasma flow conditions constant a series of measurements of V_E was made for different values of R_E. If equation (1) were valid then the graph of $1/V_E$ *vs* $1/R_E$ should be a straight line with a slope $R_p/(uBd)$. For values of R_E less than 1 Ω there is a gradual departure from the linear relationship as shown in figure 4. For R_E

greater than 1 Ω the behaviour was more complex and this is discussed in more detail in a later section. For this reason the slope of the curve in the vicinity of $R_E = 1\,\Omega$ was used to determine R_p.

The graph in figure 4 curves upwards and this may be explained qualitatively in terms of the plasma being slowed down by the braking pressure $P_z = \int (\mathbf{j} \times \mathbf{B})_z \, dz$, where z is the co-ordinate in the direction of flow and j is the induced current density. The integral is carried out over the extent of the interaction region. This braking pressure is largest at low external resistances and high induced current densities.

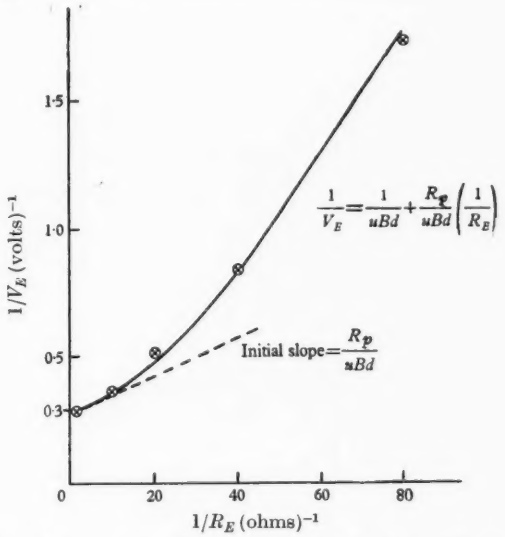

FIGURE 4. Reciprocal measured voltage V_E *vs* reciprocal external resistance R_E, for $R_E < 1\,\Omega$. The change of slope is attributed to the variation of σu, where σ is the electrical conductivity of the plasma and u is the flow velocity. For R_E close to 1 Ω the change of σu is negligible and the initial slope of the graph enables the values of σ to be calculated. Measurements recorded on this graph were made with an initial argon pressure of 1 mm of mercury.

If the graph of equation (1) were linear its slope of $R_p/(uBd)$ would equal $R'\sigma'/(\sigma uBd)$ which involves the product σu.

When the plasma slows down under the influence of the braking pressure its thermal energy (and hence its electrical conductivity) is increased at the expense of its kinetic energy. In practice the product σu is not invariant but is proportional to u^n, where n is positive and less than unity. This may be seen from the following argument, which assumes a steady-state condition with small Joule dissipation.

Mass conservation requires ρu to be constant, where ρ is the plasma density. This, with the adiabatic condition $p/\rho^\gamma = \text{const.}$ and the equation of state $p/\rho = RT$, yields $RTu^{\gamma-1} = \text{const.}$ If the temperature dependence of the conductivity follows the $T^{\frac{3}{2}}$ law, then $\sigma u \propto u^{\frac{1}{2}(5-3\gamma)}$, i.e. σu is a constant for $\gamma = \frac{5}{3}$. However, the value of γ for the plasma is nearer 1·1 than 1·66—Patrick & Brogan (1959)—and $\sigma u \propto u^{0.85}$.

As $1/R_E \to \infty$ the slope of the graph in figure 4 tends to about twice the value it has as $1/R_E \to 0$, i.e. at large current densities the observed value of σu tends to half its original value upon entering the electrode system. The current densities flowing through the small electrodes are insufficient to modify the applied field B seriously, but in the case of the large electrodes the applied field is distorted; this factor is considered later.

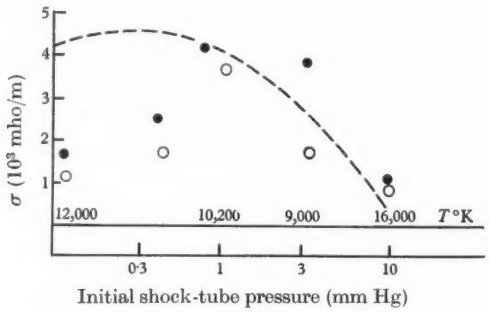

FIGURE 5. Values of the electrical conductivity of the plasma for different initial conditions in the shock-tube. ○, Experimental results; ●, results found by Pain & Smy (1960*b*). The dotted curve shows the theoretical values computed by de Leeuw (1958) using the method of Lin *et al.* (1955).

The slope of the graph as $1/R_E \to 0$, i.e. at low current densities, allows the value of the electrical conductivity of the plasma to be calculated. Measurements at low current densities were made for different plasma flow conditions, that is for different initial shock-tube pressures, and the electrical conductivity of the plasma was found in each case. These values are shown in figure 5 where the dotted curve shows the theoretical values derived by de Leeuw (1958) using the theory of Spitzer & Harm modified by Lin, Resler & Kantrowitz (1955).

These values agree quite well with results obtained by Lin *et al.* (1955) and Pain & Smy (1960*b*) using other experimental techniques.

The possibility that the external resistance is short circuited by a return current path in the plasma or the boundary layer may be discounted for the following reasons.

The magnetic field has a value of more than 5000 G over a region of 10 cm in the flow direction and a value of 10,000 G over a length of 7 cm. The electric field $\mathbf{u} \times \mathbf{B}$ is therefore unidirectional for some distance on either side of the electrodes and any current path through the plasma would be long enough to exceed the resistance of the external load. The resistance of a path through the cold boundary layer is also greater than the external load.

Large electrode system

The small pair of copper electrodes was replaced by a large pair of brass electrodes 7 cm long and 4 cm arc. The cross-section of these electrodes is shown in figure 6 which demonstrates this arrangement as the best approximation, using a circular cross-section, to the ideal case of a square cross-section with one pair

of opposite faces forming parallel electrodes. When the shock tube has a square cross-section the problem may be treated by one-dimensional analysis.

The pulsed magnetic field perpendicular to the flow has a frequency which requires the shielding effect of the brass electrodes to be considered. Search coil measurements showed that the change in the total flux across the shock-tube in the vicinity of the electrodes was less than 5 %.

The external resistances used with these electrodes varied from 0·01 to 0·00025 Ω and were constructed from resistance wire or copper strip. The dimen-

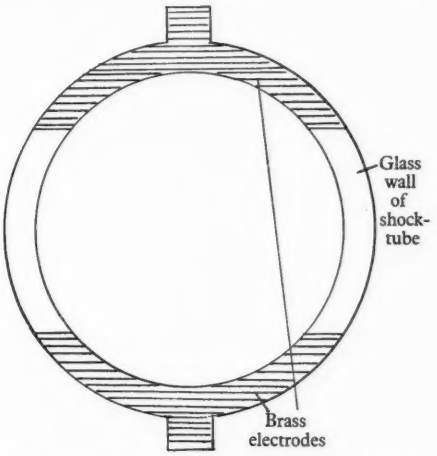

FIGURE 6. Cross-section of the large brass electrodes of 7 cm length and 4 cm arc. The external resistance arrangement is the same as in figure 2.

sions of these resistances were chosen to reduce temperature change and skin effects to a minimum.

The resistance of the external load was found by measuring the voltage across the resistances when it was conducting 10 amp and all resistance values were measured *in situ*.

No trouble with contact resistances was experienced when the metal contacts were clean and held together under strong pressure. The voltage V_E across the external load was measured in the same way as with the small electrode system.

Despite great care with the arrangement of the external load the resulting voltage wave-form showed considerable pick-up because of the large induced current flowing in the external load.

The ohmic voltage was found from the oscilloscope trace by taking the average voltage over the duration of the wave-form, i.e. the ohmic voltage V_0 is given by $\int V\,dt/\tau$, where τ is the pulse duration. The superimposed pick-up voltage V_p is thus eliminated because its integral over all time,

$$\int V_p\,dt \propto \int_{t=0}^{t=\infty} \frac{d\mathbf{i}}{dt}\,dt,$$

is zero.

The voltage oscillograms were reproducible from run to run. The magnetic field value was 10,000 G and all measurements were made with an initial pressure of argon in the shock-tube equal to 1 mm of mercury.

Measurements with the large electrode system

Given an electrode area of 28 cm² and a current density $j = \sigma uB$, then the maximum total current I_m as $R_E \to 0$ should be $28\sigma uB$ if σu is considered invariant. In table 1 the measured value of I_m is seen to be 14,000 amp so that the average value $\overline{\sigma u} = 5 \times 10^6$ m.k.s. units.

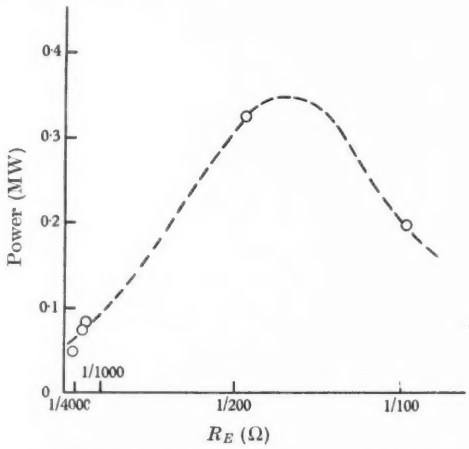

FIGURE 7. Power extracted from the plasma *vs* external load. The maximum power extracted occurs for a value of R_E of about 1/150 Ω. This matches the internal impedance of the plasma generator when it includes a resistance which arises from its behaviour as a compressible fluid.

The plasma flow conditions upon entering the electrode system yield $\sigma = 3 \times 10^3$ mho per m and $u = 4 \times 10^3$ m per sec so that the average value $\overline{\sigma u}$ is about half the original value upon entry and σu is not invariant.

The reduction of the flow velocity may be seen as a decrease in the voltage available for power generation. This may be expressed in terms of an extra resistance in series with the internal impedance R_p of the plasma generator, which represents the electrical impedance developed when the plasma is slowed down by the interaction between the induced current and the applied field. This extra resistance is a non-linear term which depends upon the strength of interaction, so that the plasma generator may have a variable internal impedance.

Writing the extra resistance as R, then as $R_E \to 0$,

$$\frac{R_p}{R+R_p} = \left\{\begin{matrix}\overline{\sigma u}\ \text{(measured)} \\ \overline{\sigma u}\ \text{(calculated)}\end{matrix}\right\} \sim \tfrac{1}{2},$$

so that

$$R \sim R_p = \frac{d}{A\sigma} = \frac{1}{300}\,\Omega.$$

In figure 7, where power extraction is plotted against the external load R_E, the maximum of the curve occurs in the region $R_E \sim 1/150\ \Omega$, where the external load matches the total impedance of the generator.

The value of the current is found directly from the voltage trace and an error of up to 15 % is probable.

R_E (Ω)	I (amp)	I^2R (W $\times 10^5$)
1/100	4,500	2
1/200	8,000	3·2
1/1800	11,400	0·7
1/2000	10,000	0·5
1/4000	14,000	0·49

TABLE 1

The arguments against short circuiting through the plasma are similar to those for the small electrodes. In this case, moreover, the existence of two currents of about 10,000 amp flowing in opposite directions in the plasma would generate interaction forces with the magnetic field acting in reverse directions. This would break up the plasma flow, an effect which has not been observed.

Modification of applied field by induced currents

When induced currents of the order of 10^4 amp flow, the induced field in the plasma may be as large as the applied field of 10,000 G and the distribution of the applied field is modified. In figure 8, z is the direction of plasma flow, the applied field is constant and in the y-direction, and the induced current is in the negative x-direction, its density j_x being equal to σuB. The applied field is B_y/μ_0 and the induced field in the y-direction is B'/μ_0 so that the total field $B/\mu_0 = (B' + B_y)/\mu_0$; μ_0 is the permeability of free space. B' opposes B_y at z_1 in figure 8 and reinforces it at z_2. We have that

$$\mu_0 j_x = \frac{\partial B'}{\partial z} = \frac{\partial B}{\partial z}, \quad \text{since } B_y \text{ is constant}$$

and

$$\sigma u \mu_0 B = \frac{\partial B}{\partial z}.$$

Now $\int \mathbf{B}.d\mathbf{l} = \mu_0 I$, where the line integral is taken around the shaded area in figure 8 and I is the total current flowing across this area so that

$$B(z_2) - B(z_1) = \mu_0 j,$$

where j is the induced current density per cm^2 along the y-axis and $B(z_2)$ is the value of the field in the y-direction at z_2. By symmetry the induced field B' is equal and opposite on either side of the current sheet so that

$$B(z_1) + B(z_2) = 2B_y.$$

The braking pressure

$$P_z = \int_{z_1}^{z_2} (\mathbf{j} \times \mathbf{B})_z dz$$

and from

$$dz = dB/\mu_0 j \tag{2}$$

we get

$$P_z = \tfrac{1}{2}[B^2(z_2) - B^2(z_1)]/\mu_0 = \tfrac{1}{2}[B(z_2) - B(z_1)]\,[B(z_2) + B(z_1)]/\mu_0 = IB_y.$$

When σu is invariant between z_1 and z_2 then (2) integrates to give

$$B(z_2) = B(z_1)\, e^{\mu_0 u\sigma(z_2 - z_1)} = B(z_1)\, e^{z/10},$$

when the appropriate values are inserted and z is measured in cm. The applied field is thus modified as shown in figure 9.

When $B(z_2)$ remains finite the limit $\mu_0 u\sigma z \to \infty$ yields $B(z_1) \to 0$, so that

$$B(z_2) = (2B_y - B(z_1)) \to 2B_y \quad \text{and} \quad P_z \to 2B_y^2/\mu_0,$$

which is the maximum pressure that the magnetic field can exert upon the plasma. When z tends to ∞ the original expression $P_z = \sigma u B_y^2 z$ also tends to ∞.

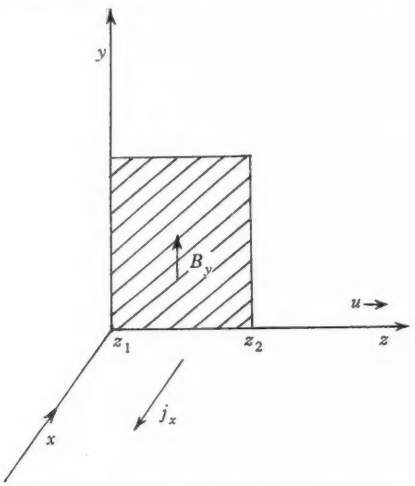

FIGURE 8. When the plasma flow velocity u is in the z-direction, and the applied field B_y is in the y-direction, the induced current j_x is in the x-direction. By considering $\int \mathbf{B}.d\mathbf{l}$ around the contour of the shaded area, the modification of B_y when j_x is large is shown not to affect the overall braking pressure, $\int_{z_1}^{z_2} j_x \times B_y dz$, by a large amount ($z_1$ and z_2 are the limits of the magnetic field region).

FIGURE 9. The applied field B_y extends from z_1 to z_2. When the total induced current is about 10,000 amp, the applied field is modified from (*a*) to (*b*).

Writing $\sigma u B_y^2 z$ as $(P_z)_0$ the ratio of the two expressions for P_z then becomes

$$\frac{P_z}{(P_z)_0} = \frac{[B(z_2)-B(z_1)]\,[B(z_2)+B(z_1)]}{2\mu_0 \sigma u B_y^2 z},$$

which, for $2B_y = B(z_1)+B(z_2)$, becomes

$$\frac{2}{\mu_0 \sigma u z}\left\{\frac{B(z_2)-B(z_1)}{B(z_2)+B(z_1)}\right\}.$$

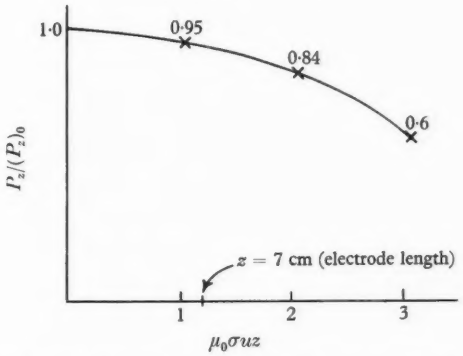

FIGURE 10. $(P_z)/(P_z)_0$ *vs* $\mu_0 \sigma u z$, when σu is considered invariant. P_z is the braking pressure developed when the magnetic field is modified by large induced currents, and $(P_z)_0$ is the braking pressure in the absence of modification. The modification for $z = 7$ cm, the length of the large electrodes, is seen to be about 5 %.

When σu is invariant, this ratio is equal to

$$\frac{2}{\mu_0 \sigma u z}\left\{\frac{e^{\mu_0 \sigma u z}-1}{e^{\mu_0 \sigma u z}+1}\right\}.$$

This expression is plotted in figure 10 with $P_z/(P_z)_0$ as the ordinate and $\mu_0 u \sigma z$ as the abscissa. With the appropriate values of $z = 7$ cm (length of large electrode) and $\mu_0 u \sigma = 0{\cdot}2$ it is seen that $P_z \sim (P_z)_0$ and that current modification of the applied field does not appreciably alter the overall braking pressure.

It should be noted that $\sigma \mu_0 u z$ is the magnetic Reynolds number so that figure 10 shows the explicit dependence upon this parameter of the reduction in braking pressure when the field is modified by induced currents.

The modification of the applied field which leads to a maximum braking pressure of $2B_y^2/\mu_0$ instead of the usual magnetohydrostatic pressure $B_y^2/2\mu_0$ also implies a corresponding change in the Lundquist number which depends on the field value B.

The significance of these modifications is greatest when the plasma is an infinite sheet of thickness $(z_2 - z_1)$ and the induced flux remains within the sheet.

Discussion

The apparent absence of boundary-layer effects when large currents flow is a feature of the experiments with the small electrodes. The Joule dissipation of a large current rapidly heats a cold boundary layer and reduces its resistance.

The various mechanisms by which a current is permitted to flow through this layer are fully discussed by Brogan (1956).

When the external load is more than 1 Ω, currents of less than 100 amp per cm² are drawn and the resistance through the plasma between the two electrodes is much greater than the plasma resistance alone and must include a cold boundary-layer resistance. A typical oscilloscope trace for a low current through an external load is shown in figure 11 to consist of an initial voltage pulse, much smaller than that expected in the absence of a cold boundary layer, on which is superimposed a series of peaks of very short duration which may be associated with a temporary local breakdown followed by a rapid recovery.

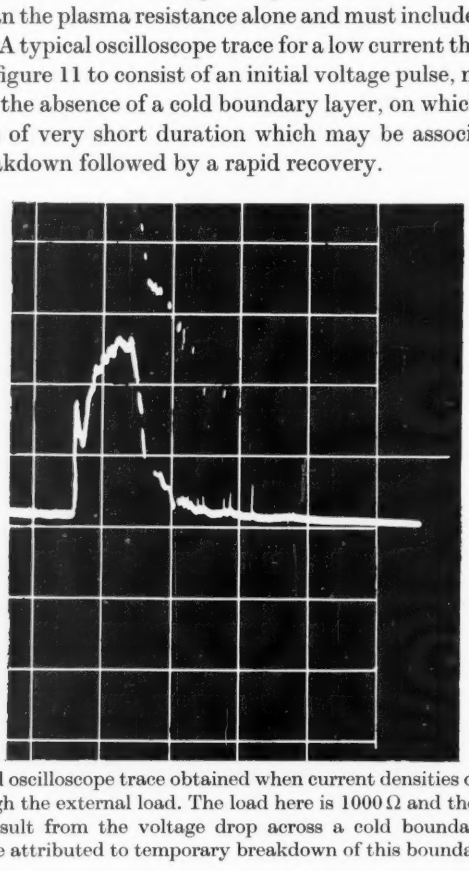

FIGURE 11. Typical oscilloscope trace obtained when current densities of less than 100 amp per cm² flow through the external load. The load here is 1000 Ω and the low initial voltage is considered to result from the voltage drop across a cold boundary-layer resistance. The sharp peaks are attributed to temporary breakdown of this boundary-layer resistance.

The recording of such a trace with large external loads supports the argument that no short circuiting occurs within the plasma, for short circuiting would make the shape of the trace independent of the value of the external load.

In the experiments with the large electrodes the maximum power is extracted when the external load matches the internal impedance of the generator which includes the resistance arising from the compressible nature of the plasma. This energy, 0·3 MW for 100 μsec represents about 30 % of the kinetic energy of plasma flow and must be the difference between the total energy content of the plasma at the entrance to and at the exit from the electrode system apart from heat losses to the electrodes.

Sakuntala *et al.* (1960) have used a similar experimental arrangement with hydrogen as a working fluid. Their measurements lead to a much lower value of

the electrical conductivity than that expected from the motion of the electrons, and it is shown that the much lower mobility of the ions is the limiting mechanism in the flow of current. This may be true when the current is small, but need not hold when the current is large, as is shown in the following argument based on work which is to be published by J. E. Lucas of this department. Lucas has examined both theoretically and experimentally the redistribution of the electric field between two electrodes in a plasma when current is drawn. For small currents the electric field falls below the applied field $E_0 = uB$ at the anode and exceeds E_0 at the cathode because of the drift of positive ions. However, except at the anode, the field is everywhere of the order of E_0. This case is shown in figure 12 (*a*) where the current is controlled by the ions, their velocity being $v = \mu^+ E_0$, where μ^+ is the ion mobility. The condition to be satisfied is that the integral $\int E\,dl$ under the curve must be equal to $E_0 d$, where d is the electrode separation.

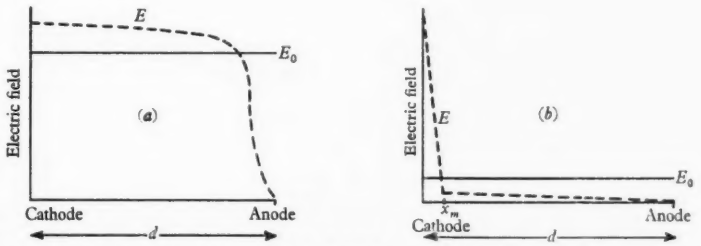

FIGURE 12. Redistribution of the electric field between the electrodes when current flows through the plasma. Case (*a*) is for a small current where the field is everywhere of the order of $E_0 = uB$ except at the anode.

Case (*b*) is for large currents where the field may be nearly zero everywhere except near the cathode where it is very large.

In both cases the condition $\int E\,dl = E_0 d$ must be satisfied, where d is the electrode separation.

When large currents flow the field distribution is much more severely distorted as shown in figure 12 (*b*). The field everywhere falls far below E_0 except in the vicinity of the cathode where it may become very large.

From Poisson's equation the field is given by

$$\frac{dE}{dx} = \frac{ne}{\epsilon_0} = \frac{I}{Av\epsilon_0},$$

where n is the ion number density, e the charge per particle, ϵ_0 the free space permittivity, I the total current, A the electrode area, and v the ion velocity.

This yields

$$\mu^+ E \frac{dE}{dx} = \frac{I}{A\epsilon_0}, \quad \text{or} \quad \frac{d}{dx}(\tfrac{1}{2}E^2) = \frac{I}{A\mu^+\epsilon_0}.$$

This gives on integration

$$[\tfrac{1}{2}E^2]_{E_{max}}^{E_x} = \left[\frac{Ix}{A\mu^+\epsilon_0}\right]_0^x, \quad \text{or} \quad E_{max}{}^2 - E_x^2 = \frac{2Ix}{A\mu^+\epsilon_0},$$

where x lies between 0 and d.

If x_m denotes that position where E becomes negligible then it follows (from $\int E\,dl = E_0 d$) that $\frac{1}{2}E_{\max} x_m = E_0 d$, to a close approximation, and

$$E_{\max}{}^2 = \frac{2I}{A\mu^+\epsilon_0}\frac{2E_0 d}{E_{\max}} \quad \text{or} \quad E_{\max}{}^3 = \frac{4IE_0 d}{A\mu^+\epsilon_0}.$$

Inserting the appropriate values for the present experiment of $E_0 d = 200$ V, $I = 10{,}000$ amp and $A = 28$ cm^2 gives $E_{\max} \doteqdot 10^5$ V per cm. This field is sufficient to accelerate ions to a high velocity and, as they strike the cathode, electron emission will follow. For argon the ratio of electron mobility to ion mobility is about 300 and it may be shown that the ion velocity at the cathode is an order of magnitude larger than the electron velocity at the anode. Thus, when large currents are drawn, the electron mobility is the controlling mechanism and the electron conductivity of the plasma is the significant factor.

The authors wish to thank Professor P. M. S. Blackett for his encouragement in this work and Dr R. Latham and other members of the High Temperature Physics Group who have helped them. In particular, this work owes much to Mr A. H. Chapman who operated the shock-tube and constructed the electrode and magnetic field systems. One of us (P. R. S.) receives a maintenance grant from D.S.I.R.

REFERENCES

Brogan, T. R. 1956 Thesis, Cornell University. The Conduction of Electric Current to Cold Electrodes in Shock Tubes.

de Leeuw, J. H. 1958 *University of Toronto Institute of Aerophysics Report*, no. 49.

Lin, S. C., Resler, E. L. & Kantrowitz, A. 1955 *J. Appl. Phys.* **26**, 95.

Neuringer, J. L. 1960 *J. Fluid Mech.* **7**, 287.

Pain, H. J. & Smy, P. R. 1960*a* *Proc. Phys. Soc.* **76**, 849.

Pain, H. J. & Smy, P. R. 1960*b* *J. Fluid Mech.* **9**, 390.

Patrick, R. M. & Brogan, T. 1959 *J. Fluid Mech.* **5**, 289.

Rosa, R. J. 1960 *J. Appl. Phys.* **31**, 735.

Sakuntala, M., von Engel, A. & Fowler, R. G. 1960 *Phys. Rev.* **118**, 1459.

Gaskinetics and gasdynamics of orifice flow

By HANS W. LIEPMANN

California Institute of Technology, Pasadena, California

(Received 4 October 1960)

The paper gives the result of a study on the efflux of gases through circular apertures. The problem is considered as an example of a transition from the gasdynamic to the gaskinetic régime.

The mass flow of helium, argon and nitrogen was measured for a range of upstream pressures corresponding to (mean free path)/(aperture diameter) from about 50 to 5×10^{-3}; within this range the transition from molecular effusion to inviscid, transonic flow takes place. The theory for the two asymptotic limits is discussed and first-order corrections to the free molecular and inviscid limit formulae are given.

1. Introduction

Consider steady gas flow from one large container to another through a circular aperture of negligible lip thickness. The symbols p_1, ρ_1, T_1, etc., denote the variables of state in the upstream container, and p_2, ρ_2, T_2 the corresponding variables downstream, both measured at a sufficient distance from the aperture.

This is called 'orifice' flow here. For upstream densities such that the mean free path Λ is large compared to the aperture diameter D, the flow corresponds to Knudsen's 'effusion' (Knudsen 1909); for sufficiently high pressure the flow approaches the potential problem of outflow of a fluid from a vessel, first studied by Kirchhoff for incompressible flow, and by Chaplygin (1904), Frankl (1947) and Guderley (1957) for compressible-fluid flow.

The study of orifice flow presented here has its origin in an attempt to find one simple and experimentally realizable flow problem for which both the Euler limit at infinite Reynolds number and the free molecular limit at zero Reynolds number are well defined and, at least in principle, theoretically understood, if not worked out in detail. In studying such a problem it is hoped to make some step in the direction of a better understanding of the transition from gasdynamic to gaskinetic flow. There do not exist many flow problems which fall within this category. Usually the free molecular limit involves unknown or only empirically known surface interaction parameters like slip and accommodation coefficients.

In this paper we will discuss only the mass flow $\dot{m}$ through a circular aperture for the case of large pressure ratios across it. To define the range of parameters and the relation of the present investigation to Knudsen's classical work and the various theoretical and experimental studies of orifice flow at high Reynolds number, it is most convenient to present all possible orifice flow régimes in a

suitably defined Mach number *vs* Reynolds number plane. From the six variables $p_1, \rho_1, T_1, p_2, \rho_2, T_2$, one can eliminate three by the equation of state and by simple thermodynamics, which yields $T_1 = T_2$ since we deal with the Joule–Thomson process of a perfect gas. Choosing the three variables p_1, ρ_1 and p_2, we can define a characteristic velocity W by

$$W = \left(\frac{p_1 - p_2}{\rho_1}\right)^{\frac{1}{2}},$$

and consequently Mach and Reynolds numbers by

$$Ma = \frac{W}{(p_1/\rho_1)^{\frac{1}{2}}} = \left(\frac{p_1 - p_2}{p_1}\right)^{\frac{1}{2}},$$

$$Re = \frac{WD}{\nu_1} = \frac{D}{\nu_1}\left(\frac{p_1 - p_2}{\rho_1}\right)^{\frac{1}{2}}.$$

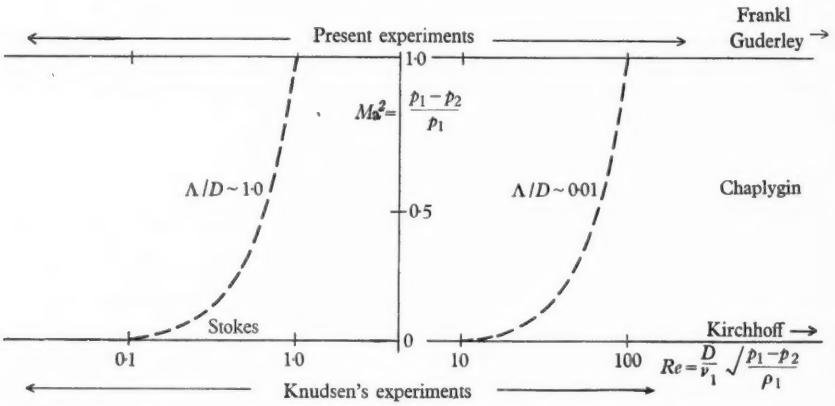

FIGURE 1. Plane of (Mach number)^2 *vs* Reynolds number for orifice flow.

Here ν_1 is the kinematic viscosity of the gas evaluated at the equilibrium upstream conditions. It is often more convenient to use Ma and Re rather than the Knudsen number Λ/D because one does not have to adopt a specific Λ as related to ν and because Ma and Re are better suited to the high-pressure limit; however, one may of course replace Ma/Re by Λ/D if one prefers this notation.

Ma and Re can be chosen independently in the experimental arrangement. In a (Ma^2, Re)-plane (figure 1), all possible (adiabatic) orifice flows are contained within a strip $0 \leqslant Ma^2 \leqslant 1$; $0 \leqslant Re < \infty$. $Re = 0$ is the free molecular limit, $Re = \infty$ the Euler limit. Two paths between these limits are particularly distinct. For pressure ratios near unity, i.e. $p_1/p_2 \doteqdot 1$ and thus $Ma \doteqdot 0$, one passes from Knudsen flow at $Re = 0$ through a Stokes-type régime to Kirchhoff flow at $Re = \infty$. For large pressure ratios, i.e. $p_1/p_2 \gg 1$, $Ma \doteqdot 1$, one passes from free molecular flow through a region of viscous compressible fluid flow to transonic orifice flow at $Re = \infty$. Knudsen's investigations followed the paths $Ma \doteqdot 0$; the present experiments cover the range for $Ma \doteqdot 1$.

The mass flow through the orifice can be written in terms of the orifice area A and the characteristic velocity W simply in the form

$$\dot{m} = \Gamma \rho_1 W A,$$

where Γ is a dimensionless factor which depends on the dimensionless parameters Ma, Re, the ratio of specific heats γ, and in the transition region possibly on slip, accommodation coefficients, and possibly a Reynolds number based on the bulk viscosity coefficient. The functional form of Γ and hence of $\dot{m}$ in the various limits can then be deduced.

More than fifty years ago Knudsen (1909) derived his 'effusion' formula from the kinetic theory of gases; in the present notation Knudsen's result becomes

$$\Gamma_{Re \to 0} = \frac{Ma}{\sqrt{(2\pi)}}.$$

The numerical factor here is a direct (but unfortunately not very sensitive) consequence of the analytical form of the Maxwell distribution. Knudsen's experiments which did check this numerical factor were therefore at the time considered crucial in verifying the existence of a Maxwell distribution in a gas.

In the opposite limit where $Re \to \infty$, one has

$$\Gamma_{Re \to \infty} = f(\gamma, Ma);$$

in particular for the conditions with $Ma \doteqdot 1$ which are of prime interest in this paper, Γ can be written

$$\Gamma_{Re \to \infty} = f(\gamma, 1) = \alpha(\gamma) \left[\gamma \left(\frac{2}{\gamma + 1} \right)^{(\gamma+1)/(\gamma-1)} \right]^{\frac{1}{2}},$$

where $\alpha(\gamma)$ is a theoretically well-defined coefficient which accounts for the difference in mass flow between a smooth nozzle ($\alpha = 1$) and an orifice ($\alpha < 1$). Many experiments have been performed on orifice flow at high Reynolds numbers because of its technical importance in metering problems. Curiously enough, no experimental work on the orifice flow as an interesting and challenging problem in transonic aerodynamics seems to have been carried out. In the engineering tests the transonic character of the flow has not been appreciated, e.g. the large pressure ratios necessary to obtain maximum mass flow come as a surprise to many workers in the field.

In the present paper mass-flow measurements at pressure ratios of about 10^3 are discussed. The measurements cover a range of Reynolds numbers from about 5×10^{-2} to 5×10^2, or Λ/D ratios from 50 to 5×10^{-3}. In this range the transition from free molecular flow to essentially inviscid flow is completed. Some of the results have been discussed before (Liepmann 1959, 1960). Further work for small pressure ratios is under way.

2. The free molecular limit

Choose a system of co-ordinates such that the wall with the orifice lies in the (y, z)-plane. The number n of molecules striking an area A of the *wall* per unit time is then given by

$$n = NA \int_{-\infty}^{0} \int_{-\infty}^{\infty} \int_{-\infty}^{\infty} u f(u, v, w)\, du\, dv\, dw, \tag{1}$$

where f denotes the normalized equilibrium distribution function and N the number of molecules per unit volume. The same type of formula gives the number of molecules passing through an aperture of area A, except that f is now a non-equilibrium distribution function. Knudsen's effusion formula is based on the assumption that in the limit of large mean free path Λ the lack of reflected molecules from the orifice area has a negligible effect on the distribution function, and hence the number n of molecules passing through A is obtained from (1) using the equilibrium distribution function. Thus one obtains the well-known expression

$$n = \tfrac{1}{4}\bar{c}_1 N_1 A \tag{2}$$

in terms of the number of molecules per unit volume N_1 and the mean molecular velocity $\bar{c}_1 = \sqrt{[(8/\pi)RT_1]}$ far upstream of the orifice. The mass flow is then given by

$$\dot{m} = \frac{1}{\sqrt{(2\pi)}}\rho_1 A\sqrt{(RT_1)},$$

or

$$\Gamma_{Re\to 0} = \frac{1}{\sqrt{(2\pi)}}. \tag{3}$$

To assess the validity of this limit and to estimate the degree of approximation for finite Λ/D, one has to study the nearly free molecular flow, i.e. the flow for large but finite Λ/D.

This can be carried out in a systematic fashion by iteratively solving the Boltzmann equation in order to obtain the non-equilibrium f, which then yields the number of passing molecules or the mass flow from (1). This has been done by Narasimha (1960). The computations are quite involved and require a number of approximations. A less systematic but simpler demonstration of the approach to free molecular flow is the following.

Following Present (1958) one can obtain Knudsen's formula (equation (2) above) in a slightly more refined way by computing the number of molecules scattered from a volume element dV in the direction of dA which do not suffer a collision between dV and dA. Let ϵ denote the mean number of collisions of a molecule per unit length travelled, i.e.

$$\epsilon \equiv \Lambda^{-1} = \sqrt{2}QN,$$

where Q is the collision cross-section. The number of molecules scattered per unit time in dV is thus equal to $N\epsilon\bar{c}\,dV$. In the free molecular limit, $N = N_1$ everywhere and hence the number of molecules scattered such as to pass dA without further collision is given by

$$dn = \int_V N_1\epsilon_1\bar{c}_1\frac{dA\cos\theta}{4\pi r^2}\exp(-\epsilon_1 r)\,dV,$$

where r is the distance from the volume element dV to dA and θ is the angle made with the normal to dA. Integration then gives

$$dn = \tfrac{1}{4}\bar{c}_1 N_1 dA.$$

The primary effect of the aperture is the reduction of the number of molecules in the neighbourhood of the opening due to the lack of reflexions. Thus N varies

from $\frac{1}{2}N_1$ in the plane of the orifice to N_1 at infinity. Consequently, ϵ depends on r and the computation of dn has to be slightly generalized to yield

$$dn = dA\,\frac{1}{4}\int_0^\infty N\epsilon\bar{c}\exp\left\{-\int_0^r \epsilon\,dr'\right\}dr. \tag{4}$$

Actually $\bar{c}$ will depend on r as well (due to the predominant loss of fast molecules $\bar{c} < \bar{c}_1$) but this effect is small and will be neglected. To evaluate dn, let $N = \frac{1}{2}N_1$ for $r < \frac{1}{2}D$ and $N = N_1$ for $r > \frac{1}{2}D$, $\bar{c} = \bar{c}_1$. Then

$$dn = \tfrac{1}{4}N_1\bar{c}_1(1+\tfrac{1}{8}\epsilon_1 D+\ldots)\,dA.$$

For large Λ/D, i.e. small values of ϵD, this formula applies approximately to a finite orifice area A, and hence

$$\dot{m} = \tfrac{1}{4}\rho_1\bar{c}_1 A\left(1+\frac{D}{8\Lambda}\pm\ldots\right). \tag{5}$$

Knudsen's limit is thus justified, but the approach of Γ to the limit is quite slow since

$$\Gamma_{Re\to 0} = \frac{1}{\sqrt{(2\pi)}}\left(1+\frac{D}{8\Lambda}\pm\ldots\right).$$

The numerical factor of $\frac{1}{8}$ agrees very well with Narasimha's computation which gave 0·13.

The increase in mass flow with increasing D/Λ in equation (5) is due to the increase in mean free path near the orifice. For still larger D/Λ the decrease in the density and the decrease in the temperature—and hence in $\bar{c}$—will tend to check the mass flow increase. Qualitatively the process will continue toward the isentropic conditions at very large D/Λ. But to follow the process in detail beyond the first-order terms soon becomes hopelessly complicated.

3. The Euler limit

We now consider the flow at infinite Reynolds number and large pressure ratio p_1/p_2.

For inviscid flow there exists a definite critical pressure ratio $(p_1/p_2)_c$ beyond which the downstream conditions cease to influence the upstream conditions. The maximum mass-flow is thus reached for $(p_1/p_2)_c$ for given upstream conditions. For a smooth nozzle critical pressure ratio and maximum mass flow are

$$\left(\frac{p_1}{p_2}\right)_c = \left(\frac{\gamma+1}{2}\right)^{\gamma/(\gamma-1)},$$

$$\dot{m} = \rho^* a^* A = \left(\frac{2}{\gamma+1}\right)^{(\gamma+1)/2(\gamma-1)}\rho_1 A(\gamma RT_1)^{\frac{1}{2}},$$

i.e.

$$\Gamma_{Re\to\infty} = \left(\frac{2}{\gamma+1}\right)^{(\gamma+1)/2(\gamma-1)}\gamma^{\frac{1}{2}}.$$

The sonic line in a sharp-edged orifice is S-shaped, and hence in the plane of the orifice the flow is partially subsonic and partially supersonic. Since the largest mass flow density occurs at local sonic velocity, the mass flow through an orifice

must be less than through a comparable smooth nozzle for which the sonic line is straight. Thus we can write

$$\Gamma_{Re\to\infty} = \alpha\left(\frac{2}{\gamma+1}\right)^{(\gamma+1)/2(\gamma-1)}\gamma^{\frac{1}{2}}$$

with $\alpha = \alpha(\gamma)$.

The two-dimensional problem, i.e. the flow through a slit, is sketched in figure 2 following Guderley (1957). The problem is a typical transonic one and, when transformed into the hodograph plane, leads to a Tricomi boundary-value problem. The flow becomes sonic at the lip of the slit and expands around the sharp

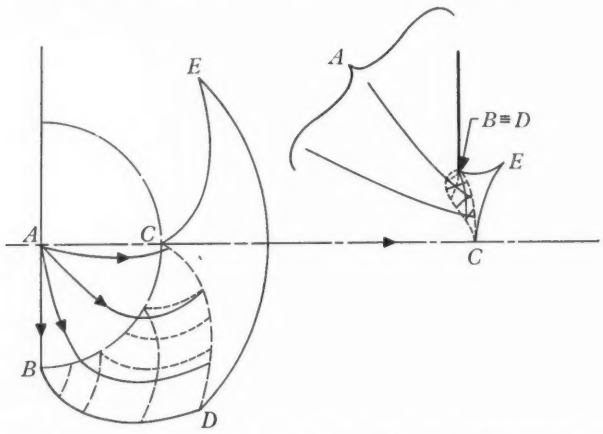

FIGURE 2. Sketches of hodograph and physical planes for the two-dimensional problem of flow through a slit (after Guderley).

edge locally like Prandtl–Meyer flow. The streamline thus maps on a characteristic in the hodograph plane. There exists a 'last characteristic' such that the flow downstream of this characteristic has no influence on the upstream conditions. This last characteristic connects the sonic point on the axis of the nozzle with the corner. In the hodograph plane this characteristic is an epicycloid from the sonic circle on the u-axis. Due to the symmetry in the pattern this characteristic meets the corner streamline or characteristic at $\theta = 45°$. Consequently the critical pressure ratio p_1/p_2 necessary for maximum mass flow is the one for which the flow past this last characteristic is established, i.e. the critical ratio is equal to the pressure ratio for a 45° turn from sonic in Prandtl–Meyer flow. This fact, though well known to the experts on transonic flow, has apparently not been generally recognized. Table 1 gives some typical values for the critical local Mach number and the critical pressure ratio; they are interesting mainly because of their large values compared with Laval nozzle flow.

The computation of the corresponding mass flow $\dot{m}$ is much more difficult; the Tricomi problem for the full hodograph equation (i.e. not the transonic approximation) has to be solved. Only one numerical computation seems to have been made: Frankl (1947) computed the flow through a two-dimensional slit for a gas with $\gamma = 1{\cdot}40$. He found $\alpha = 0{\cdot}85$.

The axisymmetrical flow corresponding to the circular orifice is even more difficult to compute because the hodograph transformation here does not lead to linear equations. Hence even the characteristics of the equation in the hodograph plane are not known *a priori*, so that the simple and general statement for the critical pressure ratio given above does not apply. One can give some simple qualitative arguments to show that the critical pressure ratios are even larger in axisymmetrical flow. Hence one expects smaller mass flow; but both should differ but little from the corresponding values for a slit.

γ	Ma_c	$\left(\frac{p_1}{p_2}\right)_c$
5/3	3·50	58·3
7/5	2·76	25·6
4/3	2·63	21·5

TABLE 1

First of all note that the flow near the sharp lip is locally two-dimensional. Hence the streamline here maps again on the epicycloid in the hodograph plane. Thus the critical pressure ratio is smaller or larger than in the planar case depending on whether the characteristic from the axis intersects the epicycloid at a point corresponding to $\theta \lesssim 45°$.

Now near the axis the transonic approximation to the flow equation is adequate. Let u denote the excess velocity beyond a^*, θ the streamline angle, and r the radial co-ordinate; u and θ are related along the characteristic by

$$\frac{d(r\theta)}{du} = r\sqrt{(\gamma+1)}\sqrt{\left(\frac{u}{a^{*3}}\right)}.$$

For plane flow

$$\frac{d\theta}{du} = \sqrt{(\gamma+1)}\sqrt{\left(\frac{u}{a^{*3}}\right)},$$

thus

$$\frac{d\theta}{du} = \left(\frac{d\theta}{du}\right)_{\text{planar}} - \frac{\theta}{r}\frac{dr}{du};$$

near the axis $dr/du > 0$, and hence

$$\left(\frac{d\theta}{du}\right)_{\text{axisym.}} < \left(\frac{d\theta}{du}\right)_{\text{planar}}.$$

Furthermore, at the intersection point of the characteristic with the epicycloid, i.e. at the corner, the flow is locally two-dimensional and hence the characteristic there approaches the slope of an epicycloid through the point. Hence the 'last characteristic' for the axisymmetrical flow intersects the epicycloid corresponding to Prandtl–Meyer flow at the corner at an angle $\theta > 45°$ and hence $(p_1/p_2)_c$ and Ma_c are both larger than the corresponding two-dimensional values; one can thus expect $\dot{m}$ to be smaller for the orifice than the corresponding value for the slit.

The difference should be very slight: the difference in characteristic slope can be estimated from the transonic nozzle expansion near the axis and is small;

hence considering that even a drastic change from a critical Mach number of $Ma_c \doteq 1$ for nozzle flow to a critical Mach number of about 2·75 in two-dimensional orifice flow reduces α only from unity to 0·85, one has reason to believe that the circular orifice will have nearly the same orifice coefficient as the slit. The difference lies probably within the error limits of both the numerical computation and the experiments.

For large but finite Reynolds numbers, boundary-layer effects have to be considered. Along the orifice lip a viscous layer will exist and continue into the orifice, thus reducing the effective orifice area. From boundary-layer similarity one expects a mass-flow formula of the type

$$\dot{m} = \dot{m}_{Re\to\infty}(1 - CRe^{-\frac{1}{2}}),$$

where C is some constant. A crude estimate of this constant can be obtained either by reducing the axisymmetrical problem to a Falkner–Skan flow using Mangler's transformation and approximating to the outer flow (for example by three-dimensional sink flow) or by applying—since the flow is accelerating—a simple method of the Kármán–Pohlhausen type, e.g. Walz's method as extended by Rott & Crabtree (1952) using the pressure distribution near the lip as computed by Frankl for slit flow.

A few computations like this have been carried out. However, near the lip pressure gradients are large and the actual flow is complicated by interaction effects between outer flow and boundary layer, and there does not seem to be much point in giving all the computational details. Experimentally the constant in the formula is of the order of $\frac{1}{2}$; the limiting formula for Γ at high Reynolds number is thus roughly

$$\Gamma = \Gamma_{Re\to\infty}\left(1 - \frac{1}{2\sqrt{Re}} \pm \dots\right).$$

The complications near the lip were emphasized by the experiments, which indicated a maximum, i.e. an overshoot, in the approach to the asymptotic value at high Re. Such an overshoot is indeed conceivable since the boundary layer not only restricts the area but also rounds off the lip, thus tending to increase the mass flow. However, neither the experiments nor the theoretical considerations are sufficiently definite to pursue this point as yet.

4. Free molecular effusion

It is of interest to collect here a few simple results valid for free molecular effusion, i.e. in the limit $D/\Lambda \to 0$. We use a cylindrical system of co-ordinates in velocity space with w the velocity in the plane of the orifice and u normal to it. The normalized local velocity distribution of the effusing particles can then be written

$$f(u,w)\,du\,dw = 4\beta^2 uw\,e^{-\beta(u^2+w^2)}\,du\,dw,$$

with $\beta = \frac{1}{2}(RT_1)^{-1}$. The mean normal velocity and transport of momentum through the hole are then

$$\bar{u} = \sqrt{(\tfrac{1}{2}\pi RT_1)}$$

and

$$\dot{m}\bar{u} = A\rho_1\sqrt{\left(\frac{RT_1}{2\pi}\right)}\sqrt{\left(\frac{\pi RT_1}{2}\right)} = \tfrac{1}{2}p_1 A.$$

The latter result is obvious since $p_1 A$ is the net rate of change of momentum at an area A of a wall; thus without reflecting the molecules back, momentum $\frac{1}{2}p_1 A$ passes through A per unit time.

The flux of kinetic energy becomes

$$\dot{m}\frac{\overline{u^2+w^2}}{2} = \dot{m}2RT_1,$$

i.e. one obtains the well-known result that the flux of kinetic energy through the orifice is larger by $\frac{1}{2}RT_1$ than the product of mass flow and mean kinetic energy of the gas in the container.

The result has an interesting consequence on the energy balance. In the steady state, the mass flow $\dot{m}$ is continuously replaced. Consequently, if the effusion formula is taken literally, there appears to be a net loss of energy from the container since excess energy $\frac{1}{2}RT_1$ flows out through the orifice. Consequently the temperature in the effusing jet must differ from T_1 and a heat flow q must exist in the container. One can work out the heat flow approximately by matching a continuum heat conduction solution for $r > \Lambda$ to the heat flux $\dot{m}2RT_1$ at a half sphere with $r = \Lambda$. One finds that the difference in temperature is of order $(D/\Lambda)^2$ and hence negligible in the limit. Furthermore, one can estimate the entropy production in the upstream container and show that it too is negligible, in agreement with more general considerations given below.

The momentum and the excess kinetic energy are imparted to the walls in the downstream container by direct wall collisions. For example, if the beam effuses into a cylindrical pipe of radius R_0 with $\Lambda > R_0 \gg D$, one obtains a shear stress distribution $\tau(x)$ along the wall

$$\tau(x) = \frac{p_1 A}{4\pi R_0}\frac{3x^2R_0^2}{(x^2+R_0^2)^{\frac{5}{2}}},$$

with a maximum stress at $x = \sqrt{(\frac{2}{3})}R_0$ and, of course, the integral of τ with respect to x from 0 to ∞ is $\frac{1}{2}p_1 A$. The heat flux q due to the excess beam energy is distributed similarly. Half the total number of effusing molecules collide with the wall for $x < R_0$. Consequently a density gradient along the axis of the downstream container is built up and the flow is similar to, for instance, Knudsen flow through a long tube. Note that in the effusion case the far downstream pressure p_2 and the mass flow $\dot{m}$ are given by the experimental conditions. The pressure p_2' just downstream of the orifice is larger than p_2. If $p_1/p_2' \gg 1$ is required, then R_0 has to be chosen sufficiently large.

5. Entropy production in orifice flow

The total change of entropy for the complete flow from the equilibrium state (1) to the equilibrium state (2) is given by

$$\frac{S_2 - S_1}{R} = \log\frac{p_1}{p_2},$$

where S denotes the entropy per unit mass and R the gas constant per unit mass.

If $p_1 \gg p_2$, the entropy increase per unit mass is large, but the gas flow upstream of the orifice is independent of p_2. Consequently the entropy increase has to be produced downstream of the orifice.

In the limit $Re \to \infty$, the flow is isentropic upstream of a shock wave and the macroscopic mechanism for entropy production is the shock wave system in the supersonic jet downstream of the orifice. For example, with the pressure ratio of 10^3 used here, a normal shock at a Mach number somewhat larger than 10 suffices.

In the opposite limit $Re \to 0$, the problem is more interesting. From the general thermodynamic argument given above, the irreversible entropy production upstream of the orifice must be negligibly small. Consequently, the molecular distribution function must be almost everywhere locally Maxwellian. This is true for the limiting distribution in the effusing beam which can be transformed into a locally Maxwellian distribution function. It must also be true for the next approximations valid at finite Reynolds numbers.

The entropy in free molecular flow is produced downstream by the irreversible processes in the pipe flow, e.g. as in Knudsen flow through a long tube.

6. Apparatus and measurements

(i) *General technique*

To obtain the mass flow $\dot{m}$, one can follow essentially two different approaches. (1) One measures the decay of the pressure in the upstream container as function of time and obtains $\dot{m}$ by differentiating the resulting decay curve. (2) One can operate at steady-state conditions, i.e. by continuously pumping the gas through the orifice and leaking a metered quantity of gas into the upstream container. When the pressure in the upstream container has reached a stationary value, the metered gas quantity equals the mass flow through the orifice at this pressure.

In the present measurements the second method was applied. The general particulars of the apparatus are dictated by the choice of the orifice diameter D. Here one has to compromise between the need to make D large in order to reduce the corrections for finite lip thickness (the so-called Clausing correction (1932)) and to insure a nearly perfect circular hole and the limitations due to the available pumps. The ultimate vacuum and the pumping speed must be such that one can operate at large Λ/D still maintaining a large pressure ratio across the aperture.

The pressure ratio was chosen to be 10^3 or higher. With the ultimate vacuum of a good standard diffusion pump of approximately 5×10^{-7} mm of mercury, one has to limit the upstream pressure to the micron range. The mean free paths for the three gases investigated, He, A and N_2, are at 1μ pressure 12·7, 4·50 and 4·44 cm respectively. The orifice diameter was thus chosen to be about 0·1 cm. The dimensions of the upstream container have to be large compared to D and Λ. The dimensions of the downstream container are limited only by the conditions that the number of back-scattered molecules passing through the orifice should be negligibly small. Both the upstream and downstream conditions are met by using a cylindrical vessel of about 40 cm internal diameter. Originally it was

intended to use glass tubing. However, it proved impossible to obtain tubing with a wall thickness uniform enough and sufficiently free of stresses for safe operations. Hence the tank was made of steel.

The general layout of the apparatus is shown in figure 3 which is largely self-explanatory. All pressures were measured with McLeod gauges. For low pressures a cathethometer was used to read the gauge. A Pirani gauge was used only to monitor the pressure variation in the tank and to check on the attainment of a

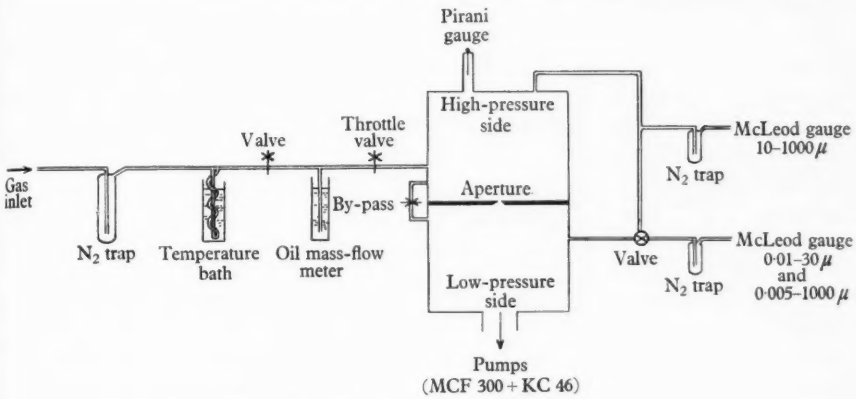

FIGURE 3. Apparatus for effusion studies.

constant pressure, i.e. steady conditions. The large volumes and the relatively small mass flows made the time constant of the system large. This had two unpleasant consequences: the time needed to measure a simple point was on average about 1 hr, and the system became quite sensitive to temperature changes in the room. The maximum permissible rate of temperature change was about 1 °C/hr.

(ii) *Detailed construction and techniques*

Orifice construction

Two orifices were used. One was a circular hole drilled into a piece of 0·0025 cm thick shim stock and cemented on a circular plate with a hole of about 1 cm diameter with tapered edges. This plate in turn fitted with *O*-ring seals into the dividing wall in the tank. The orifice was selected by inspection under a large optical comparator from a large number of similarly made samples. The orifice was very nearly circular with well-defined edges and a diameter $D = 0{\cdot}1047$ cm.

This orifice construction had the disadvantage that it was impossible to check the cemented section for leaks. Hence a second orifice of integral construction was built with roughly the same dimensions: lip thickness 0·0025 cm and a diameter $D = 0{\cdot}09855$ cm. Measurements were made with both orifices; within the experimental scatter no difference was found.

Seals, leak rate, degassing

Steel and glass construction was used throughout. No seals except *O*-ring seals or glass-blown seals were used. The main tank was helium-tested before use. The

whole apparatus remained at pressures of a micron or less for months at a time in order to reduce the degassing rate since the system could not be baked. The ultimate leak plus degassing rate thus obtained raised the pressure in the tank from the ultimate pump pressure of 10^{-6} mm by approximately $0{\cdot}2\mu$/hr. For most measurements this rate of pressure rise was entirely negligible. The measurements at the lowest pressure, however, show an increased scatter which can be attributed to variable degassing.

Gases, mass-flow measurements

Most measurements were made with He, A and N_2. A few measurements were also made with CO_2. The gases used were taken from commercially available tanks cleaned only by removing condensable gases in a liquid nitrogen trap. Argon was liquified in the trap and redistilled.

To regulate the mass flow into the system a number of more or less complicated schemes were tried. Actually it turned out that a good steel needle valve proved superior over most of the more complicated devices, in particular because when such a valve was used the volume in the mass-flow measuring device could be made very small indeed. This was very important because of the need to reduce scatter by temperature variation.

The mass flow was measured by timing the displacement of a silicone oil meniscus in a calibrated burette with a precision stop watch. The volume flow at atmospheric pressure which was measured in this fashion varied from about 2 to 10^5 cm^3 per hour.

Accuracy

Each of the plotted points is an average of at least three measurements at the same setting and represents a separate absolute measurement of the mass flow; some of the points were taken more than a year apart. The estimated error from known sources, e.g. the mass-flow measurements, temperature variation, orifice geometry, etc., is about $\pm 2\,\%$. Additional errors which are difficult to assess explicitly arose from uneven degassing at low pressure, lack of attainment of complete equilibrium, and the well-known difficulties in reading absolute pressures on a McLeod gauge with great accuracy. The over-all error is apparent from the scatter in the measured points.

With an improved design and improved techniques one could certainly improve the accuracy considerably, particularly if one restricted the measurements to a limited pressure range or flow régime.

7. Results of the measurements

The bulk of the mass-flow measurements is shown in figures 4–6. Figure 4 gives the over-all behaviour of Γ normalized by Γ_k, the theoretical asymptotic value for free molecular flow, as functions of Re^{-1} for three gases. The figure serves mainly to show the general trend of the transition curve as well as the similarity between the three gases with molecular weights of 4, 28 and 40 respectively.

Figure 5 shows the approach of Γ to the free molecular limit. The ratio of Γ for He and A to the limit value corrected for finite channel length is plotted versus D/Λ. The general agreement in behaviour with the approximate theoretical formula for near free molecular flow is shown.

Knudsen's measurements (1909) as usually given in text-books agree to within 2 or 3 % with the limiting value at about $D/\Lambda \leqslant 0{\cdot}1$; however, it appears that Knudsen's values have not been corrected for finite lip thickness. If the Clausing

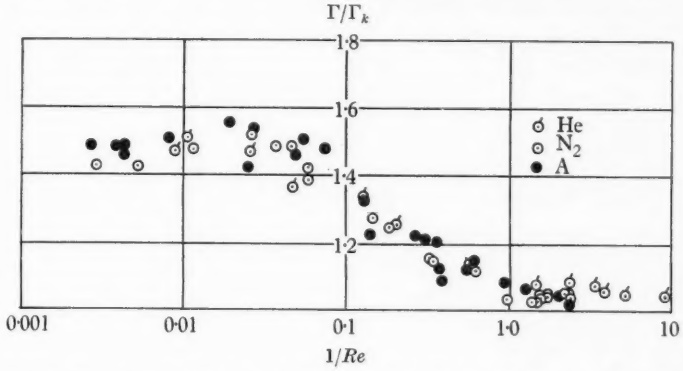

FIGURE 4. Experimental values of Γ/Γ_k *vs* $1/Re$; Γ_k is the theoretical asymptotic value of Γ for free molecular flow.

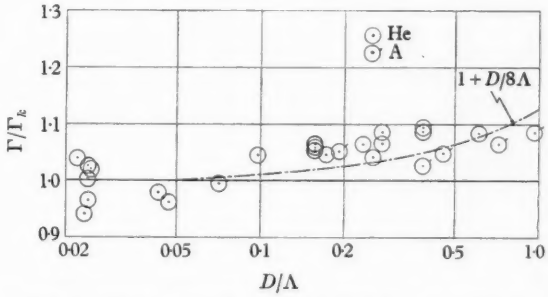

FIGURE 5. Graph showing approach of Γ to free molecular limit.

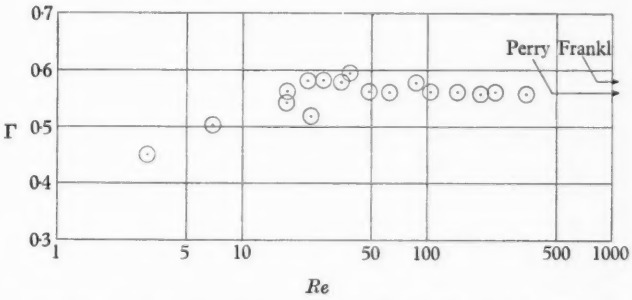

FIGURE 6. Experimental values of Γ *vs* Re for N_2 at high pressures.

correction is applied to Knudsen's results one obtains the values in table 2. Knudsen's measured Γ's are averages of a number of measurements; the two values for H_2 and O_2 refer to the two different holes used by Knudsen which require a different correction. The Clausing correction was applied to the circle of area equal to that of the somewhat irregular holes. The corrected results are evidently internally quite consistent and in good agreement with the present measurements.

Gas	Γ/Γ_k	Γ/Γ_k (corrected)
H_2	0·979	1·07
	1·02	1·07
O_2	0·980	1·07
	1·04	1·095
CO_2	0·949	1·04

TABLE 2

Gas	γ	Ma_c	α (measured)	Γ (measured)
A	1·66	3·50	0·812	0·591
N_2	1·40	2·76	0·824	0·564
CO_2	1·30	2·63	0·830	0·550

TABLE 3

Figure 6 shows Γ for N_2 plotted versus Re at the high pressures. Since Γ for $Re \to \infty$ is not exactly known, the absolute value of Γ is plotted. The measured points approach an asymptote of $\Gamma \doteqdot 0{\cdot}56$. Frankl's theoretical value for a slit is $\Gamma = 0{\cdot}582$. Perry (1949) carried out a set of orifice measurements in air at very high Reynolds number ($\sim 10^5$). His measurements give $\Gamma = 0{\cdot}575$.

This last value should be the closest to the true theoretical limit. Still, the differences between Perry's value at high Reynolds numbers and the asymptotic value reached in the present measurements at a much lower Reynolds number are not significant in view of the experimental error limits. Even Frankl's numerical computations could conceivably be off by a few per cent, and hence the data do not yet suffice to demonstrate definitely a mass-flow difference between a slit and an equivalent orifice in transonic flow.

Finally a set of measurements at a high Reynolds number $Re \sim 200$ was made to investigate the trend of the transonic orifice flow with γ. The results are given in table 3. The measured variation of Γ and hence α with γ is surprisingly small and hardly outside the experimental scatter. More accurate measurements in the transonic limit seem definitely worth while.

8. Conclusions

In general the measurements demonstrate the transition between the free molecular limit and the Euler limit. The transition region is relatively narrow, the Reynolds number ranges from about 0·1 to 100.

The first-order corrections valid for nearly zero and large Reynolds numbers agree with the measurements fairly well and do actually cover the larger part of the transition zone. As always, the remaining intermediate range near $Re \sim 1$ is theoretically the most difficult. The flow here should resemble compressible viscous sink flow. According to the general entropy argument, the entropy production in the flow must be small; hence dissipation and heat flow must be small or restricted to narrow zones.

The investigation has certainly posed more problems than it has solved. For example, transonic orifice flow is well worth a separate experimental study; in particular orifice flow with complex gases and reacting gases promises to be most interesting. The limiting pressure ratios and Mach numbers depend strongly on γ; for $\gamma < 5/4$, even the turning angle for expansion to zero pressure is larger than π. The theoretical conditions near the lip for this case are rather interesting. The expansion time in this restricted Prandtl–Meyer region is very short and hence relaxation effects should be observable.

In the free molecular and near free molecular régime there remain a host of problems for flows for which the wall temperature is much different from the gas temperature. This problem arises in connexion with molecular beams produced by shock-wave heated gases, which have begun to receive much attention recently. A particular problem here is the effusion of charged particles (Sturtevant 1960).

The investigations at the California Institute of Technology are being continued with the aim of studying different régimes in the (Ma^2, Re)-plane and in order to improve the accuracy of the measurements as well as the theoretical description.

The author would like to acknowledge very helpful discussions with R. Narasimha; in particular the (Ma^2, Re)-representation is due to him. Dr J. Broadwell kindly corrected an early misconception on the transonic problem. The work was carried out with the support of the Office of Naval Research, Contract Nonr-220(21).

REFERENCES

Chaplygin, S. A. 1904 *Scientific Annals of the Imperial University of Moscow, Physics-Mathematical Division Publication*, no. 21.

Clausing, P. 1932 *Ann. Physik.* **12**, 961.

Frankl, F. I. 1947 *Trans. Acad. Sci., U.S.S.R.* **58**, no. 3.

Guderley, K. G. 1957 *Theorie Schallnaher Strömungen*. Berlin: Springer.

Knudsen, M. 1909 *Ann. Physik.* **28**, 75.

Liepmann, H. W. 1959 A study of effusive flow. *Durand Centennial Conference, Stanford University.*

Liepmann, H. W. 1960 Gaskinetics and gasdynamics of orifice flow. First All-Union Congress on Theoretical and Applied Mechanics, Moscow.

Narasimha, R. 1960 *Phys. Fluids*, **3**, 476.

Perry, J. A. 1949 *Trans. Amer. Soc. Mech. Engrs*, **71**, 757.

Present, R. D. 1958 *Kinetic Theory of Gases*. New York: McGraw-Hill.

Rott, N. & Crabtree, L. F. 1952 *J. Aero. Sci.* **19**, 553.

Sturtevant, B. 1960 Effusion of charged particles from a shock heated gas. *GALCIT Rep. California Institute of Technology.*

Theory of flame-front stability

By WIKTOR ECKHAUS

Massachusetts Institute of Technology†

(Received 25 July 1960)

A study of the stability of a plane laminar flame front is made. The effects of disturbances on the flame structure are investigated by a small perturbations technique, taking into account the mechanism of diffusion, heat conduction and unsteady combustion. By use of a simplified model of the flame structure, and the assumption that the flame thickness is small compared with the wavelength of disturbances, a formula for the perturbation of the flame propagation velocity is derived. The flame velocity is shown to depend on the curvature of the flame, and on the rates of change of fluid velocities at the flame boundary. From stability analysis it then follows that properties of the mixture, as expressed in terms of the coefficient of heat conductivity and various coefficients of diffusion, play an important role in determining the stability picture. For some estimated values of these parameters the theoretical results are shown to agree with the general trend of the experimentally observed behaviour.

1. Introduction

The problem of stability of a plane flame front in a laminar flow is, from the theoretical point of view, a problem of unsteady dynamics of a fluid in which heat conduction, multicomponent diffusion and complex reactions resulting in heat release take place. A body of experimental evidence on the behaviour of distorted flame fronts is at present available; the theoretical investigations, however, have so far failed to produce a satisfactory explanation of the observed phenomena. The situation is in one respect a very puzzling one: while the experiments show a well-defined behaviour, which seems to be caused by some dominant mechanism, the theory finds it difficult to pin-point such a dominant mechanism. To be more specific let us now briefly outline the problem and summarize the available experimental and theoretical evidence.

We consider a plane flame front which propagates into a combustible mixture with a velocity u_0, the flame propagation velocity. From the point of view of an observer stationed at the moving flame front (figure 1), by approximation three regions of flow can be distinguished: the upstream region, occupied by the combustible mixture, which enters the flame with velocity u_0; the downstream region, occupied by products of combustion, which leave the flame with a different velocity u_f (and at a different temperature); and the flame region itself. In the upstream and downstream regions, heat conductivity, diffusion and reactions can be neglected; while, due to low velocities (u_0 of the order of magnitude of

† Now at the Institut Henri Poincaré, Paris.

30 to 100 cm/sec), compressibility can be neglected as well. Thus, these two regions can be considered to be occupied by ideal fluid. In the flame region, which is usually very thin (of the order of magnitude of a fraction of a millimetre), multicomponent diffusion, heat conductivity and reactions resulting in heat release must be taken into account.

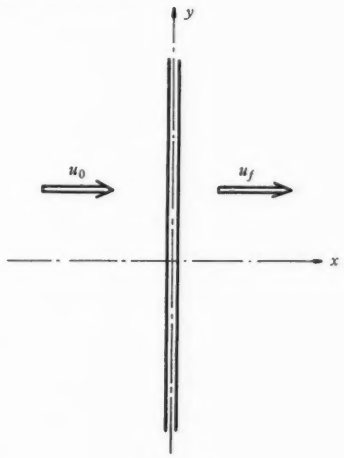

FIGURE 1

Now consider the flame front to be initially slightly distorted. The resulting stability problem was first treated by Landau in 1944 (see Landau & Lifshitz 1953; Emmons 1958). Taking disturbances harmonic in y and linearizing the equations of motion, one can easily find the perturbation fields in the upstream and downstream region. For most observable disturbances the ratio of wavelength to flame thickness will be very large, so that by approximation the flame front may be treated as a discontinuity in the field of fluid. This leads to a simple formulation of the stability problem, provided that a condition is postulated for the propagation velocity of the disturbed flame front. Landau assumed that the disturbances have negligible effect on the flame propagation velocity, hence that, even in disturbed conditions, the normal component of the velocity of fluid relative to the flame front is u_0. He then found the flame to be unstable for all wavelengths.

Let us now turn to experimental evidence. Markstein (1951) studied plane flame fronts for a series of hydrocarbon fuels pre-mixed with air. He found in a great many cases that the flame has a cellular structure: the plane flame front breaks down into many small cells which remain in the plane of the original flame, but which dance around and oscillate. Varying the composition of the mixture, Markstein was able to establish beyond any doubt that almost all fuels produced cellular structure when the mixture was rich, but that no breakdown occurred, and the flame remained plane, when the mixture was lean.†

† The only exception to the rule was produced by methane flames, for which the behaviour was reversed. Of the fuels that were tested, methane happens to be the only one that is considerably lighter than the oxidizer.

If the cellular structure of the flame is interpreted as a result of instability, the conclusion that, for a wide range of fuels, rich mixtures are unstable while lean mixtures are stable must be drawn. The transition point from unstable to stable situations was established by Markstein to be exactly at the stochiometric composition.

Hence it appears that Landau's theory must be modified, so as to take into account the effects of the disturbances on the flame propagation velocity. Markstein proposed that the variation of the flame velocity should be proportional to the ratio of flame thickness to the local radius of curvature of the flame. The proportionality constant remains undetermined in Markstein's analysis and, depending on its value, the effect is stabilizing or destabilizing.

Further theoretical understanding of the flame stability problem can be achieved only if the theory of flame propagation is extended to unsteady and slightly curved flames. But, to date, even the problem of one-dimensional steady-state flame propagation has not been truly solved. The great complexity of the phenomena that take place inside the flame zone, together with partial ignorance about the chemistry of reactions, make the problem very difficult. Nevertheless, based on various assumptions, various theories are available, and, in the words of Spalding (1955), 'no single theory fits all the facts but all fit some of the facts remarkably well'. So there is some hope that, by making reasonable assumptions in the present case, a reasonable theory can be produced. This paper presents an attempt in this direction.

The theory is based on a highly idealized model of the flame structure, which may justifiably be criticized for over-simplification. In many respects the present theory can be described as the simplest possible flame perturbation theory, a counterpart of the stationary Mallard–LeChatelier formula (see Emmons 1958).

As compared with Markstein's hypothesis, the theory shows that the perturbation of the flame velocity is not only proportional to the curvature of the flame, but also to the rate of change of the tangential fluid velocities along the flame, and to the relative acceleration of the flame. The proportionality constants follow from the theory, and are expressed in terms of the physical properties of the burning mixture, such as the coefficients of heat conductivity and various coefficients of diffusion. Stability analysis then shows that rich and lean mixtures indeed behave differently, and that a situation can arise in which the lean mixture is stable for a range of wavelengths, while the rich mixture is unstable.

2. The model of the flame structure

In the present work we adopt the concept of thermal flame propagation. This permits us to subdivide the flame zone by approximation into two regions: a pre-heat region, where the temperature rises mainly because of heat conduction and where the rates of reaction are low; and a burning region, where the rates of reaction are high and where most of the actual combustion takes place (figure 2).

Although little is known about the actual rates of reaction for any complex fuel–oxygen mixture, there are good reasons to assume that the rates of reaction rise very rapidly with temperature. We shall presently assume that the depen-

dence on temperature is so strong that in the pre-heat zone, $\xi < 0$, rates of reaction can be neglected altogether. Moreover, we shall assume that in the burning zone the rates of reactions are very high, so that this zone can be thought to be very thin, and the rate of reaction can be approximated by a constant independent of the temperature. The boundary between the two zones is given by the fictitious ignition temperature T_i which is assumed to be very close to the final

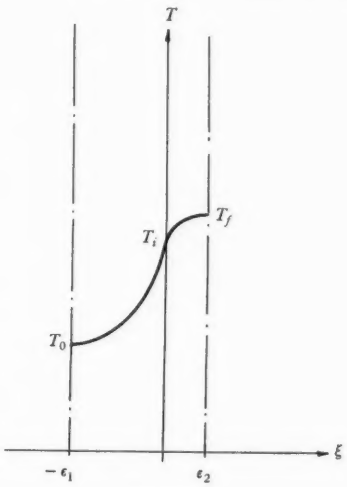

FIGURE 2

flame temperature T_f. Let us now put these assumptions in a more mathematical form. As we shall see very shortly, the parameter that governs the heat conduction in the pre-heat zone is

$$\tau = \frac{5}{2}\frac{knu}{\lambda},$$

where k is the Boltzmann constant, n the number density of the gas, u the velocity, and λ the coefficient of heat conductivity. The inverse of τ measures the width of the pre-heat zone.

Similarly, if we denote the constant rate of reaction in the burning zone by α^*, the inverse of the quantity

$$\frac{\alpha^*}{u_f}$$

measures the width of the burning zone. The fundamental assumption of the present model is

$$\frac{\alpha^*}{u_f \tau} \gg 1.$$

So far we have considered the flame as a temperature wave. This, of course, is only part of the story. The gas that flows through the flame is a mixture of many species. In the pre-heat zone we have predominantly fuel and oxidizer; in the burning zone these species disappear partially or completely and are replaced by products of combustion. There are thus large concentration gradients, and

consequently appreciable diffusion. Products of combustion diffuse into the pre-heat zone, while fuel and oxidizer diffuse into the burning zone.

Consider now a slightly curved flame front, which moves with respect to some reference axis (its original plane position) with velocity $\dot{x}_0$, and let the fluid velocities relative to the flame front vary with time. In a co-ordinate system ξ, η attached to the flame front, the flame structure may be assumed to be essentially the one-dimensional stationary flame structure, but with some small perturbations. Let us attempt a qualitative description of these perturbations.

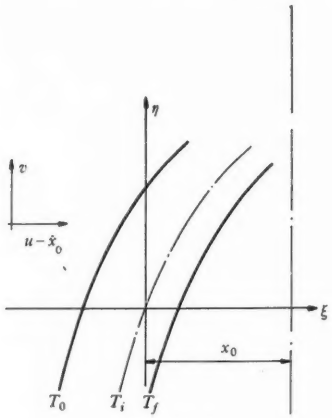

FIGURE 3

The heat conduction is affected by the fact that the flame is no longer plane (and thus one-dimensional) but curved. This is the effect proposed by Markstein; however, there are others too. The heat conduction is also affected by convection due to the perturbation velocities. The result is that locally along the flame the amount of heat needed to raise the temperature in the pre-heat zone to the ignition point is different from that needed in the undisturbed situation.

Next we consider the diffusion processes. In the one-dimensional situation there is a distribution of the relative densities of the various species along the ξ-axis. By the perturbation velocities the species will be convected and redistributed, while there will also be diffusion in the direction tangential to the flame front, due to the flame curvature. The net effect of these processes will be that, as we proceed along the ξ-axis, the ratio of fuel to oxidizer of the mixture which enters the preheat zone, and that of the mixture which enters the burning zone, will no longer be the same. There will be an effective change of composition and thus a perturbation of the amount of heat produced by combustion in the burning zone.

Some of these effects can easily be put in a mathematical form by very simple reasoning (see Eckhaus 1959). However, in order to obtain all the effects correctly, one must proceed from the system of equations that describes the flame structure, develop the perturbation equations and construct their solutions.

3. The system of equations describing the flame structure†

We define a Cartesian co-ordinate system $x-y$, in which the y-axis coincides with the unperturbed position of the flame, and consider the flow of a mixture of species, in which diffusion, heat conduction and reactions take place. Gravitational, viscous and acoustic effects, however, are neglected. The equations that we shall use are adopted from Hirschfelder, Curtiss & Bird (1954) where detailed derivations are given.

To begin with, we have the hydrodynamic equations of continuity and momentum

$$\frac{\partial \rho}{\partial t}+\frac{\partial}{\partial x}(\rho u)+\frac{\partial}{\partial y}(\rho v)=0, \tag{3.1}$$

$$\frac{Du}{Dt}=-\frac{1}{\rho}\frac{\partial p}{\partial x}, \quad \frac{Dv}{Dt}=-\frac{1}{\rho}\frac{\partial p}{\partial y}. \tag{3.2}$$

The velocities u and v are defined as mean mass velocities in the x- and y-directions respectively.

Next we consider separately the species constituting the mixture. The continuity equation for any species $[i]$ is

$$\frac{\partial n_i}{\partial t}+\frac{\partial}{\partial x}[n_i(u+V_{ix})]+\frac{\partial}{\partial y}[n_i(v+V_{iy})]=K_i, \tag{3.3}$$

where n_i is the number-density of species $[i]$, V_{ix} and V_{iy} are diffusion velocities of this species in the x- and y-directions, and K_i represents the number of molecules of species $[i]$ which disappear or are produced per unit of time and volume as a consequence of the combustion process.

The sum of equations (3.3) over all species gives

$$\frac{\partial n}{\partial t}+\frac{\partial}{\partial x}(nS_x)+\frac{\partial}{\partial y}(nS_y)=\Sigma K_i, \tag{3.4}$$

where
$$n=\Sigma n_i, \quad S_x=u+\Sigma\frac{n_i}{n}V_{ix}, \quad S_y=v+\Sigma\frac{n_i}{n}V_{iy}. \tag{3.5}$$

In reality the gas mixture within the flame has a great many components. We idealize this situation by considering a mixture of three species only: fuel, oxidizer, and the products of combustion. Thus, symbolically, we have the reaction $[1]+[2]\rightarrow[3]$. We shall adopt subscript [3] for the products of combustion. With respect to fuel and oxidizer we introduce the following convention: one of the species [1] and [2] disappears completely after combustion. We shall always denote by [1] the species that disappears in the combustion process. Thus, if the mixture is rich [1] will stand for oxygen, if the mixture is lean [1] will denote the fuel.

† We consider here the two-dimensional problem. The final results of the present theory can, however, easily be extended to three-dimensional disturbances, as described by Eckhaus (1959).

The diffusion law for a three component mixture can be written as follows

$$\left(\frac{n_1}{n}\right)\left\{\left(\frac{n_2}{n}\right)\frac{1}{D_{12}}(\mathbf{V}_2-\mathbf{V}_1)+\left(\frac{n_3}{n}\right)\frac{1}{D_{13}}(\mathbf{V}_3-\mathbf{V}_1)\right\}=\operatorname{grad}\left(\frac{n_1}{n}\right), \tag{3.6}$$

$$\left(\frac{n_2}{n}\right)\left\{\left(\frac{n_1}{n}\right)\frac{1}{D_{21}}(\mathbf{V}_1-\mathbf{V}_2)+\left(\frac{n_3}{n}\right)\frac{1}{D_{23}}(\mathbf{V}_3-\mathbf{V}_2)\right\}=\operatorname{grad}\left(\frac{n_2}{n}\right), \tag{3.7}$$

$$n_1m_1\mathbf{V}_1+n_2m_2\mathbf{V}_2+n_3m_3\mathbf{V}_3=0, \tag{3.8}$$

where D_{ij} is the binary diffusion coefficient between species $[i]$ and $[j]$, and m_i is the molecular weight. By definition $\rho=\Sigma n_i m_i$.

If we now attempt to eliminate the diffusion velocities from the system of equations (3.3), (3.6), (3.7) and (3.8), the resulting differential equations for the number densities become non-linear. It appears thus desirable to introduce some form of approximation. This has been done by Eckhaus (1959). Omitting here the derivation we state the result: in the pre-heat zone, where $K_i=0$, the approximate laws of diffusion read

$$n_1\mathbf{V}_1=-\frac{n^2}{\rho}m_2D_{12}\operatorname{grad}\left(\frac{n_1}{n}\right)+\frac{n^2}{\rho}m_3D_3\left(\frac{n_1}{n}\right)_0\left[1-\frac{m_2D_{12}}{m_3D_{13}}\right]\operatorname{grad}\left(\frac{n_3}{n}\right), \tag{3.9}$$

$$n_3\mathbf{V}_3=-nD_3\operatorname{grad}\left(\frac{n_3}{n}\right), \tag{3.10}$$

$$\frac{1}{D_3}=\left(\frac{n_1}{n}\right)_0\frac{1}{D_{13}}+\left(\frac{n_2}{n}\right)_0\frac{1}{D_{23}}, \tag{3.11}$$

where subscript 0 denotes the values at the upstream boundary of the flame front. Using some further approximations concerning the temperature dependence of the diffusion coefficients (see Eckhaus 1959), the following system of equations can be obtained

$$\frac{D}{Dt}\left(\frac{n_3}{n}\right)-D_3\nabla^2\left(\frac{n_3}{n}\right)=0, \tag{3.12}$$

$$\frac{D}{Dt}\left(\frac{n_1}{n}\right)-D_{12}\nabla^2\left(\frac{n_1}{n}\right)=-D_3\left(\frac{n_1}{n}\right)_0\left(1-\frac{D_{12}}{D_{13}}\right)\nabla^2\left(\frac{n_3}{n}\right). \tag{3.13}$$

The above approximate diffusion equations can be interpreted as follows. Suppose we start by considering species [1] and [2] as one component $[I]$. Then equation (3.12) describes the binary diffusion between $[I]$ and [3]. Having solved this problem we want to find out how the diffusion is distributed between species [1] and [2], and this is described by (3.13).

Proceeding now to the energy equation, in Eckhaus (1959) an approximate form is derived, in which the internal degrees of freedom of the molecules are neglected, the gas velocities are assumed to be low, and the coefficient of heat conductivity is taken to be a constant. The equation then is

$$\lambda\nabla^2T-\tfrac{5}{2}kn\left[\frac{\partial}{\partial t}+S_x\frac{\partial}{\partial x}+S_y\frac{\partial}{\partial y}\right]T=-Q-\tfrac{5}{2}knT\Sigma K_i, \tag{3.14}$$

where λ is the coefficient of heat conductivity, k is the Boltzmann constant and Q the heat release per unit of volume and time. Also, use has been made of the gas law in the form

$$P=knT. \tag{3.15}$$

We must finally specify the combustion mechanism. Here is where the present model introduces the most crude approximations. Without more justification then, than that the proposed relations are the simplest ones that one can use, we take

in the pre-heat zone, $Q = 0$; $K_i = 0$;

in the burning zone, the reaction is symbolized by the equation

$$a_1[1] + a_2[2] \Rightarrow a_3[3],$$

where a_i denotes the number of molecules of every component that participates in one reaction.

For the heat production we can then write

$$Q = -\frac{q}{a_1} K_1, \tag{3.16}$$

where q is the amount of heat produced in one reaction. We now define α^* to be the fraction of n_1 that participates in the reaction per unit of time. It then follows that

$$K_1 = -\alpha^* n_1, \quad K_2 = -\frac{a_2}{a_1}\alpha^* n_1, \quad K_3 = +\frac{a_3}{a_1}\alpha^* n_1. \tag{3.17}$$

In order to consider perturbations of the flame structure we introduce a new co-ordinate system, attached to the moving flame front

$$\xi = x - x_0(y,t), \quad \eta = y, \quad x_0 = \bar{x}_0(\eta)\, e^{\nu t}. \tag{3.18}$$

Here x_0 measures the distance from the instantaneous position of the ignition point to its position before disturbance was introduced. Thus $\xi = 0$ represents the ignition point in the new co-ordinate system. We now define the perturbation quantities as follows. Let any quantity introduced in this section be $f(x,y,t)$. We write

$$f(x,y,t) = \bar{f}(\xi) + f'(\xi,\eta)\, e^{\nu t}, \tag{3.19}$$

where $\bar{f}$ is the steady-state one-dimensional quantity, and f' is the perturbation; ν can, of course, be complex. We must transform the equations of this section according to (3.18), introduce the various expressions (3.19), and linearize the equations for the perturbation quantities. Instead of summarizing here all the equations obtained in this way, we shall introduce them in the following sections, as the need for them arises.

4. One-dimensional stationary flames

For the theory of perturbations we shall need some results of the stationary one-dimensional flame front. Also, since for stationary one-dimensional flames various theories are available, it is interesting to find out what results the present simple model gives for this case, and compare them with existing flame formulas.

We consider first the pre-heat zone. The energy equation becomes

$$\lambda \frac{d^2\bar{T}}{d\xi^2} - \tfrac{5}{2} k \bar{n} \bar{S}_x \frac{d\bar{T}}{d\xi} = 0. \tag{4.1}$$

The continuity equation (3.4) is

$$\frac{d}{d\xi}(\overline{nS_x}) = 0, \tag{4.2}$$

or

$$\overline{nS_x} = \overline{n}_0\overline{u}_0. \tag{4.3}$$

Thus we introduce the parameter

$$\tau = \tfrac{5}{2}k\frac{\overline{n}_0\overline{u}_0}{\lambda}, \tag{4.4}$$

and obtain the temperature profile in the pre-heat zone

$$\overline{T} = \overline{T}_0 + (\overline{T}_i - \overline{T}_0)\,e^{\tau\xi}. \tag{4.5}$$

Next we consider the burning zone. We introduce one more approximation: we assume that the total number of molecules does not change too much in combustion, $\Sigma K_i = 0$. We then have, for the energy equation,

$$\lambda\frac{d^2\overline{T}}{d\xi^2} - \tfrac{5}{2}k\overline{n}\overline{S}_x\frac{d\overline{T}}{d\xi} + \overline{Q} = 0, \tag{4.6}$$

$$Q = \frac{q}{a_1}\alpha^*\overline{n}_1. \tag{4.7}$$

Result (4.3) still holds in the burning zone. For the continuity equation of species [1] we obtain, from (3.3),

$$\frac{d}{d\xi}[\overline{n}_1(\overline{u} + \overline{V}_1)] = -\alpha^*\overline{n}_1. \tag{4.8}$$

Now, the diffusion process is governed by parameters of the type $\mu = \overline{u}/D_{ij}$, where μ is usually of the same order of magnitude as τ. Our flame model is based on the assumption that $\alpha^*/\overline{u}_f\tau \gg 1$, and thus also $\alpha^*/\overline{u}_f\mu \gg 1$. It follows that the distribution of $\overline{n}_1$ in the burning zone is mainly governed by the rates of reaction, and thus that diffusion can be neglected.

We also make use of the fact that at low velocities the pressure changes across the flame front are negligibly small (see Emmons 1958) so that $\overline{n}\overline{T}$ is constant.

Under these conditions $\overline{n}_1$ can easily be eliminated from (4.6), (4.7) and (4.8), and we obtain

$$\left(\frac{d}{d\xi} + \frac{\alpha^*}{\overline{u}_f}\frac{\overline{T}_f}{\overline{T}}\right)\left[\frac{d\overline{T}}{d\xi} - \tau(\overline{T} - \overline{T}_f)\right] = 0. \tag{4.9}$$

Integrating over the burning zone we now have

$$\left(\frac{d\overline{T}}{d\xi}\right)_{\xi=0} = -\tau(\overline{T}_f - \overline{T}_i) + \frac{\alpha^*}{\overline{u}_f}\overline{T}_f\ln\left(\frac{\overline{T}_f}{\overline{T}_i}\right) + \frac{\alpha^*\tau}{\overline{u}_f}\overline{T}_f\int_0^{\epsilon_2}\frac{\overline{T}_f - \overline{T}}{\overline{T}}\,d\xi. \tag{4.10}$$

Equating the slope of the temperature curve at the ignition point $\xi = 0$ from (4.10) with the solution (4.5) in the pre-heat zone, we obtain

$$\overline{T}_f - \overline{T}_0 = \frac{\alpha^*}{\overline{u}_f\tau}\overline{T}_f\left\{\ln\left(\frac{\overline{T}_f}{\overline{T}_i}\right) + \tau\int_0^{\epsilon_2}\frac{\overline{T}_f - \overline{T}}{\overline{T}}\,d\xi\right\}. \tag{4.11}$$

Since $\overline{T}_f - \overline{T}_i$ is small, the first term between brackets is of the order of magnitude $\overline{T}_f - \overline{T}_i$, while the second one is of the order $\tau\epsilon_2(\overline{T}_f - \overline{T}_i)$, and consequently, much smaller than the first one ($\tau\epsilon_2 \sim \epsilon_2/\epsilon_1$). Thus, retaining only the dominant terms, we have

$$\frac{\alpha^*}{\overline{u}_f\tau}\frac{\overline{T}_f - \overline{T}_i}{\overline{T}_f - \overline{T}_0} = 1, \tag{4.12}$$

which is the Mallard–LeChatelier formula (Emmons 1958).

5. The perturbation of the flame velocity

As discussed in § 2, the perturbations produce two kinds of effects on the flame structure. There is a change of composition of the mixture, resulting from diffusion and convection perturbations, which produces a perturbation of the heat release in the burning zone, and thus a perturbation of the final flame temperature T_f. There are also the convective and curvature effects on the heat conduction process, which result in a perturbation of the amount of heat needed to raise the temperature in the pre-heat zone to the ignition point. By the energy balance, however, this also means a perturbation of the final flame temperature. The net effect of both processes is a perturbation T_f'.

The perturbation of flame propagation velocity is, in the notation of § 3, $(u' - \nu\bar{x}_0)_0$, where subscript zero means that the value at the upstream flame boundary is taken. It seems reasonable to expect that for small perturbations the flame velocity will be proportional to T_f' and therefore governed by a formula of the type

$$\left(\frac{u' - \nu\bar{x}_0}{\overline{u}}\right)_0 = c\frac{T_f'}{\overline{T}_0}, \tag{5.1}$$

where c is some constant which depends on the physical properties of the mixture.

If we consider the Mallard–LeChatelier relation (4.12) and calculate the change of the flame velocity caused by some small change of T_f, we find indeed a formula of the type (5.1), with c given by

$$c = \frac{1}{2}\left\{\left(\frac{\alpha^*}{\overline{u}_f\tau} - 1\right)\frac{\overline{T}_0}{\overline{T}_f - \overline{T}_0} - \frac{\overline{T}_0}{\overline{T}_f}\right\}, \tag{5.2}$$

or, for $\alpha^*/\overline{u}_f\tau \gg 1$,

$$c \cong \frac{1}{2}\frac{\alpha^*}{\overline{u}_f\tau}\frac{\overline{T}_0}{\overline{T}_f - \overline{T}_0}. \tag{5.3}$$

In Eckhaus (1959) it has been shown that, if the formula for the flame propagation velocity is developed from the complete perturbation equations of § 3, for sufficiently large $\alpha^*/\overline{u}_f\tau$, the result is indeed given by (5.1) and (5.3).

In the present study we shall adopt (5.1) for the flame velocity. Of course, any more sophisticated model of the flame structure would lead to a more complicated flame velocity formula. It is hoped, however, that even though the present model constitutes an over-simplification, the main effects of the perturbations on the flame velocity are reasonably represented by the formula (5.1).

We are now left with the task of evaluating T_f' which in the present theory summarizes all the effects of flame-structure perturbations. This means that we must still consider the complete system of partial differential perturbation equations as defined in § 3, and construct their solutions. However, the task

can be considerably simplified by the following consideration. For stability analysis we may assume the ratio of flame thickness to the wavelength of disturbances to be very small. (In a stationary problem of a slightly curved flame front, the ratio of flame thickness to the local radius of curvature will usually be very small.) Thus we may attempt to solve the perturbation equations in terms of power series of the flame thickness parameters. The procedure is particularly simple if only linear terms in flame thickness are retained. The problem can then be solved by an integral method, and the final results are not too complicated.

We consider first the pre-heat zone $\xi < 0$. Linear perturbation of the energy equation (3.14) gives

$$\nabla^2 T' - \tau\left[\frac{\nu}{\bar{S}}T' + \frac{\partial T'}{\partial \xi}\right] = \tau\left[\frac{S'_x - \nu\bar{x}_0}{\bar{S}} + \frac{n'}{\bar{n}}\right]\frac{d\bar{T}}{d\xi} + \frac{d^2\bar{x}_0}{d\eta^2}\frac{d\bar{T}}{d\xi}, \tag{5.4}$$

where use has been made of some results of § 4. Similarly, the continuity equation (3.4) leads to the perturbation equation

$$\frac{\nu}{\bar{S}}\frac{n'}{\bar{n}} + \frac{\partial}{\partial\xi}\left(\frac{n'}{\bar{n}}\right) + \frac{\partial}{\partial\xi}\left(\frac{S'_x - \nu\bar{x}_0}{\bar{S}}\right) + \frac{\partial}{\partial\eta}\left(\frac{S'_y}{\bar{S}}\right) = 0. \tag{5.5}$$

Finally, since the pressure is approximately constant over the flame region, the perturbation of (3.15) leads to

$$\frac{n'}{\bar{n}} = -\frac{T'}{\bar{T}}. \tag{5.6}$$

Combining the above equations we have

$$\frac{\partial^2 T'}{\partial\xi^2} = \tau\frac{\partial}{\partial\xi}\left[\bar{T}\frac{S'_x - \nu\bar{x}_0}{\bar{S}}\right] + \tau\bar{T}\frac{\partial}{\partial\eta}\left(\frac{S'_y}{\bar{S}}\right) + \frac{d^2\bar{x}_0}{d\eta^2}\frac{d\bar{T}}{d\xi} - \frac{\partial^2 T'}{\partial\eta^2}. \tag{5.7}$$

We now integrate (5.7) over the pre-heat zone, and, making use of the condition that temperature perturbations must disappear at $\xi = -\epsilon_1$, we obtain

$$\begin{aligned}\frac{1}{\tau}\left(\frac{\partial T'}{\partial\xi}\right)_i = \bar{T}_i\left[\frac{S'_x - \nu\bar{x}_0}{\bar{S}}\right]_i - \bar{T}_0\left[\frac{S'_x - \nu\bar{x}_0}{\bar{S}}\right]_0 + \int_{-\epsilon_1}^{0}\bar{T}\frac{\partial}{\partial\eta}\left(\frac{S'_y}{\bar{S}}\right)d\xi \\ + \frac{1}{\tau}(\bar{T}_i - \bar{T}_0)\frac{d^2\bar{x}_0}{d\eta^2} - \frac{1}{\tau}\int_{-\epsilon_1}^{0}\frac{\partial^2 T'}{\partial\eta^2}\,d\xi.\end{aligned} \tag{5.8}$$

Note that the last term on the right-hand side is of second order in flame thickness, and can thus be neglected.

Consider now the burning zone. Identical derivation leads to

$$\begin{aligned}\frac{1}{\tau}\left(\frac{\partial T'}{\partial\xi}\right)_i = \frac{1}{\tau}\left(\frac{\partial T'}{\partial\xi}\right)_f - \bar{T}_f\left[\frac{S'_x - \nu\bar{x}_0}{\bar{S}}\right]_f + \bar{T}_i\left[\frac{S'_x - \nu\bar{x}_0}{\bar{S}}\right]_i \\ + \frac{1}{\tau\lambda}\int_0^{\epsilon_2}Q'\,d\xi - \int_0^{\epsilon_2}\bar{T}\frac{\partial}{\partial\eta}\left(\frac{S'_y}{\bar{S}}\right)d\xi - \frac{1}{\tau}(\bar{T}_f - \bar{T}_i)\frac{d^2\bar{x}_0}{d\eta^2} + O(\epsilon^2).\end{aligned} \tag{5.9}$$

Since outside the flame region the temperature fluctuations will only be convected downstream, we have

$$\left(\frac{\partial T'}{\partial\xi}\right)_f = -\frac{\nu}{\bar{u}_f}T'_f. \tag{5.10}$$

Also, we make use of the fact that diffusion velocities must vanish at the flame boundaries. Combining (5.8) and (5.9) we then have

$$\frac{1}{\tau\lambda}\int_0^{\epsilon_2} Q'\,d\xi = \overline{T}_f\left(\frac{u'-\nu\bar{x}_0}{\bar{u}}\right)_f - \overline{T}_0\left(\frac{u'-\nu\bar{x}_0}{\bar{u}}\right)_0 + \frac{\nu}{\bar{u}_f\tau}T'_f + \int_{-\epsilon_1}^{\epsilon_2}\overline{T}\frac{\partial}{\partial\eta}\left(\frac{S'_y}{\bar{S}}\right)d\xi + \frac{1}{\tau}(\overline{T}_f-\overline{T}_0)\frac{d^2\bar{x}_0}{d\eta^2} + O(\epsilon^2). \quad (5.11)$$

We next compute the perturbation of the heat-release Q'. From (3.3), (3.16) and (3.17) we have the linear perturbation equation

$$Q' = -\frac{q}{a_1}\left\{\nu(n_1)' + \frac{\partial}{\partial\xi}[n_1(u-\nu\bar{x}_0+V_{1x})]' + \frac{\partial}{\partial\eta}[(\bar{n}_1)v' + (n_1V_{1x})']\right\}, \quad (5.12)$$

where q can easily be found to be

$$q = \tau\lambda a_1\frac{\overline{T}_f-\overline{T}_0}{(\overline{n_1u})_0}. \quad (5.13)$$

The total heat-release perturbation is thus

$$\frac{1}{\tau\lambda}\int_0^{\epsilon_1} Q'\,d\xi = -\frac{\overline{T}_f-\overline{T}_0}{(\overline{n_1u})_0}\left\{\nu\int_0^{\epsilon_2} n'_1\,d\xi - [n_1(u-\nu x_0+V_{1x})]'_i + \int_0^{\epsilon_2}\frac{\partial}{\partial\eta}[\bar{n}_1v' + (n_1V_{1y})']\,d\xi\right\}. \quad (5.14)$$

We can also integrate the continuity equation for species [1] over the pre-heat zone to obtain

$$[n_1(u-\nu x_0+V_{1x})]'_i = (\bar{n}_1)_0(u'-\nu x_0)_0 - \nu\int_{-\epsilon_1}^0 n'_1\,d\xi - \int_{-\epsilon_1}^0\frac{\partial}{\partial\eta}[\bar{n}_1\nu' + (n_1V_{1y})']\,d\xi. \quad (5.15)$$

Combining (5.11), (5.14) and (5.15), and using the integrated form of (5.5) we find

$$\left(1+\frac{\nu}{\bar{u}_f\tau}\right)T'_f = -\nu\left\{\frac{\overline{T}_f-\overline{T}_0}{(\overline{n_1u})_0}\int_{-\epsilon_1}^{\epsilon_2} n'_1\,d\xi + \overline{T}_f\int_{-\epsilon_1}^{\epsilon_2}\frac{T'\,d\xi}{\bar{S}\overline{T}}\right\} - \frac{1}{\tau}(\overline{T}_f-\overline{T}_0)\frac{d^2\bar{x}_0}{d\eta^2}$$
$$-(\overline{T}_f-\overline{T}_0)\overline{\left(\frac{n}{n_1}\right)}_0\int_{\epsilon_1}^{\epsilon_2}\left[\overline{\left(\frac{n_1}{n}\right)} - \overline{\left(\frac{n_1}{n}\right)}_0\right]\frac{\partial v'}{\partial\eta}\frac{d\xi}{\bar{S}} + \int_{-\epsilon_1}^{\epsilon_2}(\overline{T}_0-\overline{T})\frac{\partial v'}{\partial\eta}\frac{d\xi}{\bar{S}}$$
$$-(\overline{T}_f-\overline{T}_0)\frac{1}{(\overline{n_1u})_0}\int_{-\epsilon_1}^{\epsilon_2}\frac{\partial}{\partial\eta}(n_1V_{1y})'\,d\xi + \frac{1}{(\overline{n_1u})_0}\int_{-\epsilon_1}^{\epsilon_2}(\overline{T}_f-\overline{T}_0)\frac{\partial}{\partial\eta}\Sigma\,(n_iV_{iy})'\,d\xi$$
$$+O(\epsilon^2). \quad (5.16)$$

T'_f is expressed by equation (5.16) in terms of integrals over the flame region. Since we wish to retain in the expression for T'_f only linear terms in flame thickness, it is sufficient to retain in the integrands only terms independent of the flame thickness. Moreover, since $\epsilon_2 \ll \epsilon$, we may neglect the contribution of the burning zone to the integrals.

Consider the tangential momentum equation (3.2). The perturbation equation, when integrated from $\xi = -\epsilon_1$ to an arbitrary point inside the flame region, gives

$$v' + \bar{u}\frac{d\bar{x}_0}{d\eta} = \left[v' + \bar{u}\frac{dx_0}{d\eta}\right]_0 + O(\epsilon). \quad (5.17)$$

Similarly, for the tangential diffusion velocities, we find from (3.9) and (3.10) that

$$(n_i V_{iy})' = -\overline{n_i V_i}\frac{d\bar{x}_0}{d\eta} + O(\epsilon). \tag{5.18}$$

The magnitude $\overline{n_i V_i}$ follows from the stationary form of (3.3):

$$\overline{n_i V_i} = (\overline{n_i u})_0 - \overline{n_i u}. \tag{5.19}$$

Introducing these results into (5.16) and using (5.1), we finally obtain

$$\left(\frac{u'-\nu\bar{x}_0}{\bar{u}}\right)_0 = -\nu c\left\{\frac{\overline{T}_f-\overline{T}_0}{(\overline{n_1 u})_0}\int_{-\epsilon_1}^{0} n_1' d\xi + \overline{T}_f\int_{-\epsilon_1}^{0} T'\frac{d\xi}{\overline{S}\overline{T}}\right\}$$
$$-c\frac{\partial}{\partial\eta}\left[v' + \bar{u}\frac{d\bar{x}_0}{d\eta}\right]_0\left\{\int_{-\epsilon_1}^{0}\frac{\overline{T}-\overline{T}_0}{\overline{T}}d\xi - (\overline{T}_f-\overline{T}_0)\left(\overline{\frac{n}{n_1}}\right)_0\int_{-\epsilon_1}^{0}\left[\left(\overline{\frac{n_1}{n}}\right) - \left(\overline{\frac{n_1}{n}}\right)_0\right]\frac{d\xi}{\overline{S}}\right\}$$
$$+O(\epsilon^2). \tag{5.20}$$

Thus for the evaluation of the flame-velocity perturbation we need for the first group of terms the solutions of the perturbation diffusion and heat-conduction problems. However, we can neglect in these solutions terms of the order of magnitude of the flame thickness. For the evaluation of the second group of terms we need only the solutions of the stationary one-dimensional flame structure.

6. The diffusion problem

Solution of the diffusion equations (3.12) and (3.13) is a straightforward procedure which has been performed in some detail in Eckhaus (1959). Omitting here the calculations, we shall state the results.

Introduce the following diffusion parameters

$$\mu_1 = \frac{\bar{u}_0}{D_{12}}, \quad \mu_3 = \frac{\bar{u}_0}{D_3}, \tag{6.1}$$

$$\Omega = \frac{D_3}{D_{13}}\frac{D_{13}-D_{12}}{D_3-D_{12}}. \tag{6.2}$$

The solution of the one-dimensional steady-state problem is then

$$\overline{\left(\frac{n_3}{n}\right)} = \overline{\left(\frac{n_3}{n}\right)}_f e^{\mu_3\xi}, \tag{6.3}$$

$$\overline{\left(\frac{n_1}{n}\right)} = \overline{\left(\frac{n_1}{n}\right)}_0\left\{1 - e^{\mu_1\xi} - \Omega\overline{\left(\frac{n_3}{n}\right)}_f(e^{\mu_3\xi} - e^{\mu_1\xi})\right\}, \tag{6.4}$$

where $\overline{(n_3/n)}_f$ is the relative concentration of the products of combustion in the burned gas.

For the perturbation problem we find that

$$\left(\frac{n_3}{n}\right)' = \left(\frac{u'-\nu\bar{x}_0}{\bar{u}}\right)_0\overline{\left(\frac{n_3}{n}\right)}_f\mu_3\xi e^{\mu_3\xi} + O(\epsilon), \tag{6.5}$$

$$\left(\frac{n_1}{n}\right)' = -\left(\frac{u'-\nu\bar{x}_0}{\bar{u}}\right)_0\overline{\left(\frac{n_1}{n}\right)}_0\left\{e^{\mu_1\xi} + \Omega\overline{\left(\frac{n_3}{n}\right)}_f\left(\frac{\mu_3}{\mu_1}e^{\mu_3\xi} - e^{\mu_1\xi}\right)\right\}\mu_1\xi + O(\epsilon). \tag{6.6}$$

7. The heat-conduction problem

The stationary one-dimensional solution (4.5) we have found already. The perturbation problem is somewhat more complicated. We have a coupled system of equations, (5.4) and (5.5). Eliminating terms involving S'_x we can write the governing equation in the form

$$\frac{\partial}{\partial\xi}\left[\frac{1}{\overline{T}}\left(\frac{\partial T'}{\partial\xi}-\tau T'\right)\right]-\frac{\nu\tau}{\overline{u}_0}\frac{\overline{T}_0}{\overline{T}^2}T'+\frac{\partial}{\partial\xi}\left(\frac{1}{\overline{T}}\int_{-\epsilon_1}^{\xi}\frac{\partial^2 T'}{\partial\eta^2}\,d\xi'\right)=\tau\frac{\partial}{\partial\xi}\left[\frac{1}{\overline{T}}R(\xi)\right], \tag{7.1}$$

$$R(\xi)=(\overline{T}-\overline{T}_0)\left(\frac{u'-\nu\bar{x}_0}{\overline{u}}\right)_0+\frac{\overline{T}}{\overline{S}}\int_{-\epsilon_1}^{\xi}\frac{\partial S'_y}{\partial\eta}\,d\xi'-\overline{T}\int_{-\epsilon_1}^{\xi}\frac{1}{\overline{S}}\frac{\partial S'_y}{\partial\eta}\,d\xi'+\frac{1}{\tau}(\overline{T}-\overline{T}_0)\frac{d^2\bar{x}_0}{\partial\eta^2}. \tag{7.2}$$

The relative order of magnitude of the various terms can be analysed by the transformation $\xi^*=\tau\xi$. We then have

$$\frac{\partial}{\partial\xi^*}\left[\frac{1}{\overline{T}}\left(\frac{\partial T'}{\partial\xi^*}-T'\right)\right]-\frac{\nu}{\overline{u}_0\tau}\frac{\overline{T}_0}{\overline{T}^2}T'+\frac{1}{\tau^2}\frac{\partial}{\partial\xi^*}\left(\frac{1}{\overline{T}}\int_{-\epsilon_1}^{\xi^*}\frac{\partial^2 T'}{\partial\eta^2}\,d\xi'\right)=\frac{\partial}{\partial\xi^*}\left[\frac{1}{\overline{T}}R(\xi^*)\right], \tag{7.3}$$

$$R(\xi^*)=(\overline{T}-\overline{T}_0)\left[\frac{u'-\nu\bar{x}_0}{\overline{u}}\right]_0+\frac{1}{\tau}\left\{\frac{\overline{T}}{\overline{S}}\int_{-\epsilon_1}^{\xi^*}\frac{\partial S'_y}{\partial\eta}\,d\xi'-\overline{T}\int_{-\epsilon_1}^{\xi^*}\frac{1}{\overline{S}}\frac{\partial S'_y}{\partial\eta}\,d\xi'+(\overline{T}-\overline{T}_0)\frac{d^2\bar{x}_0}{\partial\eta^2}\right\}. \tag{7.4}$$

We are looking for some form of expansion of T' in terms of the inverse powers of τ (the flame-thickness parameter), and, as discussed in §5, it is sufficient for the present purpose to evaluate only the term of T' which is independent of τ. This suggests that we should neglect directly in (7.3) and (7.4) all terms of order τ^{-1} and τ^{-2}. The resulting equation is a very simple one, but unfortunately it does not lead to correct results. If we solve it, and consider the solution as a first step in an iteration process, we find that the next approximation to T', which is of the order τ^{-1}, does not satisfy the boundary condition that T' should vanish in the vicinity of the outer flame boundary. A more careful approach is thus needed. We must consider a more complete form of (7.3) and (7.4), construct a solution with a proper behaviour, and evaluate the term of T' that is of interest as a limit of the solution for $\tau\to\infty$.

Consider now the equation

$$\frac{\partial}{\partial\xi^*}\left[\frac{1}{\overline{T}}\left(\frac{\partial T'}{\partial\xi^*}-T'\right)\right]-\frac{\nu}{\overline{u}_0\tau}\frac{\overline{T}_0}{\overline{T}^2}T'=\left(\frac{u'-\nu\bar{x}_0}{\overline{u}}\right)_0\frac{d}{d\xi^*}\left(\frac{\overline{T}-\overline{T}_0}{\overline{T}}\right). \tag{7.5}$$

This may seem a somewhat inconsistent approximation, since in (7.3) we have retained terms of the order τ^{-1}, while in the definition (7.4) of $R(\xi^*)$ we have neglected them. However, $R(\xi^*)$, which is the forcing function of the problem, is not responsible for the behaviour of the solution. If more terms of $R(\xi^*)$ are retained, they prove to contribute only to the labour; in the final results their contribution can be neglected. In the present presentation they have therefore already been neglected at the outset.

Introduce now a new unknown function

$$T'=\frac{\overline{u}_0\tau}{\nu}\left[\frac{u'-\nu\bar{x}_0}{\overline{u}}\right]_0(\overline{T}-\overline{T}_0)(T^*-1). \tag{7.6}$$

Equation (7.5) then becomes

$$\frac{\partial}{\partial \xi^*}\left[\frac{\overline{T}-\overline{T}_0}{\overline{T}}\frac{\partial T^*}{\partial \xi^*}\right]-\frac{\nu}{\overline{u}_0\tau}\frac{\overline{T}_0}{\overline{T}}\frac{\overline{T}-\overline{T}_0}{\overline{T}}T^*=0. \tag{7.7}$$

The most convenient form can be obtained by putting

$$T^*=e^{\sigma\xi^*}G(\xi^*), \quad \sigma=-\tfrac{1}{2}+\tfrac{1}{2}\sqrt{\left(1+4\frac{\nu}{\overline{u}_0\tau}\right)}, \tag{7.8}$$

and transforming the co-ordinates by

$$z=\frac{\overline{T}}{\overline{T}_0}. \tag{7.9}$$

We then obtain

$$z(1-z)\frac{d^2G}{dz^2}-[1+(z+\sigma)z]\frac{dG}{dz}-\sigma^2G=0, \tag{7.10}$$

which is the standard form of the hypergeometric equation. From Erdelyi (1953) we find the two independent solutions

$$G(z)=\mathscr{C}_1F[\sigma,\sigma;2\sigma+2;1-z]+\mathscr{C}_2z^2F[\sigma+2,\sigma+2;3;z], \tag{7.11}$$

where F is the hypergeometric function. We apply now the boundary condition that the temperature perturbation must vanish near the outer flame boundary; thus $T'\to 0$ when $z\to 1$.

Investigation of the behaviour of the two hypergeometric functions shows that the condition can only be satisfied if $\mathscr{C}_2=0$. To determine $\mathscr{C}_1$ we need a boundary condition at the ignition point, where we can have a perturbation of the ignition temperature T_i'. But since the ignition temperature is a fictitious magnitude, it is difficult to postulate a condition for its perturbation. In fact, this is one of the points in which the over-simplification of the flame model brings the theory into trouble. We may, however, reason as follows. Physically, the ignition temperature represents an approximation of the fact that rates of reaction are very low at low temperature and increase rapidly at a sufficiently high temperature. Therefore the question is really whether the perturbations of the flame structure influence rates of reaction so that, in comparison with unperturbed conditions, this rapid rise takes place at a somewhat different temperature. For a thermally propagating flame there seems to be not much reason for effects of this kind. We shall therefore assume that $T_i'=0$. With this, somewhat speculative, boundary condition, we find that

$$\frac{1}{\mathscr{C}_1}=F[\sigma,\sigma;2\sigma+2;1-z_i], \quad z_i=\frac{\overline{T}_i}{\overline{T}_0}. \tag{7.12}$$

The temperature distribution in the pre-heat zone is now completely specified.

8. Final results of the flame propagation velocity

The results of §§ 6 and 7 must now be substituted into (5.20) and the integrals must be evaluated. Also, the integrals involving T' must be expanded in terms of inverse powers of τ. The necessary calculations have been performed in detail by Eckhaus (1959). We shall here summarize the results.

The perturbation formula for the flame propagation velocity is

$$\left(\frac{u'-\nu\bar{x}_0}{\bar{u}}\right)_0 = -c\left\{\frac{\nu}{\bar{u}_0\tau}\left(\frac{u'-\nu\bar{x}_0}{\bar{u}}\right)_0 A_1 + \frac{1}{\tau}\frac{\partial}{\partial\eta}\left(\frac{v'}{\bar{u}}+\frac{d\bar{x}_0}{\partial\eta}\right)_0 A_2\right\} + O(\epsilon^2). \tag{8.1}$$

The coefficients A_1 and A_2 can be written as follows

$$A_1 = -\frac{r-1}{r}(K_1+K_2)+K_3, \quad A_2 = \frac{r-1}{r}(K_1+K_2). \tag{8.2}$$

Here, r denotes the ratio of the final flame temperature to the temperature of the unburned mixture; thus

$$r = \overline{T}_f/\overline{T}_0.$$

Furthermore,

$$K_1 = -\tau\overline{T}_f\int_{-\infty}^{0}(e^{\mu_1\xi}-e^{\tau\xi})\frac{d\xi}{\overline{T}}, \tag{8.3}$$

$$K_2 = -\tau\overline{T}_f\overline{\left(\frac{n_3}{n}\right)}_f\,\Omega\int_{-\infty}^{0}(e^{\mu_3\xi}-e^{\mu_1\xi})\frac{d\xi}{\overline{T}}, \tag{8.4}$$

where

$$\overline{T} = \overline{T}_0+(\overline{T}_f-\overline{T}_0)\,e^{\tau\xi}.$$

Finally,

$$K_3 = \frac{3}{4}\frac{r-1}{r}+\frac{2}{r}\ln(r-1)+\ln\left(\frac{r}{r-1}\right)+\frac{3}{r(r-1)}+\frac{1}{r}\sum_{n=2}^{\infty}(-1)^n\frac{(r-1)^{-n}}{n(n-1)}. \tag{8.5}$$

The various diffusion and heat-conduction parameters have been defined in §§ 4, 6 and 7.

The flame-velocity formula (8.1) is the final result of the present theory. It shows that there is a perturbation of the flame velocity due to acceleration of the flame front and a perturbation due to curvature effects. The particular combination

$$\left(v'+\bar{u}\frac{d\bar{x}_0}{d\eta}\right)_0$$

that occurs in the curvature term permits a direct interpretation: it is the component of the velocity of fluid relative to the flame front, that is tangential to the instantaneous flame position. This interpretation leads to some interesting observations. Consider a flame front of circular shape. If the radius is large compared with the flame thickness, we can apply the present theory locally at every point of the flame. Since the fluid motion is in this case strictly in the radial direction, it is easily found that

$$\left(v'+\bar{u}\frac{dx_0}{d\eta}\right)_0 = 0$$

at every point of the flame, and thus, that up to the first order in flame thickness there is no effect whatever of the curvature of the flame on its propagation velocity.

Now, real flames are almost never two-dimensional. Fortunately, however, an extension of the present theory to three dimensions is almost trivial. As discussed in Eckhaus (1959), it is easily found that the effects of curvature are additive. Thus, if ζ is the third space direction (in a Cartesian co-ordinate system

in which the $\zeta-\eta$ plane is tangential to the flame front at the point that we consider) and if w is the fluid velocity in the ζ-direction, the extension of (8.1) to three dimensions is

$$\left(\frac{u'-\nu\bar{x}_0}{\bar{u}}\right)_0 = -c\left\{\frac{\nu}{\bar{u}_0\tau}\left(\frac{u'-\nu\bar{x}_0}{\bar{u}}\right)_0 A_1+\frac{1}{\tau}\left[\frac{\partial}{\partial\eta}\left(\frac{v'}{\bar{u}_0}+\frac{\partial\bar{x}_0}{\partial\eta}\right)_0+\frac{\partial}{\partial\zeta}\left(\frac{w'}{\bar{u}_0}+\frac{\partial\bar{x}_0}{\partial\zeta}\right)_0\right]A_2\right\}+O(\epsilon^2). \tag{8.6}$$

It follows now that for a spherical flame front there will be no effects of curvature on the flame velocity.

Consider finally the flame on a Bunsen-burner, which is nearly conical in shape. If we apply (8.6) at an arbitrary point of the flame, we find that the curvature, caused by the rotational symmetry of the flame, has no effect on the propagation velocity. The only effect that arises is that due to curvature in the meridian plane. Since this curvature is extremely small, except in the tip-region, the total effect of curvature for a Bunsen-burner flame will be extremely small.

The above holds for the spherical flame front quite independently of the magnitude of the constant c. For the Bunsen-burner flame it holds for values of c up to say $c = O(\tau)$. It follows that c can be quite large, and yet its effect will not be felt in most experimental arrangements.

It is somewhat unfortunate for the present theory that the constant c of (8.1) and (8.6) cannot be exactly determined. It is true that in § 5 we have found an approximate expression (5.3) for c. However, not much is gained by expressing c in terms of α^*, since this last quantity is a hypothetical constant rate of reaction which cannot easily be correlated with the true physical properties of the mixture. To be realistic we must accept that the present model of combustion does not determine the constant c. From § 5 we can conclude only that c is positive, and that it can be large if the ratio of thickness of the burning zone to that of the pre-heat zone is sufficiently small (which is the basic postulate of our model).

9. Application to the problem of stability

We shall now consider the stability of a plane flame front. Let the initial disturbance be sinusoidal in the η-direction: thus

$$\bar{x}_0 = \xi_0 \cos\left(\frac{2\pi}{l}\eta\right). \tag{9.1}$$

We recall that, according to § 3 we have

$$x_0(y,t) = \bar{x}_0(\eta)\, e^{\nu t}, \tag{9.2}$$

where x_0 is the instantaneous distance from the flame front to its undisturbed position.

For the stability analysis, solutions of the fluid perturbation velocities in the two regions ahead and behind the flame front are needed, together with boundary conditions at the flame front. These last ones are supplied by the requirement that mass and momentum of the fluid are preserved when passing through the flame front. Details of the derivation can be found elsewhere (Eckhaus 1959;

Emmons 1958). The results for the fluid velocities at the upstream flame boundary are

$$\left(\frac{u'-\nu\bar{x}_0}{\bar{u}}\right)_0 = -\frac{\xi_0}{2(r+\omega)}\left\{\omega^2\frac{r+1}{r}+2\omega-(r-1)\right\}\frac{2\pi}{l}\cos\left(\frac{2\pi}{l}\eta\right), \tag{9.3}$$

$$\frac{\partial}{\partial\eta}\left[\frac{v'}{\bar{u}}+\frac{d\bar{x}_0}{d\eta}\right] = \frac{\xi_0}{2(r+\omega)}\left\{\omega^2\frac{r-1}{r}+2r\omega+(3r-1)\right\}\left(\frac{2\pi}{l}\right)^2\cos\left(\frac{2\pi}{l}\eta\right), \tag{9.4}$$

where

$$\omega = \frac{\nu l}{2\pi\bar{u}_0}.$$

When Landau's hypothesis—that the flame velocity is not affected by the perturbations—is applied, we must put (9.3) equal to zero.

In the present case we introduce (8.1) for the flame velocity and after elimination obtain

$$\omega^3\frac{r+1}{r}\frac{c}{2\pi l\tau}A_1+\omega^2\left[\frac{r+1}{r}+\frac{c}{2\pi l\tau}\left(2A_1+\frac{r-1}{r}A_2\right)\right]$$
$$+\omega\left[2+\frac{c}{2\pi l\tau}\left(-\frac{r-1}{r}A_1+2A_2\right)\right]-(r-1)\left[1-\frac{3r-1}{r-1}\frac{c}{2\pi l\tau}A_2\right]=0. \tag{9.5}$$

We shall now investigate conditions for stability. If the flame is to be stable, the real parts of all roots of (9.5) must be negative. This puts requirements on the coefficients of (9.5). For stability we must have

$$\left[\frac{3r-1}{r-1}\frac{A_2}{A_1}-\frac{2\pi l\tau}{cA_1}\right] > 0, \tag{9.6}$$

$$\left[r\left(2\frac{A_2}{A_1}-\frac{r-1}{r}\right)+2\frac{2\pi l\tau}{cA_1}\right] > 0, \tag{9.7}$$

$$\left[\frac{r-1}{r}\frac{A_2}{A_1}+2+\frac{r+1}{r}\frac{2\pi l\tau}{cA_1}\right] > 0. \tag{9.8}$$

It can easily be shown that the inequalities can be satisfied if and only if A_1 and A_2 are of the same sign. Using definitions (3.2) and remarking that K_3 is a positive number, we arrive at a necessary (though not sufficient) condition for existence of stable solutions

$$\frac{r}{r-1}K_3 \geqslant (K_1+K_2) \geqslant 0. \tag{9.9}$$

Condition (9.9) does not depend on the parameter $l\tau$, which is the ratio of wavelength of disturbance to thickness of the flame front, but only on the properties of the mixture that is being burned. If the mixture is such that condition (9.9) is not satisfied, the flame will be unstable to all disturbances. If, however, the mixture satisfies condition (9.9) there may be stable and unstable regions, depending on the wavelength of the disturbances. For the flame to be stable we find then that the wavelength must satisfy the following conditions

$$\frac{c}{2\pi l\tau}(K_1+K_2) > \frac{r}{3r-1}, \tag{9.10}$$

$$\frac{c}{2\pi l\tau}(r-1)\left[K_3-\frac{3r-1}{r}(K_1+K_2)\right] < 2. \tag{9.11}$$

If the mixture is such that $K_3 < \{(3r-1)/r\}(K_1+K_2)$, then condition (9.11) is trivial and all wavelengths smaller than the value given by (9.10) are stable. If, however, $K_3 > \{(3r-1)/r\}(K_1+K_2)$ a second region of instability will occur at small wavelengths. For sufficiently small (K_1+K_2) the two regions may overlap, so that, after all, the flame will be unstable for all wavelengths.

We shall now illustrate the above discussion with some numerical examples. In order to evaluate K_1, K_2, and K_3, various parameters describing the physical properties of the mixture must be known. In the following we shall use a range of values of these parameters, which on the basis of data of Hirschfelder *et al.* (1954) are estimated to be reasonably likely to occur. It should be stressed that the examples are intended as an illustration of the various situations which can occur, rather than study of some particular fuel-oxidizer mixture.

We take in the present examples $\tau = 100\,\mathrm{cm}^{-1}$ and $r = 5$. For a range of values of μ_1, we then find the following:

μ_1/τ	1·5	2·0	3·0	4·0
K_1	0·88	1·25	1·56	1·70

Consider now K_2. Its value depends on τ as well as on various coefficients of diffusion. If we write it in the form

$$K_2 = -\overline{\left(\frac{n_3}{n}\right)}_f \left(1-\frac{D_{12}}{D_{13}}\right)\bar{K}_2, \tag{9.12}$$

then $\bar{K}_2$ is a function of μ_1/τ and μ_3/μ_1. For this last parameter we write, according to definitions (6.1),

$$\frac{\mu_3}{\mu_1} = \frac{D_{12}}{D_3},$$

where D_{12} is the binary diffusion coefficient for the fuel–oxygen diffusion and D_3 is the effective diffusion coefficient for the diffusion of products of combustion into the unburned mixture. In general, the mean molecular weight of the products of combustion will be about the same as that of oxygen, while the mean molecular weight of the combustible mixture will be higher than that of oxygen. From the behaviour of the coefficients of diffusion with respect to molecular weight we then conclude that

$$\frac{D_{12}}{D_3} < 1.$$

For some representative values we find the following:

	$D_{12}/D_3 = \frac{2}{3}$			$D_{12}/D_3 = \frac{1}{2}$	
μ_1/τ	1·5	2·0	3·0	2·0	3·0
$\bar{K}_2$	2·62	1·80	0·94	2·50	1·40

Finally, the coefficient K_3 is a function only of r, and for $r = 5$ its value is

$$K_3 = 1{\cdot}54.$$

We consider now a lean mixture. According to §3, the meanings of the diffusion coefficients are in this case

D_{12} = diffusion of fuel in oxygen,

D_{13} = diffusion of fuel in the products of combustion.

But since the molecular weights of oxygen and the products of combustion are not too different, we conclude that

$$\frac{D_{12}}{D_{13}} \doteq 1,$$

which means that K_2 is very small. Applying now the stability conditions we find that the flame is stable if the wavelength of disturbance is smaller than the value given in the following table:

μ_1/τ	1·5	2·0	3·0	4·0
l in cm	$0{\cdot}15c$	$0{\cdot}22c$	$0{\cdot}28c$	$0{\cdot}30c$

We turn now to the rich mixture. Here the meaning of the symbols is

D_{12} = diffusion of oxygen in fuel,

D_{13} = diffusion of oxygen in the products of combustion,

from which follows that

$$\frac{D_{12}}{D_{13}} < 1 \quad \text{and thus} \quad K_2 < 0.$$

Choosing $D_{12}/D_{13} = 0{\cdot}55$, and also taking $\overline{(n_3/n)_f} = 0{\cdot}9$, we now find the following behaviour:

μ_1/τ	Behaviour for $D_{12}/D_3 = \frac{2}{3}$	Behaviour for $D_{12}/D_3 = \frac{1}{2}$
1·5	Unstable for all wavelengths	—
2·0	Stable for $0{\cdot}01c \leqslant l \leqslant 0{\cdot}09c$	Unstable for all wavelengths
3·0	Stable for $l \leqslant 0{\cdot}20c$	Stable for $l \leqslant 0{\cdot}17c$

If we now consider some specific fuel and oxidizer and wish to compare the behaviour of the flame, for lean and rich mixtures, then μ_1/τ is approximately the same for both cases, so that we must compare the above results for a fixed value of this parameter. It is clear, then, that a situation can easily arise in which the lean and the rich flames will behave very differently. For instance, for μ_1/τ up to 2·0, the lean flames will have a range of stable wavelengths, while the rich flames will be unstable to practically all wavelengths.

The stability boundary for lean flames (and for rich flames, if there is one) still depends on the proportionality constant c. According to our combustion model there is some reason to believe that c will be large. If, for instance, $c = 10$, we find the stability boundary for lean flames at wavelengths of 2 to 3 cm. However, no matter how large c is, according to the present results, instability will always occur at sufficiently large wavelengths. This seems to be in disagreement with Markstein's observations; but at this point we must realize that the theory assumes the flame to be of infinite extent, or, what is more realistic, that the wavelength of disturbance is assumed to be small compared with the dimensions of the flame container. In Markstein's experiments the flame was contained in a circular tube of 10 cm diameter. Most probably, for wavelengths of 2 to 3 cm, wall effects can no longer be neglected. Markstein observed that the overall appearance of the cellular flames was different at different wall temperatures, which suggests that the wall effects can be very important.

It should finally be remarked that for large wavelengths gravitational effects must be taken into account.

10. Conclusions

We have seen in the last section that application of the present theory to the problem of stability leads to results which can be interpreted to be in qualitative agreement with the experimentally observed behaviour. Therefore it appears that the essential features of the phenomena have been retained to some degree, in spite of the over-simplification of the theory.

An improvement of the theory can presumably be achieved by introducing a more correct model of the flame structure. The present method of integrating the equations will then probably still be useful. However, if the model is more complex, the increase of labour can be very large. Moreover, progress in this direction is made difficult because of the absence, at present, of a definite theory for one-dimensional, stationary flame propagation. This makes the choice of the model for the perturbation theory almost a matter of taste. As we have already remarked, the present theory can be considered to be a counterpart of the simplest available stationary one-dimensional theory. It cannot be expected to provide all the answers; it may even be incorrect at some points. It will, however, serve its purpose if it does provide the first step in a correct direction.

This paper is a condensed and somewhat revised version of Eckhaus (1959), which was a part of the author's doctoral thesis at the Massachusetts Institute of Technology, Department of Aeronautics and Astronautics. The author wishes to acknowledge gratefully the encouragement and advice that he received from Professor Leon Trilling. He is also indebted to Prof. Howard W. Emmons, of Harvard University, for discussions which helped to clarify numerous points of this work. The work was sponsored by United States Air Force Contract no. AF 49(638)-160.

REFERENCES

Erdelyi, A. 1953 (Director, Bateman Project). *Higher Transcendental Functions.* New York: McGraw-Hill.

Eckhaus, W. 1959 On the stability of laminar flame-fronts. *M.I.T. Fluid Dynamics Research Group Report* no. 59–9.

Emmons, H. W. (Editor) 1958 *Fundamentals of Gas Dynamics.* Princeton University Press.

Hirschfelder, J. O., Curtiss, C. F. & Bird, R. B. 1954 *Molecular Theory of Gases and Liquids.* New York: John Wiley and Sons.

Landau, L. D. & Lifschitz, E. M. 1953 *Mechanics of Continuous Media.* Moscow.

Markstein, G. H. 1951 Experimental and theoretical studies of flame-stability. *J. Aero. Sci.* **18**.

Spalding, D. B. 1955 *Some Fundamentals of Combustion.* Gas Turbine Series, Vol. 2.

On a momentum-mass flux diagram for turbulent jets, plumes and wakes

By B. R. MORTON

Department of Mathematics, University of Manchester

(Received 18 September 1960)

Many salient features of fully developed turbulent jets, plumes and wakes with steady mean flow are shown clearly by the relationship between the momentum flux and the mass flux in the column of moving fluid. Using a simple model for the flows, this relationship can be found from the solution of a single ordinary differential equation and the character of many related flows can be represented immediately (except for actual distribution in space) on a single momentum-mass flux diagram.

In this note some approximate solutions based on dimensional arguments are outlined briefly for cases of buoyant and non-buoyant wakes and jets directed along the axis of a uniform main stream, and momentum-mass flux curves are presented.

1. Introduction

There are sufficiently strong similarities in the behaviour of round turbulent jets and wakes in a still fluid environment or in a steady ambient stream to suggest that, for at least some purposes, this family of columnar turbulent flows can usefully be investigated as a single group. Further members of the same family are provided by buoyant wakes and plumes (i.e. buoyant jets) directed along the line of the (uniform) force field which produces the buoyancy. For each of these columnar turbulent flows a detailed treatment can be given using an approximate method described by Morton, Taylor & Turner (1956), but sufficient information for many purposes can be obtained from the same assumptions more simply by relating the momentum flow and the mass flow in the column and eliminating, in so far as this is possible, other variables. In particular, this partial solution is useful either for a comparison of different columnar flows, or for finding *whether* flows exhibit specified types of behaviour rather than *where* they may do so.

There are, of course, differences between the various flows of the family which must be borne in mind. Each flow will take a certain distance from the source to develop fully its appropriate turbulent character, and the flow in this initial region will be partly characteristic of the source and may not be fully turbulent (cf. Kuethe 1935, for the jet, and Goldstein 1938, chap. XIII, for the wake). The flow in this 'entry' or 'development' region is quite outside the scope of a treatment based on developed turbulent flow, but this is of no great importance if in each case the flow is conceived as originating from an appropriate virtual source, the position of which is determined by the fluxes of mass, momentum,

etc. at the end of the development region. In some cases source characteristics may persist for much greater distances downstream, as with the oscillations of a wake, which are specially marked over certain ranges of Reynolds number; these effects are more difficult to make allowance for, but this should to some extent be possible by suitable modification of the virtual source strength. Another difference arises from the fact that with increasing distance from the virtual source the local Reynolds number remains constant for a simple jet, increases for a simple plume, and decreases for a simple wake; hence the level of turbulence will decay far from the source of a wake.

The common features of jets, plumes and wakes make possible a single type of treatment which can be based on a common set of assumptions. All these flows show a relatively slow rate of spread with increasing distance from the source, and this suggests that mean profiles across the column of longitudinal velocity, etc., will be similar in shape at all stations along the column (such profiles are known experimentally to be approximately Gaussian). This assumption is certainly reasonable in the cases of simple jets and simple wakes; it is at least plausible in cases where there is an outer flow and may be used until further information on these flows is available. It will also be reasonable to adopt the usual boundary layer assumption that longitudinal diffusion is negligible relative to lateral diffusion; and molecular diffusion will in all cases be neglected relative to turbulent diffusion. The flow will be taken as independent of Reynolds number, and also of the relative density difference parameter (characteristic density difference divided by reference density) except in so far as density variations give rise to buoyancy forces. The turbulent mixing or entrainment of ambient fluid can now be fully represented by a speed of flow into the column at some arbitrarily defined 'mean outer edge', and as a consequence of the assumptions already made this inflow speed across the 'mean boundary' of the column must be proportional to the magnitude of the difference between a characteristic mean velocity along the column and the (parallel) velocity of the ambient fluid at a distance. This basic assumption follows immediately from dimensional considerations and must be valid wherever the physical character of the flow is adequately represented by the previous assumptions. It bears no immediate relationship to mixing length theories other than its dimensional background, and it is in fact a good deal weaker since no interrelationship is imposed on mixing processes at different parts of a section of the column. The result of assuming the inflow rate and the similarity of profiles is to suppress all detail of the *transverse* structure of the column from the solution; hence *any* profile shape can be used without loss of additional physical information, and although profiles are known to be almost Gaussian it will be simplest here to work in terms of *top-hat* profiles in which variables take a constant value (different to that in the ambient stream) across the whole width of the column.

2. Formulation

A convenient frame of reference for treatment of the axially symmetric flows that will be considered here has origin at the virtual source (as yet undetermined) and x-axis directed along the axis of the column. Take $r = r(x)$ as the mean

column radius, $u = u(x)$ as the mean velocity along the column (which for the top-hat profile is uniform over column sections), u_0 as the main stream velocity of the ambient fluid assumed to be parallel to the column axis, $\rho = \rho(x)$ as the density of column fluid and ρ_0 the ambient density. Although u_0 and ρ_0 can be permitted to vary with x, they will be regarded as constant here for simplicity. Then, if the buoyancy force arises from the action of a uniform gravitational field acting in the negative x-direction, equations representing the conservation of mass, momentum, and density deficiency (e.g. due to transported heat) can be written as

$$\left.\begin{aligned} &\frac{d}{dx}(\pi\rho r^2 u) = 2\pi\rho r E|u-u_0|, \\ &\frac{d}{dx}(\pi\rho r^2 u^2) = 2\pi\rho r E|u-u_0|\,u_0 + \pi g r^2(\rho_0-\rho), \\ &\frac{d}{dx}\{\pi r^2 u g(\rho_0-\rho)\} = 0, \end{aligned}\right\} \tag{1}$$

where E is the entrainment constant, which is defined as the ratio of the inflow speed at distance r to the speed difference between column and ambient flows, calculated in terms of the top-hat profile. It may be observed that these equations have been derived on the assumption that all entrainment is due to turbulent mixing outwards from within the column into the laminar ambient flow. Fluid flowing in the main stream cannot of itself enter the column, but will merely carry the column boundary before it until engulfed by the column turbulence.

Equations (1) can be written more concisely in terms of the variables

$$v = r^2 u, \quad m = r^2 u^2, \quad b = r^2 u g(\rho_0-\rho)/\rho_0,$$

which are porportional to the fluxes of mass, momentum and buoyancy, respectively. The further set of transformations to the non-dimensional variables V, M, X, given by

$$v = v_0 V, \quad m = m_0 M, \quad x = (v_0/2Em_0^{\frac{1}{2}})\,X,$$

is based on the measurable values v_0 for v and m_0 for m at the end of the development region, that is at the first point of the column which can be regarded as characteristic of the developed turbulent flow, say at the point $x = x_0$. Under these two sets of transformations, equations (1) reduce to

$$\left.\begin{aligned} &\frac{dV}{dx} = \frac{V}{M^{\frac{1}{2}}}\left|\frac{M}{V} - A\right|, \\ &\frac{dM}{dx} = \frac{AV}{M^{\frac{1}{2}}}\left|\frac{M}{V} - A\right| + B\frac{V}{M}, \end{aligned}\right\} \tag{2}$$

and $b = b_0 =$ constant, where $A = u_0 v_0/m_0$ is the ratio of the free stream velocity to the mean velocity in the column at $x = x_0$, and

$$B = (b_0 v_0^2)/(2Em_0^{\frac{5}{2}}) = [rg(\rho_0-\rho)/(2E\rho_0 u^2)]_{x=x_0};$$

A is necessarily positive or zero, but B can also be negative. In deriving these equations it has been assumed that variations in density need be taken into

account only where they give rise to buoyancy forces. A solution to equations (2) subject to the conditions $V = 1$, $M = 1$ at the appropriate point (though it is not obvious where this is) could be found without difficulty for any particular case (A, B), but it is very much simpler to carry out a survey of solution types if X is first eliminated to give the single equation

$$\frac{dM}{dV} = A + \frac{BV}{M^{\frac{1}{2}}|M - AV|}, \tag{3}$$

subject to the condition $M = 1$ when $V = 1$. Solutions to equations (3) will demonstrate the character of appropriate columnar flows without giving their distribution in space, so that it is no longer necessary to known *where* the boundary condition is to be applied. Once a solution to (3) has been found, the corresponding distribution in space is obtained by integrating the equation

$$\frac{dX}{dV} = \frac{M^{\frac{1}{2}}}{|M - AV|}, \tag{4}$$

subject to the condition that $X = 0$ when V takes the value appropriate to the virtual source (and this value is given by the solution to equation 3). The whole solution is then determined in the parametric form $X = X(V)$, $M = M(V)$.

For a survey of the family of columnar flows it will be convenient to define two groups, using slightly more general definitions for jets and wakes than are usual. Columnar flows having $A < 1$ will be termed jets, and those with $A > 1$ will be wakes; this is a classification according to the relative motion of the column and its environment at the beginning of the developed flow, and in jets the column velocity is greater than the ambient velocity while in wakes it is smaller.

In general there will be different types of virtual source for the two groups. This can be seen most readily by considering curves on the momentum–mass flux diagram representing different columnar flows. For each flow there is an M–V curve which passes through the 'initial point,' $(1, 1)$ corresponding to the start of the developed flow. The volume flux V must necessarily increase monotonically with increasing distance along the column from the virtual source since there is no possibility of 'detrainment' (i.e. removal of 'marked' column fluid due to the motion of the ambient fluid, possible only when the ambient flow is turbulent), and indeed it is this monotone increasing character of V with X which makes V a suitable independent parameter for the solution. Thus M is a single-valued function of V, and it follows that each M–V curve must cut either the V-axis in the range $0 < V < 1$ or the M-axis with $0 \leqslant M$ (a negative value of M would correspond to a reversed flow). These points of intersection with the axes represent the virtual sources; intercepts $(0, M)$ on the M-axis correspond in general to virtual sources for jet flows, and intercepts $(V, 0)$ on the V-axis are virtual sources of wakes, though there are exceptions caused by buoyancy effects. It is an advantage of this approach that the strength of the virtual source is given as a natural product of the solution.

The two groups will now be considered in greater detail.

2.1. *Jets*

This group will include all columnar flows for which $u > u_0$ at $x = x_0$, the start of the developed turbulent flow, irrespective of whether or not the initial flow in the column is buoyant. The virtual source for a jet has strength (0, M, B), where B provides a measure of the constant buoyancy flux along the jet. It follows that the virtual source must be a *point* source, since $V \propto r^2 u \propto M/u$, and hence as $x \to 0$, $u \to \infty$ and $r \to 0$.

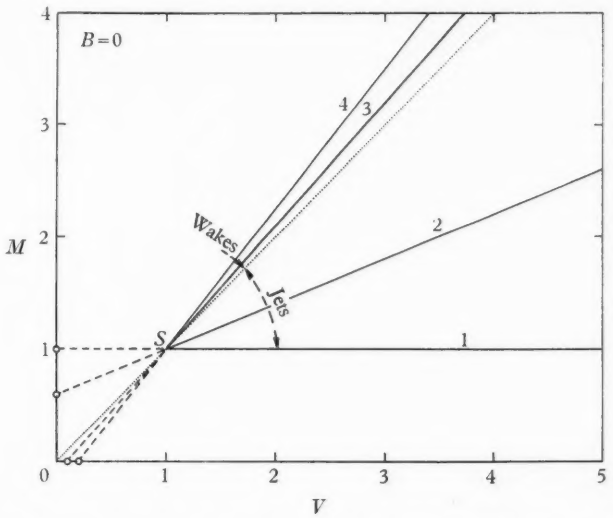

FIGURE 1. A diagram showing in non-dimensional form the relationship between the momentum flux M and the volume flux V for axially symmetrical turbulent jets and wakes released along the flow of a uniform main stream. The point $S(1, 1)$ represents conditions at the equivalent source of the flow, the unbroken lines proceeding to the right of S represent flow in the columns at increasing distance from the source and the broken lines to the left of S cut the axes in points (marked by circles) corresponding with the appropriate virtual sources and represent the hypothetical part of the column flow. The dotted line ($M = V$) provides a division into broad classes of 'jet-like' and 'wake-like' flows. The lines shown represent: (1) the simple jet ($A = 0$) in a still environment; (2) a jet in a uniform stream ($A = 0{\cdot}4$); (3) a forced wake ($A = 1{\cdot}1$) produced by emitting fluid at a mean velocity below that of the main stream; (4) the simple wake ($A = 1{\cdot}25$) of a bluff body. There are no buoyancy effects.

2.1 (*a*). *The simple jet* without buoyancy in a uniform environment at rest has $A = 0$, $B = 0$ and equation (3) reduces to $dM/dV = 0$, with solution $M = 1$, which is merely an expression of the well-known constancy of momentum in the simple jet. The *actual* flow in a simple jet is represented on the M–V diagram by the half-line $M = 1$, $V \geqslant 1$; the virtual source strength is given from the point of intersection of the line $M = 1$ with the M-axis as (0, 1), and the segment of the line for $0 \leqslant V < 1$ represents the *hypothetical* flow between the virtual source and the supposed starting point for the well-developed flow. This behaviour is represented on figure 1, where the actual flow is shown with a continuous line

and the hypothetical part of the flow by a broken line. Equation (4) has solution $X = V$; hence the full solution for the simple jet is $V = X$, $M = 1$.

2.1(*b*). *A jet in a uniform stream* with the jet emitted in the direction of the main stream. In this case $0 < A < 1$ and $B = 0$, and equation (3) has the form $dM/dV = A$ with $M = 1$ at $V = 1$. Hence $M - 1 = A(V-1)$, that is, jet momentum increases linearly with increasing volume flow because of the momentum of the fluid entrained. Actual flow in the jet is represented by the half-line of slope A through the point (1, 1) and with $V \geqslant 1$, and the strength of the (virtual) point source is $(0,\ 1-A)$ obtained from the intersection of the line with the M-axis. Possible flows of this kind are given for $0 < A < 1$, and a typical example is illustrated in figure 1 (with a developed jet velocity two and a half times the main stream velocity i.e. $A = \frac{2}{5}$). The solution to equation (4) with $X = 0$ at $V = 0$ is

$$X = \tfrac{2}{3}A^{-1}(1-A)^{-1}\{[1+A(V-1)]^{\frac{3}{2}} - (1-A)^{\frac{3}{2}}\};$$

hence the actual (effective) source is at $X_0 = \frac{2}{3}A^{-1}(1-A)^{-1}\{1-(1-A)^{\frac{3}{2}}\}$. The full solution is

$$u = u_0 \frac{(X+L)^{\frac{2}{3}}}{(X+L)^{\frac{2}{3}} - L^{\frac{2}{3}}}, \quad r = \frac{[(1-A)m_0]^{\frac{1}{2}}}{u_0} \frac{(X+L)^{\frac{2}{3}} - L^{\frac{2}{3}}}{L^{\frac{1}{3}}(X+L)^{\frac{1}{3}}},$$

where $L = \frac{2}{3}(1-A)^{\frac{1}{2}}/A$ and $A = u_0 v_0/m_0$. It may be noted that the asymptotic behaviour of a jet in a uniform stream is given by

$$\frac{u-u_0}{u_0} \sim \frac{L^{\frac{2}{3}}}{(X+L)^{\frac{2}{3}}}\left\{1 + \frac{L^{\frac{2}{3}}}{(X+L)^{\frac{2}{3}}} + \ldots\right\},$$

$$\frac{u_0 r}{[(1-A)m_0]^{\frac{1}{2}}} \sim \frac{(X+L)^{\frac{1}{3}}}{L^{\frac{1}{3}}}\left\{1 - \frac{L^{\frac{2}{3}}}{(X+L)^{\frac{2}{3}}} + \ldots\right\},$$

so that the asymptotic behaviour is that of the wake (see below). Figure 2 shows curves for the dimensionless velocity excess $(u-u_0)/u_0$ in the jet relative to the ambient fluid and for the dimensionless jet radius $u_0 r/[(1-A)m_0]^{\frac{1}{2}}$ plotted against dimensionless distance X/L from the virtual source; in each case curves for the simple jet and for the asymptotic wake behaviour are superimposed in the best form for comparison.

2.1(*c*). *A forced plume* (*or buoyant jet*) in a uniform still environment: the flux of buoyancy is constant and equal to the flux from the source; $A = 0$ and B may take any value, hence equation (3) reduces to

$$\frac{dM}{dV} = \frac{BV}{M^{\frac{1}{2}}},$$

and the solution with $M = 1$ at $V = 1$ is

$$M^{\frac{5}{2}} = 1 + \tfrac{5}{4}B(V^2 - 1).$$

This curve represents for $V > 1$ the flow that might be observed in a buoyant jet; for large values of V, $M \sim (5B/4)^{\frac{2}{3}}V^{\frac{4}{3}}$, and hence for sufficiently large V these curves will always lie under the line $M = V$, indicating jet-like flow. It may be seen by following the curve back ($V < 1$) that there is a normal jet-type point source of strength $(V, M, B) = [0, (1-5B/4)^{\frac{2}{5}}, B]$ provided that $B < 4/5$,

and this includes the case $B < 0$ of negative buoyancy forces; $dM/dV = 0$ at $V = 0$ and the flow in a sufficiently close neighbourhood of the virtual source approximates to that of a simple jet (i.e. is momentum controlled). If, on the other hand, $B > 4/5$ then the curve cuts the V-axis first, and there is a virtual source of strength $[\{1-4/(5B)\}^{\frac{1}{2}}, 0, B]$. This is a virtual source of quite a dif-

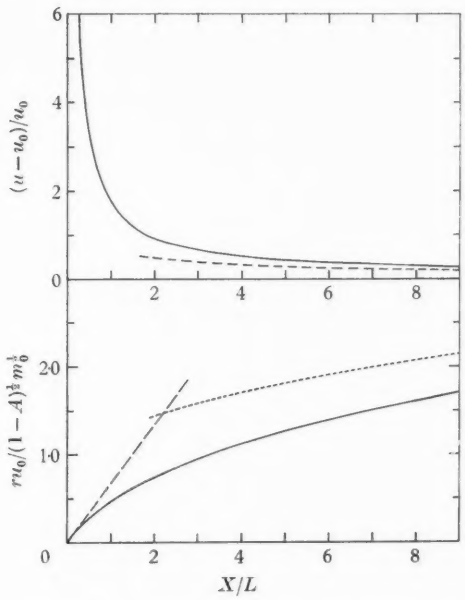

FIGURE 2. The non-dimensional velocity $(u-u_0)/u_0$ and radius $u_0(1-A)^{-\frac{1}{2}}m_0^{-\frac{1}{2}}r$ of a jet released along the flow of a uniform stream of speed u_0, plotted against the non-dimensional distance X/L from the virtual source. The broken curves for larger values of X/L represent the asymptotic behaviour of a simple wake, and the broken line for small X/L shows the spread of a simple jet in a still environment.

ferent kind, characteristic of *wake* rather than jet flow; it has infinite radius and zero efflux velocity (see below, under wakes), dM/dV is now infinite at $M = 0$ and the plume is buoyancy controlled in a neighbourhood of the source. A treatment for the forced plume has already been described in detail (Morton 1959*a*). These solutions are illustrated in figure 3 by the curves: (i) $B = -0{\cdot}462$, in which case heavy fluid is discharged and will be continuously decelerated by buoyancy forces (in addition to entrainment effects) until a greatest height is reached ($M = 0$)—the solution cannot be continued beyond this point; (ii) $B = 0{\cdot}185$, a normal example of a jet with positive buoyancy; (iii) $B = 0{\cdot}8$, the case of a simple plume from a source of pure buoyancy, for here $M = V^{\frac{4}{3}}$ and there is a point source $(0, 0, B)$ at $X = 0$; (iv) $B = 1{\cdot}6$, when the virtual source is of 'wake' type and the curve representing the early part of the actual flow lies above the dividing line $M = V$, but falls below it for larger values of V (i.e. reverts to 'jet' behaviour).

2.1(*d*). *Simple plume in a stably stratified environment* at rest: useful information can be carried on an M–V diagram even in more complicated cases where there are other dependent variables (e.g. buoyancy flux); to illustrate this a curve has been drawn in figure 3 for the simple plume projected upwards into stably stratified ambient fluid. The results (taken from Morton *et al.* 1956) are plotted for $V > 1$ only as they are hard to distinguish from those of the simple plume in $0 \leqslant V \leqslant 1$. There is again a maximum height to which plume fluid can be projected.

2.1(*e*). *A buoyant jet projected along a uniform upward stream* of uniform density: neither A nor B vanishes, and hence the full solution to equation (3)

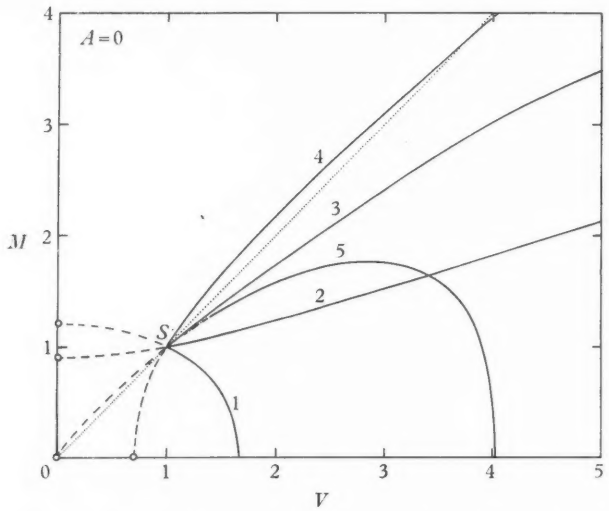

FIGURE 3. An M-V diagram for buoyant jets in a uniform still ambient fluid ($A = 0$). The curves shown represent: 1 flow from a source of heavy fluid ($B = -0{\cdot}462$) with negative buoyancy; 2 flow from a weak source of positive buoyancy ($B = 0{\cdot}185$); 3 the simple plume from a virtual source of pure buoyancy ($B = 0{\cdot}8$); 4 flow from a strong source of buoyancy ($B = 1{\cdot}6$), in which case the virtual source is of 'wake' type and the early stages of the actual flow are buoyancy dominated; 5 the simple plume in a stably stratified environment at rest, where again a maximum height is reached. Except in cases of negative buoyancy these flows are all ultimately jet-like.

satisfying $M = 1$ at $V = 1$ is required. An analytic solution might be found for this equation, but it is likely to be complicated in form and to need a good deal of numerical evaluation. Thus it may well be easier to solve the equation numerically—a simple task—and it is here that the use of an M–V diagram has some advantages since it permits a survey of the range of expected solutions with a minimum of labour. Particular cases which appear to have desired properties can subsequently be solved in detail. For example, the behaviour of jets with weak negative buoyancy might be investigated in this way to find the interaction between the retarding effect of the buoyancy and the accelerating effect of the entrained momentum on the jet. For present purposes it seems enough to

give curves for the integrations: (i) $(A, B) = (0{\cdot}5, -1{\cdot}0)$, $(0{\cdot}5, -0{\cdot}0625)$ and $(0{\cdot}5, -0{\cdot}0025)$ with negative buoyancy, and (ii) $(A, B) = (0{\cdot}5, 0{\cdot}2)$ for positive buoyancy; these are shown on figure 4.

2.2. *Wakes*

This group includes all columnar flows with $u < u_0$ at $x = x_0$, the point which may be taken as the start of developed turbulent flow, and again includes buoyant columns that lie along the line of the buoyancy producing force field. The virtual

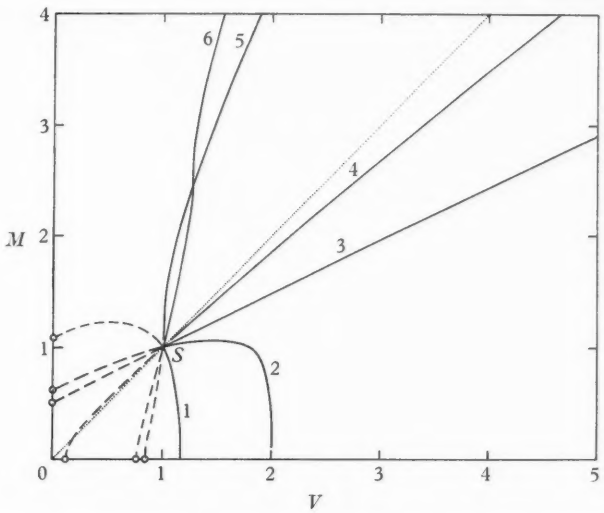

FIGURE 4. An M-V diagram for buoyant jets and wakes in a uniform stream. The curves shown represent: **1** a negatively buoyant jet ($A = 0{\cdot}5, B = -1{\cdot}0$) of heavy fluid with strong deceleration which rapidly reaches its greatest height ($M = 0$); **2** a weaker negatively buoyant jet ($A = 0{\cdot}5$, $B = -0{\cdot}0625$) which still suffers fairly rapid deceleration; **3** a buoyant jet with very weak negative buoyancy ($A = 0{\cdot}5$, $B = -0{\cdot}0025$) which is little affected; **4** a positively buoyant jet ($A = 0{\cdot}5$, $B = 0{\cdot}2$) where the discharge of buoyancy at the source S is sufficient to call for a 'wake-type' virtual source; **5** a forced wake ($A = 1{\cdot}2$, $B = 2$) with sufficiently strong positive buoyancy to cause transition from wake flow to jet flow close to the source S (shown by the infinite gradient there); **6** a more weakly buoyant forced wake ($A = 2$, $B = 1$) showing transition to jet flow at a rather greater 'distance'.

source for a wake has strength $(V, 0, B)$ in general, and since in this case $M \propto r^2u^2 \propto Vu$, it follows that when $x \to 0$, $u \to 0$ and $r \to \infty$, in such a way that there is a non-zero volume flux carrying zero momentum from the virtual source. This is, perhaps, a less commonly discussed type of virtual source, but as the flow predicted by the solution for $V < 1$ is purely hypothetical this is of no significance physically.

2.2(*a*) *Forced wakes* are column flows produced from a source emitting fluid at mean velocity u which is smaller than the free stream velocity u_0, so that $A > 1$; if there are no buoyancy effects $B = 0$, and equation (3) reduces to

$dM/dV = A$, subject to $M = 1$ at $V = 1$. These form a continuation of the solutions for jets in a uniform stream (case 2.1*b*), with the same solution

$$M - 1 = A(V - 1).$$

Observable flow in the forced wake is again represented by the half-line of slope A through $(1, 1)$ with $V > 1$, and the strength of the virtual source (of infinite area) is $\{(A-1)/A, 0\}$. Forced wake flows are possible for values of $A > 1$ lying in a range which is certainly bounded above, though it is not immediately clear what this upper bound will be; a typical example, calculated for $A = 1{\cdot}1$, is shown in figure 1. Equation (4) has solution satisfying $X = 0$ at $V = (A-1)/A$,

$$X = \tfrac{2}{3}A^{-1}(A-1)^{-1}[1 + A(V-1)]^{\frac{3}{2}},$$

so that the effective source is at $X = \frac{2}{3}A^{-1}(A-1)^{-1}$. The full solution is

$$u = u_0 \frac{X^2}{X^2 + L^2}, \quad r = \frac{[(A-1)\,m_0]^{\frac{1}{2}}}{u_0} \frac{X^2 + L^2}{L^{\frac{1}{2}} X^{\frac{1}{2}}},$$

where in this case $L = \frac{2}{3}(A-1)^{\frac{1}{2}}/A$; the asymptotic behaviour is

$$\frac{u - u_0}{u_0} \sim \frac{L^2}{X^2}\left\{1 - \frac{L^2}{X^2} + \ldots\right\},$$

$$\frac{u_0 r}{[(A-1)\,m_0]^{\frac{1}{2}}} \sim \frac{X^{\frac{1}{2}}}{L^{\frac{1}{2}}}\left\{1 + \frac{L^2}{X^2}\right\}.$$

2.2(*b*). *The simple wake* is the limiting case of a forced wake and is produced when a bluff body modifies the flow of a steady uniform stream (or when a bluff body is moved at constant speed through a still environment, but here take a reference frame moving with the body). The modification to the uniform flow u_0 outside the wake will be disregarded. The simple wake is a special case of the forced wake for limiting A, and to find the value of A it is necessary to know the mean velocity in the wake at $x = x_0$. Between $x = x_0$ and the rear surface of the body there is an attached circulating flow, the nature of which depends strongly on the Reynolds number for flow past the body and on body shape (including the existence of a defined edge for separation), roughness, etc.; and except at small Reynolds numbers this circulating flow is bordered by a turbulent mixing layer which gradually thickens until it spreads completely across the wake at a point that is probably somewhat short of $x = x_0$ (there is some loss of fluid from the mixing layer to the circulating flow near this closing point). From this very rough description it may be expected that the appropriate value for A is likely to vary with Reynolds number (even at such relatively high values as 10^5) and with other factors; moreover, the task of finding A is made more difficult by the rather limited amount of experimental data which appears to be available for the attached flow. There is a temptation to take the virtual source actually at the rear of the body, but there is no possible justification for this even though u vanishes there. However, there are two ways in which A can be estimated. The first is to use direct measurements of wake velocity, for example using results for a circular flat plate normal to the stream and at Reynolds number

$1{\cdot}6 \times 10^5$ given by Fail, Lawford & Eyre (1957) of $u/u_0 = 0{\cdot}85$ approximately, at a distance 1·6 'attached bubble lengths' behind the plate (converting into terms of the top-hat profile); the corresponding value is $A = 1{\cdot}2$. The second method for estimating A is based on the drag of the body which is $\frac{1}{2}C_D\pi a^2\rho u_0^2$ in terms of the drag coefficient C_D and the area πa^2 presented by the body to the oncoming stream, and is also $\rho\pi r^2 u(u_0 - u)$ in terms of the wake disturbance to the flow. Hence, to the present accuracy,

$$C_D = 2\frac{r^2(A-1)}{a^2A^2},$$

and A is given in terms of C_D, which is widely known, and the relative area of section of the wake downstream of the attached flow in terms of the area presented by the body, and this is as hard to find as the related information on wake velocities. The results of Fail and others are not easy to interpret for this purpose, but an estimate of the wake diameter at 1·6 attached bubble diameters indicates a value $A = 1{\cdot}3$ for the circular disk (with $C_D = 1{\cdot}12$); this agreement is probably much better than should be expected. Results for the sphere are more sensitive to Reynolds number, and the only really safe statement is that A is a good deal closer to unity, especially after transition to turbulence in the boundary layer. These results are of very limited use, but at least they show what information is needed if any particular problem is to be handled. A line is drawn in figure 1 for the simple wake with $A = 1{\cdot}25$, and this is probably close to the upper limiting line for axially symmetric simple wakes.

2.2(*c*). *A buoyant forced wake* in a vertical stream of uniform density: the full equation (3) can again be solved numerically in a survey of solutions. Solution curves are shown in figure 4 for $A = 1{\cdot}2$, $B = 2$ and for $A = 2$, $B = 1$; the fluid in the wake is accelerated by entrainment of momentum and by buoyancy until it is moving with the ambient fluid (at which point dM/dV is infinite), and thereafter the behaviour changes over to that of a buoyant jet.

3. Application of the solution

How seriously should these solutions be taken? They add nothing to physical understanding of the flows described, and the formulation based on dimensional arguments has been reduced to such a state of simplicity that only the barest bones of the problem can have survived. Whenever more sophisticated methods of solution are available these will undoubtedly be superior; but the unfortunate fact is that more sophisticated methods of attack are often not available, especially for the more complicated problems which involve diffusion and convection of buoyant material along the column. In such cases the methods described will produce a solution which is correct at least in order of magnitude and usually much more closely, and the simplicity of the formulation ensures that the physical significance of the assumptions is exposed fully and is not likely to be overlooked in making an application.

Finally, a value or values must be chosen for the entrainment constant E. This question has already been discussed at some length by various authors (see Ellison & Turner (1959) and Morton (1959*b*)). Various values for E have

been suggested for the case of jets and plumes in which the relative density variations are small; the differences are due partly to small variations in definition of the entrainment constant, and partly to the somewhat unequal quality of the available experimental results and to the difficulty in extracting accurately the required information from that which has been published. The results from jets suggest a value of about $E = 0{\cdot}116$ in the form used above; the less reliable results from plumes suggest a higher value although the difference is small if the unequal spread of momentum and heat is taken into account Values of E in cases of a moving environment are not at all easy to estimate, as there is a considerable scarcity of suitable results especially sufficiently far downstream to be of use, but it is hard to see why they should differ greatly from values for a simple jet. Moreover, E enters the various expressions mainly as a power with fractional exponent smaller than unity so that there is a tendency for errors in E to be reduced in importance. Thus while a good deal of further information on values of the entrainment constant is needed, the solutions given above are still of potential use in practical applications with E regarded as a known (or determinable) function of the column type.

REFERENCES

Ellison, T. H. & Turner, J. S. 1959 *J. Fluid Mech.* **6**, 423.

Fail, R., Lawford, J. A. & Eyre, R. C. W. 1957 *R.A.E. Tech. Note Aero.* no. 2516.

Goldstein, S. (ed.) 1938 *Modern Developments in Fluid Dynamics.* Oxford University Press.

Kuethe, A. M. 1935 *J. Appl. Mech.* **2**, 87.

Morton, B. R. 1959*a* *J. Fluid Mech.* **5**, 151.

Morton, B. R. 1959*b* *Int. J. Air Pollution*, **1**, 184.

Morton, B. R., Taylor, G. I. & Turner, J. S. 1956 *Proc. Roy. Soc.* A, **234**, 1.

A continuum theory of the isothermal flow of liquid helium II

By A. A. TOWNSEND
Emmanuel College, Cambridge

(Received 1 October 1960)

Recent work by Hall and Vinen has established that mutual friction between the normal and superfluid components of liquid helium II is caused by interactions between quantized vortex-lines and the normal fluid. If the mean separation of the vortex-lines is small compared with the channel width, the general character of the flow may not depend on the discrete nature of the lines except in so far as this is the cause of the mutual friction. Equations of motion are developed which refer to components of the velocity field with a scale large compared with the line separation, and these are used to discuss the nature of possible turbulent motions. Reasons are given for believing that isothermal flow is very similar to that of a Newtonian fluid, and the theory is developed for turbulent pressure flow along a channel and a circular pipe. The predicted variation of flow rate with pressure gradient is in good agreement with experimental measurements for Reynolds numbers (based on tube diameter and normal fluid viscosity) above 1400, and it is likely that turbulent flow can exist only above this critical Reynolds number. For Reynolds numbers which are not too small, the equations of motion apply to steady 'laminar' flow and these lead to a relation between flow rate and pressure gradient in reasonable agreement with experiment.

1. Introduction

The flow properties of liquid helium can be described in some detail by the two-fluid theory that assumes the liquid to be an intimate mixture of two components each capable of independent movement. One, the normal fluid, is a 'gas' composed of the thermal excitations (phonons and rotons) moving randomly through the whole liquid, and it may be accelerated by ordinary viscous forces of the gas-kinetic type. The superfluid contains the residual momentum and kinetic energy of the liquid and behaves as a perfect fluid at absolute zero without entropy or viscosity. Using the model in this form it is possible to describe quantitatively the flow of liquid helium II at not too high speeds, the essential properties being the inviscid behaviour of the superfluid, the free interpenetration of the two components and the thermodynamic mutual force which drives normal fluid down temperature gradients.

If the superfluid has zero viscosity, it should be impossible to set it in rotation from a condition of rest, but this can be done and the explanation of this anomaly is found in the theoretical result of Feynman (1955) that circulation is quantized

in units of h/m (h is Planck's constant, m is the mass of a helium atom) and in the inference that vorticity is localized in vortex-lines of diameter comparable with the interatomic spacing. Once vorticity is introduced into the superfluid it can be increased by elongation of the lines in a kind of turbulent flow and, although most of the superfluid will be in irrotational motion, the motion induced by the vortex-lines will appear rotational on the macroscopic scale. Hall and Vinen have made an important extension by pointing out that the excitations of the normal fluid will be scattered in the velocity field of the vortex-lines and that this will cause a mutual friction if the vortex-lines are moving relative to the normal fluid. In a series of papers they have presented very convincing evidence in favour of the notion that mutual friction between the two fluids is entirely caused by this effect (for details, see Hall (1960)). The existence of a mutual friction provides the simplest explanation of the existence of a critical flow velocity above which the simple two-fluid theory is no longer valid.

The development of a flow in which all the vorticity is concentrated in discrete lines is a difficult mathematical problem, but many of the difficulties are avoided if we consider only those aspects of the flow that can be described in terms of averages over regions of space large enough to contain a substantial number of vortex-lines. The purpose of this paper is to construct such a continuum theory of the rotational flow of liquid helium II, including only those effects of concentrated vorticity that appear in these space averages. It is hoped that in this way knowledge of the turbulent flow of Newtonian fluids can be applied to the flow of liquid helium, although it is possible that significant effects take place on scales too small to be described by a continuum theory.

2. The continuum equations of motion

In detail, the motion of the superfluid is the result of a distribution of vortex-lines moving in their own velocity field and acted on by mutual forces, and a Fourier analysis of the whole velocity field would contain both components of small wave-number which represent streaming of large numbers of vortex-lines and components of large wave-number representing the velocity fields around individual vortices. If each line were split into two and the parts separated by half the previous spacing, considerable changes would be expected in the large wave-number components but very small changes in the components of small wave-number, so we identify the small wave-numbers with the continuum aspects of the flow and use them to define the part of the flow obeying equations of motion of classical type. The largest wave-number belonging to the continuum spectrum may be estimated by considering the dependence of the velocity field defined by

$$\mathbf{q}_a(\mathbf{x}) = (2\pi)^{-\frac{3}{2}}\delta^{-3}\int \mathbf{q}_l(\mathbf{x}+\mathbf{r})\, e^{-\frac{1}{2}(r^2/\delta^2)}\, d\mathbf{r}, \tag{2.1}$$

on the length δ. $\mathbf{q}_l(\mathbf{x}+\mathbf{r})$ is the true velocity field and $\mathbf{q}_a(\mathbf{x}+\mathbf{r})$ is roughly the average velocity in a spherical volume of radius $1{\cdot}55\delta$ surrounding the point $\mathbf{x}$.†

† Effective volumes and areas have been estimated by approximating the error function by a 'top-hat' function of equal volume or area.

If a moderately large number of vortex-lines pass through this volume, the average velocity will not be sensitive to the individual velocity fields of the lines but will be determined by their combined effect and by the effect of neighbouring lines. Supposing four to be a moderately large number, $\mathbf{q}_a(\mathbf{x})$ is essentially a continuum average if

$$\delta > \delta_0 = \left(\frac{2}{\pi L}\right)^{\frac{1}{2}}, \tag{2.2}$$

where L is the number of lines per unit area (or length per unit volume) and δ_0 may be used in (2.1) to define the continuum field of velocity. In terms of Fourier components, it is easily shown that only spectral components of wave-number less than

$$k_0 = 1{\cdot}55\left(\frac{\pi}{2}\right)^{\frac{1}{2}} L^{\frac{1}{2}} \approx 2\left(\frac{m\omega_s}{h}\right)^{\frac{1}{2}} \tag{2.3}$$

may be considered to belong to the continuum spectrum, i.e. the spectrum of the velocity field $\mathbf{q}_a(\mathbf{x})$.

Using these space averages to define flow variables for both components, the equations of motion may be obtained. Omitting terms involving changes in density, they are

$$\frac{\partial \mathbf{q}_s}{\partial t} + (\mathbf{q}_s . \operatorname{grad})\,\mathbf{q}_s = -\operatorname{grad}(p + p_d) + \frac{1}{\rho_s}\mathbf{F}_{sn} \tag{2.4}$$

for the superfluid, and

$$\frac{\partial \mathbf{q}_n}{\partial t} + (\mathbf{q}_n . \operatorname{grad})\,\mathbf{q}_n = -\operatorname{grad} p - \frac{1}{\rho_n}\mathbf{F}_{sn} + \frac{\nu_n}{\rho_n}\nabla^2 \mathbf{q}_n \tag{2.5}$$

for the normal fluid.† The quantity p_d in (2.4) represents the momentum flux due to the pressure and velocity fields of individual vortex-lines, and is of order $\omega_s h/m$.‡ The relatively high viscosity of the normal fluid makes it unlikely that the corresponding term is appreciable in the equation for its motion. The mutual force $\mathbf{F}_{sn}$ is the sum of the thermodynamic force proportional to the averaged temperature gradient and the volume average of the mutual forces arising from the scattering of excitations by the vortex-lines. The scattering calculations of Hall & Vinen (1956*b*) show that the mutual friction has two components, a drag force in the plane of the vortex-line and the relative velocity and a lift force normal to this plane, both proportional to the strength of the vortex-line and to the relative velocity. If the lines within the volume defined by δ_0 are jumbled and random in direction, the average of the lift forces will be zero and the average of the drag forces will be parallel to the averaged relative velocity and proportional to the length of line per unit volume. Allowing for the random orientation, the total mutual force is

$$\mathbf{F}_{sn} = S \operatorname{grad} T + B\rho_s\rho_n\omega_s(\mathbf{q}_n - \mathbf{q}_s), \tag{2.6}$$

† In these and all subsequent equations, the pressures, forces and viscosities are 'kinematic', i.e. they are the ordinary quantities divided by the total density of the fluid. ρ_s and ρ_n are then the mass fractions of the two components and $\rho_s + \rho_n = 1$.

‡ Hall (1960) has shown that the vortex-lines are in a state of tension, which is really the longitudinal effect of the radial pressure gradient necessary to maintain rotation of fluid particles about the line. The tension (in the form of the pressure component) is included in p_d.

where $\omega_s = Lh/m$ is the *vorticity of the superfluid*, and B is a function of temperature and nearly equal to one-third of the constant determined by measuring the attenuation of second-sound in rotating liquid helium (Hall & Vinen 1956*a*). This form for the mutual friction should be valid in turbulent flow but it needs modification if the vortex-lines are not randomly orientated (see § 5).

To these dynamical equations must be added the equations of state, of conservation of mass and of conservation of energy, but in isothermal flow at speeds small compared with either velocity of sound, changes in total density or in mass fraction of the components are expected to be negligible and we have

$$\operatorname{div} \mathbf{q}_s = \operatorname{div} \mathbf{q}_n = 0. \tag{2.7}$$

To make the set of equations formally complete, it is necessary to find some relation between the superfluid vorticity ω_s and the velocity field. If the vortex-lines had long-range order, i.e. adjacent lines nearly parallel, the superfluid vorticity equals the continuum vorticity, $|\operatorname{curl} \mathbf{q}_s|$, but this is unlikely to be true in general and it is necessary to discuss the processes of generation and destruction of superfluid vorticity.

If an ordinary Newtonian fluid is in turbulent flow, distributed vorticity is continually generated by stretching of the vortex-lines and is being destroyed at the same rate by the action of viscous forces. In a superfluid, vortex-lines can only be destroyed if they approach the wall or another, oppositely directed line within a few atomic diameters, but they can lose energy to the normal fluid without any need for such a close approach. The rate of energy loss depends on their density and their mean square velocity with respect to the normal fluid, which is also proportional to the density, and this kind of argument suggests that it is not necessary to discuss the mechanism of vortex-line destruction in detail. The problem may then be reduced to the part played by the vortex-lines in dissipating energy supplied to the flow, and the first step is to obtain equations for the kinetic energies of the turbulent fluctuations in the two components. For fully developed flow between parallel planes, these equations are

$$\overline{u_s v_s}\frac{\partial U_s}{\partial y} + \frac{\partial}{\partial y}(\tfrac{1}{2}\overline{q_s^2 v_s} + \overline{p v_s}) = B\rho_n \omega_s(\overline{\mathbf{q}_s \cdot \mathbf{q}_n} - \overline{q_s^2}) - \epsilon_s \tag{2.8}$$

for the superfluid, and

$$\overline{u_n v_n}\frac{\partial U_n}{\partial y} + \frac{\partial}{\partial y}(\tfrac{1}{2}\overline{q_n^2 v_n} + \overline{p v_n}) = B\rho_s \omega_s(\overline{\mathbf{q}_s \cdot \mathbf{q}_n} - \overline{q_n^2}) - \epsilon_n \tag{2.9}$$

for the normal fluid. In these equations, the Ox axis is parallel to the direction of flow and the Oy axis is at right-angles to the planes; the mean velocity has components $(U, 0, 0)$, the velocity fluctuation is (u, v, w) and $q^2 = u^2 + v^2 + w^2$. ϵ_n is the energy dissipation by viscous forces in the normal fluid and ϵ_s is the rate of loss of superfluid energy by transfer to scales of motion too small to contribute to the averaged velocity field. Similar forms may be derived for other kinds of flow.

An important difference between these equations and the corresponding equation for a Newtonian fluid is that mechanical energy can be lost to the

system by mutual friction as well as by working against viscous retarding forces and that, while viscous losses hardly affect the large energy-containing eddies of the motion (for example, see Townsend 1956), this is not necessarily true of the mutual friction. Whether mutual friction affects the large eddies or not depends on the degree of correlation between the velocity fluctuations in the two fluids, and we consider the two extreme possibilities, (*a*) negligible correlation defined by

$$|\overline{\mathbf{q}_s \cdot \mathbf{q}_n}| \ll (\overline{\mathbf{q}_s^2}\,\overline{\mathbf{q}_n^2})^{\frac{1}{2}}, \tag{2.10}$$

and (*b*) nearly perfect correlation defined by

$$\overline{(\mathbf{q}_s - \mathbf{q}_n)^2} \ll \frac{\rho_s \epsilon_s + \rho_n \epsilon_n}{B \rho_s \rho_n \omega_s}. \tag{2.11}$$

If the correlation is negligible, the mutual friction acts as a damping force but, if it is large, the mutual friction couples the motions together and the damping effect is relatively small.

In the energy equation for the superfluid fluctuations, the term

$$\frac{\partial}{\partial y}(\tfrac{1}{2}\overline{q_s^2 v_s} + \overline{p v_s})$$

represents transport of energy from one part of the flow to another and it is known to be comparatively small in channel flow (Laufer 1955). Omitting this term and assuming negligible correlation, we find that

$$\omega_s \leqslant \frac{|\overline{u_s v_s}|}{\overline{q_s^2}} \frac{1}{B\rho_n} \left|\frac{\partial U_s}{\partial y}\right| < \frac{1}{B\rho_n} \left|\frac{\partial U_s}{\partial y}\right| \tag{2.12}$$

and so the superfluid vorticity must be comparable with the vorticity of the mean flow. In turbulent flow, fluctuations of vorticity are typically large compared with the vorticity of the mean flow, and this suggests what the following analysis confirms, that independent velocity fluctuations in the two components are incompatible with isothermal turbulent flow and that the energy-containing eddies are almost perfectly correlated and coherent. The extent to which this coherence of motion extends to the small-scale components of the motion is considered in the next section.

3. Spectrum of coherent turbulent flow

If the velocity fields of the two components were identical except for a difference in mean velocity, the velocity fluctuation would satisfy the equation

$$\frac{\partial \mathbf{q}}{\partial t} + (\rho_s U_s + \rho_n U_n)\frac{\partial \mathbf{q}}{\partial x} + (\mathbf{q} \cdot \operatorname{grad})\,\mathbf{q} = -\operatorname{grad} p + \nu_n \nabla^2 \mathbf{q}, \tag{3.1}$$

which is exactly the equation of motion for an ordinary fluid of the same viscosity moving with the mean flow velocity

$$U_m = \rho_s U_s + \rho_n U_n$$

in the same mean pressure gradient. This equation describes any perfectly coherent flow but it contains no terms involving thermomechanical forces. It

follows that the turbulent motion observed during thermal flow of liquid helium is either of a scale too small to be described by a continuum theory or is fundamentally incoherent. Compare this equation with the equation of motion for the superfluid in the absence of thermomechanical forces:

$$\frac{\partial \mathbf{q}_s}{\partial t} + U_s \frac{\partial \mathbf{q}_s}{\partial x} + (\mathbf{q}_s . \operatorname{grad}) \mathbf{q}_s = -\operatorname{grad} p + B\rho_n \omega_s (\mathbf{q}_n - \mathbf{q}_s). \tag{3.2}$$

On subtracting and equating $\mathbf{q}_s$ to $\mathbf{q}_n$ except in the mutual friction term, we obtain an approximate equation for the velocity difference in nearly coherent flow,

$$(U_s - U_n) \frac{\partial \mathbf{q}}{\partial x} = -B\omega_s (\mathbf{q}_s - \mathbf{q}_n) - \frac{\nu_n}{\rho_n} \nabla^2 \mathbf{q}. \tag{3.3}$$

To this approximation, the equation is linear and, in terms of the Fourier coefficients of the velocity field, it is

$$-B\rho_n \omega_s (\mathbf{a}_s - \mathbf{a}_n) = [-\nu_n k^2 + il(U_s - U_m)\rho_n] \mathbf{a}, \tag{3.4}$$

where $\mathbf{q} = \Sigma \mathbf{a}(\mathbf{k}) \exp(i\mathbf{k}.\mathbf{x})$, or

$$\mathbf{a}_s - \mathbf{a}_n = \left(-il \frac{U_s - U_n}{B\omega_s} + \frac{\nu_n}{B\rho_n \omega_s} k^2 \right) \mathbf{a}, \tag{3.5}$$

where l is the component in the direction of mean flow of the vector wavenumber $\mathbf{k}$. Two conditions must be satisfied before essentially coherent motion is possible for the Fourier component of wave-number $\mathbf{k}$:

$$l \ll \frac{B\omega_s}{|U_s - U_n|} = l_c \quad \text{and} \quad k \ll \left(\frac{B\rho_n \omega_s}{\nu_n} \right)^{\frac{1}{2}} = k_1. \tag{3.6}$$

The first condition is inertial, requiring that the mutual force should be sufficient to supply the acceleration caused by relative motion of the superfluid and the pressure field, and to this approximation failure to satisfy the condition results in a difference in phase but none in magnitude. The second condition is independent of the relative velocity and requires a mutual force sufficient to balance the viscous stresses in the normal fluid. Failure to satisfy the second condition implies a greater magnitude of the Fourier component of the velocity fluctuation in the superfluid.

An essential process in any turbulent flow is the transfer of energy between eddies of different sizes, usually a transfer from large eddies to smaller ones, and it is usual to discuss this process in terms of the three-dimensional spectrum function $E(k)$, defined so that $E(k)\,dk$ is the fraction of the total energy $\frac{1}{2}\overline{\mathbf{q}^2}$ arising from Fourier components with magnitudes between k and $k+dk$ (Batchelor 1953). So long as the conditions (3.6) are satisfied, the motion is coherent and the low wave-number part of the spectrum is expected to be identical with the spectrum of flow in a Newtonian fluid and to have the same characteristics. For the present purpose, the relevant characteristics are (i) that viscous dissipation of turbulent energy is concentrated at wave-numbers near $k_s = \frac{1}{2}(\epsilon/\nu^3)^{\frac{1}{4}}$, where ϵ is the rate at which energy is lost by the larger eddies to the dissipative processes, (ii) that, if the wave-number is large compared with the wave-numbers

characteristic of the energy-containing eddies, the motion at this wave-number is determined by the energy dissipation ϵ and by the kinematic viscosity ν_n, and (iii) that eddies with wave-numbers near k_s contain nearly all the vorticity. If these principles of local similarity are applied to a flow of liquid helium which is coherent at not too large wave-numbers, the statistical specification of the vorticity distribution in the superfluid depends on the rate of dissipation of mechanical energy, on the difference in mean velocity of the two fluids and on the physical properties of liquid helium. Dimensional considerations require then that the superfluid vorticity is given by

$$\omega_s^2 = \epsilon\nu_n^{-1} \times \text{function of} \left(\frac{\epsilon\nu_n}{(U_s - U_n)^4}, \frac{h}{m\nu_n}, B\rho_n \right). \tag{3.7}$$

To make this expression more precise, it is necessary to consider in more detail the transfer of energy from one Fourier component to another in the spectral range of coherent motion, in the range of incoherent continuum motion, and outside the continuum range. At first sight, there are a number of possibilities depending on the relative magnitudes of the wave-numbers defining the limits of coherent and of continuum motion, but in isothermal flow the limit to the coherent range is always set by the viscous condition. Then the existence of the velocity difference cannot affect the incoherent motion of the superfluid, and so the magnitude of the superfluid vorticity is independent of the velocity difference and equation (3.7) becomes

$$\omega_s^2 = \epsilon\nu_e^{-1}, \tag{3.8}$$

where ν_e/ν_n is a function of $h/(m\nu_n)$ and $B\rho_n$, i.e. of temperature.

The relative magnitudes that determine the ratio ν_e/ν_n are those of the limit of coherent motion k_1, the limit of continuum motion k_0 (defined by equation (2.3)), and the wave-number k_s near which the coherent spectrum loses energy by viscosity. Their ratios are

$$k_0/k_1 = 2\left(\frac{\nu_n m}{B\rho_n h}\right)^{\frac{1}{2}}, \quad k_s/k_1 = \frac{1}{2(B\rho_n)^{\frac{1}{2}}}\left(\frac{\nu_e}{\nu_n}\right)^{\frac{1}{2}},$$

and, on using the rough values $h/m\nu_n = 10$, $B\rho_n = 0{\cdot}05$, appropriate to a temperature near $1{\cdot}4\,^\circ\mathrm{K}$, we find that there is a substantial spectral range of incoherent motion ($k_0/k_1 = 2{\cdot}8$). The continuum representation of the motion distinguishes between the part of the superfluid vorticity that is necessary to provide the averaged vorticity, $\operatorname{curl}\mathbf{q}_s$, and the residual density of vortex-lines which is completely disordered. Since space averages are used in the definition of the continuum motion,

$$\omega_s^2 = \overline{(\operatorname{curl}\mathbf{q}_s)^2} + \omega_d^2, \tag{3.9}$$

which defines $\omega_d = (h/m)\,L_d$ as the disordered component of the vorticity. Disorder in the distribution of vortex-lines causes each line to move relatively to its neighbours with a velocity of about $2h/md$, where d is the mean spacing. From the magnitude of k_0/k_1, we expect the normal fluid to be too viscous to move with the disordered motion of the vortex-lines and the rate of working

against the mutual friction to be $B\rho_n L_d(2h/md)^2(h/m)$ per unit volume. Then the rate of energy dissipation by irregular motion of the vortex-lines is

$$\epsilon_s = \frac{\alpha B\rho_n}{\pi^2}\frac{h}{m}\omega_d^2, \tag{3.10}$$

where α is a constant of order one. The energy is the energy not dissipated by processes occurring in the continuum range of eddy sizes, and energy loss by mutual annihilation of vortex-lines is ignored.

As the details of the dissipation process for Newtonian fluids are not known in any detail, the magnitude of ν_e/ν_n will be left unspecified in the following sections. Notice that if the whole motion were coherent and all the energy were dissipated by viscous stresses, the superfluid vorticity would be $(\epsilon/\nu_n)^{\frac{1}{2}}$. Actually part of the total dissipation occurs in the incoherent range by mutual friction which is a less effective process than viscous dissipation and so more continuum vorticity will appear for the same continuum dissipation. In the disordered motion, too, more vorticity is necessary for the same energy dissipation and it seems a fair inference that ν_e is less than ν_n and more than $\alpha B\rho_n h/\pi^2 m$.

4. Pressure flow between parallel planes

In fully developed flow between parallel planes, mean values of the flow variables become independent of displacement parallel to the boundaries and functions only of y, the distance from one boundary. For this flow, the equations of mean motion are

$$\frac{\partial\overline{u_s v_s}}{\partial y} = \frac{\tau_0}{D} + B\rho_n\omega_s(U_n - U_s) \tag{4.1}$$

and

$$\frac{\partial\overline{u_n v_n}}{\partial y} = \frac{\tau_0}{D} + B\rho_s\omega_s(U_s - U_n) + \frac{\nu_n}{\rho_n}\frac{d^2U_n}{dy^2}, \tag{4.2}$$

where $2D$ is the width of the channel and the pressure gradient in the direction of flow is $-\tau_0/D$. From these equations may be obtained the equation for the mean mass flow,

$$\frac{\partial}{\partial y}[\rho_s\overline{u_s v_s} + \rho_n\overline{u_n v_n}] = \frac{\tau_0}{D} + \nu_n\frac{d^2U_n}{dy^2} \tag{4.3}$$

and the equation for the difference of mean velocity,

$$\frac{\partial}{\partial y}[\overline{u_n v_n} - \overline{u_s v_s}] = B\omega_s(U_s - U_n) + \frac{\nu_n}{\rho_n}\frac{d^2U_n}{dy^2}. \tag{4.4}$$

Equation (4.3) may be integrated to give the total stress,

$$\tau = \nu_n\frac{dU_n}{dy} - (\rho_s\overline{u_s v_s} + \rho_n\overline{u_n v_n}) = \tau_0(1 - y/D) \tag{4.5}$$

since τ_0 is the shear stress on either wall.

Arguments have already been given indicating that the motions of the large-scale eddies are nearly coherent, and if this is true the mass flow will be similar to that of an ordinary fluid in a channel of the same width and in the same pressure gradient except near the walls where the flow is unlikely to be turbulent. The validity of this notion will now be tested by calculating the amount of incoherence

in the motion, but first it is useful to review the properties of channel flow as they have been established for Newtonian fluids. For values of $\tau_0^{\frac{1}{2}} y/\nu$ greater than 20, the distribution of mean velocity is of the form,

$$U = \frac{\tau_0^{\frac{1}{2}}}{K} F(y/D) + U_l, \tag{4.6}$$

where U_l is a velocity of translation that depends on details of the flow near the wall, the function $F(y/D)$ is characteristic of channel flow in general and K is an absolute constant about 0·41. This velocity distribution defines the rate of production of turbulent energy, $-\overline{uv}\,\partial U/\partial y$, and this rate equals the rate of energy dissipation in the most important part of the flow, that for which $y/D < 0{\cdot}2$. In this same region, $F(y/D) = \log y/D$ and so

$$\epsilon = -\overline{uv}\frac{\partial U}{\partial y} = \frac{\tau_0^{\frac{3}{2}}}{Ky} \tag{4.7}$$

and the scale of the energy-containing eddies is nearly proportional to distance from the wall (Townsend 1956).

It is now possible to estimate the magnitude of the departures from coherence in the liquid helium flow. The incoherence of the motions of the two components is given by equation (3.5), but the incoherence from inertial effects does not produce any inequality between $\overline{u_s v_s}$ and $\overline{u_n v_n}$, the first-order effect being a change of phase producing a small relative displacement of the velocity patterns. On the other hand, the effect of viscosity acting only on the normal fluid is to make velocities rather greater in the superfluid, and so

$$\frac{\overline{u_s v_s} - \overline{u_n v_n}}{\overline{uv}} = \frac{\nu_n^2 k_e^4}{B^2 \rho_n^2 \omega_s^2}, \tag{4.8}$$

where k_e is the average wave-number of the Fourier components contributing to the Reynolds stress. Substituting in equation (4.4), we obtain a relation between ω_s and $(U_s - U_n)$,

$$B\omega_s(U_s - U_n) = -\frac{d}{dy}\left[\frac{\nu_n^2 k_e^4 \tau}{B^2 \rho_n^2 \omega_s^2}\right] - \frac{\nu_n}{\rho_n}\frac{d^2 U_n}{dy^2}. \tag{4.9}$$

Using the relation (3.8), $\epsilon = \nu_e \omega_s^2$, and substituting for ϵ, k_e and dU_n/dy the values for a constant-stress layer in ordinary flow, viz.

$$k_e \propto y^{-1}, \quad \epsilon = \frac{\tau_0^{\frac{3}{2}}}{Ky}, \quad \frac{dU}{dy} = \frac{\tau_0^{\frac{1}{2}}}{Ky},$$

the ratio of the velocity difference to the scale of velocity variation $\tau_0^{\frac{1}{2}}$ is found to be

$$\frac{U_s - U_n}{\tau_0^{\frac{1}{2}}} = \frac{3K^{\frac{3}{2}}}{B^3 \rho_n^2}(k_e y)^4 \left(\frac{\nu_e}{\nu_n}\right)^{\frac{3}{2}} \left(\frac{\nu_n}{\tau_0^{\frac{1}{2}} y}\right)^{\frac{7}{2}} + \frac{1}{B\rho_n K^{\frac{1}{2}}} \left(\frac{\nu_e}{\nu_n}\right)^{\frac{1}{2}} \left(\frac{\nu_n}{\tau_0^{\frac{1}{2}} y}\right)^{\frac{3}{2}}. \tag{4.10}$$

It may now be confirmed that no appreciable incoherence exists in the fluctuations contributing to the energy and the Reynolds stress. The inertial condition for coherent motion becomes

$$B^2 \rho_n \frac{\nu_n}{\nu_e}\left(\frac{\tau_0^{\frac{1}{2}} y}{\nu_n}\right)^2 \gg k_e y = O(1), \tag{4.11}$$

and the viscous condition

$$B\rho_n \frac{\nu_n}{\nu_e}\left(\frac{\tau_0^{\frac{1}{2}} y}{\nu_n}\right)^{\frac{3}{2}} \gg (k_e y)^2 = O(1). \tag{4.12}$$

Both these conditions are satisfied in that part of the flow for which $\tau_0^{\frac{1}{2}} y/\nu_n$ is large, and this is the greater part of the channel if the Reynolds number of flow, $R = \tau_0^{\frac{1}{2}} D/\nu_n$, is large.

The assumption of the previous section that the upper limit to the coherent part of the spectrum is set by viscous rather than inertial effects may also be confirmed. Using equation (4.10), it may be shown that the ratio of the inertial cut-off to the viscous cut-off is

$$l_c/k_1 = B^{\frac{3}{2}}\rho_n^{\frac{1}{2}} K^{\frac{1}{4}}\left(\frac{\nu_n}{\nu_e}\right)^{\frac{1}{4}}\left(\frac{\tau_0^{\frac{1}{2}} y}{\nu_n}\right)^{\frac{5}{4}} \tag{4.13}$$

for large values of $\tau_0^{\frac{1}{2}} y/\nu_n$. At the same large values of $\tau_0^{\frac{1}{2}} y/\nu_n$, the mutual friction is

$$B\omega_s(U_s - U_n) = \frac{\tau_0}{D}\frac{D^2}{y^2}\frac{\nu_n}{\tau_0^{\frac{1}{2}} D}, \tag{4.14}$$

and it is small compared with the pressure gradient except very close to the wall.

In an ordinary fluid, a limit to fully turbulent flow is set by the damping action of the viscous forces which prevent an appreciable level of turbulent motion for values of $\tau_0^{\frac{1}{2}} y/\nu_n$ less than 12, and the additive constant in the velocity distribution (4.6) is determined by a condition of velocity continuity at the boundary between the fully turbulent flow and the effectively laminar flow next the wall. If the fluctuations in liquid helium were everywhere coherent, the same viscous forces would exist and impose the same limit to the region of fully turbulent flow, but the conditions for coherent flow, (4.10–12), show that it will not be possible for some values of $\tau_0^{\frac{1}{2}} y/\nu_n$ greater than 12 if $B\rho_n$ is small. Then the turbulent motion in this wall region is incoherent to some extent and the levels of turbulent intensity and Reynolds stress will be reduced because of added dissipation by mutual friction. To a rough approximation, we may use the viscous condition for coherence (4.12) to set a limit, y_v say, to the region of negligible Reynolds stress so that

$$\frac{\tau_0^{\frac{1}{2}} y_v}{\nu_n} = \chi\left(\frac{\nu_e}{B\rho_n \nu_n}\right)^{\frac{2}{3}}, \tag{4.15}$$

where χ is a constant. This can only be valid if y_v is much greater than the ordinary limit, $12\nu_n/\tau_0^{\frac{1}{2}}$. Applying the condition of velocity continuity at the edge of the region of negligible Reynolds stress, the universal velocity distribution (4.6) takes the form

$$U = \frac{\tau_0^{\frac{1}{2}}}{K}\left(\log\frac{\tau_0^{\frac{1}{2}} y}{\nu_n} + C\right), \tag{4.16}$$

where C is given by

$$C = K\frac{\tau_0^{\frac{1}{2}} y_v}{\nu_n} - \log\frac{\tau_0^{\frac{1}{2}} y_v}{\nu_n}. \tag{4.17}$$

For a Newtonian fluid, $\tau_0^{\frac{1}{2}} y_v/\nu_n \approx 12$ and $C \approx 2{\cdot}3$.

It has been shown that the mass flow velocity in the fully turbulent part of the flow has the same distribution as for an ordinary fluid except for a modified

velocity of translation. Within the wall layer of negligible Reynolds stress, the flow is steady and analysis of this kind of flow (§ 5) shows that the velocity difference is nearly $2\nu_n/(3B\rho_n D)$ and the total flow in the wall layer is negligible for Reynolds numbers in the turbulent range. The volume flow may then be calculated from the universal velocity distribution as $Q_m = \frac{1}{D}\int_0^D U_m dy$, and is given by

$$\frac{Q_m}{\tau_0^{\frac{1}{2}}} = K^{-1}\left[\log R + C + \int_0^1 F(x)\,dx\right], \tag{4.18}$$

where $(R = \tau_0^{\frac{1}{2}} D/\nu_n)$. This relation between volume flow and pressure gradient is valid for flow along a tube of circular section with a suitably modified contribution from the integral of the distribution function $F(x)$.

The arguments set out here may be applied to any kind of isothermal turbulent flow and it seems that the continuum theory of turbulent flow in liquid helium II leads to the conclusion that its macroscopic structure is nearly indistinguishable from ordinary turbulent flow if the Reynolds number is large. This is not true for thermal flows in which the motion is essentially incoherent or for steady flows with vortex-lines.

5. Steady flow with vortex-lines

Many experimental measurements of flow resistance in tubes and channels have been made for Reynolds numbers between 10 and 50 and, although it is unlikely that the flow can be turbulent, the observed resistance indicates a sufficient density of vortex-lines for approximate validity of the continuum theory. It is natural to assume that the flow is steady and that the flow of the superfluid is retarded by mutual friction between the normal fluid and a steady stream of vortex-lines, generated perhaps near the channel entrance.† The continuum equations for steady flow between parallel boundaries are

$$\left.\begin{aligned} O &= +\frac{\tau_0}{D} + \tfrac{3}{2}B\rho_s\left|\frac{dU_s}{dy}\right|(U_s - U_n) + \frac{\nu_n}{\rho_n}\frac{d^2U_n}{dy^2}, \\ O &= \frac{\tau_0}{D} - \tfrac{3}{2}B\rho_n\left|\frac{dU_s}{dy}\right|(U_s - U_n), \end{aligned}\right\} \tag{5.1}$$

the factor $\frac{3}{2}$ appearing because the vortex-lines are all at right-angles to the flow direction and not randomly orientated as in turbulent flow.‡ Then,

$$U_n = \frac{\tau_0 y}{\nu_n}(1 - \tfrac{1}{2}y/D) \tag{5.2}$$

and the velocity difference between the superfluid and the normal fluid, $U_1 = U_s - U_n$, is given by

$$\tfrac{3}{2}B\rho_n U_1\left[\frac{dU_1}{dy} + \frac{\tau_0}{\nu_n}(1 - y/D)\right] = \frac{\tau_0}{D} \tag{5.3}$$

† The existence of such a flow is not certain.

‡ In steady flow the lift forces are all in the same direction and do not disappear when the averaging process is carried out, but their only effect is to induce a lateral pressure gradient.

with a boundary condition that depends on the nature of the interaction between the material of the wall and the liquid. The discussion of this boundary condition raises the same questions of the generation and continued existence of vortex-lines as arise from the existence of a critical velocity of flow. Without going into any detailed discussion it seems reasonable that there should be a layer of fluid next the wall not containing vortex-lines and moving with the critical velocity U_0 appropriate to its thickness d_0. Measurements of critical velocity suggest that these are related by

$$U_0 d_0 = \beta h/m, \tag{5.4}$$

where β is a number varying slowly with channel width. Consider now the forces acting on the layer of fluid next the wall and of thickness $d_0 + \frac{1}{2}d_1$, where d_1 is the mean separation of vortex-lines at the edge of the continuum flow. On the average, this layer is not accelerated and the pressure gradient is balanced by the mutual friction on the vortex-lines in the layer of thickness $\frac{1}{2}d_1$, so that

$$\tfrac{3}{2}B\rho_n \frac{h}{m}(U_0 - U_n) = \frac{\tau_0}{D}(d_0 + \tfrac{1}{2}d_1)\, d_1, \tag{5.5}$$

where U_n is the normal fluid velocity at distance d_0 from the wall. The mean separation of vortex-lines is related to the velocity gradient at distance d_0 from the wall by

$$\frac{dU_s}{dy} = d_1^{-2}\frac{h}{m},$$

so that these two equations provide a boundary condition.

Although solutions of equation (5.3) with this boundary condition could be computed, the essential features of the flow can be discovered by making suitable approximations. Near the wall, $y/D \ll 1$ and the solution is

$$\frac{\tau_0 y}{\nu_n} = A_0 - U_1 - \frac{\nu_n}{\frac{3}{2}B\rho_n D}\log\left[\frac{\frac{3}{2}B\rho_n U_1 D}{\nu_n} - 1\right], \tag{5.6}$$

where A_0 is a constant of integration determined by the boundary condition. This solution implies that the difference velocity approaches asymptotically the value $2\nu_n/(3B\rho_n D)$ but the final approach to the asymptotic solution requires more detail in the distribution of vorticity than can be provided by vortex-lines of finite strength. A continuum flow consistent with the physical requirements is one with the asymptotic difference flow to within a distance d_0 of the wall and a critical flow in this layer. The condition for the validity of the asymptotic solution is that $dU_1/dy \ll \tau_0/\nu_n$ or

$$R = \frac{\tau_0^{\frac{1}{2}} D}{\nu_n} \gg (\tfrac{3}{2}B\rho_n)^{-\frac{1}{2}}, \tag{5.7}$$

and in that part of the channel for which $(1 - y/D)^3 \gg (\frac{3}{2}B\rho_n R^2)^{-1}$, the solution may be continued as

$$U_1 = \frac{2\nu_n}{3B\rho_n D}(1 - y/D)^{-1}. \tag{5.8}$$

For still larger values of y/D, an approximate solution is

$$\tfrac{3}{4}B\rho_n U_1^2 = \frac{\tau_0 y}{D} + \text{constant}. \tag{5.9}$$

Using these approximate solutions in their ranges of validity, the difference flow in a channel may be calculated. It is

$$Q_1 D = \int_0^D U_1 dy = \frac{2\nu_n}{3B\rho_n} [\log (\tfrac{3}{2}B\rho_n R^2)^{\frac{1}{2}} + A'] + \beta \frac{h}{m}, \tag{5.10}$$

where A' depends on the transition between the regions of validity of (5.8) and (5.9) and is probably about one. In non-dimensional form, the volume flow is given by

$$\frac{Q_m D}{\nu_n} = \tfrac{1}{3}R^2 + \frac{2\rho_s}{3B\rho_n} [\log (\tfrac{3}{2}B\rho_n R^2)^{\frac{1}{2}} + A'] + \beta\rho_s \frac{h}{m\nu_n}. \tag{5.11}$$

These calculations have been made for flow between parallel planes but the extension to flow along a tube of circular cross-section is straightforward. In a tube of radius a, the wall stress is related to pressure gradient by

$$2\tau_0 = -a\frac{dP}{dx},$$

and the volume flow is given by

$$\frac{Q_m a}{\nu_n} = \tfrac{1}{4}R^2 + \frac{4\rho_s}{3B\rho_n} + 2\beta\rho_s \frac{h}{m\nu_n}, \tag{5.12}$$

where Q_m is the mean flow velocity of the whole liquid and the Reynolds number is defined by

$$R = \tau_0^{\frac{1}{2}} a/\nu_n.$$

These calculations refer to flow at comparatively large Reynolds numbers such that $\frac{3}{2}B\rho_n R^2 > 10$ and it is less easy to find explicit expressions for flow at lower Reynolds numbers within the continuum range. A very rough approximation is to neglect the motion of the normal fluid so that the solution of equation (5.3) is

$$U_1^2 = U_0^2 + \frac{\tau_0 y}{\frac{3}{4}B\rho_n D}, \tag{5.13}$$

and to use this solution for values of y greater than d_0, the distance from the wall of the first vortex-lines. An application of the boundary condition expressed in equations (5.4–5) leads to a slip velocity of

$$U_0 = \left[\frac{8\beta^2}{3B\rho_n}\frac{h}{m}\frac{\tau_0}{D}\right]^{\frac{1}{4}}, \tag{5.14}$$

if the normal fluid velocity is zero and the total volume flow may be calculated. It is given by

$$\frac{Q_m D}{\rho_s h/m} = \tfrac{4}{3}\beta^2 \left[\left(1 - \frac{1}{2\beta} + (3\beta^4 B\rho_n)^{-\frac{1}{3}} \left(\frac{\tau_0^{\frac{1}{2}} D}{h/m}\right)^{\frac{2}{3}}\right)^{\frac{3}{2}} - 1\right] + \beta, \tag{5.15}$$

which has meaning only if

$$\frac{\tau_0^{\frac{1}{2}} D}{\nu_n} > (\tfrac{3}{8}\beta B\rho_n)^{\frac{1}{2}} \frac{h}{m\nu_n}$$

corresponding to $d_0 < D$. Experimental measurements of critical velocity and flow resistance in wide channels suggest that β is of order 10, so that this theory

can only apply at Reynolds numbers greater than about three (for $B\rho_n \approx 0{\cdot}05$). On the other hand, neglect of the motion of the normal fluid is only possible if $U_1 D/\nu_n \ll 2/(3B\rho_n)$, corresponding to sub-critical flow rates at temperatures between 1·2 °K and the λ-point.

6. Comparison with measurements of flow resistance

The continuum theory of the flow of liquid helium II assumes that the macroscopic properties of the flow are determined by the pressure gradient, by the dimensions of the channel and by the properties of the liquid that can be

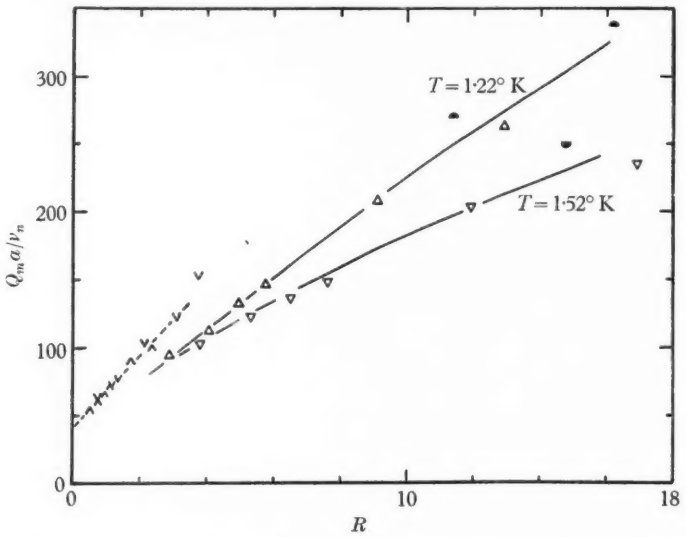

FIGURE 1. Reynolds number plot of flow measurements by Atkins (1951) at low Reynolds numbers.

$a =$	$0{\cdot}131 \times 10^{-2}$ cm	$0{\cdot}408 \times 10^{-2}$ cm	$1{\cdot}02 \times 10^{-2}$ cm
$T = 1{\cdot}22$ °K	Λ	Δ	◓
$T = 1{\cdot}52$ °K	V	∇	◒

expressed by the quantities h/m, ν_n, ρ_n, B, which are either non-dimensional or have the dimensions of viscosity. Dimensional homogeneity then requires that flows should be dynamically similar if the Reynolds number and temperature are the same, and in particular that the volume flow velocity should be related to the pressure gradient by

$$\frac{Q_m a}{\nu_n} = F\left(\frac{\tau_0^{\frac{1}{2}} a}{\nu_n}, \frac{h}{m\nu_n}, B, \rho_n\right), \tag{6.1}$$

where the function depends only on the flow geometry.† The only set of measurements that are suitable for a test of this prediction are some measurements of

† N.B. This is a test of dependence on the named quantities, not of the continuum theory as such.

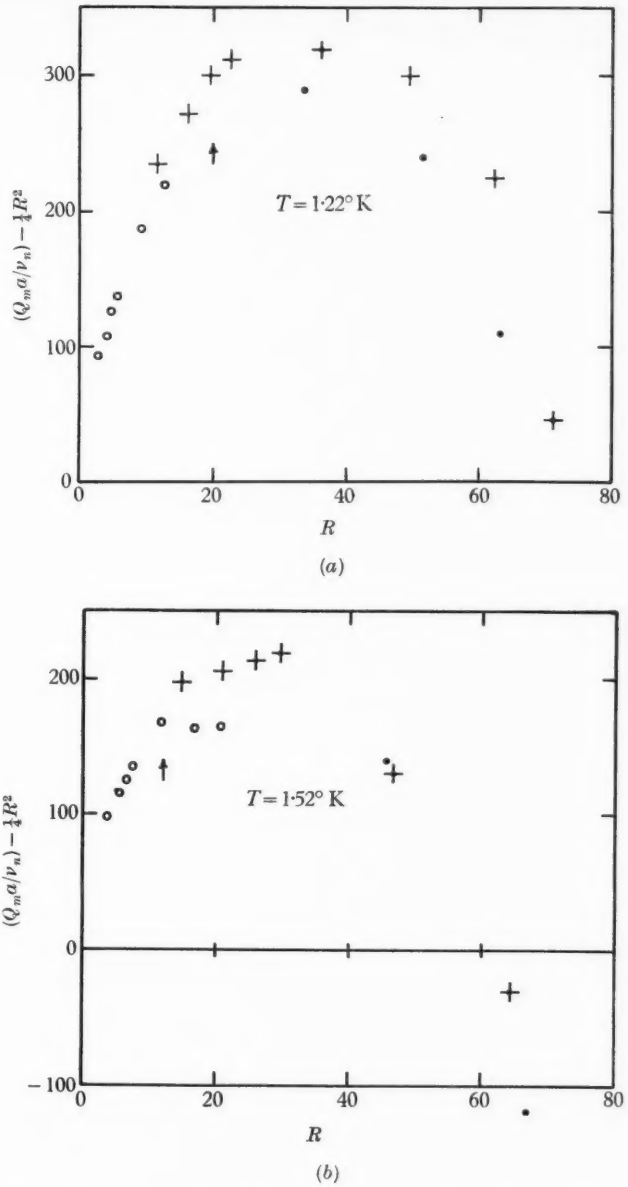

FIGURE 2. Reynolds number plot of flow measurements by Atkins (1951) at moderate Reynolds numbers for comparison with equation (5.12). ○, $a = 0{\cdot}408 \times 10^{-2}$ cm; +, $a = 1{\cdot}02 \times 10^{-2}$ cm; ●, $a = 2{\cdot}2 \times 10^{-2}$ cm. Arrows indicate lower limit to validity of equation (5.12).

flow along capillary tubes by Atkins (1951). Using tubes of four different diameters and measuring the rate of flow at two different temperatures, his measurements covered a range of Reynolds numbers from one to 300, i.e. from outside the continuum range to well within the range for turbulent flow. Points taken from his mean curves have been plotted in non-dimensional form in figures 1–3, and comparatively good agreement with the functional form (6.1) is found. The principal cause of irregular behaviour appears to be caused by uncertainty in

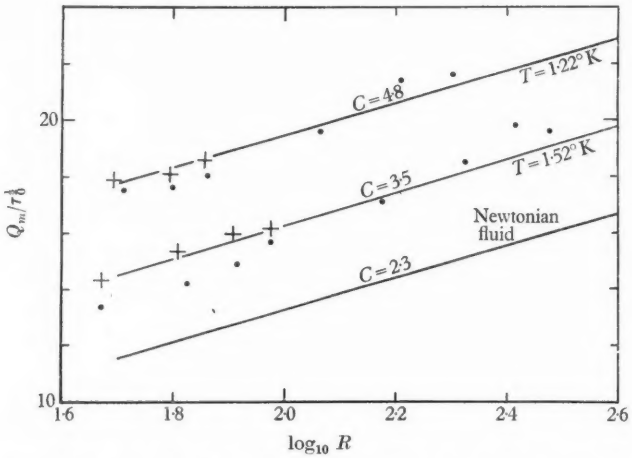

FIGURE 3. Reynolds number plot of flow measurements by Atkins (1951) at large Reynolds numbers for comparison with the logarithmic friction law (4.18). The lower line represents the mean of measurements for Newtonian fluids (Goldstein 1938).

+, $a = 1{\cdot}02 \times 10^{-2}$ cm; ●, $a = 2{\cdot}2 \times 10^{-2}$ cm.

the measured values of the tube diameter, as the discrepancies between points obtained with tubes of different diameters are of the same magnitude at both temperatures and show no consistent trend with tube diameter. On these results, there is no evidence that the absolute value of the diameter has any influence on the form of the relation (6.1) within the range of tube diameters

$$0{\cdot}262 - 4{\cdot}4 \times 10^{-2}\,\text{cm},$$

and if there is a length characteristic of the mechanism of mutual friction (e.g. the core diameter of a vortex-line) it is likely to be rather less than the smallest of these diameters.

Measurements at the smallest Reynolds numbers are shown in figure 1, most of them corresponding to average distances between vortex-lines larger than the tube radius. It is interesting that measurements with a Reynolds number less than four fall on the same curve at both temperatures (1·22° and 1·52 °K), but flow of the normal fluid must be very small in this range and a correlation of flow rate with normal fluid viscosity is very difficult to explain. Measurements at somewhat higher Reynolds numbers are compared with the steady flow theory of § 5 by plotting $(Q_m a/\nu_n) - \frac{1}{4}R^2$ against R (figure 2). Equation (5.12) requires

that this difference flow rate should be independent of Reynolds number if the flow is steady and if $\frac{3}{2}B\rho_n R^2 > 10$, i.e. if R exceeds 12 at 1·52 °K or 20 at 1·22 °K, and this is approximately true for Reynolds numbers less than 50. Above this Reynolds number the apparent difference flow decreases rapidly, and it is natural to suppose that this abrupt change in the trend of the measurements corresponds to the growth of instabilities and the onset of turbulent motion. Confirmation is found by comparing the lower critical Reynolds number for flow of a Newtonian fluid which is 63. The difference and its sign might be expected from consideration of the effect of slipping of the superfluid at the wall on the condition for critical stability of disturbances of the steady flow.

In fully developed turbulent flow, the ratio $Q_m/\tau_0^{\frac{1}{2}}$ should be a linear function of $\log_{10} R$ with a slope of $K^{-1}\log_e 10 = 5{\cdot}66$ (see equation (4.18)), and this prediction is compared with the measurements in figure 3. Remembering that the division of the flow velocities by $\tau_0^{\frac{1}{2}}$ has removed the greater part of the variation with pressure gradient, it may be claimed that experiment and theory are in good agreement. The additive constant in the logarithmic velocity distribution appears in the mass-flow equation and these results show that the constant C is larger in liquid helium flow than in air or water flow and increases as the temperature is reduced. Reasons have already been given to expect this behaviour but the magnitude of the variation is less than is given by equation (4.15). This is not unreasonable as the effective thickness of the wall layer is no more than 1·4 times the similar layer in a Newtonian fluid and the necessary condition that the extent of this layer is controlled by the mutual friction and not by viscous damping is hardly satisfied.

More recently, Bhagat (1960) has made measurements of isothermal flow along a tube of radius 0·034 cm at temperatures in the range 1·3–1·7 °K, mostly at Reynolds numbers sufficiently high to permit turbulent flow. The measurements were made by observing the rate of change of level difference between two vessels connected by the tube and Bhagat found the variation of this rate with pressure difference could be accounted for if

$$Q_m = v_0 + \frac{a^2}{8\nu_{\text{eff.}}}\operatorname{grad} P, \tag{6.2}$$

where $\nu_{\text{eff.}}$ depended on the initial pressure gradient and the constant velocity, v_0, varied from one experiment to another, increasing with initial pressure gradient. Validity of equation (6.2) implies that the flow is not quasi-steady and that the friction at any stage is not solely determined by the instantaneous flow velocity but depends strongly on the turbulence generated in the initial rapid flow. However, it is characteristic of turbulent flows that the rate of adjustment to change is proportional to the rate of rotation of the eddies which must be large for fully developed flow in a small tube. So, although hysteresis and delay might be expected in the development of turbulent flow from an initial condition of very weak fluctuations, it is difficult to believe that this flow was not quasi-steady except at the very beginning. For the purposes of comparison with the theory and with the measurements of Atkins, it is unfortunate that Bhagat gives no details of the variation of v_0 and that it is difficult to decide the pressure

difference appropriate to the measured value of $\nu_{\text{eff.}}$. In figure 4, the variations of $Q_m/\tau_0^{\frac{1}{2}}$ with R implied by equation (6.2) are shown for a number of initial pressure differences, using assumed values of v_0 that are consistent with the quoted order of magnitude, 2 cm sec^{-1}, and with the observed trend with pressure difference. All the curves fall near the line representing the logarithmic resistance law for 1·52 °K as inferred from Atkins's measurements, and the principal devia-

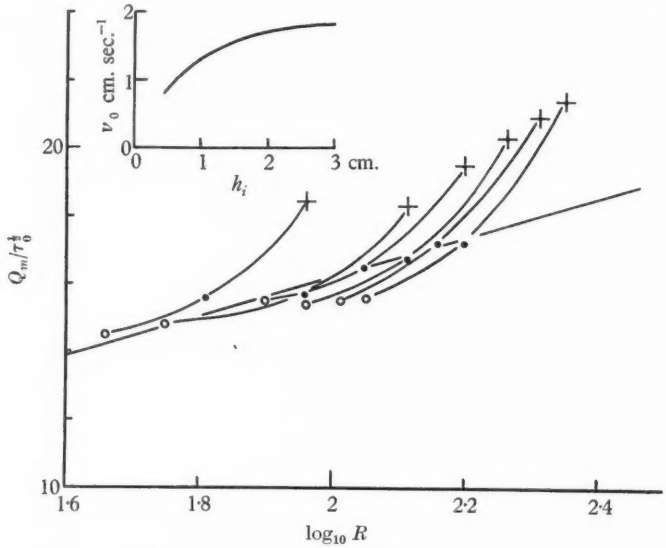

FIGURE 4. Variation of flow coefficient with Reynolds number according to Bhagat (1960) for various initial pressure gradients, assuming the values of v_0 shown in inset. The straight line is the logarithmic law for $C = 3{\cdot}5$. (The points +, ●, ○, refer to the initial gradient. one-half and one-quarter.)

tions correspond to abnormally large rates of flow while the turbulence level is increasing. It also appears from this diagram that the observed values of $\nu_{\text{eff.}}$ probably correspond to steady flow at about half the initial pressure gradient. Assuming this, a more direct comparison is possible, by comparing the observed values of $\nu_{\text{eff.}}/\nu_n$ with the values predicted by the logarithmic law,

$$\nu_{\text{eff.}}/\nu_n = \frac{R}{2(Q_m \tau_0^{-\frac{1}{2}} + K^{-1})}. \tag{6.3}$$

Reasonably good agreement is found, particularly at the lower temperatures (figure 5).

7. Discussion

This theory of the rotational flow of liquid helium depends on the demonstration by Hall and Vinen that resistance to flow of the superfluid is due to frictional forces between the normal fluid and the vortex-lines of the superfluid, and it attempts to obtain an approximate solution of the flow problem by considering

only averages over volumes large enough to contain a substantial number of vortex-lines. This procedure is similar to the derivation of the Navier–Stokes equations from the kinetic theory of gases and within its proper limits this kind of approximation should be valid and useful. The important result of the calculations in this paper is that it is possible to assume that the motions of the normal

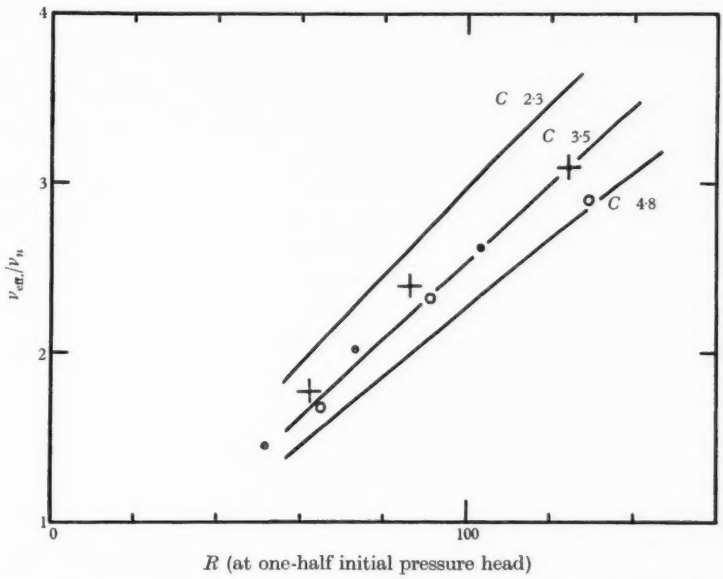

FIGURE 5. Variation of effective viscosity with Reynolds number calculated from half the initial pressure gradient (from Bhagat 1960). The lines are the variations predicted by the logarithmic law for several values of the additive constant C. ●, 1·3 °K; +, 1·5 °K; ○, 1·7 °K.

and the superfluid which contribute to the mean velocity and the Reynolds stress are almost perfectly coherent for turbulent flow in pipes and channels, the only region excepted from this being a thin layer next the walls. It is not very difficult to satisfy oneself that this will be true of any kind of isothermal flow and it appears that, if allowance is made for the peculiar properties of flow near a solid boundary, turbulent flow of liquid helium is very similar in its macroscopic aspects to turbulent flow of a Newtonian fluid.

The large differences between the flow of liquid helium and the flow of more ordinary fluids appear at Reynolds numbers less than 50, and I have attempted to describe the flow for the larger Reynolds numbers in this range by assuming the flow to be steady with vortex-lines moving in the general direction of flow in a quasi-regular array. The possibility of this kind of motion in liquid helium is not obvious and careful consideration of the flow details will be necessary before this assumption can be accepted without reservation. Meanwhile, it is interesting that the result that the excess of the superfluid flow over that of the normal fluid is, as the theory predicts, nearly independent of pressure gradient, and that

the magnitude is consistent with the known magnitude of the friction constant B and with the assumption of a slip flow at the walls with the critical velocity appropriate to a channel of the same thickness. For example, measurements by Atkins at 1·52 °K give the product of slip velocity and layer thickness as

$$125 \pm 30 \times 10^{-4}\,\mathrm{cm^2\,sec^{-1}},$$

compared with values of $v_{s,c}d$ in the range $80\text{–}130 \times 10^{-4}\,\mathrm{cm^2\,sec^{-1}}$ for wide tubes.

Vinen (1957*a–d*) has shown conclusively that a heat current can induce something resembling turbulent motion in liquid helium and that the mutual friction is uniformly distributed across the channel. Simple considerations of the supply of energy to the 'turbulent' motion show that fully coherent motion can obtain no energy from the heat flow, and it follows that the important processes of the flow take place on scales comparable with the mean separation of the vortex-lines. Until a continuum theory of incoherent turbulence driven by thermomechanical forces is available, there must be some doubt whether the thermal flow can be usefully described by a continuum representation. However thermal flow is described, it seems certain that it is a completely different motion to isothermal flow and that comparisons of mutual frictions will not be profitable.

My interest in this subject was aroused by conversations with Dr H. E. Hall and Dr W. F. Vinen, and I am grateful for their help and criticism.

REFERENCES

Atkins, K. R. 1951 *Proc. Phys. Soc.* A, **64**, 833.

Atkins, K. R. 1959 *Liquid Helium.* Cambridge University Press.

Batchelor, G. K. 1953 *The Theory of Homogeneous Turbulence.* Cambridge University Press.

Bhagat, S. M. 1960 *Proc. Phys. Soc.* A, **75**, 303.

Feynman, R. P. 1955 *Progr. Low Temp. Phys.*, vol. I, chap. II. North Holland Publishing Co.

Goldstein, S. (ed.) 1938 *Modern Development in Fluid Dynamics*, vol. II. Oxford University Press.

Hall, H. E. 1960 *Phil. Mag. Suppl.* **9**, 89.

Hall, H. E. & Vinen, W. F. 1956*a* *Proc. Roy. Soc.* A, **238**, 204.

Hall, H. E. & Vinen, W. F. 1956*b* *Proc. Roy. Soc.* A, **238**, 215.

Laufer, J. 1955 *N.A.C.A. Rep.* no. 1174.

Townsend, A. A. 1956 *The Structure of Turbulent Shear Flow.* Cambridge University Press.

Vinen, W. F. 1957*a* *Proc. Roy. Soc.* A, **240**, 114.

Vinen, W. F. 1957*b* *Proc. Roy. Soc.* A, **240**, 128.

Vinen, W. F. 1957*c* *Proc. Roy. Soc.* A, **242**, 493.

Vinen, W. F. 1957*d* *Proc. Roy. Soc.* A, **243**, 400.

Flow of a non-homogeneous fluid in a porous medium

By CHIA-SHUN YIH

Department of Engineering Mechanics, University of Michigan

(Received 27 September 1960)

If the viscosity and specific weight of a fluid are variable, the equations governing its flow in a porous medium are non-linear and in general very difficult to solve. It has been found, however, that steady flows of a fluid of variable viscosity but constant specific weight can be reduced to those of a homogeneous fluid by a remarkably simple transformation, which indicates that the flow patterns of the fluid are the same as those of a homogeneous fluid with the same boundary conditions, and that only the speed need be modified. The speed of the actual flow is obtained by dividing the speed of the homogeneous-fluid flow by a factor proportional to the actual viscosity. The transformation is also used to derive the equations governing steady two-dimensional flows and steady axisymmetric flows of a fluid of variable viscosity and specific weight. In a good many cases of practical importance these equations are exactly linear, in spite of the fact that the governing equations obtained without the use of the above-mentioned transformation are non-linear. An exact solution for a steady two-dimensional flow with prescribed boundary conditions is given. Two inverse methods for generating exact solutions for two-dimensional flows are presented, together with two illustrative examples. The theory also applies to Hele–Shaw flows, so that it can be easily verified in the laboratory.

1. Steady seepage flow of a fluid of variable viscosity

The generalized Darcy's law for steady flows of a non-homogeneous fluid in a porous medium is expressed by the equations

$$\frac{\mu}{k}u_i = -\frac{\partial p}{\partial x_i} + \rho X_i \quad (i = 1, 2, 3), \tag{1}$$

in which u_i is the (mean) velocity component in the direction of the Cartesian co-ordinate x_i, μ is the viscosity, k is the permeability (which may vary from place to place), p is the pressure, ρ is the density, and X_i is the body force per unit mass in the direction of increasing x_i. If the fluid is incompressible, the equation of continuity is

$$\frac{\partial u_i}{\partial x_i} = 0. \tag{2}$$

If μ and ρ are constant, equations (1) and (2) are linear. In particular, if (in addition) k is constant and X_i possesses a potential Ω so that

$$X_i = -\frac{\partial \Omega}{\partial x_i}, \tag{3}$$

then

$$\phi = \frac{k}{\mu}(p + \rho\Omega)$$

is the potential for the velocity components and satisfies the Laplace equation, as can be seen from the three preceding equations. If ρ and μ are not constant, equations (1) are highly non-linear, and at first sight hopelessly complicated. The following development will show that the situation is actually not as hopeless as it appears to be.

For seepage flow with a macroscopic scale large compared with the dimension of the interstices, interstitial diffusion can be neglected† (Saffman 1959). Molecular diffusion can be neglected (Saffman 1960) if the Péclet number based on a macroscopic scale is large compared with 1. Thus in most practical cases diffusion can be neglected altogether, and for steady flows

$$u_\alpha \frac{\partial \mu}{\partial x_\alpha} = 0 \tag{4}$$

and

$$u_\alpha \frac{\partial \rho}{\partial x_\alpha} = 0. \tag{5}$$

In the absence of body forces, the effect of viscosity variation is simply and conclusively embodied in the transformation

$$u_i' = \frac{\mu}{\mu_0} u_i, \tag{6}$$

in which μ_0 is a reference viscosity and u_i' the velocity of an associated flow. To isolate the effect of viscosity variation, we shall assume ρ to be constant and the body force to be conservative. Equations (1) then become

$$\frac{\mu_0}{k} u_i' = -\frac{\partial}{\partial x_i}(p + \rho\Omega). \tag{7}$$

Furthermore, because of (4), equation (2) can be written

$$\frac{\partial u_i'}{\partial x_i} = 0. \tag{8}$$

Equations (7) and (8) are those governing the flow of a homogeneous fluid. Thus, by means of the transformation (6), the flow of a fluid of variable viscosity is related to that of a homogeneous fluid. In particular, if k is constant,

$$u_i' = -\frac{\partial \phi'}{\partial x_i}, \tag{9}$$

in which the potential

$$\phi' = \frac{k}{\mu_0}(p + \rho\Omega) \tag{10}$$

satisfies the Laplace equation

$$\nabla^2 \phi' = 0. \tag{11}$$

Consequently, if k and ρ are constant, the flow *pattern* is the same as that for a homogeneous fluid, provided the boundary conditions are unchanged.‡ The actual velocity u_i is obtained by means of (6) from the velocity u_i' of the irrotational flow

† The author owes this assurance to Dr P. G. Saffman.

‡ In this connexion, remember that the conditions at surfaces of density discontinuities are satisfied in the actual flow if they are satisfied in the associated flow (with density jumps).

field determined by (11). Thus, in regions of constant u_i' (say $u_1' = U', u_2' = u_3' = 0$), the actual speed u_1 is inversely proportional to the viscosity. This conclusion applies to regions of *horizontal* flow, even if ρ is not constant.

2. The equation governing steady two-dimensional flows of a non-homogeneous fluid

The effect of variation in specific weight (or of density in a gravitational field) will now be taken into account also. If (x, z) are used for (x_1, x_3), with z measured vertically upward, and (u, w) are used for (u_1, u_3), equations (1) can be written, for two-dimensional flows,

$$\frac{\mu}{k}u = -\frac{\partial p}{\partial x}, \quad \frac{\mu}{k}w = -\frac{\partial p}{\partial z} - g\rho, \tag{12}$$

or, with

$$(u', w') = \frac{\mu}{\mu_0}(u, w), \tag{13}$$

$$\frac{\mu_0}{k}u' = -\frac{\partial p}{\partial x}, \quad \frac{\mu_0}{k}w' = -\frac{\partial p}{\partial z} - g\rho. \tag{14}$$

The permeability k will be assumed constant in the subsequent development. If p is eliminated from equations (14), and, as a consequence of (5) and the steadiness of the motion, ρ is recognized to be a function of the stream function alone, the following equation is obtained:

$$\nabla^2\psi' = \frac{kg}{\mu_0}\frac{d\rho}{d\psi'}\frac{\partial\psi'}{\partial x}, \tag{15}$$

in which ψ' is the stream function (of Lagrange) for the velocity components u' and w':

$$u' = \frac{\partial\psi'}{\partial z}, \quad w' = -\frac{\partial\psi'}{\partial x}. \tag{16}$$

The quantity $d\rho/d\psi'$ is to be determined from the upstream condition.

3. The equation governing steady axisymmetric flows of a non-homogeneous fluid

For axisymmetric flows, the equations corresponding to (14) are, in cylindrical co-ordinates (with z measured vertically upward),

$$\frac{\mu_0}{k}u' = -\frac{\partial p}{\partial r}, \quad \frac{\mu_0}{k}w' = -\frac{\partial p}{\partial z} - g\rho, \tag{17}$$

in which u' and w' are again related to u and w by (13), except that now u is the radial and w the axial component of the velocity. The equation of continuity

$$\frac{\partial(ru)}{\partial r} + \frac{\partial(rw)}{\partial z} = 0 \tag{18}$$

can again be written as

$$\frac{\partial(ru')}{\partial r} + \frac{\partial(rw')}{\partial z} = 0, \tag{19}$$

because the substantial derivative of μ is zero. Equation (19) permits the use of Stokes's stream function ψ':

$$u' = -\frac{1}{r}\frac{\partial \psi'}{\partial z}, \quad w' = \frac{1}{r}\frac{\partial \psi'}{\partial r}. \tag{20}$$

Elimination of p from (17) by cross-differentiation and utilization of the fact that ρ is a function of ψ' alone produce the following equation governing steady axisymmetric flows:

$$-\left(\frac{\partial^2}{\partial r^2} - \frac{1}{r}\frac{\partial}{\partial r} + \frac{\partial^2}{\partial z^2}\right)\psi' = \frac{kgr}{\mu_0}\frac{dp}{d\psi'}\frac{\partial \psi'}{\partial r}, \tag{21}$$

in which $d\rho/d\psi'$ is to be determined from the upstream condition.

4. Exact solutions for two-dimensional flows

As a first example, the case of stratified seepage into a two-dimensional sink will be discussed. The fluid is assumed to be confined to the porous layer between two impermeable horizontal planes, one at $z = 0$ and the other at $z = d$. The sink is situated in the upper plane.

The point in the lower plane directly below the sink will be used as the origin for the co-ordinates (x, z) in the plane perpendicular to the direction of the length of the sink. Thus the co-ordinates for the trace of the sink in that plane are $(0, d)$. Since there is symmetry about the z-axis, only one half of the flow field need be considered. The flow at $x = -\infty$ is, as can be verified later, horizontal in direction. Hence (15) demands that, at $x = -\infty$,

$$\psi' = Cz \quad (C = \text{constant}),$$

where ψ' is taken to be zero at the lower boundary. If the upstream variation of μ with z is given, C is related to the actual discharge in a straightforward manner. With the dimensionless variables defined by

$$\xi = \frac{x}{d}, \quad \eta = \frac{z}{d}, \quad \Psi = \frac{\psi'}{Cd}, \quad \text{and} \quad B = -\frac{kg}{\mu_0 C}\frac{d\rho}{d\Psi}, \tag{22}$$

(15) becomes

$$\left(\frac{\partial^2}{\partial \xi^2} + \frac{\partial^2}{\partial \eta^2}\right)\Psi + B\frac{d\Psi}{d\xi} = 0. \tag{23}$$

The quantity B is in general a function of Ψ, to be determined from the upstream condition. But if ρ changes linearly with z far upstream, where the flow is parallel, it also changes linearly with Ψ and B is a constant. The constancy of B will be assumed in the examples given.

Equation (23) is to be solved with the boundary conditions

$$\Psi = 0 \quad \text{at} \quad \eta = 0 \quad \text{and} \quad \xi = 0 \quad (\eta < 1),$$
$$\Psi = 1 \quad \text{at} \quad \eta = 1,$$
$$\Psi = \eta \quad \text{at} \quad \xi = -\infty.$$

The solution, by the method of separation of variables, is

$$\Psi = \eta + \frac{2}{\pi}\sum_{n=1}^{\infty}\frac{(-1)^n}{n}\sin n\pi\eta \exp(\alpha\xi), \tag{24}$$

with

$$\alpha = \tfrac{1}{2}(-B + \sqrt{[B^2 + 4n^2\pi^2]}).$$

The flow pattern for $B = 0$ is an irrotational flow pattern, familiar in hydrodynamics, and will not be shown here. Those for $B = \pi$, 2π and 4π are shown in figures 1–3 respectively. The flow condition at $x = -\infty$ is entirely the same for

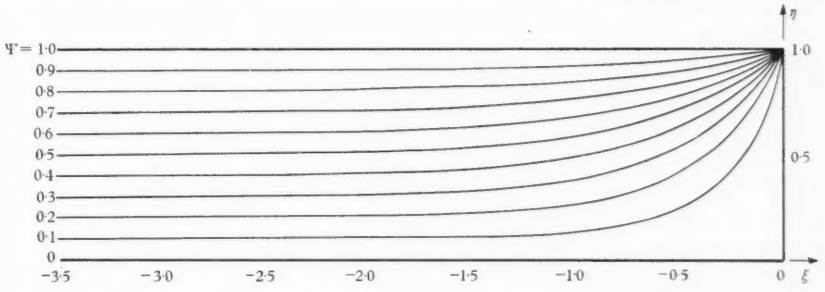

FIGURE 1. Two-dimensional flow of a stratified fluid in a porous medium into a sink, $B = \pi$.

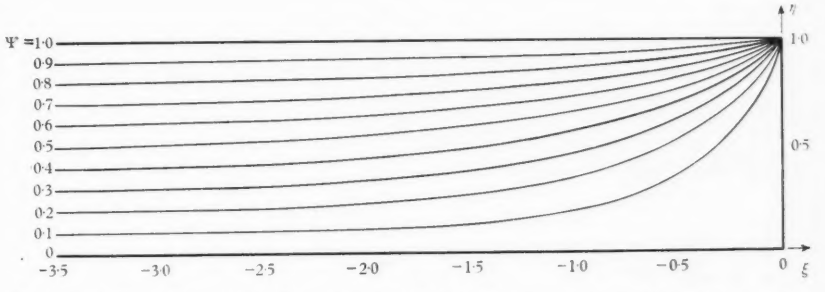

FIGURE 2. Two-dimensional flow of a stratified fluid in a porous medium into a sink, $B = 2\pi$.

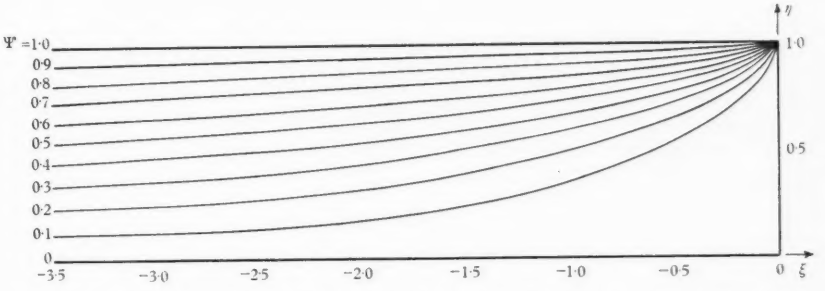

FIGURE 3. Two-dimensional flow of a stratified fluid in a porous medium into a sink, $B = 4\pi$.

any value of B (or of density variation), but the patterns show a concentration of streamlines near $\eta = 1$ for greater and greater values of B. The solution (24) and the corresponding one for axisymmetric flow may be useful for deciding whether the practice in the oil industry of forcing oil up for pumping by injecting water into the ground is an economical one.

For flows, confined between two impermeable planes $z = 0$ and $z = d$, from left to right past an impermeable barrier protruding from the lower plane (say), inverse methods can be advantageously used. Two inverse methods will now be given, which can be combined if desired. For either method the solution is of the form

$$\Psi_- = \eta + \sum_{n=1}^{\infty} A_n \sin n\pi\eta \exp(\alpha_n \xi) \quad (\xi < 0), \tag{25}$$

$$\Psi_+ = \eta + \sum_{n=1}^{\infty} B_n \sin n\pi\eta \exp(\beta_n \xi) \quad (\xi > 0), \tag{26}$$

in which
$$(\alpha_n, \beta_n) = \tfrac{1}{2}(-B \pm \sqrt{[B^2 + 4n^2\pi^2]}), \tag{27}$$

the constancy of B being assumed. The first method consists in matching Ψ_- and Ψ_+ at $\xi = 0$ through the demands

$$\Psi_- = \Psi_+ \quad \text{at} \quad \xi = 0, \tag{28}$$

$$\frac{\partial \Psi_-}{\partial \xi} - \frac{\partial \Psi_+}{\partial \xi} = f(\eta) \quad \text{at} \quad \xi = 0, \tag{29}$$

in which
$$f(\eta) = 0 \quad \text{for} \quad a \leqslant \eta \leqslant 1 \quad \text{and at} \quad \eta = 0,$$

and is arbitrary otherwise. The function $f(\eta)$ corresponds to a vortex distribution from $\eta = 0$ to $\eta = a$. Equation (28) demands that

$$A_n = B_n, \tag{30}$$

and (29) demands

$$\alpha_n A_n - \beta_n B_n = 2\int_0^1 f(\eta) \sin n\pi\eta \, d\eta, \tag{31}$$

or
$$\sqrt{(B^2 + 4n^2\pi^2)}\, A_n = 2\int_0^1 f(\eta) \sin n\pi\eta \, d\eta. \tag{32}$$

The vortex sheet does not have to be located at $\xi = 0$. If it is located at $\xi = b$, all one has to do is to change ξ to $\xi - b$ in equations (25) and (26). Thus more than one vortex sheet may be used, and the resulting barrier is then traced out as the closed streamline $\Psi = 0$. By assuming $f(\eta)$ to be a 'Dirac function' located at some non-zero elevation, equations (25)–(27), (30) and (31) provide the solution for flow over a barrier generated by a concentrated vortex located on $\xi = 0$. By shifting the origin we can obtain the solution for a concentrated vortex located elsewhere, and the solutions for different vortices can again be superposed.

If

$$f(\eta) = \begin{cases} -12 \sin 2\pi\eta & \text{in} \quad 0 \leqslant \eta \leqslant \tfrac{1}{2}, \\ 0 & \text{elsewhere}, \end{cases} \tag{33}$$

then

$$I_n \equiv 2\int_0^1 f(\eta) \sin n\pi\eta \, d\eta = \begin{cases} 0 & \text{if} \quad n \text{ is even but} \neq 2, \\ -6 & \text{if} \quad n = 2, \\ \dfrac{48}{(n^2-4)\pi}(-1)^{\frac{1}{2}(n-1)} & \text{if } n \text{ is odd.} \end{cases} \tag{34}$$

The flow patterns for this choice of $f(n)$ are shown in figures 4 and 5, for $B = \pi$ and 2π respectively. From (25) and (26) it can be seen that the flow pattern is always unsymmetric about $\xi = 0$, even if the barrier itself is symmetric.

The second method consists in matching Ψ_- and Ψ_+ at $\xi = 0$ by demanding

$$\frac{\partial \Psi_-}{\partial \xi} - \frac{\partial \Psi_+}{\partial \xi} = 0 \quad \text{at} \quad \xi = 0, \tag{35}$$

$$\Psi_- - \Psi_+ = f(\eta) \quad \text{at} \quad \xi = 0, \tag{36}$$

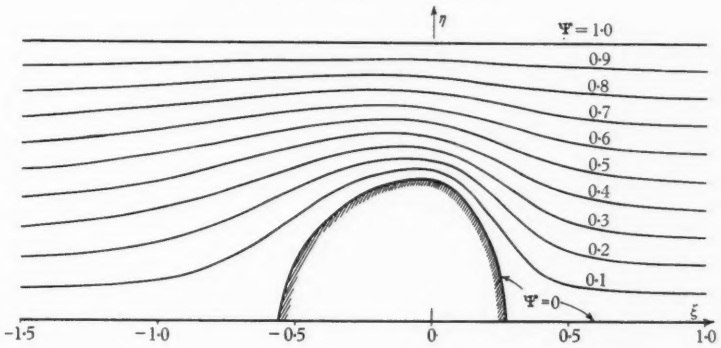

FIGURE 4. Two-dimensional flow of a stratified fluid in a porous medium over a barrier, $B = \pi$.

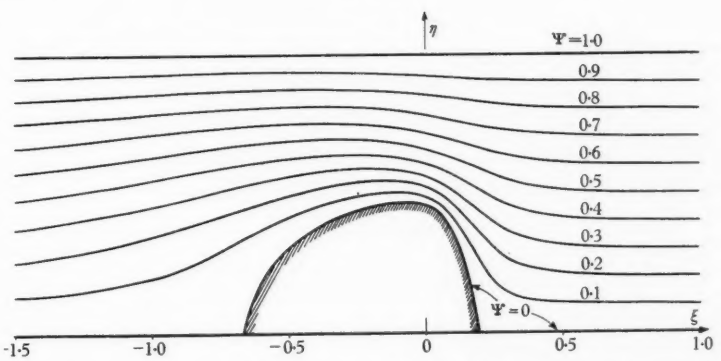

FIGURE 5. Two-dimensional flow of a stratified fluid in a porous medium over a barrier, $B = 2\pi$.

in which $f(\eta)$ is defined as in (29). The function $f(\eta)$ now corresponds to a source distribution. Equation (35) demands

and (36) demands

$$\alpha_n A_n - \beta_n B_n = 0, \tag{37}$$

$$\left(1 - \frac{\alpha_n}{\beta_n}\right) A_n = \left(2 + \frac{B}{n^2\pi^2}\beta_n\right) A_n = 2\int_0^1 f(\eta) \sin n\pi\eta \, d\eta. \tag{38}$$

Again, the source distribution may be shifted to $\xi = b$. In that case the solution is given by equations (25)–(27), (37) and (38), with ξ changed to $\xi - b$. Solutions corresponding to concentrated sources located anywhere above $\eta = 0$ can be obtained by assuming $f(\eta)$ to be a 'Dirac function', and these can be superposed on those for source distributions to obtain a solution representing a flow over a barrier which is nearly the same in form as a prescribed one. In order that a closed

barrier be obtained, however, the total algebraic sum of the sources must be zero. In fact, from the solution corresponding to a concentrated source we can obtain that for a concentrated doublet, by differentiation of (25) and (26) with respect to ξ. The solution corresponding to a doublet distribution can then be obtained by integration. The doublets and doublet distributions (over vertical lines) can be located at different places, and the corresponding solutions can be superposed. We do not have to worry now about the closure of the streamline representing the barrier.

5. Stratified flow in Hele–Shaw cells

Since Hele–Shaw flows can be much more easily investigated in the laboratory and are much easier for observation than seepage flows, it is desirable to show that all of the developments in §§ 2 and 4 can be carried over to Hele–Shaw flows. In fact, if the fluid is confined between two rigid planes $y = 0$ and $y = b$, and if b is very small, the equations of motion are, for steady flows,

$$\mu \frac{\partial^2 u}{\partial y^2} = \frac{\partial p}{\partial x}, \tag{39}$$

$$\mu \frac{\partial^2 w}{\partial y^2} = \frac{\partial p}{\partial z} + g\rho, \tag{40}$$

in which the symbols have exactly the same meanings as in § 2. Since b is small, we can assume, after Hele–Shaw, that

$$(u, w) = 6\frac{y}{b}\left(1 - \frac{y}{b}\right)(U, W),$$

where U, W are independent of y. If, furthermore, μ is assumed to be only a function of x and z, and not of y, equations (39) and (40) become

$$\frac{12\mu}{b^2} U = -\frac{\partial p}{\partial x}, \tag{41}$$

$$\frac{12\mu}{b^2} W = -\frac{\partial p}{\partial z} - g\rho, \tag{42}$$

which are identical to (12) if $\frac{1}{12}b^2$ is equated to k, and U and W identified with the u and w in (12). Since μ and ρ again do not change on a streamline in the x–z-plane, an equation identical to (15) can again be obtained, and all of the developments in § 4 can be carried over.

This work has been done at the University of Cambridge during the tenure of a Senior Post-doctoral Fellowship granted by the National Science Foundation. It is also a pleasure to acknowledge here the support of fundamental research in stratified flows by the Office of Ordnance Research in the past several years. The assistance of Mr Chintu Lai (supported by O.O.R.) in the production of the figures is much appreciated.

REFERENCES

SAFFMAN, P. G. 1959 A theory of dispersion in a porous medium. *J. Fluid Mech.* **6**, 321–49.

SAFFMAN, P. G. 1960 Dispersion due to molecular diffusion and macroscopic mixing in flow through a network of capillaries. *J. Fluid Mech.* **7**, 194–208.

The effect of a very strong magnetic cross-field on steady motion through a slightly conducting fluid

By G. S. S. LUDFORD
University of Maryland*

(Received 29 March 1960 and in revised form 3 August 1960)

The flow engendered by the steady motion of a cylindrical insulator through an inviscid, incompressible fluid of small conductivity σ is not close to potential flow when the applied magnetic cross-field H_0 is sufficiently strong. Here we determine the limiting form of this flow as $\sigma \to 0$ with $\sigma H_0^2 \to \infty$, the latter representing the ponderomotive force.

The limit equations do not have a unique solution, but it is possible to make a selection by taking into account the inertia of the fluid during the limiting process, i.e. without recourse to considerations of how the motion was set up from rest. The forces on the cylinder are found to be asymptotically proportional to $\sqrt{\sigma H_0}$.

The case of an elliptic cylinder and that of a flat plate are worked out in detail.

1. Introduction

Recently J. D. Murray and the author (1960) investigated the flow of a slightly conducting, incompressible, inviscid fluid past a fixed obstacle. The applied magnetic field was assumed to be weak (in fact, it need only be moderate) and to originate in the body itself. The same methods work for a uniform applied field.

In the present paper the fluid is again taken to be a bad conductor, but now the ambient field is assumed to be very strong, being applied at infinity at right angles to the free-stream direction. For simplicity we consider plane flow past a cylindrical insulator of the same permeability as the fluid, perpendicular to both the free stream and the applied magnetic field.

Because of the small conductivity σ, the relative change in the magnetic field $\mathbf{H}_0$, due to motion-induced currents, is small; in the previous problem this disturbance was nevertheless of some importance, but here it may safely be neglected. On the other hand, the fluid motion is no longer close to the potential flow which occurs for $\sigma = 0$. If it were, there would be induced currents of order σH_0—which may still be small—on which would act ponderomotive forces of order σH_0^2, and it is this last quantity which we take to be large in speaking of a very strong magnetic field. This contradiction can only be avoided by assuming a completely different limit flow.

In fact, as $\sigma \to 0$ with $\sigma H_0^2 \to \infty$, the flow attains a rigidity in which only the component of velocity, v, along the lines of force can be disturbed and all quantities are unvarying in this direction (y).† However, there are many such solutions

* Present address: Brown University, Providence, Rhode Island.

† Fig. 1 gives one such flow, which is not, however, the correct one (§ 6).

of the limit equations,* none of which satisfies the boundary conditions completely. The most attractive one is in general not the correct one.

The character of the possible limit flows is reminiscent of transsonic flow past a thin airfoil. As there the y-co-ordinate must be compressed, this time by a factor $\sqrt{\sigma H_0}$. Changes along the lines of force are thereby magnified and the new limit equations, which are fortunately still linear, take into account the inertia of the fluid. This leads to what may be called the outer expansions of the solution, one for y large and positive and the other for y large and negative. Their role is similar to, but somewhat simpler than, that of the Oseen expansion in slow viscous flow (Proudman & Pearson 1957) and, as there, they must be matched to an inner expansion (the Stokes expansion in the viscous case). There is only one such inner expansion, and its first two terms, which are solutions of the limit equations mentioned in the last paragraph, not only determine the correct limit flow at each point but also describe the way in which the pressure becomes infinite there.

It is easy to see how the compression factor $\sqrt{\sigma H_0}$ arises. For if changes in v take place over a distance of order R in the y-direction, then by continuity the disturbance velocity perpendicular to the field is of order $1/R$. This induces a ponderomotive force in the same direction of order $\sigma H_0^2/R$, which can only be balanced by pressure gradients and hence pressures of the same order. Thus pressure gradients along the lines of force of order $\sigma H_0^2/R^2$ occur and these can only be balanced by inertia forces, which are of order unity. Hence $R = \sqrt{\sigma H_0}$.

This also shows that the pressure and hence the forces on the cylinder are of order $\sqrt{\sigma H_0}$. The corresponding lift, drag, and moment are calculated for a flat plate at incidence and an elliptic cylinder.

The same analysis applies when the conductivity and magnetic field are both moderate, provided that then the free-stream velocity U_0 is small.† In this case our conclusions appear to be in contradiction to those of Stewartson (1956), who is forced to consider how the motion is set up from rest in attempting to determine the ultimate steady state. Although strictly speaking the two problems are not comparable—he considers a sphere of infinite conductivity while here a cylinder of zero conductivity‡ is taken—it would seem that his complete neglect of the quadratic inertia terms is not valid. Their rejection on the basis that the magnitude of the ponderomotive force is much larger is not justified for the motion along the magnetic field, since this force, however large, has no component in that direction. In fact the inertia forces play a critical role in the present treatment by dispersing the disturbance at large y-distances and thereby controlling the flow upstream and downstream of the cylinder.

We shall return to this point in a later paper, where the flow past a three-dimensional obstacle will be considered.

The author is indebted to S. Goldstein for valuable discussion during the preparation of this paper.

* This non-uniqueness was first recognized by Stewartson (1956).

† The compression factor $\sqrt{\sigma H_0}$ is replaced by $U_0^{\frac{1}{2}}$. Note that now the dimensionless pressure is of order $U_0^{\frac{1}{2}}$ so that the actual forces on the cylinder are proportional to $U_0^{\frac{1}{2}}$.

‡ The present approximation does in fact also apply to a cylinder with a small conductivity.

2. The equations of motion

The fluid is assumed to be incompressible, inviscid and electrically conducting, so that its steady motion is governed by the equations

$$\left.\begin{aligned} \rho_0 \mathbf{v}.\operatorname{grad}\mathbf{v} &= -\operatorname{grad} p + \mu \operatorname{curl}\mathbf{H}\times\mathbf{H}, \\ \operatorname{curl}\mathbf{H} &= \sigma(\mathbf{E}+\mu\mathbf{v}\times\mathbf{H}), \end{aligned}\right\} \tag{1}$$

where

$$\operatorname{div}\mathbf{v} = 0, \quad \operatorname{curl}\mathbf{E} = 0, \quad \operatorname{div}\mathbf{H} = 0. \tag{2}$$

Here $\mathbf{v}$ is the fluid velocity, ρ_0 the constant mass density, $\mathbf{E}$ and $\mathbf{H}$ the electric and magnetic fields, respectively, σ the electrical conductivity, and μ the permeability; the last two are taken to be constant throughout the fluid.

Take axes moving with the body, with Ox along the direction in which the fluid now moves at infinity, so that $\mathbf{v} = U_0\mathbf{i}$ there, and Oy along the undisturbed magnetic field $\mathbf{H}_0$.

Let a be a representative length in the body. Then, when $\mathbf{v}$, $\mathbf{r}$, and $\mathbf{H}$ are made dimensionless by referring them to U_0, a, and H_0, respectively, the equations (1) become

$$\mathbf{v}.\operatorname{grad}\mathbf{v} = -\operatorname{grad} p + \frac{1}{A^2}\operatorname{curl}\mathbf{H}\times\mathbf{H}, \tag{3a}$$

$$\operatorname{curl}\mathbf{H} = R_M(\mathbf{E}+\mathbf{v}\times\mathbf{H}), \tag{3b}$$

while equations (2) are unchanged. Here $A = U_0\sqrt{\rho_0}/\sqrt{\mu}H_0$ is the Alfvén number and $R_M = U_0 a\mu\sigma$ the magnetic Reynolds number; the electric field is now given by $(\mu U_0 H_0)\mathbf{E}$ and the pressure by $(\rho_0 U_0^2)p$. On substituting (3*b*) into (3*a*) we obtain the alternative form

$$\mathbf{v}.\operatorname{grad}\mathbf{v} = -\operatorname{grad} p + \frac{R_M}{A^2}(\mathbf{E}+\mathbf{v}\times\mathbf{H})\times\mathbf{H}. \tag{4}$$

In flows at low R_M, the disturbance of the applied magnetic field, due to the currents induced by the fluid motion, is seen to be determined by R_M [equation (3*b*)], while the influence of the field on the motion, through the force exerted by the field on these currents, is characterized by R_M/A^2 [see equation (4)]. This important parameter will be denoted by N:

$$N = \frac{R_M}{A^2} = \frac{a\mu^2 H_0^2\sigma}{\rho_0 U_0}. \tag{5}$$

When we say that the magnetic field is very strong we mean that N is large, even though R_M is small.

At large distances $\mathbf{E}$ tends to $-\mathbf{k}$. When the motion is plane, in the sense that $\mathbf{v}$ and $\mathbf{H}$ are independent of z and have no z-components, the second of equations (2) shows that $\mathbf{E}$ has this constant value throughout the flow.

3. Plane flow past a cylinder

We consider the flow past a cylinder whose generators are parallel to the z-axis, and proceed in a heuristic way, later checking the result obtained (§6).

As a first approximation for R_M small we may take $\operatorname{curl}\mathbf{H} = 0$ [see (3*b*)]. Since the permeability of the cylinder is assumed to be the same as that of the

fluid, this means that the magnetic field is undisturbed: $\mathbf{H} = \mathbf{j}$. When this and the result $\mathbf{E} = -\mathbf{k}$ are used in equation (4) it becomes

$$\left.\begin{aligned} \frac{\partial u}{\partial x} + u\frac{\partial u}{\partial x} + v\frac{\partial u}{\partial y} &= -\frac{\partial p}{\partial x} - Nu, \\ \frac{\partial v}{\partial x} + u\frac{\partial v}{\partial x} + v\frac{\partial v}{\partial y} &= -\frac{\partial p}{\partial y}, \end{aligned}\right\} \tag{6}$$

where u and v are the components of the disturbance velocity $\mathbf{v} - \mathbf{i}$.

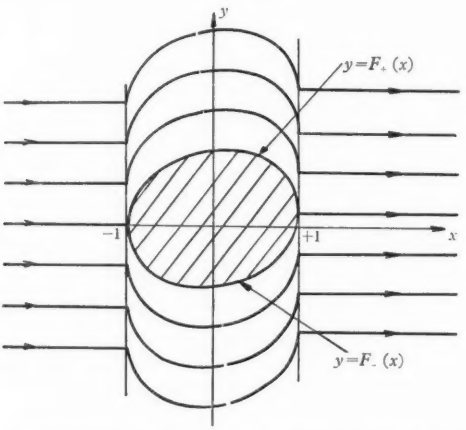

FIGURE 1. Plausible (but incorrect) solution of limit equations.

When N is large these equations reduce to

$$u = -\frac{\partial}{\partial x}\left(\frac{p}{N}\right), \quad \frac{\partial}{\partial y}\left(\frac{p}{N}\right) = 0, \tag{7}$$

if we allow for the possibility that p becomes large with N. Thus

$$p = Nf(x), \quad u = -f'(x),$$

and the equation of continuity gives

$$v = yf''(x) + g(x);$$

here f and g are arbitrary functions.

Although we shall not in fact be able to satisfy the boundary conditions completely, it is clear that $f''(x)$ must be set equal to zero. Then f' is a constant, which must be zero if u is to vanish at infinity; similarly, $f = 0$ since this is its value at infinity. There remains $g(x)$, which for $|x| \leqslant 1$* is determined by the boundary conditions at the cylinder $y = F_{\pm}(x)$ (see figure 1):

$$v = g(x) = \begin{cases} F'_+(x), & |x| \leqslant 1 \quad \text{and} \quad y \geqslant F_+(x), \\ F'_-(x), & |x| \leqslant 1 \quad \text{and} \quad y \leqslant F_-(x). \end{cases} \tag{8}$$

* The length a is henceforth taken to be one half the breadth of the cylinder in the x-direction.

This determination violates the conditions at infinity: v does not tend to zero as $y \to \pm\infty$. However, for $|x| > 1$, they can be satisfied by setting

$$v = g(x) = 0 \quad \text{for} \quad |x| > 1. \tag{9}$$

Then the violation is restricted to vanishingly small angles around the y-axis. Nevertheless, it will turn out that this is not in general the correct choice for $x < -1$.

This solution, which is apparently the only acceptable one, is illustrated in figure 1. The streamlines form two families of congruent curves. The flow is undisturbed until it comes abreast of the cylinder, where it is displaced to either side along the lines of force. Behind the cylinder it reunites into a uniform stream again. When, as in the figure, the cylinder is blunt at the front, infinite vertical velocities occur on the line $x = -1$. A similar remark applies to $x = 1$.

It would seem that this is the limiting form of the flow pattern in the vicinity of any fixed point as $N \to \infty$. However, when substituted into the neglected terms on the left-hand side of equations (6), it yields a perturbation in which, for $|x| < 1$, u and p are linear functions of y, and v is a quadratic one.

4. Compressing the y-co-ordinate

The main feature of the supposed limiting flow pattern is its frozen character in the vertical direction. Changes in this direction vanish in the limit at any fixed point. This suggests that, as this limit is being taken, the y-co-ordinate should be simultaneously compressed at a rate sufficient to retain significant changes. By reason of continuity, the disturbance velocity in the x-direction, which also vanishes in the limit, must be magnified at the same rate.

We therefore set

$$y = \sqrt{N}\,Y, \quad u = \frac{U}{\sqrt{N}}, \quad p = \sqrt{N}\,P \tag{10}$$

in equations (6), assume all the new variables and their derivatives are of order unity, and let N tend to infinity:

$$U = -\frac{\partial P}{\partial x}, \quad \frac{\partial v}{\partial x} = -\frac{\partial P}{\partial Y}. \tag{11}$$

Note that the inertia term $\partial v/\partial x$ has now survived [cf. (7)]. The choice (10) ensures that, in the new variables, the flow is the result of a balance between the inertia forces and the stress forces (both pressure and Maxwell).*

Eliminate U and P between equations (11) and the equation of continuity:

$$\frac{\partial U}{\partial x} + \frac{\partial v}{\partial Y} = 0. \tag{12}$$

Then

$$\frac{\partial^3 v}{\partial x^3} + \frac{\partial^2 v}{\partial Y^2} = 0. \tag{13}$$

* It is conceivable that the limit solution is the uniform flow and that this must be supplemented by a boundary layer at the cylinder. In the boundary layer the fluid would have to accelerate rapidly as it moved away from the front. However, the only force capable of such accelerations is the ponderomotive force and this would act in the wrong direction.

This equation will be solved separately above and below the x-axis, which is a characteristic. The two partial solutions must satisfy the boundary conditions

$$|x| \leqslant 1: \quad v = \begin{cases} F'_+(x) & \text{for} \quad Y \to +0, \\ F'_-(x) & \text{for} \quad Y \to -0, \end{cases} \tag{14}$$

see (8). For $|x| > 1$ they must lead to the same v and pressure P (and hence $\partial v/\partial Y$) on the x-axis.*

We may restrict our attention to the half plane $Y > 0$ (see figure 2), considering for the moment that v is prescribed everywhere on the x-axis. The problem is then quite similar to the initial-value problem of one-dimensional heat flow. Since the order of the derivatives in (13) is one higher, however, it would seem that the values of $\partial v/\partial Y$ also should be prescribed for $Y \to +0$. This is replaced by the requirement that v should vanish as $Y \to +\infty$, an automatic property in the heat case.†

The complete solution can be built up from the source solution, which is the x-derivative of the solution having the unit-step function for its boundary values. The latter corresponds to the error function of heat conduction and, like it, is a function of a single combination of x and Y.

5. The step-function solution

Consider the solution

$$v_0 = \frac{1}{2\pi i} \int_{c-i\infty}^{c+i\infty} \exp(\lambda Y - \lambda^{\frac{3}{2}} x) \frac{d\lambda}{\lambda} \quad (c > 0),$$

which can be obtained by use of the Laplace transform and is clearly a function of

$$\eta = \frac{x}{Y^{\frac{2}{3}}} \tag{15}$$

alone. The lines $\eta = \text{const.}$ are shown dashed in figure 2. In the first instance v_0 is defined for positive values of x only, but by deforming the path of integration in the complex λ-plane it can be continued analytically to all values of x (see Appendix).

For large values of $|\eta|$ it has the asymptotic expansions

$$v_0 \sim \frac{3}{2}\left[1 + \frac{1}{|\eta|^{\frac{3}{2}}} \sum_{n=0}^{\infty} \frac{1}{(2n+1)!\,\Gamma(-\frac{1}{2}-3n)} \frac{1}{|\eta|^{3n}}\right] \quad (\eta < 0), \tag{16a}$$

$$v_0 \sim \frac{9\exp[-4\eta^3/27]}{4(\pi\eta^3)} \sum_{n=0}^{\infty} \frac{A_n}{\eta^{3n}} \quad (\eta > 0), \tag{16b}$$

* See §6 for further clarification.

† Since the complete flow region is doubly connected the question of uniqueness of the solution arises, just as it does in the absence of a magnetic field [equations (6) with $N = 0$]. Although there is room to question uniqueness at this stage, where we are solving in the upper half plane assuming that v is prescribed on the x-axis, the real question comes later (end of next section), when we must determine v on the x-axis outside the body from the integral equation which results on joining this partial solution to a similar one in the lower half plane. However, it is known that this particular integral equation (Abel's) does have a unique solution.

where the coefficients A_n are determined by the recurrence relation

$$A_{n+1}+\tfrac{27}{4}(n+\tfrac{1}{2})A_n = \frac{\Gamma(\frac{3}{2})}{(2n+2)!\,\Gamma(-\frac{3}{2}-3n)}, \quad A_0 = 1. \tag{17}$$

Since v_0 tends to $\frac{3}{2}$ as $\eta \to -\infty$ and 0 as $\eta \to \infty$, it follows that

$$\mathscr{H}(\eta) = 1-\tfrac{2}{3}v_0 = 1-\frac{1}{3\pi i}\int_{c-i\infty}^{c+i\infty} \exp\left[\lambda Y-\lambda^{\frac{3}{2}}x\right]\frac{d\lambda}{\lambda}$$

is the required step-function solution.

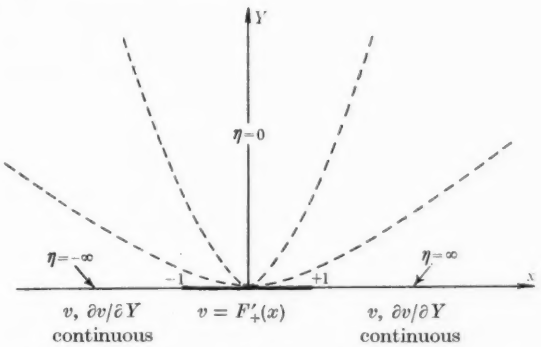

FIGURE 2. Boundary conditions on solution of equation (13) in upper half of x, Y-plane. On a dashed line the η of equation (15) has constant values.

A graph of $\mathscr{H}(\eta)$ is given in figure 3. For almost the whole range of η shown the series expansion

$$\mathscr{H}(\eta) = \tfrac{1}{3}+\tfrac{2}{3}\eta\sum_{n=0}^{\infty}\frac{(-1)^n}{(3n+1)!\,\Gamma(\frac{1}{3}-2n)}\eta^{3n}+\tfrac{2}{3}\eta^2\sum_{n=0}^{\infty}\frac{(-1)^{n-1}}{(3n+2)!\,\Gamma(-\frac{1}{3}-2n)}\eta^{3n} \tag{18}$$

was found adequate for hand computations. The asymptotic expansions (16) confirmed values at the extremes. Note the gradual (algebraic) decay of $\mathscr{H}$ for negative η, determined by (16a), in contrast to the sharp (exponential) rise to its limiting value when η is positive, governed by (16b).*

The solution of (13) taking on the values $V(x)$ on the x-axis is therefore

$$v = \frac{1}{Y^{\frac{2}{3}}}\int_{-\infty}^{\infty} V(\xi)\mathscr{H}'[(x-\xi)/Y^{\frac{2}{3}}]\,d\xi, \tag{19}$$

since the x-derivative of $\mathscr{H}$ is clearly the source solution. The corresponding U and P now follow from (11) and (12). However, since we are mainly interested in the values of P as $Y \to +0$, which can be determined directly from the expansions (16), we shall not write the resulting formulas down. To satisfy (14) we set

$$V(x) = F'_+(x) \quad \text{for} \quad |x| \leqslant 1. \tag{20}$$

There remains the determination of V outside this range.

* For the case of heat conduction, the decay is exponential.

Consider the pressure P due to a unit source at the origin. Since

$$v = \frac{\partial \mathscr{H}}{\partial x} = -\frac{2}{3}\frac{\partial v_0}{\partial x},$$

we have

$$\frac{\partial^2 P}{\partial x^2} = \frac{\partial v}{\partial Y} = -\frac{2}{3}\frac{\partial^2 v_0}{\partial x \partial Y}.$$

Hence from the asymptotic expansions (16) we find that, as $Y \to +0$,

$$\frac{\partial^2 P}{\partial x^2} = \frac{\partial}{\partial x}\left[\frac{1}{2\sqrt{\pi}|x|^{\frac{3}{2}}}\right], \quad P = \frac{1}{\sqrt{\pi}|x|^{\frac{1}{2}}} \quad \text{for} \quad x < 0,$$

$$\frac{\partial^2 P}{\partial x^2} = 0, \quad P = 0 \quad \text{for} \quad x > 0,$$

since $P \to 0$ as $x \to \pm\infty$. This means that a source creates pressure upstream but not downstream of itself.

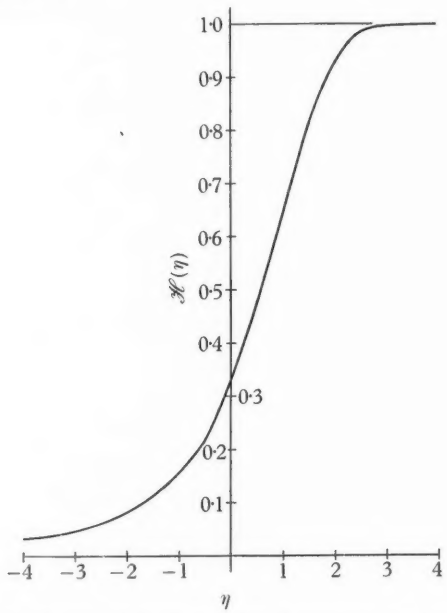

FIGURE 3. The step-function solution $\mathscr{H}(\eta)$ of equation (13), where $\eta = x/Y^{\frac{2}{3}}$.

It follows that

$$V(x) = 0 \quad \text{for} \quad x > 1 \tag{21}$$

in (19), and that correspondingly

$$P = \frac{1}{\sqrt{\pi}}\left[\int_x^{-1} \frac{V(\xi)}{(\xi - x)^{\frac{1}{2}}}\, d\xi + \int_{-1}^{1} \frac{F'_+(\xi)}{(\xi - x)^{\frac{1}{2}}}\, d\xi\right] \tag{22}$$

on the x-axis for $x < -1$. Similarly, for the solution in $Y < 0$ we have the values

$$P = -\frac{1}{\sqrt{\pi}}\left[\int_x^{-1} \frac{V(\xi)}{(\xi - x)^{\frac{1}{2}}}\, d\xi + \int_{-1}^{1} \frac{F'_-(\xi)}{(\xi - x)^{\frac{1}{2}}}\, d\xi\right], \tag{23}$$

where the same function V occurs by reason of the continuity of v across the x-axis.

Now equate the right-hand sides of (22) and (23). The result is an Abel integral equation for V, whose unique solution* is

$$V(x) = \frac{1}{2\pi}\frac{d}{dx}\int_x^{-1}\frac{d\eta}{(\eta-x)^{\frac{1}{2}}}\int_{-1}^{1}[F'_+(\xi)+F'_-(\xi)]\frac{d\xi}{(\xi-\eta)^{\frac{1}{2}}}$$

$$= -\frac{1}{2\pi}\frac{1}{\sqrt{(-1-x)}}\int_{-1}^{1}[F'_+(\xi)+F'_-(\xi)]\frac{(1+\xi)^{\frac{1}{2}}}{\xi-x}\,d\xi \quad \text{for} \quad x<-1. \quad (24)$$

6. Discussion of solution: the force on the cylinder

We must now indicate in a more precise way the character of the solution which has been obtained. What is in fact involved in a matching procedure similar to those in boundary-layer theory [see Goldstein (1960, p. 131 *et seq.*)] and slow viscous motion [see Proudman & Pearson (1957)], though of a simpler kind.

The variables u, v, p as functions of x, y will be called the inner solution, while U, v, P as functions of x, Y, for $Y>0$ and $Y<0$ separately, will be referred to as the outer ($\pm$) solutions. Correspondingly, we shall speak of the inner layer and outer regions.

In §3 we showed, by plausible arguments, that the first approximation to the inner solution for large values of N was

$$u=0, \quad v=\begin{cases} F'_{\pm}(x) & \text{for} \quad |x|\leqslant 1, \\ g(x) & \text{for} \quad |x|>1, \end{cases} \qquad p=O(N), \qquad (25)$$

correct to $O(1)$, $O(1)$, and $O(N)$ respectively, where now we shall not take $g=0$. In §4 we assumed that the outer solutions would have to satisfy these conditions (translated into U, v, P-variables) as $Y\to\pm 0$. For $|x|\leqslant 1$ this prescribes definite (but in general different) values for v as $Y\to\pm 0$. For $|x|\geqslant 1$ it merely requires the values to be the same, $g(x)$. However, since in the outer regions a velocity v induces a pressure P of the same order, a pressure p of order $\sqrt{N}$ must be expected in the inner layer, and such a pressure is transmitted unaltered across the layer. This leads then to the additional requirement that the P of the outer solutions should tend to the same values as $Y\to\pm 0$, for $|x|>1$.†

Thus the disturbance created by the cylinder transmits itself through the inner layer along the magnetic lines of force into the outer regions, where it disperses and thereby influences conditions upstream (but not downstream) in the inner layer.

The first approximation to the outer ($+$) solution was determined in the last section. The velocity v is given by (19) where V has the values (20), (21) and (24). Similar formulas hold for the outer ($-$) solution. This determines not only g,

$$g(x)=V(x) \quad (|x|>1),$$

but also most of the next approximation in the inner solution. For, in order to provide appropriate $\sqrt{N}$-terms, the latter must be a solution of (7), rather than

* See second footnote, p. 146.

† There is a similar requirement on U but this is satisfied automatically [see (11)].

the result of perturbing (25) by means of (6); consequently it may be written in the form

$$u = -\frac{1}{\sqrt{N}} P_0'(x), \quad v = V(x) + \frac{1}{\sqrt{N}} \begin{cases} [y - \tilde{F}_\pm(x)] P_0''(x) & \text{for } |x| \leqslant 1, \\ [y - h(x)] P_0''(x) & \text{for } |x| > 1, \end{cases}$$
$$p = \sqrt{N} P_0(x). \quad (26)$$

The choice $$\tilde{F}_\pm(x) = F_\pm(x) + \frac{P_0'(x)}{P_0''(x)} F'_\pm(x)$$

ensures that the boundary condition at the cylinder is satisfied to order $1/\sqrt{N}$. Also, setting $P_0(x)$ equal to either of the expressions (22) and (23) for $x < -1$, or the equivalent expression $$\frac{1}{2\sqrt{\pi}} \int_{-1}^{1} \frac{F'_+(\xi) - F'_-(\xi)}{(\xi - x)^{\frac{1}{2}}} d\xi; \quad (27)$$

zero for $x > 1$; and $$\pm \frac{1}{\sqrt{\pi}} \int_x^1 \frac{F'_\pm(\xi)}{(\xi - x)^{\frac{1}{2}}} d\xi \quad \text{for} \quad |x| < 1; \quad (28)$$

makes the pressure p join smoothly with that in the outer regions.

As was the case for $g(x)$ in the approximation (25), $h(x)$ is left undetermined. It has to be found from the common limit for v in the next approximation to the outer solutions as $Y \to \pm 0$ with $|x| > 1$. Note that the y-terms in (26) already appear in the expansions (small Y) of the previous approximation to the outer solutions, and that any part $k(x)$ of the functions $\tilde{F}_\pm$ and h can be absorbed by them if we now set $$Y = [y - k(x)]/\sqrt{N} \quad (10')$$

[cf. (10)]. This appears to be of some importance since otherwise, for example, unmanageably singular data.

$$v = F'_\pm(x) - \frac{1}{\sqrt{N}} \tilde{F}_\pm(x) P_0''(x) \quad \text{as} \quad Y \to \pm 0 \quad \text{with} \quad |x| \leqslant 1$$

occur for this next approximation (see next section). The pressure P of order $1/\sqrt{N}$ which is introduced must once again be continuous across $Y = 0$, as is easily checked by determining the form of the term of order unity in p for the inner solution [from (6)].

The next approximation to the outer solutions involves a perturbation of the previous approximation, and cannot be expressed in simple form. In any event, it is not needed in order to obtain the pressure p, and hence the forces on the cylinder, to order $\sqrt{N}$ [see (26)]. We find from (28) the following lift, drag, and moment.

$$\left.\begin{aligned} \frac{L}{\rho_0 U_0^2 a} &= -\sqrt{\frac{N}{\pi}} \int_{-1}^{1} dx \int_x^1 \frac{F'_+(\xi) + F'_-(\xi)}{(\xi - x)^{\frac{1}{2}}} d\xi \\ &= -2\sqrt{\frac{N}{\pi}} \int_{-1}^{1} (\xi + 1)^{\frac{1}{2}} [F'_+(\xi) + F'_-(\xi)] d\xi, \\ \frac{D}{\rho_0 U_0^2 a} &= \sqrt{\frac{N}{\pi}} \int_{-1}^{1} dx \int_x^1 \frac{F'_+(x) F'_+(\xi) + F'_-(x) F'_-(\xi)}{(\xi - x)^{\frac{1}{2}}} d\xi, \\ \frac{M}{\rho_0 U_0^2 a^2} &= -\sqrt{\frac{N}{\pi}} \int_{-1}^{1} dx \int_x^1 \{[F_+(x) F'_+(x) + x] F'_+(\xi) \\ &\qquad + [F_-(x) F'_-(x) + x] F'_-(\xi)\} \frac{d\xi}{(\xi - x)^{\frac{1}{2}}}. \end{aligned}\right\} \quad (29)$$

7. Examples: flow past a flat plate and elliptic cylinder

Some general conclusions can be drawn from the formulas. From (24) we find

$$\int_{-\infty}^{-1} V(x)\,dx = -\frac{1}{2}\int_{-1}^{1} [F'_+(\xi)+F'_-(\xi)]\,d\xi = d,$$

where

$$d = F_+(-1)-F_+(1) = F_-(-1)-F_-(1)$$

is the downward displacement of the rear point of the profile with respect to its front point. Since the dividing streamline is straight behind the profile, this means that the total displacement of this streamline is zero in the first approximation (see figure 4).

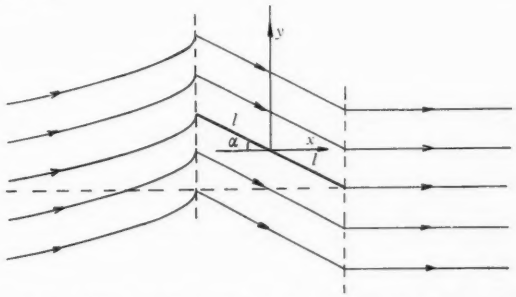

FIGURE 4. Limiting form of flow past a flat plate at incidence.

The pressure upstream of the profile depends only on the values of $F_+(x)-F_-(x)$, i.e. on the thickness in the y-direction but not on the position of the mean surface $y=\frac{1}{2}[F_+(x)+F_-(x)]$ [see (27)]. On the other hand, the lift depends on the mean surface but not on the thickness.

(*a*) *Flat plate.* Let the breadth be $2l$ and the angle of attack α (figure 4). Then $F_\pm = -x\tan\alpha$, $a = l\cos\alpha$ and

$$V = \frac{2\tan\alpha}{\pi}\left[\sqrt{\left(\frac{2}{-1-x}\right)}-\tan^{-1}\sqrt{\left(\frac{2}{-1-x}\right)}\right] \quad \text{for} \quad x<-1,$$

$$P_0 = \mp\frac{2\tan\alpha}{\pi}\sqrt{(1-x)} \quad \text{for} \quad |x|<1.$$

Elsewhere P_0 is zero, in accordance with the remarks just made. The forces on the plate are

$$L = \frac{16}{3}\sqrt{\left(\frac{2N}{\pi}\right)}\rho_0 U_0^2 l\sin\alpha = 4{\cdot}255\sqrt{N}\rho_0 U_0^2 l\sin\alpha,$$

$$D = \frac{16}{3}\sqrt{\left(\frac{2N}{\pi}\right)}\rho_0 U_0^2 l\sin\alpha\tan\alpha = 4{\cdot}255\sqrt{N}\rho_0 U_0^2 l\sin\alpha\tan\alpha,$$

with a resultant perpendicular to the plate; while the moment is

$$M = -\frac{16}{15}\sqrt{\left(\frac{2N}{\pi}\right)}\rho_0 U_0^2 l\tan\alpha = -0{\cdot}851\sqrt{N}\rho_0 U_0^2 l\tan\alpha,$$

so that the resultant acts at a point $l/5$ forward of the centre.

(*b*) *Elliptic cylinder.* Let the major axis be horizontal and of length $2a$. Then $F_{\pm} = \pm (b/a)\sqrt{(1-x^2)}$, where $2b$ is the length of the minor axis. From the symmetry, $V = 0$ for $x < -1$, and $L = M = 0$.

We find

$$P_0 = \begin{cases} \dfrac{2}{\sqrt{\pi}}\dfrac{b}{a}\sqrt{(1-x)}\left[\dfrac{-x}{1-x}K\left(\sqrt{\dfrac{2}{1-x}}\right) - E\left(\sqrt{\dfrac{2}{1-x}}\right)\right] & \text{for } x < -1, \\ \sqrt{\dfrac{2}{\pi}}\dfrac{b}{a}\left[K\left(\sqrt{\dfrac{1-x}{2}}\right) - 2E\left(\sqrt{\dfrac{1-x}{2}}\right)\right] & \text{for } |x| < 1, \end{cases}$$

where K and E are complete elliptic integrals of the first and second kind, respectively. Finally, the drag is

$$D = \frac{1}{\sqrt{(18\pi)}} B^2(\tfrac{1}{4}, \tfrac{1}{2}) \frac{b^2}{a^2}\sqrt{N}\rho_0 U_0^2 a = 3{\cdot}656 \frac{b^2}{a^2}\sqrt{N}\rho_0 U_0^2 a,$$

where B is the beta function.

A circular cylinder of diameter $2a$ experiences a drag equal to that of a flat plate of breadth $2a$ inclined at an angle α of about 49°.

Finally, we note that the function $\tilde{F}_{\pm}(x) P_0''(x)$ which occurs in equation (26) is infinite of order $\frac{3}{2}$ as $x \to 1$ in (*a*) and as $x \to -1$ in (*b*). Both these singularities can be avoided in the boundary data for the second approximation to the outer solutions by suitable non-singular choices of $k(x)$ in (10′). Whether this leads to an acceptable approximation remains an open question. In any event the case of the elliptic cylinder, which is bluff both forward and aft, appears to be no more singular than that of the flat plate.

These successively worse singularities on $x = \pm 1$ seem to form an integral part of the expansion of the inner solution, since they arise from matching with expansions of the outer solutions, which in turn derive from essentially asymptotic representations of the type (16).

This research was sponsored by the Office of Ordnance Research, U.S. Army, under contract DA-36-034-ORD-1486.

Appendix

Here we derive the properties of the function

$$v_0 = \frac{1}{2\pi i}\int_{c-i\infty}^{c+i\infty} \exp\left[\lambda Y - \lambda^{\frac{3}{2}} x\right] \frac{d\lambda}{\lambda} \quad (c > 0) \tag{30}$$

quoted in the text (see figure 5).

For $x > 0$, the integral is convergent and the path of integration may be deformed into $ABCD$ starting at $-\infty$, encircling the origin in the anti-clockwise direction, and returning to $-\infty$. Thus, for $0 \leqslant \arg\lambda < 3\pi/4$, $|\exp(-\lambda^{\frac{3}{2}}x)|$ is less than unity, while, for $3\pi/4 \leqslant \arg\lambda \leqslant \pi$, $\exp\lambda Y$ is dominantly small in the integrand, i.e. $|\exp(\lambda Y - \lambda^{\frac{3}{2}}x)| < \exp(-m|\lambda|)$ for any positive $m < Y/\sqrt{2}$. A slight modification of the usual argument (Carslaw & Jaeger 1948, p. 76) now shows that the integral taken over the infinite circular arc Q_1 is zero. Similar remarks apply to Q_2. Hence

$$v_0 = \frac{1}{2\pi i}\int_{-\infty}^{(0+)} \exp\left[\lambda Y - \lambda^{\frac{3}{2}} x\right] \frac{d\lambda}{\lambda}, \tag{31}$$

the integral now converging for all values of x.

If $\exp(-\lambda^{\frac{3}{2}}x)$ is expanded and term-by-term integration is made [a procedure which is valid for (31) but not (30)], we obtain*

$$\begin{aligned} v_0 &= \frac{1}{2\pi i}\int_{-\infty}^{(0+)} \frac{e^{\lambda Y}}{\lambda}\left[1 - x\lambda^{\frac{3}{2}} + \frac{x^2\lambda^3}{2!} - \frac{x^3\lambda^{\frac{9}{2}}}{3!} + \ldots\right] d\lambda \\ &= 1 - \frac{x}{\Gamma(\frac{1}{3})\, Y^{\frac{3}{2}}} + \frac{x^2}{2!\Gamma(-\frac{1}{3})\, Y^3} + \ldots \\ &= 1 - \sum_{n=0}^{\infty} \frac{(-1)^n}{(3n+1)!\,\Gamma(\frac{1}{3}-2n)}\left(\frac{x}{Y^{\frac{3}{2}}}\right)^{3n+1} + \sum_{n=0}^{\infty} \frac{(-1)^n}{(3n+2)!\,\Gamma(-\frac{1}{3}-2n)}\left(\frac{x}{Y^{\frac{3}{2}}}\right)^{3n+2}, \end{aligned}$$

from which follows (18) [see (15)]. These series converge (exponentially) for all values of $\eta = x/Y^{\frac{3}{2}}$.

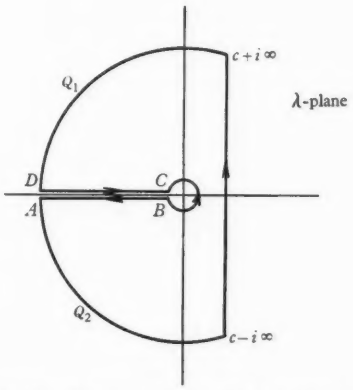

FIGURE 5. Paths of integration in λ-plane for (30) and (31).

On the other hand, when x is restricted to negative values we may expand $\exp\lambda Y$ and integrate term by term, thus obtaining the asymptotic representation for η large and negative†

$$\begin{aligned} v_0 &= \frac{1}{2\pi i}\int_{-\infty}^{(0+)} \frac{e^{-\lambda^{\frac{1}{2}}x}}{\lambda}\left[1 + Y\lambda + \frac{Y^2\lambda^2}{2!} + \frac{Y^3\lambda^3}{3!} + \ldots\right] d\lambda \\ &= \frac{3}{2}\left[1 + \frac{Y}{\Gamma(-\frac{1}{2})\,(-x)^{\frac{3}{2}}} + \frac{Y^3}{3!\Gamma(-\frac{7}{2})\,(-x)^{\frac{9}{2}}} + \ldots\right] \\ &= \frac{3}{2}\left[1 + \sum_{n=0}^{\infty} \frac{1}{(2n+1)!\,\Gamma(-\frac{1}{2}-3n)}\left(\frac{Y^{\frac{3}{2}}}{-x}\right)^{3n+\frac{3}{2}}\right]. \end{aligned}$$

Here we have used the transformation $\kappa = \lambda^{\frac{3}{2}}$ and have noticed that the resulting path of integration in the κ-plane can be deformed into one similar to that in the λ-plane. For $m = 0, 1, 2, \ldots$

$$\int_{-\infty}^{(0+)} e^{-\lambda^{\frac{1}{2}}x}\lambda^m\, d\lambda = \frac{3}{2}\int_{-\infty}^{(0+)} e^{\kappa(-x)}\kappa^{\frac{1}{2}(3m+1)}\, d\kappa = \begin{cases} 0 & \text{if } m \text{ is odd,} \\ \dfrac{3}{2}\dfrac{2\pi i}{\Gamma(-\frac{1}{2}-\frac{3}{2}m)\,(-x)^{3(m+1)/2}} & \text{if } m \text{ is even.} \end{cases}$$

Thus we obtain (16*a*).

* See, for example, Jeffreys (1927, p. 23 *et seq.*).

† In the heat-conduction case, where $\lambda^{\frac{3}{2}}$ is replaced by $\lambda^{\frac{1}{2}}$, this does not work: the function is exponentially small.

To obtain the asymptotic representation of v_0 when x is positive and η is large we set $\lambda = x^3 z^3 / Y^3$ in (31). With $k = x^3/Y^2$ ($= \eta^3$),

$$v_0 = \frac{3}{2\pi i} \int_{(1-\sqrt{3}i)\infty}^{(1+\sqrt{3}i)\infty} \exp\left[k(z^3 - z^2)\right] \frac{dz}{z}, \tag{32}$$

where the path of integration passes to the right of the origin (see figure 6). The integral is now in standard form for applying the method of steepest descent (Copson 1946; Erdélyi 1956).

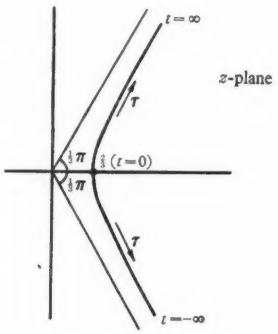

FIGURE 6. The steepest descent paths, leading from the col $z = \frac{2}{3}$, used in finding the asymptotic expansion of (32) for large k.

There are two cols, $z = 0$ and $z = \frac{2}{3}$. The first is not acceptable; through the second passes the steepest descent curve

$$3x^2 - y^2 - 2x = 0.$$

Since the right branch of this hyperbola tends to infinity in the directions $\arg z = \pm \frac{1}{3}\pi$, it may be used as the path of integration in (32). Let

$$z^3 - z^2 = -\tfrac{4}{27} - t^2,$$

so that on the hyperbola t is real and increases monotonically from $-\infty$ through 0 (at $z = \frac{2}{3}$) to $+\infty$. Then we must determine $\log z$ as a function of t [since $dz/z = d(\log z)$].

Let

$$\log z = \log \tfrac{2}{3} + W;$$

then

$$\frac{2}{3\sqrt{3}} W \left(\frac{e^W - 1}{W}\right) (2e^W + 1)^{\frac{1}{2}} = it,$$

where $(2e^W + 1)^{\frac{1}{2}}$ denotes the branch which reduces to $\sqrt{3}$ when $W = 0$ (i.e. $t = 0$). By Lagrange's formula for the reversion of series (Copson 1935) the solution is

$$W = \sum_{n=1}^{\infty} B_n (it)^n,$$

where $$nB_n = \text{residue of}\left[\frac{2}{3\sqrt{3}}W\left(\frac{e^W-1}{W}\right)(2e^W+1)^{\frac{1}{2}}\right]^{-n} \quad \text{at} \quad W=0$$

$$= \text{residue of}\,(1+w)^{-1}\left[\frac{2}{3\sqrt{3}}w(2w+3)^{\frac{1}{2}}\right]^{-n} \quad \text{at} \quad w=0^*$$

$$= \text{sum of the first } n \text{ coefficients in } (-1)^{n-1}(\tfrac{3}{2})^n(1-\tfrac{2}{3}w)^{-\frac{1}{2}n}$$

$$= (-1)^{n-1}(\tfrac{3}{2})^n\left[3^{\frac{1}{2}n}-(\tfrac{2}{3})^n\frac{\Gamma(\frac{3}{2}n)}{\Gamma(\frac{1}{2}n)\,\Gamma(n+1)}F(\tfrac{3}{2}n,1,n+1;\tfrac{2}{3})\right].$$

The integral (32) may now be written in terms of t. Then if we set $t=\sqrt{\tau}$ for $t>0$ and $t=-\sqrt{\tau}$ for $t<0$ it becomes

$$v_0 = \frac{3}{4\pi i}\exp\left[-\frac{4k}{27}\right]\int_0^\infty e^{-k\tau}\left[\sum_{n=1}^{\infty}\{i^n-(-i)^n\}nB_n\tau^{\frac{1}{2}(n-1)}\right]\frac{d\tau}{\sqrt{\tau}}$$

$$= \frac{3}{2\pi}\exp\left[-\frac{4k}{27}\right]\sum_{m=0}^{\infty}(-1)^m(2m+1)\,\Gamma(m+\tfrac{1}{2})B_{2m+1}k^{-(m+\frac{1}{2})}$$

$$= \frac{9\exp[-\frac{4}{27}k]}{4\sqrt{(\pi k)}}\sum_{m=0}^{\infty}A_m k^{-m},$$

where

$$A_m = \frac{4}{3\sqrt{\pi}}(-1)^m\,\Gamma(m+\tfrac{3}{2})\,B_{2m+1}$$

$$= \frac{2}{3\sqrt{\pi}}(-1)^m\,\Gamma(m+\tfrac{1}{2})\left[(\tfrac{27}{4})^{m+\frac{1}{2}}-\frac{\Gamma(3m+\frac{3}{2})}{\Gamma(m+\frac{1}{2})\,\Gamma(2m+2)}F(3m+\tfrac{3}{2},1,2m+2;\tfrac{2}{3})\right].$$

Since $k=\eta^3$ this is (16*b*). The recurrence relation (17) easily follows, and can be checked by direct substitution of (16*b*) into the differential equation (13).

REFERENCES

Carslaw, H. S. & Jaeger, J. C. 1948 *Operational Methods in Applied Mathematics*, 2nd ed. Oxford University Press.

Copson, E. T. 1935 *An Introduction to the Theory of Functions of a Complex Variable.* Oxford University Press.

Copson, E. T. 1946 *The Asymptotic Expansion of a Function Defined by a Definite Integral or Contour Integral.* Admiralty Computing Service (Ref. No. S.R.E./ACS 106).

Erdélyi, A. 1956 *Asymptotic Expansions.* New York: Dover.

Goldstein, S. 1960 *Lectures on Fluid Mechanics.* New York: Interscience.

Jeffreys, H. 1927 *Operational Methods in Mathematical Physics* (Cambridge Tracts in Mathematics and Mathematical Physics, No. 23). Cambridge University Press.

Ludford, G. S. S. & Murray, J. D. 1960 On the flow of a conducting fluid past a magnetized sphere. *J. Fluid Mech.* **7**, 516–28.

Proudman, I. & Pearson, J. R. A. 1957 Expansions at small Reynolds numbers for the flow past a sphere and a circular cylinder. *J. Fluid Mech.* **2**, 237–62.

Stewartson, K. 1956 Motion of a sphere through a conducting fluid in the presence of a strong magnetic field. *Proc. Camb. Phil. Soc.* **52**, 301–16.

* Setting $W=\log(1+w)$ in the contour-integral representation of the residue.

REVIEWS

Handbook of Supersonic Aerodynamics. Published by Bureau of Naval Weapons, U.S. Navy, and for sale by U.S. Government Printing Office, Washington D.C.

Eleven sections of this *Handbook* have been published so far, the first appearing in 1950, and ten more are to be published eventually. All the editorial work has been done by a group at the Applied Physics Laboratory, Johns Hopkins University. According to the Preface: 'The primary criterion used in selecting material for the *Handbook* is its expected usefulness to designers of supersonic vehicles. Thus a collection of data directly useful in the design of supersonic vehicles, results of the more significant experiments, and outlines of basic theory are included at the risk of producing a handbook that may be considered somewhat unconventional and heterogeneous in content'.

The sections of the book, either already published or to be published in the future, are as follows:

Section			Year of publication
	Volume 1		
1	Symbols and Nomenclature. 21 pp.		
2	Fundamental Equations and Formulae. 35 pp.		
3	General Atmospheric Data. 123 pp.	$1.75	1950
4	Mechanics and Thermodynamics of Steady One-Dimensional Gas Flow. 155 pp.		
	Volume 2		
5	Compressible Flow Tables and Graphs. 188 pp.	$1.50	1953
	Volume 3		
6	Two-Dimensional Airfoils. 85 pp.	$1.50	1957
7	Three-Dimensional Airfoils. 67 pp.	$1.50	1958
8	Bodies of Revolution, by D. Adamson	—	Future
	Volume 4		
9	Mutual Interference Phenomena, by Cornell Aeronautical Laboratory	—	Future
10	Stability and Control Analysis Techniques, by R. S. Swanson	—	Future
11	Stability and Control Parameters, by R. S. Swanson	—	Future
12	Aeroelastic Phenomena. 107 pp.	$1.25	1952
	Volume 5		
13	Viscosity Effects, by R. E. Wilson	—	Future
14	Heat Transfer Effects, by R. E. Wilson	—	Future
15	Properties of Gases. 228 pp.	$2.00	1953
16	Mechanics of Rarified Gases, by S. A. Schaaf and L. Talbot. 75 pp.	$1.25	1959

Section	Volume 6		Year of publication
17	Ducts, Nozzles, and Diffusers, by C. L. Dailey	—	Future
18	Shock Tubes, by I. I. Glass and J. G. Hall. 598 pp.	$3.75	1959
19	Wind Tunnel Design, by A. Pope	—	Future
20	Wind Tunnel Instrumentation and Operation, by R. J. Volluz	—	Future
21	Ballistic Ranges	—	Future

Sections 6, 7 and 12 were prepared at the Applied Physics Laboratory, Johns Hopkins University; section 5 at the Ordnance Aerophysics Laboratory, Consolidated Vultee Aircraft Corporation; and section 15 by staff at both these laboratories, working in collaboration.

A large part of the *Handbook* is made up of tables and graphs, with only an outline of the relevant theory. This arrangement is appropriate for a handbook intended primarily for designers, as this one is, but as with all handbooks there are disadvantages as well as advantages. Those who already have a good understanding of the fundamentals of supersonic flow will undoubtedly find it useful, but the inexperienced user of the book may find that he is tempted to make use of theoretical results without understanding clearly the limitations imposed by the assumptions on which they are based. Some attempts are made to deal with this difficulty; for example in section 7, which is based entirely on the linearized equation of motion for an inviscid gas, a few pages at the end are devoted to comparison of some experimental and theoretical results.

In section 2 there is a condensed account of the equations of motion and basic thermodynamics. The usual expressions are derived for one-dimensional steady isentropic flow, Prandtl-Meyer flow, and flow through plane shock waves. Corresponding numerical tables are given in section 5, for $\gamma = 9/7$, $7/5$ and $5/3$.

Section 3 is very comprehensive, but as it was published in 1950 the data for the upper atmosphere are now out of date.

Section 4 consists of a verbatim reprint of a paper by A. H. Shapiro and W. R. Hawthorne (*J. Appl. Mech.* **14**, 1947, A–317), together with numerical tables issued by the same authors with G. M. Edelman in 1947.

In section 6, on two-dimensional aerofoils, there are numerous graphs giving results of calculations by first-, second- and third-order theories and by the shock-expansion method. Some comparisons with experimental results are also given.

Section 7, dealing with three-dimensional aerofoils, and based on the linearized equation of motion, is comparatively brief in relation to the magnitude and practical importance of the subject, being no longer than section 6.

Section 12 is a collection of data for use in flutter calculations. The approximations made in computing the coefficients are not made very clear and some users of the book may perhaps be misled by the large number of significant figures given in the tables.

Despite its title, section 15 deals only with the properties of *air*, and in particular with departures from the perfect gas laws and effects of dissociation at

high temperatures. Tables are given for dry air and also for air with various amounts of moisture. Effects of non-zero relaxation times are not considered. The tables are based on the ones compiled by Hirschfelder and Curtis in 1948 and on the NBS-NACA tables issued in 1949 and later years.

In section 16 some results are given for a *perfect gas* in slip flow and in free-molecule flow.

In section 18 the declared object of the *Handbook* has apparently been set aside temporarily, for there is little here that is likely to be useful to a 'designer of a supersonic vehicle'. This section, unlike the others, is directed more to the research worker than to the designer. It is very long and the index is poor, so that although there is much useful information a particular item cannot easily be found. For example, a prolonged search was needed in order to find the equation relating the pressure ratio across a diaphragm to the strength of the shock wave that is formed in a shock tube; moreover this equation, which is of fundamental importance, does not appear until page 65. In contrast to this, imperfect gas effects are introduced as early as page 35, which makes difficulties for a reader who is new to the subject. In the chapter on instrumentation (75 pages) the measurement of force components on a model seems to have been overlooked.

With the exception of section 18, the whole of the *Handbook* should be useful to designers. Some of the sections, notably, 2, 4, 5, 15, 16 and 18, should also be useful to research workers. It is unfortunate that some of the indexes are poor, since the book is intended more for quick reference than for prolonged study.

Most of the sections can be purchased individually, at fairly low prices. Those who frequently have to make calculations in supersonic aerodynamics are likely to find some of them useful.

W. A. Mair

Hydromagnetic Channel Flows. By Lawson P. Harris. M.I.T. Technology Press, 1960. 90 pp. 22*s*. or $2.75.

Wanted: Strong lad, willing and able to perform experiments on the turbulent flow of liquid metals in transverse magnetic fields.

This appeal is inspired by reading the volume under review along with several other theoretical or speculative treatments of the problem. The only experimental observations available to relate these various discussions to reality are the very early ones of Hartmann and Lazarus and those made by Murgatroyd ten years ago. Both were exploratory investigations with features now open to criticism; the results could certainly be improved upon; and yet they have been treated as holy writ by the many empirico-theoreticians who have considered turbulent magnetohydrodynamic flow, building elaborate analyses on this very limited experimental foundation. The pressing need is for fresh experimentation which would repeat the pressure gradient measurements of the earlier workers and also go further and investigate the mean and eddying velocity distributions. Then it will be appropriate for some would-be Copernicus from the many to extract order from the established facts.

In his book Harris remarks that the results of Hartmann and Lazarus cannot be taken as particularly reliable. With only two pressure tappings to establish the pressure gradients, errors could easily arise owing to defects of the tappings. The pipes were so small as to be somewhat uncertain in size and shape, and, as Hartmann was aware, the pressure drops included small contributions due to the current loops at the edges of the magnetic field. In addition, they would include small contributions associated with the adjustment of the velocity profile in the magnetic field.

Murgatroyd used several tappings and deduced his pressure gradients from readings in the region away from the edges of the field, where the pressure fell in reasonably linear fashion. However, the edge current loops still exert a baleful influence here because of their tendency to create vorticity at the edge of the field. As a result the velocity profile is deformed. To be completely satisfactory any new experiments would need to eliminate this complication by the use of streamwise baffles or deliberately broadened fringes at the edges of the field. This distortion of the profile is most pronounced at the higher field strengths and lower flow rates, where laminar flow tends to occur. Thus it may be that Murgatroyd's results for turbulent flow do not suffer on this account. His magnet only permitted a relatively short length of apparently fully developed flow, and any new experiments should employ magnets with pole-faces long enough for it to be certain that a steady state of flow was reached. This is particularly necessary where critical Reynolds numbers for transition to or from turbulence are concerned.

Harris's discussion and analysis of the experimental results is sensible and his assumptions plausible. The book is actually a reproduction of an unusually lucid and mature Ph.D. thesis. The approach adopted is a generalization of the derivation of the universal velocity distribution in ordinary channel flow, using the ideas that the flow near the wall is independent of channel size while the velocity defect away from the wall is independent of viscosity, there being a substantial region where both ideas apply. Harris argues sensibly that the effect of induced fields may be neglected so that only the Hartmann number M and the Reynolds number R govern the problem. His analysis leads to a formula for the friction factor f in terms of two unknown functions, one of which he discards for not wholly convincing reasons. However, the available experimental results do correlate quite well under the scheme thus developed, which states that, for a given pressure gradient, $f^{-\frac{1}{2}}$ (which is proportional to flow rate) differs from its value in the absence of magnetic field by a function of M^2/R^*, R^* being the Reynolds number based on friction velocity. At low values of M^2/R^* the flow is increased slightly and at high values it decreases markedly. In the first case the damping of turbulence is dominant, while in the second the deformation of the mean velocity profile produces high rates of shear near the walls. Harris goes on to deduce further consequences of his theory such as the distributions of velocity and Reynolds stress across the channel. The theoretical analysis is probably more sophisticated than the experimental information warrants, but the ideas presented are undoubtedly stimulating, particularly in indicating what details should be scrutinized in further experiments.

A typical case in point is the conclusion that when the magnetic field is nearly but not quite strong enough to suppress the turbulence completely, it restricts it to the boundary layers, the central motion being at a uniform steady velocity. This should be readily observable by the use of probes to detect fluctuating induced voltages. Going further than Harris, one can argue that when this broad central laminar region occurs, the channel width ceases to affect the boundary layers, the representative length scale controlling them now being the Hartmann laminar boundary layer e-folding length. A simple-minded proposal is then to use the universal friction factor formula of ordinary channel flow with the channel width replaced by the Hartmann length and with numerical coefficients chosen to suit Murgatroyd's results for the régime in question. The resultant formula

$$f^{-\frac{1}{2}} = 6\log_{10}(R^*/M) - 1{\cdot}6,$$

accounts adequately for those of Murgatroyd's results for which f depends only on R/M or R^*/M until M gets too small and the turbulence too strong. Note that $R = 4R^*(8/f)^{\frac{1}{2}}$ here. Rough limits on the region where the formula appears to hold are $2000M > R > 900M$, where the lower limit is the one given by Murgatroyd for complete suppression of turbulence. It is not surprising that this suppression should occur at a fixed value of R/M if by then the channel width is irrelevant. The quantity f may still be a function only of R/M when $2000M > R$ as Murgatroyd observed, provided R is large enough, but the form of relation given above ceases to apply.

Harris's correlation in terms of M^2/R^*, a quantity which depends on channel size but is independent of viscosity, is more appropriate to the case of vigorous turbulence which spans the channel.

In this review I have concentrated on those aspects of the book that are of general fluid-dynamical interest, leaving aside the technologically important later chapters which deal theoretically with laminar and turbulent flow in a.c. induction pumps. In discussions of skin friction in pumps and other situations where there is current flow to and from the liquid, in contrast to the Murgatroyd case, it must be remembered that the pressure gradient no longer simply defines the skin friction.

To conclude, this is a stimulating book which deserves close study by all who are interested in magnetohydrodynamic channel flow and particularly by those who are proposing, or who can be induced, to undertake further experiments.

J. A. Shercliff

JOURNAL OF FLUID MECHANICS

Volume 10, Part 1 February 1961

CONTENTS

Diffraction of strong shocks by cones, cylinders, and spheres
by A. E. BRYSON and R. W. F. GROSS *page* 1

Slow steady rotation of axially symmetric bodies in a viscous fluid
by R. P. KANWAL 17

Analysis of vibrational relaxation regions by means of the Rayleigh-line method
by N. H. JOHANNESEN 25

Comparison of exact and approximate methods for analysing vibrational relaxation regions
by P. A. BLYTHE 33

A further note on the speed of floating bodies in a stream
by J. R. D. FRANCIS 48

Experiments on power generation from a moving plasma
by H. J. PAIN and P. R. SMY 51

Gaskinetics and gasdynamics of orifice flow
by HANS W. LIEPMANN 65

Theory of flame-front stability
by WIKTOR ECKHAUS 80

On a momentum-mass flux diagram for turbulent jets, plumes and wakes
by B. R. MORTON 101

A continuum theory of the isothermal flow of liquid helium II
by A. A. TOWNSEND 113

Flow of a non-homogeneous fluid in a porous medium
by CHIA-SHUN YIH 133

The effect of a very strong magnetic cross-field on steady motion through a slightly conducting fluid
by G. S. S. LUDFORD 141

REVIEWS

Handbook of Supersonic Aerodynamics 156

Hydromagnetic Channel Flows 158

Printed in Great Britain at the University Press, Cambridge
(Brooke Crutchley, University Printer)